DISSERTATION

FLAVIVIRUS CONTROL OF LIPID METABOLISM: IMPLICATIONS FOR VIRION FORMATION, FUNCTION AND PATHOGENESIS

Submitted by

Rebekah Gullberg

Department of Microbiology, Immunology and Pathology

In partial fulfillment of the requirements

For the Degree of Doctor of Philosophy

Colorado State University

Fort Collins, Colorado

Summer 2018

Doctoral Committee:

Advisor: Rushika Perera

Dean Crick
Santiago Di Pietro
Brian Geiss
Jeff Wilusz

ABSTRACT

FLAVIVIRUS CONTROL OF LIPID METABOLISM: IMPLICATIONS FOR VIRION FORMATION, FUNCTION AND PATHOGENESIS

Dengue viruses (DENV) are the most aggressive arthropod-born viruses worldwide with no currently available antivirals. There is a clear need to understand host viral interactions that can be exploited for therapeutic options. DENV are members of the *Flaviviridae* family with a positive sense single-stranded RNA genome surrounded by a virally encoded capsid protein, a host cell derived lipid envelope and an icosahedral shell of virally encoded glycoproteins. Its genome is replicated in virally–induced invaginations in the endoplasmic reticulum of the host cell that consistently develop in a time-dependent manner. These invaginations display a highly curved architecture and seem to increase the membrane contact sites within the ER and its vicinity. Functionally, these membranes condense the replication machinery, provide a scaffold to coordinate replication, and hide the viral double stranded RNA intermediate from the host cellular defenses. It has been shown that fatty acid synthesis is increased during infection to provide substrates for this membrane expansion. To identify further changes to cellular metabolism, we have profiled the metabolome of DENV serotype 2 (DENV2) infected Human Hepatoma cells (Huh7) cells at key time-points in virus replication. We have found time-dependent changes in cellular essential fatty acid metabolism. Furthermore, we have interrogated a library of siRNAs directed at the unsaturated fatty acid biosynthesis pathway to determine key enzymes involved in viral replication. We have identified that stearoyl Co-A desaturase 1 (SCD1), the rate-limiting enzyme responsible for converting stearic to oleic acid, is critical for

viral replication, maturation and infectious particle formation. Finally, we have profiled the serum metabolome of acute-phase patients with dengue diseases, chikungunya virus infection, or an unknown febrile illness to identify metabolic changes with potential use as prognostic biomarkers. Hypothesis: Since dengue viruses are enveloped viruses, lipid metabolites in the human host are a critical resource hijacked by these viruses for their replicative advantage. Important metabolites will be altered during infection in a time dependent manner and can be quantified and correlated directly to their role in viral genome replication and infectious particle assembly and release. These metabolic changes could also be identified in human bio-fluids and could function as early biomarkers of disease manifestation.

ACKNOWLEDGEMENTS

I would like to express my deepest gratitude to the members of my graduate committee: Drs. Crick, Di Pietro, Geiss, Perera and Wilusz. Their generous commitments of time, resources, knowledge and creative ideas have been instrumental in my training and development as a scientist. It has been a true honor to be constantly challenged by each of them.

A very special thanks goes to my advisor Dr. Perera, whose commitment of time and resources has gone above and beyond the call of duty. She has consistently invested in my education and training with particular emphasis on the development of my career. I am extremely grateful for this investment that will contribute to my future work and studies.

It has been a great pleasure to work with so many amazing people, in particular all of my fellow graduate students, members of the Perera lab, CSU, IDA and AIDL personnel, especially, Nunya Chotiwan, Jordan Steel, Kimberly Anderson, Stephanie Mills, Elena Lian, Nurul Islam, Venugopal Pujari, Barbra Grahm, Tach Costello, Tyler Eike, and Susi Bennett. I would also like to thank the members of the metabolomics working group and MINDR initiative, who have provided me with extensive training in metabolomics and given me helpful feedback along the way.

There have been many CSU faculty that have spent time guiding, training and inspiring me along the way, including Drs. Belise, Blair and Beaty. A special thanks goes to Drs. Rovnak and Quackenbush who have spent considerable time training me, discussing my data and have always provided me with encouragement.

Finally, I would like to thank my family and friends for their continual support, encouragement and love throughout my education. In particular, I want to thank my father, Rod

Gullberg, for his continual inspiration in science and statistics. Many additional thanks and love also go to Karen, Scott, Melissa, and Luke Gullberg for always believing in me. Lastly, I want to thank Patrick Martin for the love, courage and support that he has continuously provided for me without fail throughout this journey.

TABLE OF CONTENTS

CHAPTER 1. LITERATURE REVIEW

1.1 Introduction

Positive-strand RNA viruses share a common need for expansion and rearrangement of cellular membranes utilized for their propagation. These membranes serve as a platform for the replication of viral genomes, to concentrate resources, and to protect the replication intermediate from the immune response. In order for these membrane changes to occur, cellular metabolism must be altered to produce biomass for membrane expansion. Here, we have discussed what is currently known about changes to cellular metabolism induced by multiple flaviviruses. Since membranes also serve as sites of virion assembly and are the source of the viral lipid envelope, the lipid content of the virion has direct implications for its stability outside of the cell and ability to fuse with a new cell. Thus, we have also discussed what is currently known about the lipid content of envelope viruses and the challenges of these investigations. Additionally, given the need for highly curved membranes in virus infected cells, we have discussed unsaturated fatty acid biosynthesis and its implication in human disease as a preface to discussion of its importance for flavivirus infection investigated in this dissertation. Finally, we address the link between cellular metabolism and dengue disease pathology and the current state of biomarker discovery across various cohorts of DENV-infected patients. Therefore, this chapter introduces the major thematic elements of this dissertation and provides evidence from the literature that serves as a basis for each of our experimental approaches.

1.2 The Flavivirus lifecycle

Flaviviruses

The family *Flaviviridae* is composed of enveloped positive strand RNA viruses. *Flavus* is the Latin word for yellow, giving name to this virus family based on the prototypic member yellow fever virus. The four genera belonging to the *Flaviviridae* are: *Pestivirus*, *Hepacivirus*, *Pegivirus,* and *Flavivirus*. Pestiviruses cause diseases in animals and have bovine viral diarrhea virus (BVDV) as the prototypical member (1). Hepatitis C virus is the prototype of the Hepaciviruses and typically causes a persistent disease in humans. The Pegiviruses are less well understood and contain some viruses previously known as GB-viruses. The Flavivirus genus is composed of arthropod-borne viruses that cause diseases in humans. Among them are: dengue viruses (DENVs), yellow fever virus (YFV), West Nile virus (WNV), Zika virus (ZIKV) and Japanese encephalitis virus (JEV), which are highly pathogenic and contribute to significant global health problems. They can be broadly separated into encephalitic viruses and hemorrhagic viruses. Flaviviruses share similar genomic organization and a similar replication strategy.

Dengue viruses (DENV)

The DENVs are composed of 4 serotypes (DENV1-4). Infection with one virus provides life-long immunity, however this immunity is serotype specific and there is no cross protection (2). A secondary infection is often associated with more severe diseases (3–5). It is hypothesized that a common ancestor to the four serotypes of DENV emerged about 1000 years ago and maintained a cycle between non-human primates and mosquitoes (6,7). Then, four independent spill-over events, potentially as recent as a few hundred years ago, generated the four serotypes we have today. Despite previous outbreaks, it was not until the early 1940's that isolates of

DENV were generated for research purposes. DENV1 was isolated in Japan in 1943 and DENV2 was isolated in Hawaii in 1945 (8).

Initially, the four serotypes had distinct geographical distributions, however with increased globalization and vector spread, we have seen co-endemicity of all of them (9). However, in some locations we observe sequential endemicity, where one year will have an outbreak of, for example, DENV3 followed by DENV1 the next year. Young children who are naïve to the current outbreak are susceptible to severe infection due to this constant cycling of serotypes. Infection with DENV can range from asymptomatic to life-threatening (4,10,11). Dengue fever (DF) begins with a fever, pain, vomiting, and malaise, which can last for approximately 7 days. This can resolve or it can progress to a more severe form of disease, dengue hemorrhagic fever (DHF). At this stage supportive care and fluid replacement is critical for survival. Some patients will progress to dengue shock syndrome (DSS), which typically results in death.

In 2009 the World Health Organization (WHO) switched the case definition for dengue diseases in order to help clinicians better manage patients (12). The new definition emphasizes the signs of severe disease more than the current symptoms (12,13). It is estimated that this new definition has led to a significant over-reporting of severe disease (13). The over-reporting caused by the new case definition is likely beneficial for patient care by ensuring that patients with severe disease get the care they need. However, there is a co-incident strain on hospitals in resource-poor settings where staffing and supplies are limited and not equipped to deal with the increase in patient numbers. Additionally, this definition has not been adopted by many research groups and clinicians, due to the need for cohesive definitions across years of studies and the difficulty in implementation.

Despite many efforts, there are currently no US Food and Drug Administration (FDA) approved antivirals and only a sub-optimal vaccine for dengue (14–16). Prevention, through vector control, remains the best strategy for a global reduction in dengue diseases.

Stages of the virus life cycle

Attachment and entry

Unfortunately, the field has yet to find a consensus on the receptor required for DENV attachment and entry into a cell. It is likely that the virus is promiscuous and able to use a variety of receptors on different cell types. Prior to internalization, the virion moves randomly along the cell surface and then binds to attachment molecules via non-specific interactions (virion adhesion) (17). These attachment molecules include but are not limited to several C-type lectins, the mannose receptor, dendritic cell-specific intercellular adhesion molecule-grabbing non-integrin (DC-SIGN), liver/lymph node-specific intercellular adhesion molecule-3-grabbing integrin (L-SIGN), as well as TIM (T cell/transmembrane, immunoglobulin, and mucin) and TAM (Tyro3, Axl, and Mer) receptors (18–21). After attachment the virus is loaded onto a pre-existing clathrin-coated pit for internalization (22,23).

Once the virion is internalized, it traffics through the endocytic pathway. Beginning in the early endosome (EE), cargo contents are sorted into intraluminal vesicles and transported to late endosomes via endosomal carrier vesicles (ECVs) along microtubules. The ECVs undergo an additional sorting step in the late endosome where they are targeted to the trans-Golgi network (TGN), degradation in the lysosome, or released into the cytoplasm. DENV is transported in an ECV into the late endosome where it escapes the endocytic pathway through fusion with a Rab7-positive endosome (24). Fusion independent of Rab7 has also been observed, thus this may be strain specific. Fusion appears to be an event distinct from genome delivery into

the cytoplasm, which may require additional host proteins to accomplish (25). Hence, the virion may fuse with the ECV completely or as an intermediate state and subsequently the ECV back-fuses with the late endosome (LE), resulting in the final release of the genome into the cytoplasm (25). This process is depicted in Figure 1.

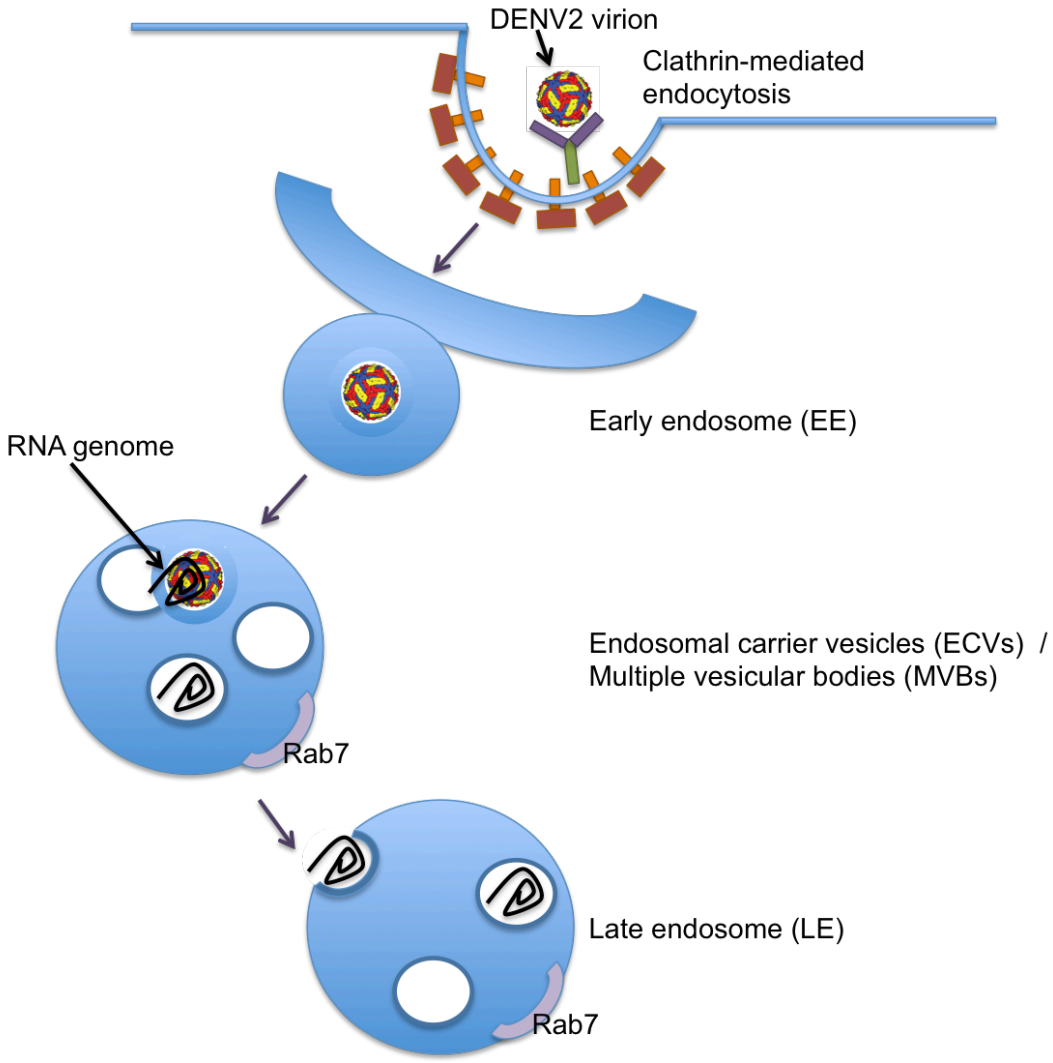

Figure 1 DENV2 entry and travel through the endocytic pathway. As described in the text, DENV2 enters the cell through clathrin-mediated endocytosis, then enters an early endosome (EE) filled with endosomal carrier vesicles (ECV). It fuses with an ECV, and is targeted to a Rab7 endosome. When the endosome develops into a late endosome, the ECV will fuse with the endosomal membrane and release the viral RNA into the cytoplasm. Adapted from (22-25)

The structural changes that occur to the virion envelope glycoprotein (E) to allow for fusion are well characterized (26–28). The E glycoprotein has 3 domains (D): DI, DII and DIII.

In the mature virion, E glycoproteins lay flat on the surface as homodimers. The drop in pH in the late endosome disrupts these homodimers into monomers (26). This causes the monomers to project outward from the surface of the particle, exposing the fusion loop at the distal end of the DII domain. The fusion loop inserts into the target membrane and three E glycoproteins in close proximity form a trimer. The hemi-fusion intermediate then forms and the DII domains folds back against the trimer. Initially the outer leaflets of the membranes begin to mix, then the inner membranes mix as the fusion pore forms. Then the capsid protein and RNA complex are released into the cytoplasm, or into the ECV depending on the membrane used for the fusion event.

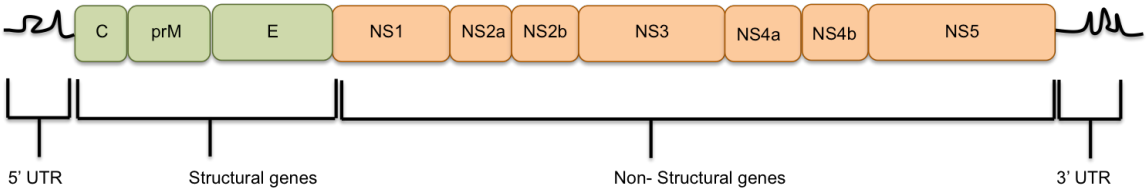

Figure 2 Flavivirus Genome Organization. The organization of the flavivirus genome is depicted with the location of each structural and non-structural gene. UTR: untranslated region, C- capsid, prM:premembrane/membrane, E: envelope, NS1: Non-structural protein 1, NS2a: Non-structural protein 2a, NS2b: Non-structural protein 2b, NS3: Non-structural protein 3, NS4a: Non-structural protein 4a, NS4b: Non-structural protein 4b, NS5: Non-structural protein 5. [Adapted from (29,30)].

Translation and polyprotein processing

Since flaviviruses have a positive sense RNA genome it is ready to be translated as soon as the genome is released into the cytoplasm and encounters a ribosome. The viral genome has one open reading frame and is translated into a polyprotein that is co- and post- transnationally cleaved by viral and host proteases into 10 individual proteins. The genomic organization is depicted in Figure 2.

Structural proteins:

The capsid protein interacts with the viral genome as it packs into the virion. No icosahedral symmetry of the capsid structure has ever been observed (31). Furthermore,

populations of capsid protein localize to the nucleus of the cell, where they are implicated in nucleosome disruption and induction of apoptosis (32–34). Capsid is anchored to ER membranes through its C-terminal sequence, however it also takes on a dimeric form in solution (35). The functional importance of this dimerization is still unclear due to its functional flexibility, but mutations that are structurally predicted to disrupt dimerization prevent virion assembly (36).

The pre-membrane (prM) protein is a key structural protein that takes on a heterodimeric form and associates with the E glycoprotein to make up the virion glycoprotein shell (37). The pr portion of the prM protein acts to cover the fusion loop of E to prevent a premature fusion event within infected cells, while the M portion is membrane bound and anchors the heterodimer in the virion envelope (38,39). A pH change as the virion transits through the TGN triggers a structural change that exposes a furin cleavage cite on prM. After cleavage the pr peptide remains associated with the virion until it returns to a neutral pH in the extracellular milieu.

The envelope (E) glycoprotein provides much of the structure of the protein shell and contains the fusion loop allowing the virion to penetrate a host cell (40). The E glycoprotein is a class II fusion protein. It is also the primary source of structural heterogeneity of flavivirus particles (37,41–43). Hence, it has a critical role in viral transmission and evolution.

The non-structural proteins

The non-structural proteins are numbered according to their genomic organization. Intracellularly, NS1 is in a membrane bound dimeric form that aids in viral replication (44). In its secreted form it is hexameric and is found in association with lipids. This proteo-lipid particle is found circulating in patient serum and is an antigen used in diagnostic tests for DENV infections (45). NS1 plays a role in severe disease forms of dengue by enhancing degradation of the

endothelial glycocalyx (46,47). The recent structure of WNV and DENV NS1 as a hexamer and dimer provided insight into membrane interactions and immunogenicity (48,49).

NS2A is a transmembrane protein that has been implicated to function in both viral replication as well as assembly. The structure of NS2A has not been solved but extensive biochemical analysis implicates 5 membrane spanning domains. It is speculated that it may exist in different forms to mediate its roles in replication and assembly (50). NS2B is required as a co-factor for the protease activity of NS3. NS3 is the helicase and nucleotide triphosphatase required for RNA replication. It is also a serine protease that post-translationally cleaves the viral polyprotein (51). NS3 is also implicated in the disruption of many different cellular pathways (52). For example, NS3 cleaves the antiviral protein, stimulator of interferon genes (STING), and thereby suppresses interferon production and the immune response (53,54).

NS4A and NS4B are membrane bound proteins with no known enzymatic activity. Early studies demonstrated that they alone are sufficient for membrane rearrangements in the ER (55,56). The C-terminal region of NS4A (referred to as 2K) is a signal sequence that assists in the localization of NS4B in the ER lumen to facilitate these membrane changes. Interactions between the two proteins may be through 2 helices in the N-terminal region of NS4B and are important for viral replication (57) and may also suppress the innate antiviral response (58,59).

NS5 is a multifunctional protein possessing methyltransferase, RNA-dependent RNA polymerase and guanylyltransferase activities (60–62). The N-terminal one-third of the protein is responsible for capping the viral RNA and internal methylation of the RNA. An alpha-helical linker region with a nuclear localization signal connects the capping region to the C-terminal two-thirds of the protein responsible for RNA-dependent RNA polymerase activity that replicates the viral genome. Interestingly, there may be two populations of NS5 in cells where

the nuclear localization signal directs a large population of the protein to the nucleus (63). This population is hyperphosphorylated and transits to the nucleus immediately after translation. Given its role in RNA replication, another population of NS5 remains in the cytoplasm to replicate the viral RNA.

Replication on the ER membranes

Ultrastructural characterization of flavivirus infected human and mosquito cells have demonstrated massive expansion and rearrangement of ER membranes. Flavivirus infected cells demonstrate three distinct types/structures of membranes: convoluted membranes (CM), paracrystalline arrays (PC) and vesicle packets (Vp) housing internal smaller vesicles (Ve). The CM and PC are proposed as sites of translation and polyprotein processing due to the presence of NS3 and NS2B within the structures (64,65). The Ve structures are connected to the cytoplasm through neck-like open pores and are packaged within the Vps. Viral RNA-dependent RNA polymerase and double stranded RNA (dsRNA) intermediates are observed in the Vp/Ve structures suggesting that this is the location of viral replication. The lack of single-stranded RNA in these locations suggests that after it is capped it exits the Ve and interacts with capsid in a neighboring location.

Assembly/ budding

Flaviviruses do not possess a packaging signal and so encapsidation of viral RNA is not well understood. However, only complete and actively replicated viral RNA is packaged (66). This occurs in close proximity to the Vp/Ve sites of viral replication. These sites appear to be directly opposed to the neck-like structures of the Ve. Hence, newly replicated RNA may exit the Ve and immediately interact with viral structural proteins and assemble. The capsid protein aids in packaging of the viral RNA on the cytoplasmic side of the ER, where the capsid interacts with

prM and E in the membrane. Together, the particle forms and buds into the ER lumen. The assembled particle has T=3 icosahedral symmetry due to the arrangement of the glycoproteins (37). These proteins are anchored in the host-derived lipid-bilayer that encircles the capsid and RNA.

Maturation

As the virion transits through the TGN it undergoes a maturation process involving significant structural rearrangements in its glycoprotein shell. Initially, the particles are considered "immature" where 90 prM-E heterodimers are arranged in 60 trimeric spikes that protrude orthogonally from the particle surface. As the particle transits through the TGN, the pH drops which induces a rearrangement of E into 90 homodimers that lay flat on the particle surface. This is a reversible rearrangement. This transition exposes the furin cleavage site on prM and allows processing of pr from M. The pr peptide however, remains associated with the virion, likely to cover the fusion loop of E and prevent pre-mature fusion. It dissociates from the virion when it encounters a neutral pH external to the cell. Virions that are free of the pr peptide are fusogenic and can enter new cells.

1.3 Flavivirus manipulation of cellular metabolism

Cellular metabolism is a tight balance between anabolic and catabolic processes that are necessary for cells to function and proliferate. Viruses usurp these processes to meet their metabolic needs [reviewed in (67)]. These needs broadly range from production of new virions to immune evasion. Substrates needed for progeny production include nucleic acids for RNA replication, amino acids for protein synthesis and lipids to build virion envelopes. In addition to the substrates that viruses gain through cellular synthesis or degradation pathways, they can also gain energy to drive replication. In the midst of building new virions, viruses must evade the host

immune system that is seeking to destroy them [reviewed in (68)]. Metabolic manipulation can enable viruses to obtain their substrate needs and avoid the immune response.

Metabolomics-based studies have provided significant insight into biochemical pathways that viruses rely on or change during the course of infection. However, when we observe accumulation of certain lipid species, it is difficult to determine if these species come from a synthesis or degradation pathway. Metabolic flux experiments, using isotope tracers coupled to high-resolution mass spectrometry, can help us to tease these pathways apart. Flux analyses allow us to determine the distribution of metabolites in a pathway under steady-state conditions and quantify the response of the metabolic network to perturbation. This technique has been used to elucidate metabolic control mechanisms of certain viruses but has not yet been used for flaviviruses (69). Detailed flux analysis of flavivirus infections would answer many of the questions outlined below.

Cellular metabolism is often a limiting factor in viral infections, thus every virus family uses novel strategies to replicate at their own optimal rate. Different virus families manipulate many different branches of metabolism [reviewed in (70)]. Thus far, it has been demonstrated that flaviviruses manipulate glycolysis, the pentose phosphate pathway and lipid biosynthesis. We will discuss each of these pathways below, the current understanding of virion lipid composition and explore how manipulation of these metabolic pathways alters virion function.

Central Carbon Metabolism

Under standard conditions mammalian cells undergo mitochondrial oxidative phosphorylation to produce ATP. However, certain conditions can drive cells to uptake excessive glucose and “ferment” it into lactate, despite the presence of sufficient oxygen. Typically, this occurs in cancer cells due to oncogenic mutations that drive the need for an increase in biomass

necessary for proliferation. This phenomenon is known as the Warburg effect and has been studied for many years in the context of cancer cell metabolism and proliferation (71–73). The precise reason for cancer cell utilization of this route of metabolism is unclear, the original hypothesis was that it is due to mitochondrial dysfunction, however many have shown that this is not the case [reviewed in (71)]. This "aerobic glycolysis" is an interesting phenomenon that also occurs in some virus-infected cells implying that it is not unique to cancer cells. The Warburg effect impacts central carbon metabolism (CCM), or the enzymatic transformation of carbon via glycolysis, the PPP, or the tricarboxcylic acid (TCA) cycle. There is still much to be understood regarding CCM and its uses by flaviviruses, with the current understanding being limited and controversial. Here we present an update on what is known about flaviviruses DENV, HCV and ZIKV and their ability to manipulate CCM.

Glycolysis:

Glycolysis is a series of enzymatic reactions that convert glucose to pyruvic acid, NADH and ATP. Viruses manipulate glycolysis to obtain these resources. Briefly, the glycolytic process is increased in HCV-infected cells to provide ATP for replication (74,75). DENV increases glycolytic processes, but it is not clear if this is uniform throughout the pathway. For example, the activity of some glycolytic enzymes, the downstream fates of the carbons from glucose and the source of energy production in infected cells are still unclear (76,77). Finally, it was recently demonstrated that ZIKV enhanced levels of multiple genes involved in regulation of cellular metabolism, specifically glycolysis (78).

In order for glycolytic activities to proceed, there must be a supply of glucose in the cell. This is accomplished by a variety of glucose transporters that import exogenous glucose. GLUT1 is widely expressed and responsible for basal uptake in all cells, with increased expression in

erythrocytes and endothelial cells in barrier tissues (i.e. blood brain barrier) (79). During infection of primary human foreskin fibroblasts (HFFs), DENV increases GLUT1 expression (76). It is unclear if other glucose transporters are additionally impacted, perhaps different cell types or different flaviviruses may result in various glucose transporter usages.

It is important to note that increased glucose uptake does not imply an increase in glycolysis since glucose can feed into multiple metabolic pathways. Hence, the entire pathway must be characterized to identify the fate of glucose. The first step in glycolysis is the phosphorylation of glucose by hexokinase 2 (HK2) to convert it into glucose-6-phosphate. The addition of the charged phosphate group directs glucose-6-phosphate towards glycolysis and depletes cellular pools of glucose maintaining a gradient and allowing for its continued facilitated import into the cell. In DENV-infected cells hexokinase expression is increased, effectively stimulating the import and retention of glucose (76). No dengue viral protein was found to be responsible for the increased HK2 activity, but in HCV infected cells, the D2 or D3 domain of NS5A modifies the catalytic parameters of HK2 to stimulate its activity (74). Further characterization of this interaction may implicate other flaviviral proteins in this process. This pool of modified glucose in the cell can now be shunted towards glycolysis or the pentose phosphate pathway (PPP). These carbons may flux completely through either one of these pathways or may be diverted depending on the regulation of key enzymes in the pathway. A profiling of the metabolites in glycolysis found that the first few metabolites produced in the glycolytic pathway build up during DENV infection, while the later metabolites appeared to decrease (76). This could indicate that there is increased flux through the pathway where the final metabolites are shunted elsewhere and thus decreased. Or the decrease in downstream metabolites could be due to inhibition of the final enzymatic reactions. Interestingly, the DENV

NS1 protein increases glyceraldehyde 3-phosphate dehydrogenase (GAPDH) activity, which is a downstream enzyme in glycolysis and its increased activity suggests that carbon fluxes all the way through glycolysis in DENV-infected cells (80).

In order to complete the Warburg effect there must be an increase in lactate dehydrogenase activity and extracellular lactate. This both completes the cycle and produces NAD^+ to support continued glycolysis. One group found that this was not the case in DENV-infected cells suggesting that flux is not the true role of the increased glucose supply, but that it is diverted elsewhere (77). This contradicts findings from our lab, where we do see an increase in lactate dehydrogenase expression and extracellular lactate production (Steel *et al*, unpublished). Furthermore, others have observed increased lactate production in HCV infected cells and inhibition of lactate dehydrogenase leads to a reduction in DENV replication, suggesting that glucose flux is important in flavivirus infected cells (74,76). These findings are not mutually exclusive, as increased glucose supply may lead to some percentage of glycolytic intermediates being diverted and some completing the glycolytic pathway to lactate. Further work is needed to define the relative role of these pathways, the cell-type specificity and the control points in regulating these processes.

TCA cycle/mitochondria:

In addition to the question of whether carbon fluxes through glycolysis in virus infected cells, there are other important questions: 1) where could carbon divert instead of through glycolysis and 2) what is the main source of ATP? These are still largely unclear. However Fernandes-Siqueira *et al* shed light on this phenomenon using high-resolution respirometry to evaluate the contribution of fatty acids (FAs), glutamine, glucose and pyruvate to mitochondrial oxygen consumption in the presence of dengue infection (77). They found viral inhibition of the

Crabtree effect, a phenomenon where cellular respiration is inhibited in the presence of glucose (81). Hence, the excess glucose that flavivirus infected cells take up does not inhibit mitochondrial respiration to favor glycolysis as one might expect. Instead they found that oxidized FA are the main energy source in infected cells and that glucose plays an anapleurotic role (replenishes unspecified intermediates in the pathway) in the use of these FAs. Hence, glucose utilization favors oxidation of endogenous substrates. Thus the increase in glucose uptake results in more pyruvate that shunts into the TCA cycle in order to oxidize endogenous fatty acids (77). This is again in contrast to what was found with HCV infection where it causes severe impairment of mitochondrial oxidative phosphorylation and a switch to reliance on non-oxidative glucose metabolism (75).

The critical role of β-oxidation in energy production during dengue infection is supported by the increase in autophagy to degrade TGs from lipid droplets for β-oxidation (82). Multiple groups have demonstrated that DENV causes mitochondria to elongate, increasing respiration, thus corroborating the idea that DENV is dependent on oxidative metabolism (83,84). However, it was demonstrated that DENV causes cellular respiration to uncouple from ATP synthesis (85). This indicates that ATP production from β-oxidation is not efficient and not the primary source of ATP in DENV-infected cells. These studies would imply that glycolysis is a likely route of ATP production, similar to the Warburg effect. Higher resolution techniques and comparisons across cell types are needed to clearly define this unique energy balance in DENV-infected cells.

Pentose phosphate pathway:

Tightly coupled to and running in parallel with glycolysis is the PPP, an anabolic process that takes glucose derivatives and generates pentose rings to be used in purine, pyrimidine and histamine synthesis among others. During the initial oxidative phase of the pathway NADPH is

produced, which is required for lipid biosynthesis and prevention of oxidative stress. Both the NADPH and the pentose rings are substrates needed by the virus to replicate its genome, make proteins and synthesize lipids to expand membranes. Given the significance of this pathway, flaviviral control of it seems inevitable. One hypothesis is that the increase in glucose uptake during DENV infection is primarily shunted towards the PPP to drive nucleotide and fatty acid biosynthesis (77). One way to accomplish this channeling of glucose is for the rate-limiting enzyme to be enhanced in some manner to drive metabolism. Glucose 6-phosphate dehydrogenase (G6PD) is the enzyme that catalyzes the first and rate-limiting step in the oxidative branch of the PPP and produces NADPH.

Very little evidence supports the idea of G6PD involvement in PPP channeling in DENV infection. However, some have taken advantage of the fact that many humans have a spontaneous mutation causing a deficiency in G6PD. To explore the impact of this deficiency primary monocytes from these patients were cultured and infected with DENV. This resulted in an increase in viral replication compared to control cells (86,87). The impact on viral replication was hypothesized to be due to lowered levels of NO and O_2 and increased oxidative stress (86). Hence, G6PD may not be involved in shunting substrates towards the PPP in DENV-infected cells, or it may be that the impacts on oxidative stress mask the effects of G6PD on the PPP. Further mechanistic detail of this enzyme will likely tease this apart and demonstrate the importance of the PPP.

On the other hand, metabolomics experiments of HCV infected cells over time observed increased nucleotide synthesis and PPP intermediates (88). Proteomic profiling of HCV infected cells coupled to lipidomic analysis highlighted an early perturbation in the non-oxidative PPP to sustain viral replication (89). Clearly, both branches of the PPP are important to generate species

for flavivirus genome replication. Whether the viruses achieve control of this pathway or if it is a cellular response to stress is still unclear.

Importantly, many of these processes can be inhibited to control viral infection. There are inhibitors that target most steps in central carbon metabolism and their use can demonstrate the significance of each branch point in metabolism during dengue virus infection. However, many of them lack specificity and thus need to be corroborated with other means of experimentation. Currently, it has been published that inhibition of lactate dehydrogenase and hexokinase both reduce dengue virus replication (76). Interestingly, ZIKV replication can be inhibited with nucleoside analogues, implicating another arm of central carbon metabolism in replication (78). Ideally, with further understanding of viral control of these pathways and the impact on the cell we can identify host-targeted therapeutics to control viral infection.

Lipid biosynthesis:

Despite the ambiguous destination and usage of increased glucose uptake in flavivirus infected cells, there is clearly added carbon in these cells that can be used as substrates for complex organic compounds. Currently, the best-characterized reductive biosynthetic process manipulated by flaviviruses is lipid synthesis. This represents a likely destination for these carbons, however a complete picture of the biosynthetic processes perturbed by these viruses is still being explored.

Fatty Acids:

The first class of lipid we will discuss is a fatty acid chain. These provide hydrophobicity and are primarily responsible for maintaining the bi-layer nature of membranes in cells. Fatty acids can be synthesized *de novo* in the cell, scavenged from the environment or recycled from

existing lipid species. Here we will discuss their synthesis in relation to flaviviruses and replication complex formation.

At the top of the fatty acid biosynthetic pathway is acetyl Co-A carboxylase (ACC) that catalyzes the carboxylation of acetyl-CoA to malonyl-CoA and commits these carbons to the production of fatty acids. Knockdown of ACC results in inhibition of DENV replication (90). Furthermore, ACC is important for WNV replication and is hypothesized to play a key role in the rearrangement of cellular ER membranes (91). Inhibition of ACC disrupts the formation of membranous complexes in virus infected cells as seen in EM images (91). Presumably, this is due to depletion of fatty acid substrates preventing membrane expansion. Without the expansion of these membranes, WNV cannot sufficiently protect and replicate its genome. Whether there is a dose-dependent relationship between membrane expansion and viral genome copies produced is unclear, however intriguing.

Immediately downstream of ACC is fatty acid synthase (FAS), which takes malonyl-CoA and turns it into palmitic acid. FAS is recruited to replication complexes in the ER in DENV-infected cells where it produces fatty acids (90). Inhibition of FAS is well recognized to limit the genomic replication of multiple flaviviruses in multiple cell types (90–93). However, a recent report stated that ZIKV was not sensitive to FAS inhibition, this was unexpected and more work needs to be done to validate this observation (95). Together, ACC and FAS generate fatty acid species that serve as a biomass for the expansion and rearrangement of ER membranes into viral replication factories.

Complex lipids:

Complex lipid species can be broadly classified as glycerophospholipids, sphingolipids or sterols. They play critical roles in cellular signaling events and structural organization of membranes, further discussed below.

Glycerophospholipids (GPLs):

GPLs are the most abundant component of cellular membranes, with phosphatidylcholine (PC) representing the most abundant of the GPLs (45-55% of all lipid species) (96). PCs have cylindrical geometry and act as the skeleton of the membrane giving a stabilizing force with neither positive nor negative curvature (97,98). PC is synthesized via the Kennedy pathway in the ER and Golgi or via a scavenger pathway that breaks down phosphatidylethanolamine (PE) to PC (99). Due to the massive overall expansion of membranes in flavivirus infected cells, one would assume that cells would display a significant increase in PC levels. Many metabolomic profiling studies using various flaviviruses and cell types have indeed found increases in PC and total GPL content compared to uninfected cells as expected (88,89,92,100,101). When looking more specifically at PC localization in virus infected cells Zhang *et al* found that many plus-strand RNA viruses recruit PC to their replication complexes and inhibition of this process is detrimental to their replication (102). However, they did not observe this phenomenon in DENV-infected human cells, calling into question the significance of increased PC content in flavivirus infected cells. Perhaps location may explain this seemingly contradictory finding, where DENV-infected cells may have an overall expansion of membranes containing PC, while they specifically recruit other lipid species to their replication complexes.

Not many large-scale metabolomics experiments have been carried out with ZIKV thus far, presumably it is quite similar to DENV. A MALDI Mass Spectrometry Imaging (MALDI-MSI)

approach to characterize the lipidome in ZIKV infected mosquito cells (103). Similar to previous work on the lipidome of DENV-infected mosquito cells, they found an increase in glycerophospholipid metabolism in ZIKV infected compared to uninfected cells. Furthermore, they found one putative sphingolipid molecule previously implicated in antiviral defense. Few other changes were observed, likely due to the low-resolution methods used.

Another interesting GPL species is the lysophospholipid (LPL), key to many signaling pathways and instrumental in membrane structure. LPLs consist of a glycerol backbone esterified to a variable head group and one variable fatty acid chain. These species have an inverted cone-shape that promotes positive curvature. Lysosphospholipase enzymes: PLA_1 and PLA_2 in conjunction with lysophospholipase D (lysoPLD) or phospholipase D (PLD), remove a fatty acid from phosphatidic acid (PA) to generate LPLs [reviewed in (104,105)]. Lysophosphatidic acid (LPA) acts as an extracellular signaling molecule by binding to G protein-coupled receptors (GPCRs). The pathways impacted by LPA stimulation have been implicated in cancer, obesity, and diabetes [reviewed in (104)]. Many of the metabolic pathways impacted by these diseases are also altered by flaviviruses [reviewed in (70)]. Perera *et al* found elevation of multiple lysophosphocholine (LPC) and lysophosphoethanolamine (LPE) species in DENV-infected mosquito cells (92). Simultaneously, they found that PLA_2 activity was increased in these cells. When looking closer at replication complex associated membranes they found elevation of an LPE species (PE P-16:0e). Enrichment of this lipid near replication complexes is likely due to the need for highly curved membranes surrounding the replication intermediate. These sites are also close to viral assembly sites and incorporation of LPLs into virions could support their high degree of curvature. A similar increase in LPL content in total cells was also seen in WNV infected cells (100). However, this was not found in a recent metabolomics study

of DENV-infected mosquitoes, who primarily had decreases in LPLs compared to uninfected controls (106). This may reflect a difference in biological systems, cell type or timing of infection. Further interrogating the role of PLA_2 in DENV-infected cells such as its cell type specificity, timing of action, and the role of its enzymatic products in the infection process may shed light on this process.

Sphingolipids (SL):

SLs are the second key membrane lipid species. They contain a common sphingoid backbone that is N-acylated with a fatty acid to form ceramide (Cer). Complex SLs are formed through modifications to ceramide such as phosphorylation, or glycosylation (107). These bioactive molecules act in signaling pathways throughout the cell such as signal transduction, cell growth, differentiation, and apoptosis (108–110). They also provide key structural support to cellular membranes and are particularly enriched in lipid rafts in conjunction with cholesterol. The dysregulation of genes in sphingolipid biosynthesis is implicated in diseases such as, type 2 diabetes, Alzheimer's disease, and hepatocellular carcinoma [reviewed in (111)].

Sphingolipid biosynthesis includes both *de novo* synthesis and salvage pathways, providing for multiple control points (112). WNV causes an increase in both ceramide and sphingomyelin in cells (100). The high levels of SLs in the cell are utilized both in the virion envelope (discussed in detail in section 1.4), and in formation of the replication complexes (100,113). Prolonged inhibition of serine palmitoyltransferase, the rate limiting enzyme in the *de novo* biosynthesis of sphingolipids, reduces levels of ceramide in the cell and leads to a reduction in WNV replication (113). The salvage pathway to generate ceramide involves the removal of the phosphocholine group of SM by acid sphingomeylinase to generate ceramide. Inhibition of acid sphingomeylinase results in a reduction in the release of viral particles from infected cells (100).

DENV similarly increases sphingolipids in infected mosquito cells (92). However, sphingolipids seem to be utilized differently for these two flaviviruses. For instance, DENV-infected cells do not recruit ceramide to RCs. Additionally, DENV replication is increased when ceramide synthesis is inhibited (113). However, these studies were carried out in mammalian cells. Therefore, it is possible that DENV may utilize sphingolipids differently in mosquito versus mammalian cells.

Cholesterol:

The final class of membrane lipids is sterols. Cholesterol is a ubiquitous component of cellular membranes with significant interest across biological disciplines. It is typically found highly concentrated in the plasma membrane of the cell where it provides a rigid structure and presumably aids in the formation of lipid rafts by associating with certain lipid species that have high-melting temperatures. Lipid rafts function as key initiators of signaling cascades in the cell by concentrating receptors and other signaling proteins (114). Misdistribution of cholesterol in the cell is typically indicative of a disease state and contributes to varying shapes of membranes [reviewed in (115)]. Cholesterol, its synthesis, location, trafficking and role in replication of many different viruses have been widely studied and many unique ways to alter cholesterol homeostasis have been discovered.

Huh7 cells infected with DENV display an early increase in cellular cholesterol and lipid raft formation (116). Specifically, an increase in the activity of the rate limiting enzyme in the mevalonate pathway (which is part of cholesterol biosynthesis), 3-hydroxy-methylgluteryl-COA reductase (HMG-CoA reductase) was shown by an increase in its phosphorylation and an increase in cholesterol levels (116). Additionally, Fluvastatin treatment, which inhibits HMG-CoA reductase, reduced viral replication, which could be partially rescued with mevalonate,

geranylgeranyl pyrophosphate (GGPP), or farnesyl pyrophosphate (FPP), three downstream metabolites (117). Loss of function of mevalonate diphospho decarboxylase (MVD), another key enzyme in this pathway, also reduced DENV replication (117).

During ZIKV infection, an interferon stimulated gene (ISG): cholesterol-25-hydroxylase was upregulated to produce 25-hydroxycholesterol, which is a strong antiviral agent (118). The protective effects of 25-hydroxycholesterol against ZIKV were further demonstrated in brain organoids, fetal mice and macaques.

WNV infection also increased the biosynthesis of cholesterol via control of HMG-CoA reductase. This enzyme and pools of cholesterol were re-located to sites of viral replication (119). The re-distribution of cholesterol lead to a depletion of lipid rafts and the down-regulation of interferon-stimulated Jak-STAT antiviral signaling (119). These observations, collectively demonstrate a role for cholesterol in flavivirus replication.

1.4 Lipid content of Flavivirus Virions

Thus far we have discussed metabolic changes in host cells caused by viral infection with structural or signaling implications for the host cell. However, the impact of metabolic changes on the final product of replication, the virion is also of significance due to the direct inclusion of a host-derived lipid envelope as a structural component of the virion. Additional components of the virion include the viral genome and viral glycoproteins. While the manipulation of host cell lipids by flaviviruses is a clear phenomenon, the criteria that govern the inclusion of these lipids into the virion envelope has not been investigated.

Some virus families bud from lipid rafts and so control the lipid content of their envelope (120–122). Flaviviruses do not appear to bud from lipid rafts but they may control their lipid content in other ways. Perhaps the virion incorporates specific lipids into the envelope to achieve

stability or functionality (i.e. fusion with the target cell). This could be controlled by altering the lipid content of the ER in a localized manner, i.e. near the site of assembly, through localized metabolism or lipid organizational enzymes (flipases/flopases). Alternatively, sites of assembly could be targeted by the virion based on their existing lipid content. Profiling the lipid content of viral envelopes can provide significant insight into these processes. If the lipid content of the virion differs significantly from that of the cellular membrane from which it originates, it would indicate selectivity. Here we will discuss the current understanding of the biogenesis of the flavivirus lipid envelope.

One of the largest difficulties faced in profiling the lipid content of virions is the inclusion of proper controls and sufficient replicates. Virus purification can be a complex process and the final prep is often a mixture of viral particles, sub-viral particles, exosomes and other cellular debris depending on the type of purification. As such comparison to uninfected cellular supernatant and the originating cellular membranes need to be included as important controls. For flaviviruses this is the ER membrane, which is very difficult to clearly separate from other cellular membranes. With the use of these controls the lipid content of virions can be accurately queried and compared to the originating cellular membranes.

Most studies of the lipid composition of enveloped viruses have focused on more complex lipid species and have not characterized the fatty acid content. It is clear that certain lipid species are enriched in viral envelopes and are functionally relevant for virion infectivity (100,123–126). Here, we will describe the lipid content of flaviviruses that have thus far been characterized.

West Nile virus (WNV):

To characterize the WNV particle lipidome, sucrose gradient purified virions were compared to recombinant subviral particles (RSPs) and total HeLA cellular membranes (100).

The comparison to RSPs is useful as they come from the same cellular membrane, however comparing to total cellular membranes is less than ideal since the lipid content varies between cellular membranes (i.e. Golgi vs. ER vs. PM) under normal conditions. Differences found between total cellular membranes and the virus may reflect the re-distribution of lipid species from replication, rather than a specific control of lipid content in the virion. Nonetheless, profiling total lipids is informative. For this experiment they looked specifically at glycerophospholipid and sphingolipid content. They found less PC in virions and RSPs compared to the cellular membranes, meanwhile, SM was enriched in virions and RSPs compared to cellular membranes. More specifically, they found 4 PE, a dihydroCer and 3 SM species that were enriched and one PE that was reduced. When comparing virions, RSPs, and infected cell membranes, they only found 5 lipid species that were enriched in all of these. These species were annotated as PEs and SMs. They hypothesized that enrichment of these species in the cell provides for their increase in the virion envelope (100).

Bovine viral diarrhea virus (BVDV):

The second flavivirus we will discuss here is bovine viral diarrhea virus (BVDV). This virus is from the pestivirus family in the genus *Flaviviridae*. It is a pathogen of livestock with similar biology to HCV (127). To characterize the lipidome of BVDV, Callens *et al* purified particles from Madin-Darby Bovine Kidney Epithelial (MDBK) cells and using standards, profiled 20 specific classes of lipid species: 13 GPLs, 3 SLs, 3 neutral lipids, and cholesterol (126). They identified 398 total unique molecular features that were quantified within this list. They found a ~2.3-3.5 fold increase in cholesterol, SM and hexosylCer in the virion envelope compared to the originating cellular membrane. Collectively these three species account for ~70 mol% of the lipid envelope while they account for 30 mol% of the cellular membranes,

representing a significant increase in the virions. Furthermore, there was a 1.5-5% decrease in GPL species in the virions. Interestingly, when profiling the PC species, they found a tendency towards saturated PC species and shorter acyl chains in virions. Taking together, they concluded that the total lipid composition of BVDV is most similar to influenza virus and surprisingly quite dissimilar to HCV.

Hepatitis C virus (HCV):

The lipid envelope of the flavivirus, HCV, the archetypal hepacivirus, has also been profiled. Merz *et al* used Huh7.5 cells to produce the Jc1 chimera strain of HCV as well as $Jc1E2^{FLAG}$, with a tagged envelope protein for affinity purification (128). This enabled separation of the virus from other lipid membranous debris. Additionally, they were able to subtract out the lipid content of the WT virus preparation from the affinity purified virus to subtract out cellular debris. They determined that the major lipid composition of the virus was PC, SM and cholesterol esters. Other lipids were also measured, but not determined to be above background (cell debris) levels. They compared the virus lipidome to that of the originating Huh7.5 cells and found that the virus had lower levels of phospholipids and higher levels of cholesterol esters. Finally, compared to vesicular stomatitis virus (VSV) and Semliki Forest virus, HCV was enriched in cholesterol esters (128).

Functional consequences of lipid content:

The lipid envelope of a virion is a multifunctional entity, which serves to protect the genome from extracellular dangers, assist its transport to new cells and release when a favorable environment (late endosome) is encountered.

The process of fusion was described briefly in section 1.2 and is reviewed here (129). Here we will discuss the impact of lipid content on virion fusion. Studies on lipid content

functionality and relevance for fusion have largely been carried out in liposome systems. Primarily people have looked at the requirements for specific lipid content in the target (cellular) membrane for fusion to occur. There is still limited understanding about flavivirus virion lipid content requirements, however some progress has been made.

Cellular membrane lipid requirements:

The endocytic pathway displays an overall gradient in lipid composition, where early endosomes are rich in cholesterol, phosphatidylserine (PS) and phosphatidylinositols (PI), and cholesterol content gradually decreases in vesicles along the pathway (130,131). Late endosomes are enriched in ceramide, which maintains membrane fluidity. Additionally, bis(monoacylglycero)phosphate (BMP) is an anionic lipid that is enriched in the inner membranes of late endosomes and is absent in early endosomes. This gradient of lipid composition may be an important control feature to prevent pre-mature fusion and direct the viral entry process.

Alphaviruses have an absolute dependence on cholesterol and sphingolipids in the target membrane for fusion to occur. The need for these specific lipids is not quite shared by flaviviruses, however the process is enhanced by their presence in the membranes used for fusion. Specifically the membrane binding and trimerization steps of the viral fusion protein are enhanced by cholesterol and sphingolipids (132). The 3β-hydroxyl group of cholesterol is the key moiety in these interactions similar to alphavirus fusion (132,133). JEV entry but not attachment is dependent on cholesterol-rich microdomains (134). HCV also fuses with membranes in a pH dependent manner and its fusion with liposomes was enhanced with both cholesterol and sphingomeylin in the target membrane (135). Despite this enhancement, flavivirus fusion is quite flexible and will still proceed even when cholesterol and sphingolipids

are absent from the target membrane (132,136). Interestingly, a more recent study demonstrated that DENV requires anionic lipids, such as BMP and PS, in order to fuse with the cellular membrane (137). As mentioned above, BMP in enriched on the internal late endosomal membrane and there it regulates membrane sorting and dynamics. Interestingly, BMP may be more specifically required for delivery of the viral RNA into the cytoplasm, an event distinct from membrane fusion (Figure 1) (25). PS may be responsible for the upstream event of virion fusion with the endosomal carrier vesicle membrane inside of the late endosome (25). The distribution of these lipids in the cell enables DENV to specifically fuse with the late endosome under low pH conditions, thus delaying its actual entry into the cell. Whether these lipids are necessary and sufficient for DENV fusion is still unclear [reviewed in (129)].

Virion envelope lipid requirements:

Initial studies of lipid content in virions were carried out by simply correlating the density of particles with their functional impact. For example, infectious HCV found in patient sera has a low density (138). It was determined that the low density fractions produced in cell culture were more successful at fusion and thus more infectious (135). Improvements in purification methods have produced high quality purified virions that have increased our understanding of not only their lipid content, but also the significance of specific lipids within their envelopes. For example, purified BVDV was treated with sphingomyelinase to degrade sphingomeylin in the lipid envelope and this reduced the infectivity of the virions (1). This implied that SM is a critical component of the envelope and may stabilize it or play a role in the fusion process. Similarly, treatment of BVDV virions with methyl-β-cyclodextrin (MCD), a cholesterol scavenger, resulted in a dose dependent decrease in virus release from cells. This effect was not seen when cells were treated with MCD (1). Furthermore, exposure of DENV virions to MCD reduced infectivity

in a dose-dependent manner. A reduction in infectivity was not seen when cholesterol was depleted from the cellular target membrane. This finding indicates that the cholesterol in the DENV virion envelope was critical for infection (139). Partial rescue of virion infectivity was achieved following incubation with fetal bovine serum (FBS) after MCD treatment (139). Addition of exogenous cholesterol to BVDV virions that had partial removal of cholesterol from their virion envelopes resulted in a partial rescue of infectivity. This rescue was not seen when virions were incubated with higher levels of MCD (to extract more of the envelope cholesterol) and then incubated with exogenous cholesterol. These studies indicated that when most of the cholesterol was removed from the envelope an irreversible change occurred to the virion structure, but when it was partially removed infectivity was just lowered (126). These findings are significant and interesting, however they do not necessarily implicate cholesterol in the fusion process, since the defects in fusion could be due to alterations in the structure of the virion and not its reduced cholesterol content. It is truly remarkable that cholesterol could be re-integrated into the virion envelope to restore infectivity, increasing the plausibility that it does play a functional role in the fusion process.

Clearly, lipids play significant roles in in the functionality of flavivirus virions and their ability to fuse with a target membrane. Whether the requirement for particular lipid species is due to the need for efficient lipid mixing of the particle and the cellular membrane or for the interactions of the fusion loop of E with the cellular membrane is unclear. Future work on lipid requirements and functionality will shed light on these processes and likely reveal potential antiviral targets.

1.5 Unsaturated fatty acid biosynthesis

As described above, fatty acids (FA) play key roles in the cell and have functions in signaling and structural support. The regulation of the synthesis of diverse FAs determines many cellular functions and has been implicated in a variety of diseases. Furthermore, unsaturated fatty acids (UFAs) drive curvature and fluidity of membranes. Given the complex structure of the ER membrane in virus infected cells (described in section 1.2) UFAs are likely to be involved in enabling this high degree of curvature. As such, we carried out an siRNA screen of the UFA biosynthesis pathway to identify control points used during DENV replication (described in Figure 16A). Here, we will describe the function of these various enzymes and their roles in human diseases.

FA synthesis and modifications take place in the cytosol, mitochondria, peroxisomes and ER. In the cytosol, *de novo* FA synthesis is carried out by FAS described in section 1.4. We will primarily discuss FA elongation and unsaturation in the ER, peroxisomes and the mitochondria. Substrates for the elongation of fatty acids can be synthesized by FAS or from a dietary source. FAs are elongated through a four-step cycle in the ER that adds two carbons to a growing FA chain each cycle. The four steps are: condensation, reduction, dehydration, and reduction. These four reactions are outlined in Figure 3 and details regarding the enzymes are outlined in Table 1. We will discuss the enzymes that perform these reactions below and highlight those that were included in our siRNA screen.

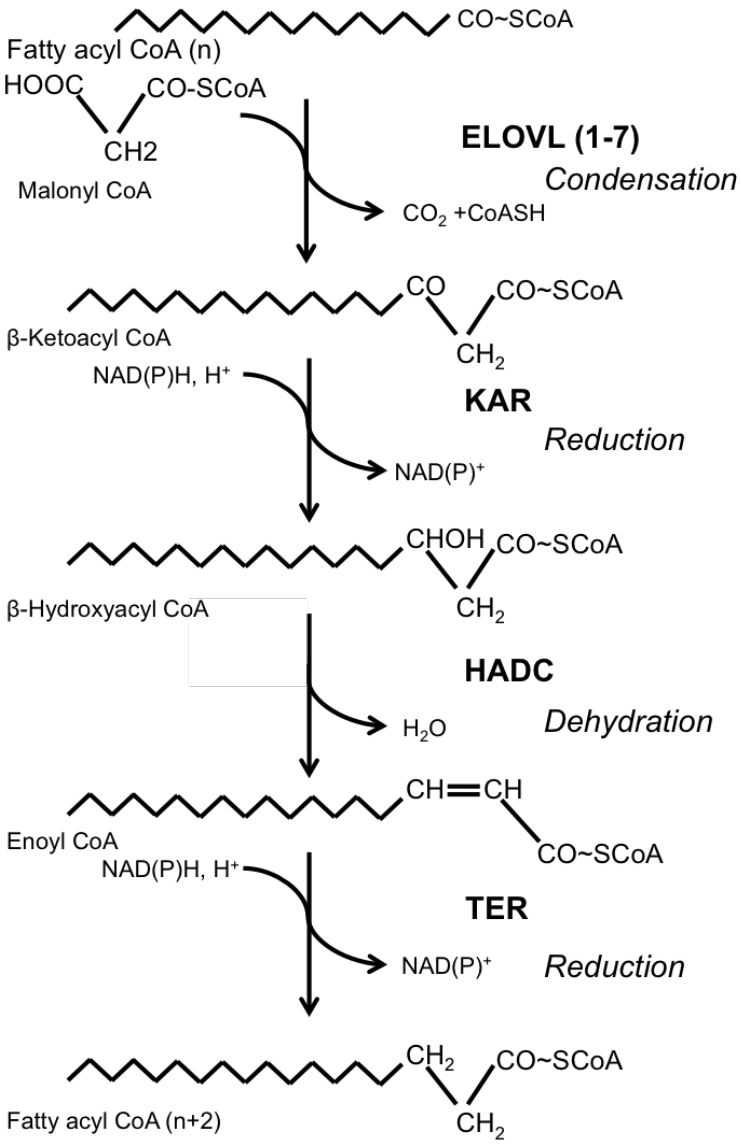

Figure 3 Fatty acid chain elongation. The reaction sequence for the elongation of fatty acids in the endoplasmic reticulum. Adapted from (140 - 142).

Table 1 Enzymes in fatty acid chain elongation (Adapted from (140–142))

Enzyme	Reaction	Specificity
ELOVL1, ELOVL3, ELOVL4, ELOVL7	Elongation-**condensation**	Saturated LCFAs-C18:0, C20:0
ELOVL2, ELOVL5	Elongation-**condensation**	MUFAs and PUFAs-C16-, C18-, C20- and C22-
ELOVL6	Elongation-**condensation**	C16:0 and C16:1
hydroxysteroid 17-beta dehydrogenase 12 (KAR)	Elongation- **reduction**	β-Ketoacyl CoA
3-Hydroxyacyl-CoA Dehydratase 1 and 2 (HACD1, HACD2)	Elongation-**dehydration**	β-Hydroxyacyl CoA
trans-2,3-enoyl-CoA reductase (TER)	Elongation-**reduction**	Enoyl CoA
Stearoyl-CoA desaturase 1 and 5 (SCD1, SCD5)	Desaturation	Δ9
fatty acid desaturase 2 (FADS2)	Desaturation	Δ6
fatty acid desaturase 21 (FADS1)	Destauration	Δ5

Condensation (elongases):

The rate limiting step in elongation of unsaturated fatty acids is a condensation step carried out by members of the elongation of very long chain fatty acids family (ELOVLs), also referred to as elongases. There are 7 human elongase enzymes that differ in their substrate specificity and tissue distribution. The details of each enzyme are included in Table 1. Given these characteristics we included ELOVL2, 5 and 6 in our siRNA screen described in Figure 16A.

Elongase family members are ER membrane-bound 3-keto acyl-CoA synthase enzymes. They catalyze the condensation of malonyl CoA with a variable fatty acid precursor. In so doing,

they add 2 carbons to the fatty acid per cycle. This reaction is shown in Figure 3 and substrate specificity is shown in Table1.

ELOVL2 is specific for polyunsaturated fatty acid (PUFA) elongation. It shows a preference for 20 and 22 carbon PUFAs (143). The highest expression of ELOVL2 is in liver, placenta, testis, and brain. Single nucleotide polymorphisms (SNPs) in ELOVL2 in human populations have been associated with increased plasma n-3 PUFA levels and this is correlated with protection from cardiovascular disease (144,145). PUFAs are important signaling molecules that regulate the balance between pro-inflammatory and anti-inflammatory states, lending support to the significance of ELOVL2.

ELOVL5 most often uses the PUFA, C18:3(n-6) acyl-CoA as a substrate, but can work on both n-3 and n-6 family members. Given the significance of PUFAs in many diseases, it is not surprising that ELOVL5 has been implicated in a variety of diseases. For example, gene expression of ELOVL5, along with 1 and 6, was increased in an aggressive form of breast cancer (146) yet had transcriptional repression in a specific colorectal cancer (147). Many types of cancer show differential metabolic profiles and perhaps ELOVL5 plays a role in these different profiles.

The final elongase we profiled is ELOVL6 which elongates fatty acids with 12, 14 and 16 carbons and has a higher activity toward C16:0 acyl-CoAs. Hence, ELOVL6 is associated with the *de novo* fatty acid synthesis pathway and indeed works with SCD1 (delta 9 desaturase) to generate oleic acid. Likely due to its involvement in *de novo* fatty acid synthesis and the tendency for these fatty acids to be incorporated into storage lipids, ELOVL6 is implicated in obesity induced insulin resistance (148). Interestingly, we have found that ELOVL6 gene expression is increased at early time points of DENV infection, again likely due to its

involvement in *de novo* fatty acid synthesis and the need for increased biomass during infection (Read *et al*, unpublished).

Reductase:

The second step in fatty acid elongation in the ER is a reduction step carried out by a 3-keto-acyl carrier protein reductase (KAR). Hydroxysteroid 17-beta dehydrogenase 12, very-long-chain 3-oxoacyl-CoA reductase (HSD17B12) was identified as the human analogue of yeast KAR that uses NADPH to reduce 3-ketoacyl-CoA to 3-hydroxyacyl-CoA (149). Given that this is currently the only known enzyme in humans that can carry out this reaction it is likely very important. Indeed, knockout of *KAR* in mice results in embryonic lethality due to disruption of organogenesis (150). It has widespread tissue distribution, but is most highly expressed in tissues such as liver, kidney, heart, and skeletal muscle that are responsible for much of lipid homeostasis (151). Interestingly, this enzyme also catalyzes the final step in steroid biosynthesis and converts estrone into estradiol in ovarian tissue (151,152). Most studies of this enzyme have focused on its role in steroid biosynthesis rather than fatty acid elongation, but it has been implicated as a prognostic biomarker in certain cancers due to its role in fatty acid elongation (152,153). More work is needed to understand this enzyme and the diverse roles that it plays in cells.

Dehydratase:

Once a 3-hydroxyacyl-CoA is formed it has to be dehydrated into a trans-2,3-enoyl-CoA. Two enzymes that carry out this reaction will be discussed here: 3-Hydroxyacyl-CoA Dehydratase 1 and 2 (HACD1/2). Previously these enzymes were called, Protein-Tyrosine Phosphatase-Like Member A and B (PTPLA/)B and are labeled in our siRNA screen as such (Figure 16A). In fact, there are four enzymes in this family all in the ER, HACD1-4, but HACD3

and HACD4 were only recently recognized as processing 3-hydroxyacyl-CoA dehydratase activity (154). Even more recently still was the identification of their substrate specificity (155). HACD4 still has no identified substrate specificity, while HACD3 displayed weak activity towards both saturated and monounsaturated FAs. HACD1 and 2 have broad specificities, capable of acting on both saturated and polyunsaturated FAs of varying chain length. HACD 1 and 4 are restricted to muscle tissues and leukocytes (154,155). HACD2 is ubiquitously expressed and HACD3 is widely expressed with highest expression in the brain, kidney, liver, and placenta (154,156).

Reductase:

The final reaction to complete the 2-carbon elongation of a FA chain is carried out by a member of the oxidoreductase family: trans-2,3-enoyl-CoA reductase (TECR). The ER resident enzyme reduces trans-2,3-enoyl-CoA to a saturated acyl-CoA, while consuming NADPH and producing NAD^+. TECR was identified as the yeast homologue of Tsc13p, the *trans*-2,3-enoyl-CoA reductase, and found to possess the same activity (149). Mutation of this gene in yeast is lethal (157). The *TER* P182L mutation in the human TECR gene is associated with nonsyndromic mental retardation. This is likely due to the reduction in VLCFAs and the impact of this reduction on the sphingolipid profile (158).

Desaturases:

De novo synthesized or exogenously obtained fatty acids can undergo further modifications and be shuttled to various cellular destinations. Here, we will discuss the desaturase enzymes in the ER that act on endogenously synthesized or dietary derived FAs. The desaturation reaction is depicted in Figure 4. Mammalian fatty acid desaturases are composed of

an N-terminal cytochrome B5-like domain and a C-terminal membrane-spanning domain with conserved histidine motifs and desaturase activity.

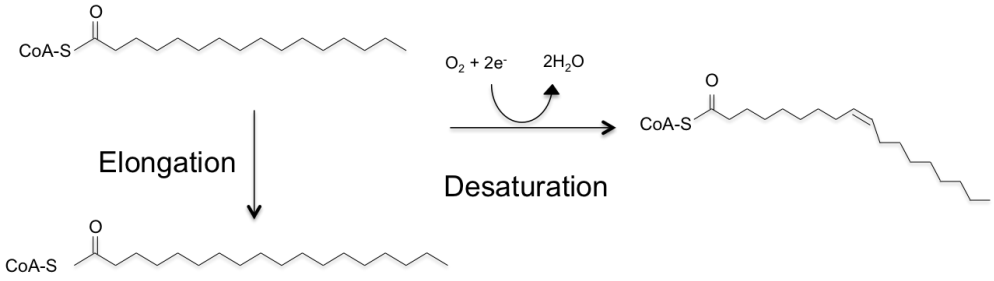

Figure 4 Fatty acid elongation and desaturation. The biochemical reactions that can occur to modify fatty acid chains include elongation and desaturation. Elongation includes the addition of two carbons (Shown in Figure 3). Desaturation is the incorporation of a double bond in the carbon chain. [Adapted from (142,159,160)].

Polyunsaturated fatty acid desaturases:

PUFAs are essential components of complex lipid species, particularly phospholipids. Arachidonic acid (20:4n-6) can be released from phospholipids either in a membrane-bound form or secreted [reviewed in (161,162)]. The membrane bound form subsequently acts on signaling pathways and the secreted form primarily acts as an inflammatory molecule.

Mammals cannot synthesize n-3 or n-6 fatty acids independently and so derive them from their diet giving them the name "essential fatty acids". Mammals can consume simple n-3 and n-6 species and use them to synthesize longer PUFAs. Fatty acid desaturase 1 and 2 (FADS1/2) are the rate limiting enzymes in PUFA biosynthesis. FADS1 is a delta-5 desaturase, as it desaturates the 5^{th} carbon from the carboxylic end of a fatty acid chain (163). The delta-6 desaturase, FADS2, acts primarily on the 6^{th} carbon, but also has activity towards the 4^{th} and 8^{th} carbons. FADS2 is rate-limiting in generating arachidonic acid from a linoleic or α-linoleic acid precursor. More specifically, it catalyzes the desaturation of dihomo-gamma-linoleic acid (DHGLA) (20:3n-6) and eicosatetraenoic acid (20:4n-3) to generate arachidonic acid (AA) (20:4n-6) and eicosapentaenoic acid (EPA) (20:5n-3).

Despite the shared metabolic pathway and similar structure, circulating n-3 and n-6 FAs display distinct effects. n-3 PUFAs tend to be anti-inflammatory while n-6 PUFAs, such as arachidonic acid, are pro-inflammatory. Furthermore, n-3 are associated with reduced risk of cardiovascular disease (CVD), while increased n-6 in adipocyte phospholipids is associated with an increase in CVD [reviewed in (164)]. More specifically, n-3 FAs in the serum reduces circulating TG levels which are implicated in CVD (165). Consumption of foods high in n-3 FAs such as marine products is associated with cardioprotective and anti-inflammatory effects. However, results of dietary interventions are variable likely due to genetic polymorphisms in human populations (164,166–169).

FADS1/2 levels are associated with circulating levels of PUFAs, and so are implicated in many disease processes. Given the significance of FADS1/2 in regulating serum FA levels, it is not surprising that their polymorphisms in human populations are associated with obesity, type 2 diabetes and coronary artery disease (170–173).

de novo FA synthesis desaturase:

The initial desaturation event to a new FA chain is the rate-limiting and key step in UFA biosynthesis and is catalyzed at the Δ9 position by stearoyl-CoA desaturase 1 (SCD1) (174,159). The preferred substrates for this enzyme are stearic and palmitic acid, which are converted into oleic or palmitoleic acid respectively. SCD1 is a 40kD integral membrane bound protein in the ER and is a highly conserved enzyme from bacteria to mammals (175). In humans, it is encoded on chromosome 10 and has two isoforms, SCD1, which is ubiquitously expressed, and SCD5, which is expressed in the liver (176). SCD1 regulates the balance between saturated and monounsaturated fatty acids in the cell. Monounsaturated fatty acids are the preferred building blocks for complex lipids such as phospholipids, sphingolipids, or triglycerides. SCD1 knockout

animals display decreased fat stores and are resistant to diet-induced weight gain (177). As such, SCD1 is a potential therapeutic target for obesity and metabolic syndrome. SCD1 and its role in flavivirus infection will be discussed extensively in Chapter 3.

Thioesterases:

Free FAs are toxic to a cell since their hydrophobic nature causes them to act as detergents. As such, cells attach a coenzyme A (CoA) molecule to one end of a fatty acid chain to protect and activate it. Once the CoA is attached, then FA can move through the cell, undergo further enzymatic processes and be incorporated into complex lipid species. However, in order for FAs to enter the mitochondria and undergo β-oxidation for ATP production, the CoA group must be removed. Acyl-CoA thioesterase enzymes carry out the removal of the CoA from the fatty acid, by breaking the thioesterase bond between the sulfur atom and the carbonyl group. Thus, these enzymes regulate the balance between free and activated fatty acids in the cell.

This enzyme family is highly diverse with differences in structure and substrate specificity. There are two types of ACOTS: type I and type II and the only similarity is their shared enzymatic reaction. For our screen we used type I ACOT 1 and 2 and type II ACOT 7. ACOT 1 and 2 are highly similar only differing by the N-terminal mitochondrial localization sequence on ACOT2. ACOT1 is cytosolic and has a preference for long chain saturated and monounsaturated acyl-CoAs [reviewed in (178)]. Through regulating the balance and distribution of FFAs and acyl-CoAs, ACOT1 may play a cardioprotective role (179,180). ACOT2 also prefers long chain acyl-CoAs and due to its localization in the mitochondria, seems to increase oxidative phosphorylation (181). ACOT4 localizes to peroxisomes and acts on both short-chain dicarboxylyl-CoAs and medium- to long-chain acyl-CoAs. It is hypothesized that

ACOT4 acts to direct acyl-CoAs that have been shortened in the peroxisome to a new location or for their recycling within the peroxisome (182).

Type II ACOTs have a completely different structure, composed of a "HotDog" domain and tend to be oligomeric in structure. ACOT7 is highly expressed in the mammalian central nervous system and was originally termed brain acyl-CoA hydrolase (BACH) (183) (and is referred to as such in our siRNA screen Figure 16A). ACOT7 is also expressed in macrophages. It has a preference for long chain acyl-CoAs and when overexpressed leads to a reduction in prostaglandins, indicating a key role in PUFA metabolism and inflammatory pathways (184).

Peroxisomes

A peroxisomal FA chain elongation system has been controversial, however there is good evidence for its existence. β-oxidation consists of the catabolic process of removing 2 carbons to produce acetyl-CoA, NADH and $FADH_2$. This can occur in the mitochondria or the peroxisome (for longer chain FAs) and represents a key downstream processing event of UFA biosynthesis and metabolism. *β*-oxidation of long-chain FAs is crucial to synthesize shorter long chain FAs that mammals can't synthesize any other way. For example, it is hypothesized that eicosapentaenoic acid (C20:5) can be elongated and desaturated at the delta-6 position to 24:6 in microsomes and then *β*-oxidized to DHA in peroxisomes (163). The lack of a delta-4-desaturase in mammals prevents this pathway from proceeding through a simpler process. Hence mammals are able to use peroxisomal *β*-oxidation to generate a variety of diverse and necessary FAs that may be in short dietary supply.

Acyl-CoA oxidase 1 (ACOX1) is the first enzyme in the peroxisomal FA β-oxidation pathway. It catalyzes the desaturation of acyl-CoAs to 2-trans-enoyl-CoAs (185). It is widely

expressed, with the highest abundance in the liver. Diseases associated with ACOX1 are characterized by accumulation of very long chain fatty acids (186).

A similar peroxisomal enzyme is pristanoyl-CoA oxidase 3 (ACOX3), which is involved in the desaturation of 2-methyl branched FAs. It has very low expression in the liver, but may be expressed during certain developmental stages. ACOX3 may be increased in prostate cancer samples and thus contribute to peroxisomal branched chain fatty acid β-oxidation prostate cancer (187).

Peroxisomal *trans*-2-enoyl-CoA reductase (PECR) is a reducing enzyme involved in fatty acid elongation (similar to those mentioned above) in the peroxisome. This enzymes is key for peroxisomal FA elongation (188). However, it has also been implicated in the degradation of fatty acids in the peroxisome such as phytol, a dietary derived branched chain fatty acid (189). Clearly more work needs to be done to tease apart the role of PECR in peroxisomal FA metabolism.

Acetyl-CoA acyltransferase 1 (ACAA1), is a peroxisomal acyl transferase enzyme involved in *β*-oxidation. It is not well characterized, however mutations in this gene lead to pseudo-Zellweger syndrome. A transcriptomics study also found ACAA1 downregulated in hepatocellular carcinoma (187).

Bile Acids:

Bile acids are made in the liver (191). They are a way to absorb and excrete excess cholesterol, fats and fat-soluble vitamins from the intestines. Bile acids are made from cholesterol, which is enzymatically transformed, and finally undergoes β-oxidation in the peroxisome to form chenodeoxycholoyl-CoA (C24 bile acid). The final step in the process is the formation of bile acid-amino acid conjugates via the transfer of C24 bile acids from the acyl-

CoA thioester to either glycine or taurine. Once conjugated bile acids are excreted in the bile. The Bile Acid-CoA:Amino Acid N-Acyltransferase (BAAT) carries out this final amidation reaction and is primarily a peroxisomal enzyme, however it has been postulated that there is a second pathway in the cytoplasm for the conjugation of the bile acid to glycine or taurine [reviewed in (192)].

Mitochondrial *β*-oxidation:

Mitochondrial *β*-oxidation uses unique enzymes but overall a similar process to peroxisomes. The last 3 steps are catalyzed by the enzymatic activities of the mitochondrial trifunctional protein (MTP): hydroxyacyl-CoA dehydrogenase, 3-ketoacyl-CoA thiolase, enoyl-CoA hydratase. This is a tri-functional protein composed of four alpha and four beta subunits. The gene in our siRNA screen (discussed in Chapter 3) encodes for one of the alpha subunits that catalyzes the 3-hydroxyacyl-CoA dehydrogenase and enoyl-CoA hydratase activities, HADHA. Thus, it converts medium- and long-chain 2-enoyl-CoA compounds into 3-ketoacyl-CoA when NAD is solely present and acetyl-CoA when NAD and CoASH are present (193). The MTP protein complex is located on the inner mitochondrial membrane.

Human mutations in HADHA are associated with accumulation of long-chain fatty acids and long-chain 3-hydroxyacyl coenzyme A dehydrogenase (LCHAD) deficiency, with symptoms of hypoglycemia, Reye-like syndrome, cardiomyopathy, or sudden unexpected death (194). Furthermore, HADHA was found to be downregulated in renal cell carcinoma and this was associated with a poor prognosis (195). This implies that preventing the buildup of long-chain fatty acids is critical to maintain homeostasis and prevent disease onset.

Interestingly, HCV has been shown to interact with HADHA. The viral protein NS5A interacts with both the α and the β subunit and downregulates their expression. They also found

an attenuation of β-oxidation in HCV infected cells. Knockdown of HADHA and HADHB did not reduce viral replication but did suppress the type I IFN response (196).

1.6 Dengue Disease Serum Metabolomics

The application of metabolic changes caused by DENV to human health is most apparent in studies of biomarker discovery. Many efforts have been made over the years to characterize metabolites in the serum of dengue disease patients in order to identify diagnostic biomarkers and understand disease pathology. Here we will discuss the findings from a variety of efforts from all over the world.

Untargeted metabolomics of dengue disease serum

Untargeted metabolomics, or a chemometrics approach, involves extraction of metabolites en masse from a sample and measurement of the metabolites with a mass spectrometer to acquire accurate masses. Molecular features are extracted from the mass spectrometer and their presence/absence and intensities are compared across samples. Accurate masses [mass/charge (m/z) ratios] are aligned with databases and annotated accordingly. Accuracy of metabolite annotations from mass spectrometry are scored on a point system from 1-4 depending on the degree of certainty associated with the annotation and the techniques used according to the Metabolomics Standard Initiative (MSI) level of identification (197). Level 1 identification involves the use of a standard and fragmentation data, while level 2 just requires fragmentation data. The accuracy of annotations from untargeted metabolomics is typically MSI level 3, where there is no fragmentation data, just annotation of accurate mass. When no annotation can be found it is level 4; this generally occurs for a large percentage of the metabolites in these datasets. Nonetheless, a large dataset is generated from these studies that can be validated using targeted analyses to accurately identify and quantify a subset of features. This

approach is ideal for hypothesis generation and identifying trends and patterns in metabolite profiles.

One of the main groups using this approach is located in Singapore, where they have access to a cohort of adult patients with dengue infections. Their samples are well characterized, often followed over time and compared to matched healthy controls. Their seminal paper profiles the total serum metabolome and lipidome of adult dengue disease patients with a primary infection, followed over time (198). Serum was collected from these patients on their first, second and third visits to the clinic after a positive diagnosis for dengue infection and compared to healthy controls. They used two different chromatography platforms to characterize patient serum. Liquid chromatography (LC) was used for metabolomic analysis and gas-chromatography (GC) for lipidomic analysis.

In the acute infection phase, visits 1 and 2 to the clinic, the authors identified extensive metabolic changes in dengue diseases compared to healthy controls. Interestingly, they found a variety of free fatty acids including PUFAs such as arachidonic acid, linoleic acid, docosohexenoic acid, and α-linoleic acid increased during acute infection. These are hallmarks of increased inflammation. Whether the increase in these molecules is a cause or effect of increased inflammation is unknown but presents an intriguing future direction to investigate. Multiple acylcarnitines, sphingolipids, and glycerolipids were also increased. However, they identified a decrease in certain phosphocholine and lysophosphocholine species. This replicates the studies mentioned above, where PL species are decreased in serum from dengue patients, again likely representing liver damage or retention of PLs in cells.

The next major work done by the same group in Singapore, characterized one component of dengue disease pathophysiology from a metabolomics dataset. Using untargeted LC-MS

metabolomics they characterized the serum from adult patients with dengue fever (DF) and dengue hemorrhagic fever (DHF) in the febrile phase (<96 h) (199). They determined that serotonin was significantly decreased in DHF patients. This is physiologically relevant because serotonin is involved in platelet aggregation and activation (200), processes which are impaired in DHF. This observed decrease may explain some of the thrombocytopenia characteristic of severe dengue diseases. Furthermore, they found that kynurenine, an immunomodulator, increased significantly in patients with DHF, which may represent a host response to infection. Kynurenine and serotonin are metabolites of tryptophan, which has been implicated in dengue and a variety of other diseases (201).

Dengue diseases are difficult to distinguish at an early phase, can progress to more severe diseases and are marked by a long recovery phase. To address some of these challenges Cui *et al* characterized the differences between DF and DHF at early and later phases of disease (202). Using sera from adult DF and DHF patients at critical (<96hrs) and convalescent (21-28 days) phases, they identified 29 differentially expressed metabolites at the critical phase including bile acids, purines, acylcarnitines, phospholipids and amino acids. The same group of patients had eight different metabolites between DF and DHF during the convalescent phase. Among the identified metabolites, they identified a decrease in uric acid in DHF vs. DF patients at the critical phase, indicating increased oxidative stress. Several studies have observed oxidative stress during DENV infections in model systems, however, the role that it plays may depend on a variety of factors. It has typically been implicated as a host response to infection that reduces viral replication and biogenesis (203) however others have shown that oxidative stress specifically aids in viral replication (204). Interestingly, one of the bile acids, chenodeoxyglycocholic acid, was significantly higher at both critical and convalescent phases.

This likely indicates long-term liver damage due to severe infection that is not found in DF. These findings shed light on dengue disease pathology, particularly the prospect of long-term liver damage raising concerns for continued patient care.

To confirm their findings from the human serum metabolome Cui *et al* performed a serum metabolomics study of humanized mice infected with DENV (205). Their findings demonstrated the replicability of the human serum metabolome in these mice and validated the use of the humanized mouse model to identify biomarkers for dengue diseases. Mouse models have not replicated other aspects of DENV biology accurately, but in this study they were successful. They used a humanized mouse model where the immunodeficient NOD-*scid Il2rg-/-* (NSG) mouse received an adoptive transfer of human CD34+ fetal liver cells for the experiments. The mice were infected with DENV and serum was collected on 0, 3, 7, 14, and 28 days post infection. They used LC-MS to characterize the metabolome and included both reverse-phase-ultra high-performance liquid chromatography (RP-UHPLC) and hydrophilic interaction (HILIC)-UHPLC to fully cover both hydrophobic and hydrophilic molecules. Results were consistent with their human studies. FFAs, purine and pyrimidines, acylcarnitines and SMs were mostly elevated at 3 and 7 days post-infection (dpi) and returned to normal levels later during the infection. Meanwhile, PLs were decreased at 3 and 7 dpi and returned to normal at 14 and 28 dpi. The change in PLs, in particular, mimicked studies from their human cohort and others. Pathway analyses found that purine and pyrimidine metabolism, fatty acid β-oxidation, phospholipid catabolism, arachidonic acid and linoleic acid metabolism, sphingolipid metabolism, tryptophan metabolism, phenylalanine metabolism, lysine biosynthesis and degradation and bile acid

biosynthesis were all perturbed. Findings from metabolomics studies have been slow to progress to the clinic. However, studies like this demonstrate the potential for progress and reproducibility across platforms, infection models, sample types and sources.

In collaboration with the Sustainable Sciences Institute, Managua, Nicaragua and Universidad Autónoma de Yucatán (UADY), Mérida, Yucatán, México, Voge *et al* set out to identify metabolites in acute phase serum that were predictive of progression to severe disease (206). In a cohort of children from Nicaragua they found 83 molecular features that differentiated DHF/DSS and DF outcomes. In the Mexican cohort, comprised of children and adults, they found 37 molecular features that statistically differentiated DHF/DSS and DF outcome. Of the features that differentiated DF and DHF/DSS in the Nicaraguan samples, 13 metabolites were structurally identified using tandem mass spectrometry (MS/MS). These features were classified as amino acids and lipids such as fatty acids and phospholipids, as well as vitamins. Of particular interest, they identified 3 different forms of vitamin D_3 that were all downregulated in severe (DHF/DSS) vs. non-severe disease (DF) in both the Nicaraguan and the Mexican cohort. Among these, 1,25-vitamin D_3 is the active form. It is synthesized in the vascular endothelium following stimulation of vitamin D_3 1α-hydroxylase activity by inflammatory cytokines and its decrease in the serum is associated with increased mortality in sepsis patients (207). Vitamin D_3 has many implications in diseases and is actively being explored for its role in DENV replication and disease. Furthermore, they identified long-chain polyunsaturated fatty acids such as DHA (C22:6) and ALA (C18:3) that were increased in abundance in DHF/DSS versus DF and ND groups. These long chain n-3 fatty acids are anti-inflammatory agents and may represent a host response as an attempt to dampen the immune response to the infection.

A key question with all of these studies is whether metabolomic data can predict disease progression, outcome or response to treatment. The difficulty in answering this question often lies with the correct experimental design and procurement of the proper samples. Fortunately, this group obtained acute phase serum samples from the Nicaraguan cohort that were initially diagnosed as DF and then progressed to DHF/DSS. Comparing these samples to DF patients who did not progress to a severe disease, they found 65 metabolites that were significantly different. Of these, six were structurally identified (MS level1) and they were annotated as proline, alpha-linolenic acid, arachidonic acid, docosahexaenoic acid, and two lysophosphatidylcholines. These six features were quantified and each of them were found in higher abundance in the patients who progressed to severe disease. Hence, this study confirmed that diseases were biochemically distinct even at an early phase. Furthermore, using acute-phase serum, they quantified metabolites that could predict disease outcomes. Further testing of these and other metabolites in the proper experimental setting may yield results with prognostic potential that can be moved forward to clinical settings.

Another analytical platform used in metabolomics is ^{1}H nuclear magnetic resonance (NMR) spectroscopy. This technique is reliable and reproducible, however the computational platforms to analyze the spectra from NMR experiments are limited and difficult to use at this point. This will likely change in the near future, as bioinformatics improves. One group recently used NMR exploratory metabolomics to analyze patient plasma from a patient cohort in Recife, Brazil (208). The samples were collected during a DENV3 outbreak from both adults and children. They obtained 2 samples from each patient: 1 at the onset of symptoms and 1 at the defervescent phase. Patients were grouped as DF primary infection, DF secondary infection, DHF primary infection, DHF secondary infection, and non-dengue febrile illness. They built a

sparse partial least squares discriminant analysis (sPLS-DA) pairwise model and found metabolites in lipid, glucose, and protein metabolism that were changed. In particular they found a decrease in VLDL/LDL in severe vs. non-severe samples, similar to others (209). Interestingly, when the patients were followed over time to the defervesent phase they identified an increase in the plasma lipoprotein levels in DF patients that recovered, likely representing a recovery of liver function. This increase was not seen in the DHF patients who appeared to experience long-term liver damage. These observations indicated that plasma VLDL and LDL levels may be good prognostic markers for severe dengue diseases. Further evidence for liver damage in severe patients was gathered with the increase in acetate, citrate and formate. Increases in acetate levels are often seen from liver dysfunction, specifically due to a decrease in acetyl-CoA synthetase activity (210). Plasma glutamine and choline were also decreased in severe diseases (208). The differences in glutamine levels were discriminatory for severe vs. non-severe patients implicating glutamine as another potential prognostic feature. The longitudinal decrease in glutamine levels observed is consistent with the hypermetabolic state observed in DENV-infected cells. In particular, immune cells require increased glutamine as a biosynthetic precursor for metabolic processes and functionality (211). However, in cell culture glucose and not glutamine was shown to be important for DENV replication (76), but as is often the case, this observation may not be replicated *in vivo*.

Each of these un-targeted metabolomics studies highlights differing metabolites that play a role in dengue disease pathology. Taken together, they provide a broad picture of metabolite dysregulation across patient cohorts from differing genetic backgrounds and age-ranges with primary or secondary DENV(1-4) infections, measured on multiple analytical platforms. Clearly, there is variability in the findings from these studies, however they consistently highlight liver

dysfunction in severe disease and provide us with a set of metabolites with prognostic potential. Further testing of these metabolic profiles in prospective studies will be crucial as we move forward in determining patient care options.

Metabolic indicators of vascular permeability

An intriguing and deadly phenomenon in dengue disease pathology is the vascular permeability and endothelial barrier leakage leading to hemorrhaging. Precisely how this occurs and whether it is virally mediated or a host response to the infection, has remained unclear. However, excellent hypotheses have been put forth that will be discussed here.

Recent work on the DENV non-structural protein 1 (NS1) has suggested its role in mediating vascular permeability through disruption of the endothelial glycocalyx (47,212). These findings shed light on the mechanism of endothelial barrier failure. Many other metabolomic studies add to this by identifying host factors that may either contribute to endothelial barrier dysfunction or are a downstream effect of this cascade. For example, an increase in chymase was observed in DHF vs. DF patient serum from adult patients in Singapore (213). Chymase is a serine protease found primarily in mast cells, but also in skeletal muscle and skin. This group hypothesized that activated mast cells during infection produce excess chymase and causes an increase in vascular leakage (213).

Recently, others have found serum immunomodulators that may play a role in endothelial barrier function. Using serum from dengue patients with plasma leakage they found a reduction in endothelial barrier function in cultured cells compared to serum from patients without plasma leakage (214). They identified various immunomodulators that differed in the leakage and non-leakage serum samples and hypothesized that these may mediate the observed effects. In particular, leakage was strongly associated with augmented levels of IP-10, GM-CSF, IL-1α, and

IL-8, as well as decreased levels of CXCL1 and platelets (214). Indeed, many other metabolites found elevated in DSS patients may be a cause or an effect of plasma leakage. Likely endothelial barrier dysfunction is a product of both virally mediated efforts and host factors responding to the infection. Teasing these metabolites apart and testing them in model systems will be critical to gain mechanistic understanding of this phenomenon.

Comparison with other viruses:

Of course, a big question in this field is how well metabolomics can distinguish one disease vs. another rather than just a healthy vs. a disease state. Specifically, can we identify biochemical features that are uniquely and consistently altered by a given infection rather than simply due to a generalized immune or stress response from the host?

Chikungunya virus (CHIKV) is an alphavirus that shares a common vector with DENV: the *Aedes aegypti* and *Aedes albopictus* mosquitos. It has co-circulated with DENV in parts of South East Asia for a long time. It was first detected in the Americas in 2013 and now co-circulates with DENV in these areas as well. Due to this co-circulation, the prospect of human co-infection with these viruses is a real possibility. However, this phenomenon and particularly the metabolic impacts are poorly understood. The first report of co-infection was in 1967 in South India (215). Furthermore, with the recent introduction of Zika virus (ZIKV) into the Americas, and the common vector that it also shares with CHIKV and DENV, there are now multiple reports of all combinations of co-infection with these three viruses (216–220). Metabolomics of ZIKV infection are still preliminary with only one report where serum from ZIKV patients was compared to a control group of healthy and febrile patients negative for ZIKV (221). They identified an up-regulation of Angiotensin (1-7) and Angiotensin I as well as a disturbance of the PI3K-AKT-mTOR Pathway. While, they did not specifically compare to

DENV disease, their inclusion of healthy and non-healthy individuals highlighted interesting metabolic differences unique to ZIKV that will be interesting to confirm in future studies.

Naturally, metabolomic comparisons of DENV and CHIKV infections were in order. Thus, Shrinet *et al* conducted an NMR based metabolomics study of serum from patients in India who were infected with DENV, CHIKV or co-infected with both (222). They stratified their groups multiple different ways in order to find confounding factors that detract from the main findings. They found that age, fever duration and intensity of joint involvement in CHIKV disease all contributed to the variation in the data. However, they were able to correct for these and identify features whose differences were attributed to the disease states. They found eleven compounds dysregulated in the CHIKV infections, fourteen compounds in DENV and twenty compounds in the co-infected patients. Glycine, serine, threonine and galactose metabolism were all dysregulated in CHIKV, DENV and the co-infections. Hence, they identified similarities amongst the infections, but were also able to identify specific features that biochemically differentiated DENV vs. CHIKV infection vs. a co-infection.

Another febrile illness with symptoms that overlap with DENV diseases is influenza. Cui *et al* used their expertise in DENV metabolomics to compare it with H3N2 influenza infections (223). They used untargeted metabolomics and targeted oxylipidomics to characterize serially collected patient serum, comparing first, second, third visits to see metabolic changes overtime. They identified disturbances in purine metabolism, fatty acid biosynthesis and β-oxidation, tryptophan metabolism, phospholipid catabolism, and steroid hormones over time. Significant overlap between the two diseases was observed, however they were able to metabolically distinguish them. They identified eight oxylipins associated with early influenza infection, and

found that dengue infection attenuated serotonin, bile acids and biliverdin. Despite the clinical similarities and general host response to inflammation and disease, it is remarkable that these infections can be metabolically distinguished.

Other bio-fluids

A major critique of using serum for many of these metabolomics studies is the difficulties it presents in clinics in resource poor settings. For example, it is relatively invasive, time-consuming and the material needs are costly. These studies using serum are proof-of-principle and identify trends and biological concepts. Translation of these concepts to biological samples that are cheaper and less invasive will be critical for developing quality diagnostic and prognostic tests.

Due to the ease of serum analysis, few metabolomics studies have been carried out on other bio-fluids. However, a group in Malaysia recently collected mid-stream urine from ninety six adult males serologically positive for dengue infection at the Penang General Hospital (PGH), and compared to matched healthy controls (224). ^{1}H NMR spectroscopy was used to characterize the metabolome of these patients. They identified dysregulation of amino acid metabolism, tricarboxylic acid cycle intermediates and β-oxidation of fatty acids in DENV-infected patients. They found an increase in 4-hydroxyphenylpyruvic acid, which is an intermediate in the metabolism of the amino acid phenylalanine. The observation of perturbation of phenylalanine metabolism was confirmed by other groups (202,225). High levels of phenylalanine indicate oxidative stress due to its accumulation and lack of conversion to tyrosine. This is due to reduced levels of tetrahydrobiopterin (BH_4), which is a necessary cofactor for converting phenylalanine

to tyrosine. In conditions of oxidative stress, BH_4 is increasingly oxidized and thus unavailable as a substrate. Again, we see the theme that dengue disease contributes to increased oxidative stress.

While many viral diseases have excellent diagnostic tests available, prognosis remains a problem. Metabolomics has revealed great potential to change this by identifying biomarkers that can predict disease outcome. In the case of DENV infections, these metabolites tend to result from liver damage and oxidative stress caused by the virus that regulates multiple biochemical pathways. Furthermore, it is very promising to see similar biochemical pathways disturbed across studies, genetic backgrounds, analytical platforms and bio fluids. Application of these findings to longitudinal and blinded test sets will demonstrate the reproducibility of these findings and translatability to the clinic.

1.7 Conclusions

Here, we have discussed the current understanding of the flavivirus life-cycle, flavivirus manipulation of cellular metabolism, the lipid content of flavivirus envelopes, enzymes in the unsaturated fatty acid biosynthesis pathway and their contribution to human diseases, and the current state of metabolite biomarker discovery in biofluids from dengue patients.

Each of these sections provides the scientific premise for our experiments in this thesis. Given the vast evidence in the literature it is clear that DENV2 induces changes in cellular metabolism to meet its needs. We have identified outstanding questions in the field and proposed directions to answer them. In the following chapters, we will present our findings of the metabolic changes induced by DENV2 infection over time in an *in vitro* human cell culture model (Chapter 2), discuss the importance of the unsaturated fatty acid biosynthesis pathway for the DENV2 life cycle (Chapter 3), describe our efforts towards the discovery of metabolite

biomarkers in serum from dengue patients as well as our efforts to identify common themes in specific pathways perturbed between model systems (Chapter 4). Taken together, this dissertation will provide insight into how cellular metabolism plays a key mechanistic role in the DENV life cycle and dengue disease prognoses.

CHAPTER 2. DENGUE VIRUS 2 PERTURBS ESSENTIAL FATTY ACID SYNTHESIS AND METABOLISM IN HUMAN HEPATOMA CELLS

2.1 Introduction

The DENV-induced ER membrane rearrangements form multiple complex structures (described in section 1.2). These membranous structures serve to concentrate metabolites required for the assembly and function of viral replication complexes. Furthermore, they protect replicating viral genomes from the innate immune response and serve as the site for assembly and budding of progeny virions (29,226).

The extensive reorganization of ER membranes for the construction of complex structures is not trivial. Engineering the characteristics of membranes can occur in many ways. Primary among these is through alteration of cellular metabolism to concentrate or deplete a given lipid species. Interestingly, it was previously demonstrated that cellular fatty acid synthase (FAS) is recruited to these membrane sites during DENV2 replication (90). Hence, virus infection may be driving the concentration of particular lipid species [i.e.: long-chain fatty acids (C>16)] in these virus-induced membranes by changing the location of FAS to promote local fatty acid synthesis. It was also shown that the activity of FAS is required for DENV2 replication in both human and mosquito cells (90,92). Furthermore, significant changes in the lipid repertoire of mosquito cells as well as mosquito midguts following infection with DENV2 have also been demonstrated (92,106). Highly unsaturated fatty acids and lyso-phospholipids, both species that induce membrane curvature and fluidity (97), were significantly altered in virus infected mosquito cells and midguts. These studies indicate that not only does DENV2 expand the total area of ER membranes, but it also enriches cells in lipid species that facilitate the curvature of these complex replication platforms.

The completion of the virus life cycle from entry and fusion through replication, assembly and egress is a tightly coordinated process that occurs in a timely manner. This is essential so that the virus can evade the cellular response and effectively generate progeny virions. How viruses coordinate metabolic changes in the host in a timely manner is less well understood. However, cellular metabolism is a powerful limiting factor in viral replication and the tight control of these processes is absolutely imperative for viruses to complete the steps in their life-cycle [reviewed in (67)]. The timing of a life cycle differs widely amongst families of viruses. Interestingly, metabolic differences in central carbon metabolism between a relatively fast and slow growing virus have been characterized, clearly demonstrating the importance of well-timed metabolic control (69). Characterizing other changes to biochemical pathways, or their dysregulation, will provide further insight into the metabolic requirements of viral replication.

Given that flaviviruses significantly alter cellular membranes in a consistent time-dependent manner (227), temporal controls of specific metabolic pathways must occur to cater to changing needs as infection progresses. These temporal changes can be used as a tipping point to alter the outcomes of infection. Using high-resolution mass spectrometry and a chemo-enrichment approach, we have identified changes in the cellular metabolome caused by DENV2 infection over time. Specifically, we found a time-dependent enrichment of *de novo* fatty acid synthesis and arachidonic acid metabolism that coincided with viral replication. Disruption of these pathways resulted in a reduction of viral replication. Through these studies, we have demonstrated that DENV2 infection induced changes in key metabolic pathways to cater to its changing needs over time and we can alter these pathways to control viral infection.

2.2 Results

To identify metabolic changes caused by DENV2 over time we used liquid chromatography-high-resolution mass spectrometry (LC-MS) to profile DENV2 infected cells during a time course of infection. Specifically, we analyzed metabolic changes in Huh7 cells infected with DENV2 at 6, 18, 30 and 48 hr post-infection (hpi) (Figure 5, and Table 2), representing early, peak, advanced and late time points of infection. Mock infected cells and a UV-inactivated (UVI) virus, which can attach to and enter cells but cannot replicate its genome, were used as controls. The UVI, enabled us to differentiate between metabolic changes that occurred following exposure to and entry of a virus versus during replication of the viral genome. We expected that any metabolic changes observed that are similar in the DENV2 infected and UVI samples should be a result of early signaling events following virus attachment, while similarities between mock and UVI treated cells should be due to normal cell growth conditions. Where these features differ from DENV2 infected cells, represents metabolic changes caused by virus infection and replication.

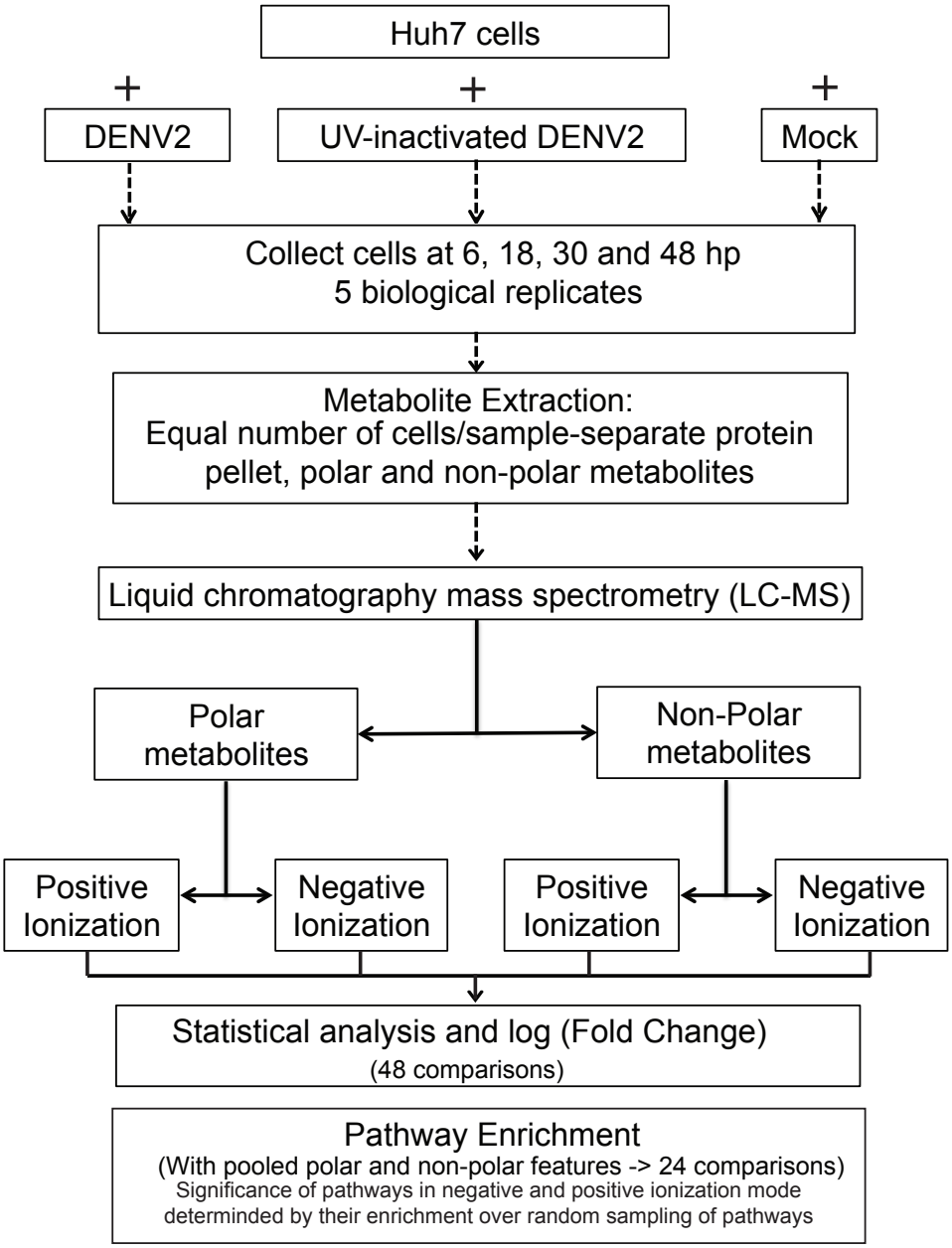

Figure 5 Experimental design used to identify temporal metabolic changes during DENV2 infection. Huh7 cells were infected with DENV2, a UV-inactivated DENV2 or mock infected for 6, 18, 30 or 48 hr. At each time point cells were harvested and metabolites extracted into polar and non-polar phases from an equal number of cells from each sample. These metabolites were then analyzed by LC-MS in positive and negative ionization modes. A linear model was built to identify significant differences between all the comparisons and log fold change values calculated between each comparison. Mass to charge (m/z) ratios and statistical measures were fed into a network analysis platform to annotate the features and identify biochemical pathways enriched during infection.

LC-MS reveals changes in the DENV2 infected cellular metabolome

LC-MS was run to evaluate the cellular metabolites extracted into the polar and non-polar phases, each in both positive and negative ionization mode to acquire maximal metabolite coverage. For our initial multivariate analyses, we kept each of the phases and modes separate, giving us four sample sets to analyze (Figure 5). Molecular features observed were defined as unique mass to charge ratios (m/z) and retention times (rt). Those features found to be absent in 50% or more of a group were removed. We further removed all features found in only one group and imputed missing values as described in the materials and methods section.

Due to the multiple variables in this experiment, we ran a variety of rigorous statistical analyses. The different comparisons are outlined in Table 2. As an initial overview of the data we performed principle component analyses (PCA) on all four phases and modes (Figure 6A and 6B). We first looked at the effect of time on the metabolic profiles of the samples. Samples are colored; 6 hpi (black), 18 (red), 30 (green) and 48 (blue) (Figure 6A). The samples are circled with the 95% confidence interval (CI) around the mean. We see that the principle components separate the samples by time very clearly for non-polar metabolites analyzed by negative ionization mode. General separation between the early (6 and 18 hpi) and late (30 and 48 hpi) time points are seen in the polar phase metabolites analyzed by both positive and negative ionization modes. However, distinct temporal separation is not observed in the non-polar metabolites analyzed by the positive ionization mode (Figure 6A). These analyses provide valuable insight into the chemical characteristics of metabolites that change over time as cells grow in culture.

Table 2 Statistical comparisons made between samples in all phases, ionization modes, time points and treatment groups.

Hours post infection	Non-Polar features in positive ionization mode	Polar features in positive ionization mode	Polar features in negative ionization mode	Non-Polar features in negative ionization mode
6	DENV2 vs mock DENV2 vs UVI mock vs UVI	DENV2 vs mock DENV2 vs UVI mock vs UVI	DENV2 vs mock DENV2 vs UVI mock vs UVI	DENV2 vs mock DENV2 vs UVI mock vs UVI
18	DENV2 vs mock DENV2 vs UVI mock vs UVI	DENV2 vs mock DENV2 vs UVI mock vs UVI	DENV2 vs mock DENV2 vs UVI mock vs UVI	DENV2 vs mock DENV2 vs UVI mock vs UVI
30	DENV2 vs mock DENV2 vs UVI mock vs UVI	DENV2 vs mock DENV2 vs UVI mock vs UVI	DENV2 vs mock DENV2 vs UVI mock vs UVI	DENV2 vs mock DENV2 vs UVI mock vs UVI
48	DENV2 vs mock DENV2 vs UVI mock vs UVI	DENV2 vs mock DENV2 vs UVI mock vs UVI	DENV2 vs mock DENV2 vs UVI mock vs UVI	DENV2 vs mock DENV2 vs UVI mock vs UVI

Next, we looked at the global effect of virus infection or exposure on the metabolome (Figure 6B). The PCA plots show DENV2 infected samples colored in black, UVI samples are in green and mock in red (Figure 6B). The samples are circled with the 95% confidence interval (CI) around the mean. Similar to the above, we see a strong separation of DENV2 from mock and UVI samples in all of the phases and modes except for the non-polar metabolites analyzed by the positive ionization modes (Figure 6B). These analyses indicate that UVI-exposed and mock-infected cells are quite similar, while DENV2 infection drastically changes the cellular metabolome.

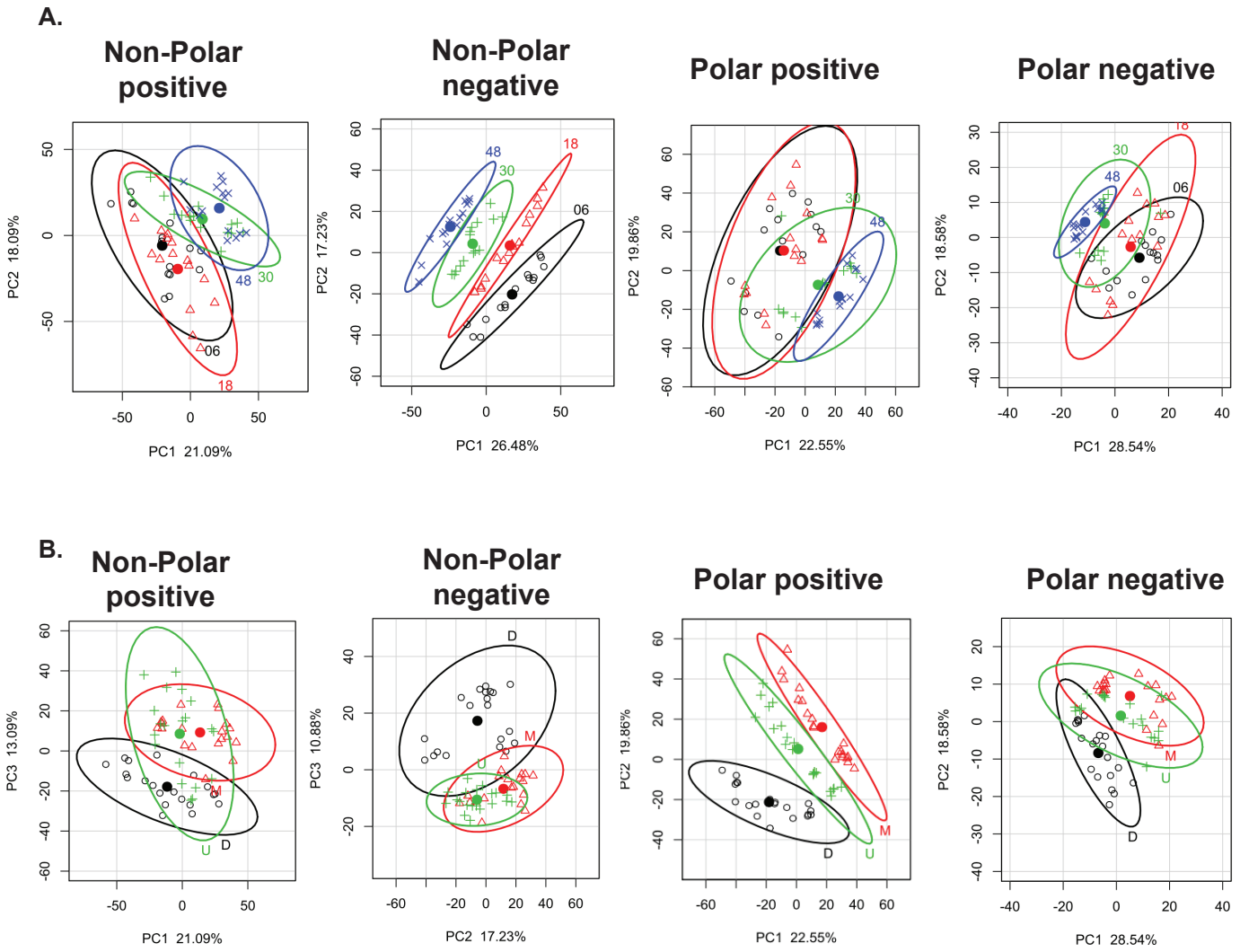

Figure 6 Principle component analyses (PCA) show segregation of the global metabolite profiles. (A) PCA plots for each phase and ionization mode with all the samples color-coded by time; 6 hpi (black), 18 (red), 30 (green) and 48 (blue). The circle around the data represents

the 95% confidence interval of those samples. (B) PCA plots for each phase and ionization mode with all the samples color-coded by treatment; DENV2 (black), UVI (green) and mock (red). The circle around the data represents the 95% confidence interval of those samples. DENV2; dengue virus serotype 2, UVI; UV-inactivated DENV2.

To test for dysregulation of metabolites we used the limma package in R (228) to generate a linear model measuring the log fold change (logFC) in abundance of each metabolite between the 12 different comparisons. These were plotted against their p-values on volcano plots (Supplementary Figures 1 and 2). Metabolites were considered significantly different when the absolute log fold change was at least 1 and adjusted *p*-value was less than 0.005. A low *p*-value was used to decrease the likelihood of false discovery because of the large number of comparisons that are looked at simultaneously.

We quantified the number of molecular features (unique m/z values) increased (logFC>0), decreased (logFC<0) or those that remained unchanged (NA) in each of the comparisons by time-points. The number of molecular features from each phase and mode were summed to give the total number of metabolites that changed in each comparison (Table 3). These numbers were color-coded according to their values. The red cells correspond to the most number of features changed and green corresponds to fewer changes (Table 3). The highest numbers of features we see are those that did not change in abundance in each comparison, this is expected. The highest number of features that changed was downregulated at 6 hpi. At peak viral replication (18 hpi) we also see numerous metabolites significantly different between DENV2-infected and mock-infected cells. Changes are also observed between DENV2 and UVI, although fewer than compared to mock. Comparing mock to UVI we see far fewer differences overall. Furthermore, at later time points (48 hpi) we see fewer differences between all comparisons. These trends can also be observed looking at the volcano plots in Supplementary Figures 1 and 2. Overall, the number of features changing reflects the effects of DENV2 infection on the cellular metabolome and demonstrates the quality of our controls.

Table 3 Changing metabolites over time. The numbers of metabolites increased, decreased or remaining unchanged (NA) in each of the comparisons by time-points are shown. The numbers of molecular features (based on m/z) from each phase and ionization mode were summed to give the total number of metabolites in each comparison. These numbers were color-coded according to their values. Color scale is indicated.

	DENV vs Mock			DENV vs UV			Mock vs UV		
	Up	Down	NA	Up	Down	NA	Up	Down	NA
6	895	1313	3001	508	1094	3607	391	251	4565
18	1033	1108	3067	735	824	3651	434	471	4303
30	933	760	3515	767	520	3920	555	669	3983
48	679	668	3861	674	283	4250	362	727	4119

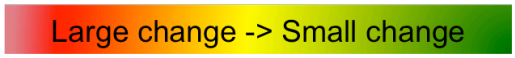

Pathway analysis of DENV2 induced metabolic changes

Untargeted mass spectrometry is an invaluable tool for discovery of novel molecular features and characterizing global trends. However, the annotation of specific metabolites with this approach is still weak. This is because the methodology typically relies on matching only the mass to charge (m/z) ratios of molecular features against databases of known metabolites. These databases only cover ~2% of the complete human metabolome leaving extensive un-annotated data [reviewed in (229–231)]. Furthermore, a given m/z value can often map to multiple metabolites in the databases. Therefore, without further fragmentation of the molecule, it is often impossible to distinguish between them. Recent advances in bioinformatics has improved this outlook [reviewed in (232)]. An alternative to traditional untargeted metabolomics is the chemo-enrichment approach where m/z values are mapped onto a network and connectivity data between the metabolites is used to obtain putative identifications. This removes human bias in selecting metabolite annotation.

Thus, we used the *mummichog* software to generate a network of all the detected metabolites and to identify biochemical pathways that were enriched in the different comparisons (233). The biochemical pathways found to be enriched in each of our comparisons at each time point is listed in Supplementary Tables 1 and 2. We observed significant dysregulation of pathways in DENV2-infected cells compared to uninfected cells. Other pathways were perturbed in both DENV2 and UVI samples compared to mock, indicating a stress response or signaling event caused by virus entry. To further tease these relationships apart we looked at enriched pathways shared amongst these comparisons. The number of pathways shared (following pooling of metabolites from all time points) is depicted in the Venn diagram in Figure 7A. We reasoned that pathways enriched in both the DENV2 vs. mock comparison and the DENV2 vs. UVI comparison that are absent in mock vs. UVI must represent a metabolic shift caused by viral replication distinct from viral attachment and entry (Figure 7B). We observed that a substantial amount (41%) of the total enriched pathways attributed to virus replication were involved in fatty acid synthesis or metabolism (Figure 7B).

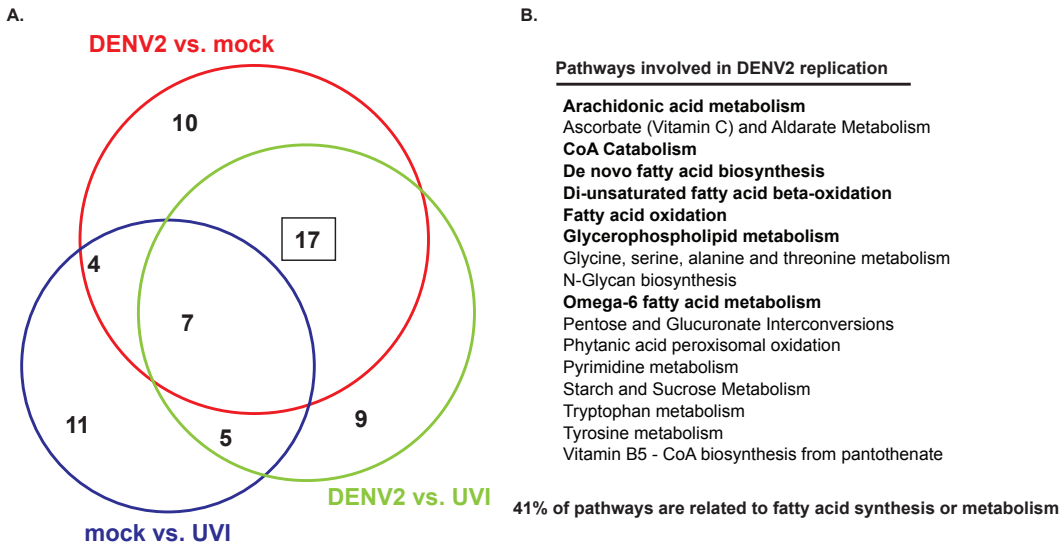

Figure 7 DENV2-infected cells show enrichment of pathways in fatty acid biosynthesis and metabolism. (A) Pathway analysis was run to identify enriched pathways in the indicated comparisons. Venn diagrams show the number of pathways that are common or unique amongst the comparisons. Pathways shared between DENV2 vs. mock and DENV2 vs. UVI represent pathways that are specifically enriched during viral replication. (B) The 17 pathways that fall in this group are listed. 41% of these pathways involve fatty acids. These are shown in bold. DENV2; dengue virus serotype 2, UVI; UV-inactivated DENV2.

To determine which biochemical pathways changed with the progression of viral infection, we performed similar analyses of shared and unique pathways at each individual time-point (Figure 8). The numbers of pathways attributed to viral replication at each time point are highlighted in yellow (Figure 8A-D). These biochemical pathways are listed below with their corresponding p-value as an indication of how significant the enrichment of the pathway is in DENV2 infected cells compared to mock (Figure 8D).

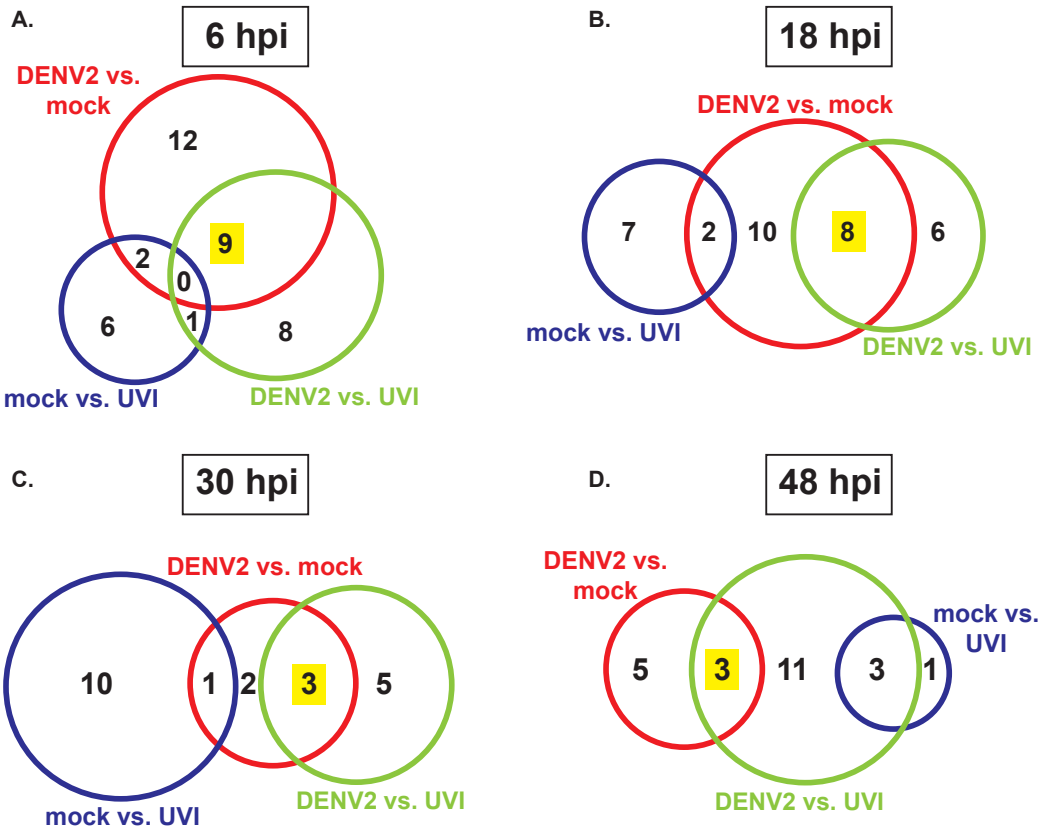

E.

6 hpi	p-value	18 hpi	p-value	30 hpi	p-value	48 hpi	p-value
Aspartate and asparagine metabolism	8.40E-05	**Arachidonic acid metabolism**	0.0006	**Arachidonic acid metabolism**	0.003	TCA cycle	0.015
Vitamin B5 - CoA biosynthesis from pantothenate	0.003	Purine metabolism	0.003	Glycerophospholipid metabolism	0.004	Phytanic acid peroxisomal oxidation	0.038
Pyrimidine metabolism	0.011	Pyrimidine metabolism	0.004	***De novo* fatty acid biosynthesis**	0.018	Glycolysis and Gluconeogenesis	0.042
Pentose and Glucuronate Interconversions	0.017	Vitamin B5 - CoA biosynthesis from pantothenate	0.016				
Tryptophan metabolism	0.024	N-Glycan biosynthesis	0.022				
Fatty acid oxidation	0.042	***De novo* fatty acid biosynthesis**	0.024				
Vitamin D3 (cholecalciferol) metabolism	0.042	Glycerophospholipid metabolism	0.034				
Tyrosine metabolism	0.042	CoA Catabolism	0.041				
Glutathione Metabolism	0.046						

Figure 8 DENV2-infected cells show a temporal enrichment of pathways. Pathway analysis was run to identify enriched pathways at each time point in the indicated comparisons. (A-D) Venn diagrams show the number of pathways that are common or unique at each time point. Pathways shared between DENV2 vs. mock and DENV2 vs. UVI represent pathways that are specifically enriched during viral replication. The number of pathways that fall in this comparison at each time point are highlighted in yellow. (E) The pathways that correspond to the highlighted numbers are listed for each time point. They are ordered by their p-value (only $p<0.05$ were included), which indicates the level of significance for the enrichment of the pathway in DENV2 vs. mock. DENV2; dengue virus serotype 2, UVI; UV-inactivated DENV2.

In general, we see an initial disturbance of pathways involved in anabolic processes, particularly amino acid and nucleotide synthesis. At time points representing peak and advanced viral infection we see pathways involved in fatty acid synthesis and metabolism. Finally, at later time points we see a switch to more catabolic and energy producing pathways that are disturbed (Figure 8E). This is similar to what has been observed for other viruses (234) and demonstrates the changing needs of the virus over time.

For enhanced detail, we show the metabolic network of DENV2 vs. mock at each time point. The metabolic networks for DENV2-infected vs. mock-infected samples at 6 hpi is shown in Supplemental Figure 3, 18 hpi in Supplemental Figure 4, 30 hpi in Supplemental Figure 5, and 48 hpi in Supplemental Figure 6. For each time point we show a sub-network of metabolites derived from the significantly perturbed biochemical pathways (Figure 9, 10). The red nodes are metabolites that are increased in DENV2 infected cells, while blue are metabolites that are decreased. At 6 hpi we see metabolites involved in amino acid biosynthesis that tend to be downregulated (Figure 9A). We have shown the sub-network of tryptophan metabolism that is dysregulated at this time point (Figure 9A and Figure 8E). Then at 18 hpi (Figure 9B) we see that metabolites in arachidonic acid (AA) metabolism are strongly upregulated in virus-infected cells (Figure 9B and Figure 8E). This trend is maintained at 30 hpi (Figure 10A). Finally, we see far fewer overall altered metabolites at 48 hpi. (Supplemental Figure 6). We have highlighted the observed features in glycolysis (Figure 10B). The increase in downstream metabolites in glycolysis such as phosphoenolpyruvate potentially indicates a shift towards gluconeogenesis at 48 hpi. (Figure 10B).

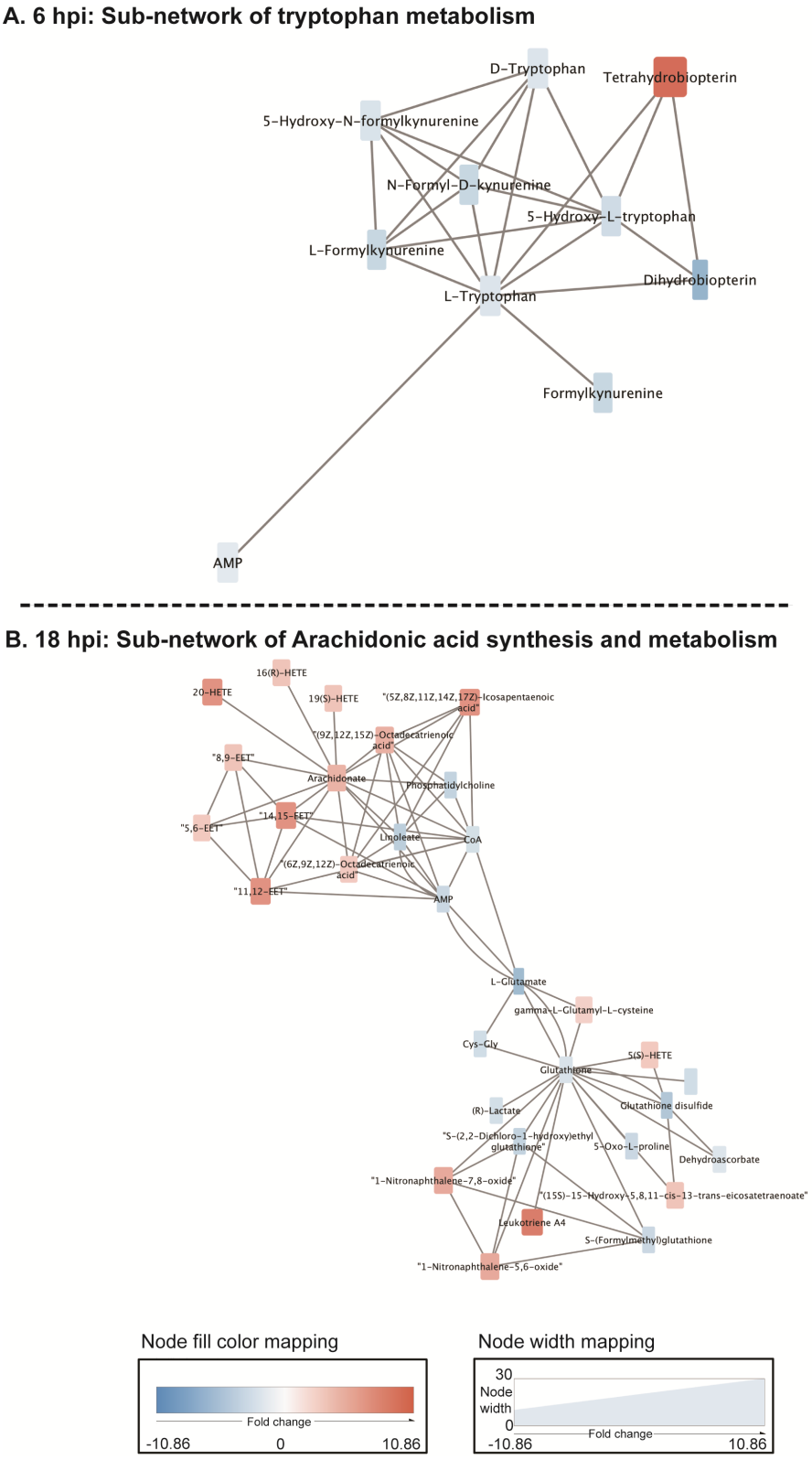

Figure 9 Metabolic sub-networks at early viral replication. Metabolites annotated by network analysis that are observed following comparison of DENV2-infected samples to mock controls. The node size and color are determined by the statistical differences between DENV2 and mock with the values noted in the

legend. The large nodes (red) are metabolites that are upregulated and the small nodes (blue) are metabolites that are downregulated in DENV2 vs. mock samples. The edges connecting the nodes represent enzymatic reactions between the connected metabolites. Their length has no significance. (A) A sub-network of tryptophan metabolism at 6 hpi showing decreases in most features of this pathway. (B) A sub-network of features in arachidonic acid metabolism as 18 hpi. These sub-networks were chosen based on pathway analysis that indicated their enrichment at this time point (Figure 8). The legend indicates values of size and color for the nodes.

A. 30 hpi: Sub-network of arachidonic acic synthesis and metabolism.

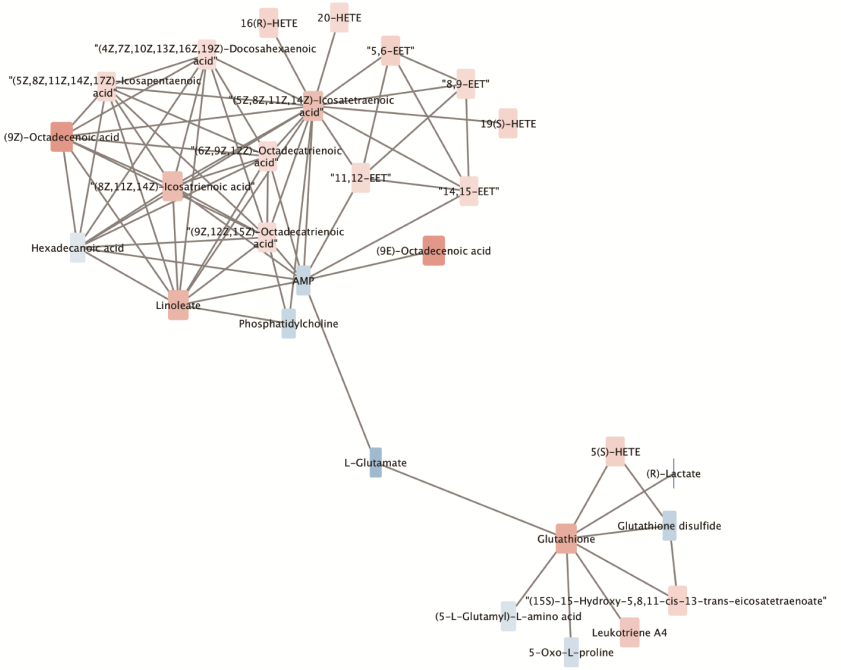

B. 48 hpi: Sub-network of glycolysis

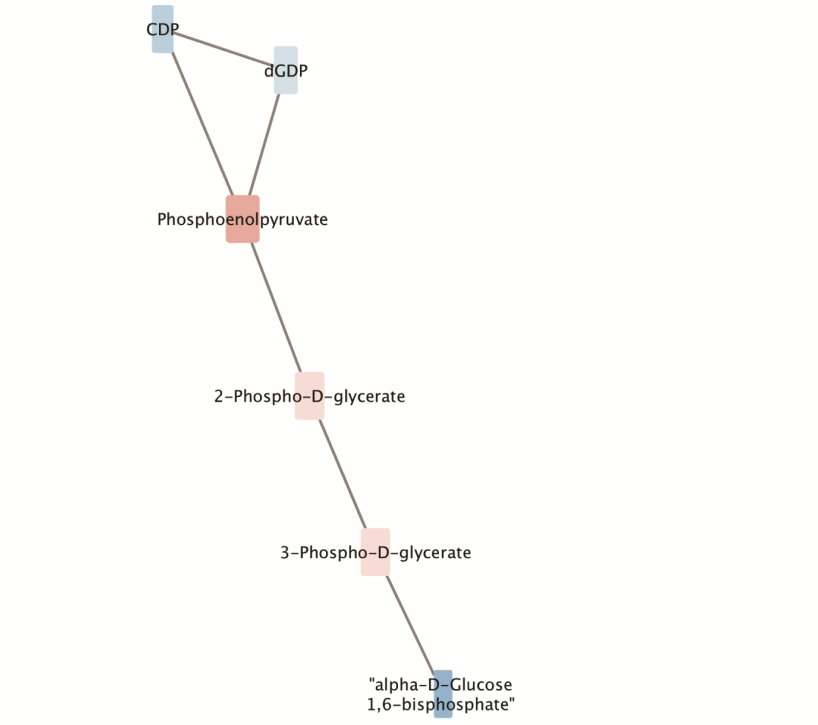

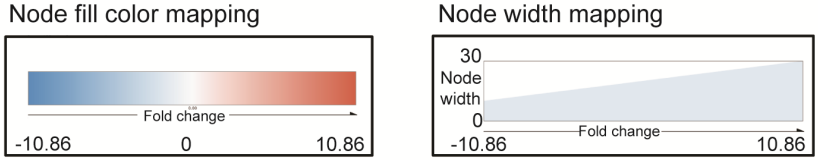

Figure 10 Metabolic sub-networks at late viral replication. Metabolites annotated by network analysis that are found when comparing DENV2-infected samples to mock controls, similar to Figure 9. (A) A sub-network of arachidonic acid metabolism at 30 hpi showing increases in most features of this pathway. (B) A sub-network of features in glycolysis at 48 hpi is shown. These sub-networks were chosen based on pathway analysis that indicated their enrichment at this time point (Figure 8). The legend indicting values of size and color for the nodes.

De novo fatty acid synthesis

Previously, we demonstrated that FAS activity was upregulated during DENV2 virus infection and re-located to centers of viral replication (90). Furthermore, we have shown that stearoyl-CoA desaturase 1 (SCD1) and its product, oleic acid, increased during DENV2 infection in a time-dependent manner. Inhibition of this enzyme resulted in the production of immature virus particles (Chapter 3). These are both enzymes in *de novo* FA biosynthesis that act on medium to long-chain FAs. Here we observed that *de novo* FA biosynthesis was perturbed at 18 and 30 hr of viral replication (Figure 8E). Specifically, we observed an increase in palmitic and oleic acids at peak viral replication (Figure 11A). Additionally, when we mapped the metabolites that were observed (from all phases and modes) onto the KEGG unsaturated fatty acid biosynthesis pathway we saw consistent disturbances in these metabolites over time (Figure 11A). In the n-3 family of unsaturated fatty acids, we observed an early increase in eicosapentanoic acid, indicating some increase in essential fatty acid uptake or prevention of its degradation (Figure 11B). This fatty acid can be elongated and desaturated to docosahexanoic acid, which we measured in this study with a moderate but not statistically significant increase at 18 hpi (Figure 11B).

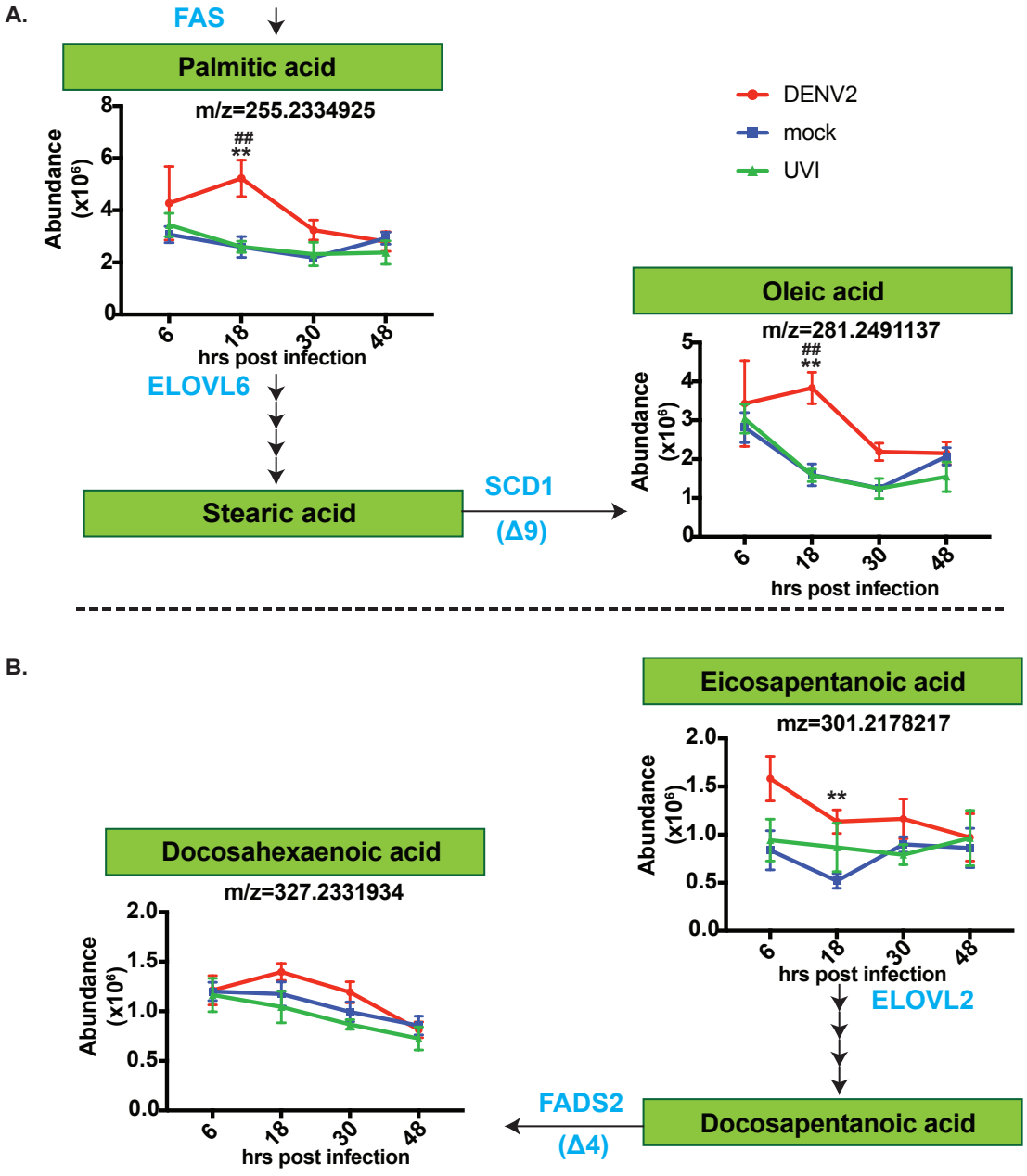

Figure 11 Metabolites observed in the biosynthesis of unsaturated fatty acids. (A-B) Using Kegg pathways (235) we have mapped the metabolites we observed in *de novo* fatty acid biosynthesis and unsaturated fatty acid biosynthesis. The common name for each fatty acid is shown in green with the measured m/z value for each molecular feature indicated below. The graphs show the normalized abundance of the metabolites over time in DENV2 infected cells, UVI-exposed cells and mock-infected cells. The arrows indicate enzymatic reactions with rate-limiting enzymes of interest labeled. DENV2vsMock (*=p<0.005, **p<0.001), DENV2vsUVI (#=p<0.005, ##=p<0.001), m/z; mass to charge ratio, FAS, Fatty acid synthase, SCD1; Stearoyl-CoA desaturase 1, ELOVL6; Elongation of very long-chain fatty acids 6, FADS2; Fatty acid desaturase 2, ELOVL2; Elongation of very long-chain fatty acids 2,

The elongation of fatty acids is regulated by seven elongation of very long chain fatty acid (ELOVLs) enzymes in mammalian cells, which differ by substrate specificity and tissue distribution (140,236). The desaturase enzymes that act on the fatty acid products we see are stearoyl-CoA desaturase 1 (SCD1) and fatty acid desaturase 2 (FADS2). Using siRNA analyses we screened the ELOVL and desaturase enzymes responsible for the observed reactions shown in Figure 11A and 11B. We observed that inhibition of the enzymes that elongated and desaturated both de novo synthesized FAs and essential FAs were important for viral replication (Table 4). Hence, the increases in fatty acids that we see in DENV2 infected cells are likely viral induced changes in the cell and disruption of their synthesis is detrimental to the virus.

Table 4 DENV2 replication is reduced with inhibition of unsaturated fatty acid synthesis. siRNAs were used to knockdown enzymes of interest in Huh7 cells. These cells were infected with DENV2 and viral titers measured after 24 hrs. Shown here is the fold change in viral replication compared to a matched irrelevant siRNA control (IRR) and the p-value from a statistical comparison of three replicates. The mechanistic analyses of the desaturase enzymes (SCD1 and FADS2) are also shown in Figures 14 and 16.

	Essential FAs		***de novo* FAs**		
	ELOVL2	FADS2**	ELOVL6	SCD1***	
logFC*	-2.48	-2.704	-3.045	-5.813	
p-value	0.0023	0.0201	0.0002	0.0002	
		**Chapter 2 Figure 14		***Chapter 3 Figure 16	

*logFC change in DENV2 replication comparing siRNA knockdown of indicated gene to a matched irrelevant (IRR) siRNA control

Arachidonic acid synthesis and metabolism

Next, we characterized the role of n-6 fatty acids and their oxygenated products in DENV2 replication. Arachidonic acid (AA) is synthesized in the cell from n-6 fatty acid precursors. It is then stored in cellular membrane phospholipids by lysoacyltransferase enzymes and freed upon cleavage by PLA_2 [reviewed in (237)]. When freed, it can be oxygenated

randomly by free radicals or by enzymes to produce eicosanoids, which are potent signaling molecules. The enzyme that acts on AA determines the production of each unique eicosanoid. The three main pathways to make eicosanoids are modulated by cyclooxygenase (COX), lipoxygenase (LOX), and cytochrome P450 (CYP) enzymes. These enzymes have a specific tissue distribution and are often concentrated in cells of the immune system [reviewed in (238)]. We identified that the AA metabolism pathway is dysregulated in DENV2- vs. mock-infected cells at 18 and 30 hpi (Figures 8E, 9B, 10A). We have reconstructed this pathway with representative features identified in our dataset by the *mummichog* software in both the synthesis of AA, its liberation from phospholipids, and its downstream effectors (Figure 12). Overall, we see a consistent increase in the precursors to AA as well as its downstream effectors in DENV2 infected cells at peak viral replication (Figure 12). This increase is not seen in cells exposed to UVI-virus or mock treatment. Therefore, these data suggest that the replication of DENV2 causes an increase in AA synthesis and metabolism. However, the data do not inform us on whether this pathway is required for viral replication or if it is a host-response to infection.

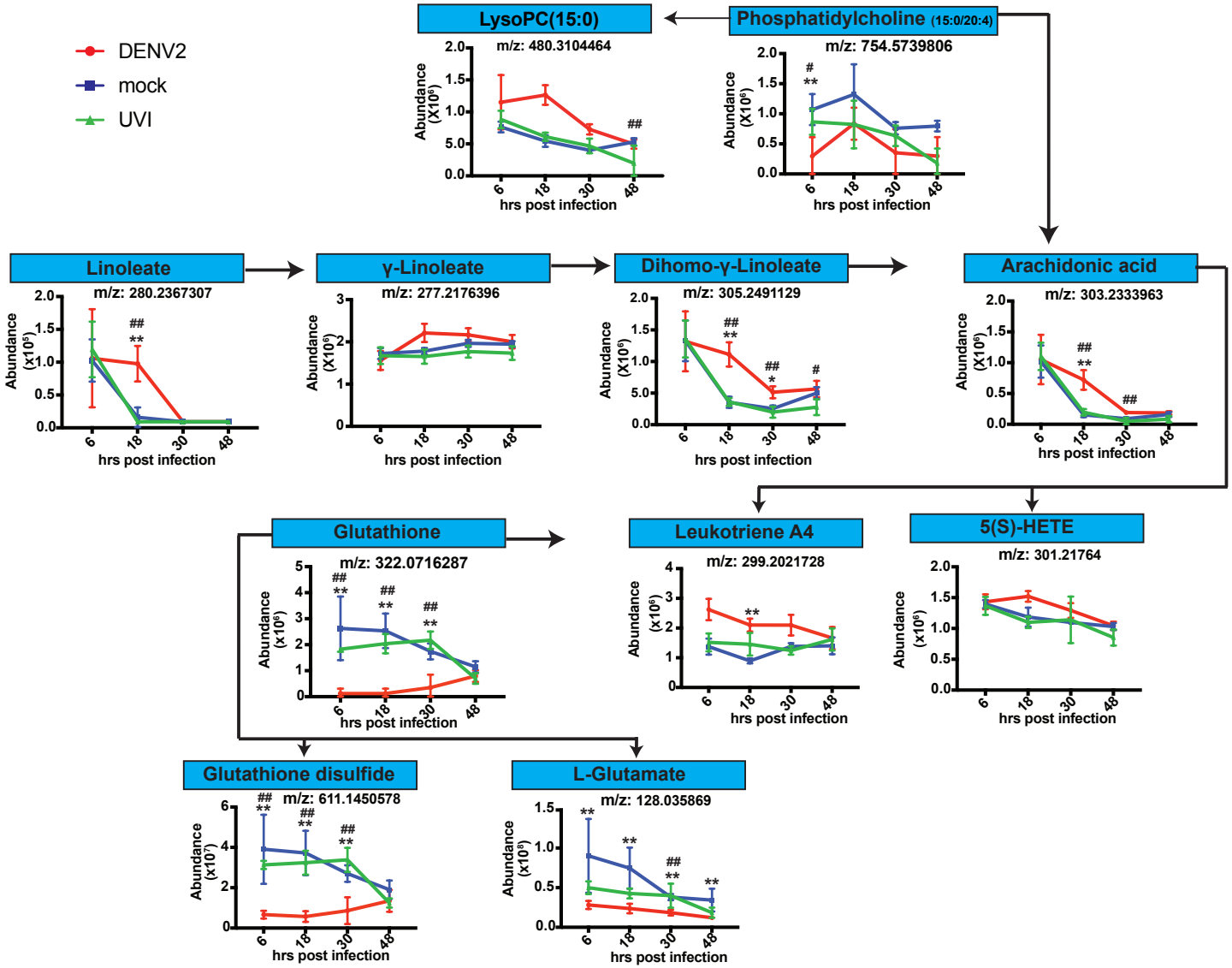

Figure 12 Metabolites observed in Arachidonic acid (AA) synthesis and metabolism. Using Kegg pathways (235) we have mapped the metabolites we observed in AA synthesis and metabolism. The common name for each metabolite is shown in blue with

the m/z value for each molecular feature indicated below. The graphs show the normalized abundance of the metabolites over time in DENV2 infected cells, UVI-exposed cells and mock-infected cells. DENV2 vs Mock (*=p<0.005, **p<0.001 DvsM), DENV2 vs UVI (#=p<0.005, ##=p<0.001). m/z; mass to charge ratio.

Given the metabolic disturbances we observed, we propose that both the synthesis and metabolism of AA is important for DENV2 replication. Therefore, disruption of this pathway would be detrimental to the virus. The observed trends in specific metabolites in this pathway are summarized in Figure 13. We have also highlighted the critical enzymes in blue and have indicated what is known about their role in flavivirus replication. For instance, PLA2 is activated during DENV infection and inhibition of this process is detrimental to West Nile Virus (WNV) replication (94,239). 5-LOX expression was also upregulated in DENV-infected human neutrophils resulting in increased leukotriene B_4 (240). Here, we investigated the importance of fatty acid desaturase 2 (FADS2) and 5-lipoxogenase (5-LOX) in the DENV2 life cycle in Huh7 cells.

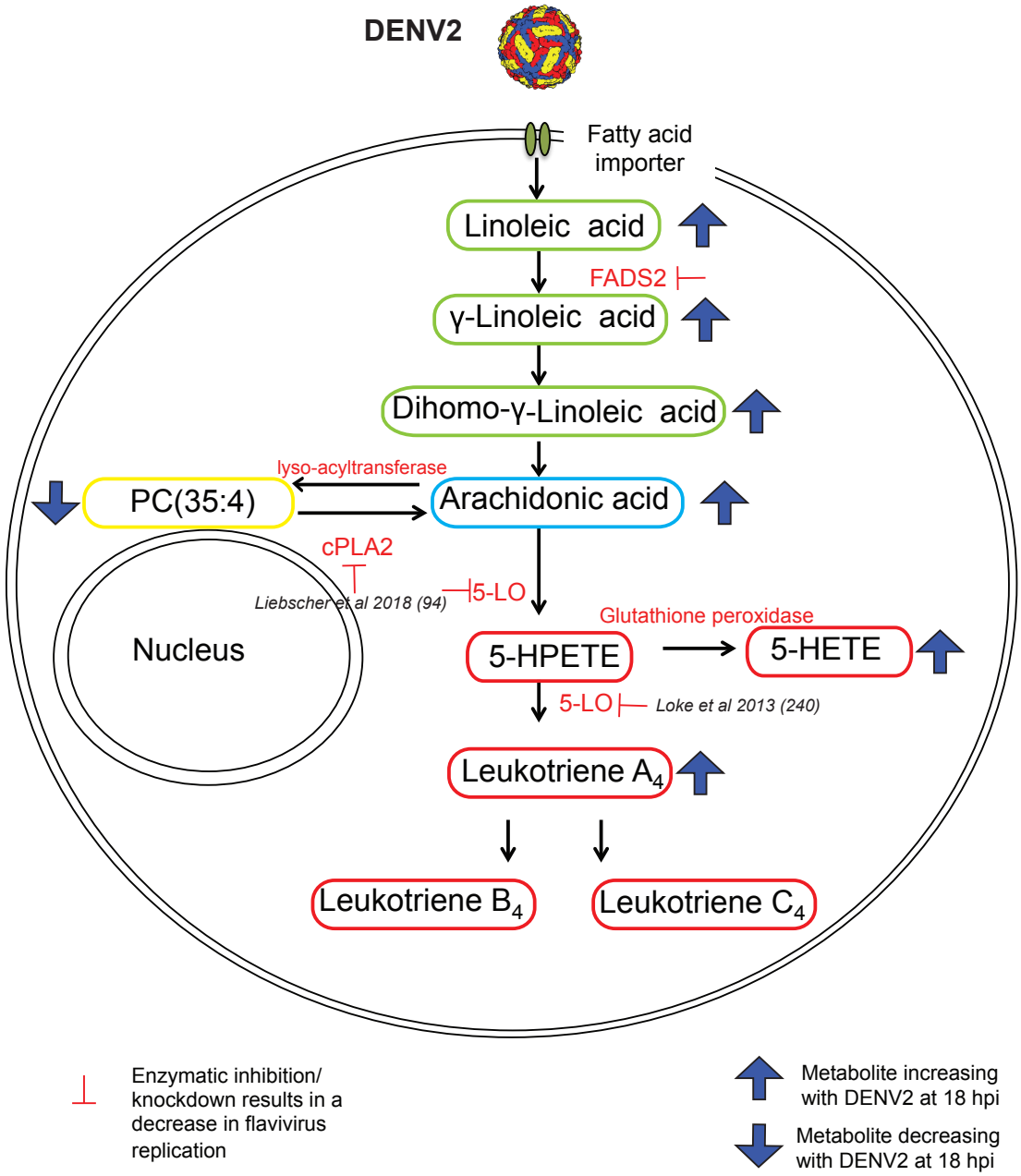

Figure 13 DENV2 perturbs essential fatty acid biosynthesis and metabolism. Here we show a model of a cell infected with DENV2 causing perturbed AA synthesis and metabolism. The metabolites in these pathways are listed along with a blue arrow indicating the trend in DENV2 infected cells at 18 hpi compared to mock infected cells. The arrows pointing up indicate an increase in the indicated metabolite, while the arrow pointing down indicates a decrease in abundance. Critical enzymes in these pathways are labeled in red with a citation for data showing that inhibition of the indicated enzyme reduces viral replication.

Fatty acid desaturase2

We observed a modest (insignificant) increase in γ-linoleic acid in DENV2 infected cells but significant increases in downstream metabolites (Figure 12). This could be due to an increase in flux of metabolites through this pathway. Hence, we reasoned that further interrogation of key regulators of this pathway was warranted. The rate-limiting enzyme in this pathway is FADS2. It converts linoleic (C18:2*n*-6) or α-linoleic acid (C18:3*n*-3) to γ-linoleic acid (C18:4*n*-6) or stearidonic acid (C18:4*n*-3) respectively. The n-6 family member γ-linoleic acid is further converted to AA while the n-3 stearidonic acid is further converted to eicosapentanoic acid. Both of these polyunsaturated fatty acids (PUFAs) can be further elongated and desaturated to other PUFAs or can be oxygenated to become eicosanoids with potent signaling capabilities (Figure 12).

Since we observed that the linoleic acid metabolism pathway was modulated in a temporal manner over the course of DENV2 infection (Supplementary Table 1 and 2) we wanted to test the expression levels of FADS2. Like many other fatty acid metabolism enzymes, FADS2 is primarily regulated at the transcriptional level [reviewed in (140)]. Thus, we infected cells with DENV2 and harvested infected and mock-infected cells at the indicated time points. RNA was extracted and FADS2 gene expression was measured. We observed an early (6 hpi) increase in FADS2 gene expression followed by a decrease in expression at later time points (Figure 13A). The decrease in expression may be due to the accumulation of PUFAs in cells that can reduce gene expression via SREBP-1 (241). These data suggest that DENV2 infection may increase FADS2 expression in a time-dependent manner to ensure an early increase in essential PUFA metabolism.

To determine the role of FADS2 in DENV2 infection we used a FADS2 specific siRNA to knockdown gene expression and measured its impact on viral replication. We first determined that treatment of cells with an siRNA for FADS2 was not significantly cytotoxic for the cells (Figure 13B) and that treatment with the siRNA resulted in a decrease in FADS2 gene expression (Figure 13C). Thus, we infected cells after 48 hr of knockdown and allowed for viral replication to proceed for 24 hr. We then measured infectious virus and viral genome copies in the cell (Figure 13D and 13E). Interestingly, we found that while viral genome copies in the cell were not reduced significantly upon FADS2 knockdown, we did observe a significant reduction of infectious virus release from cells at multiple time points (Figure 13E). These data suggest that PUFA products of FADS2 enzymatic activity are dispensable for viral genome replication, but they are critical for the production of infectious virions.

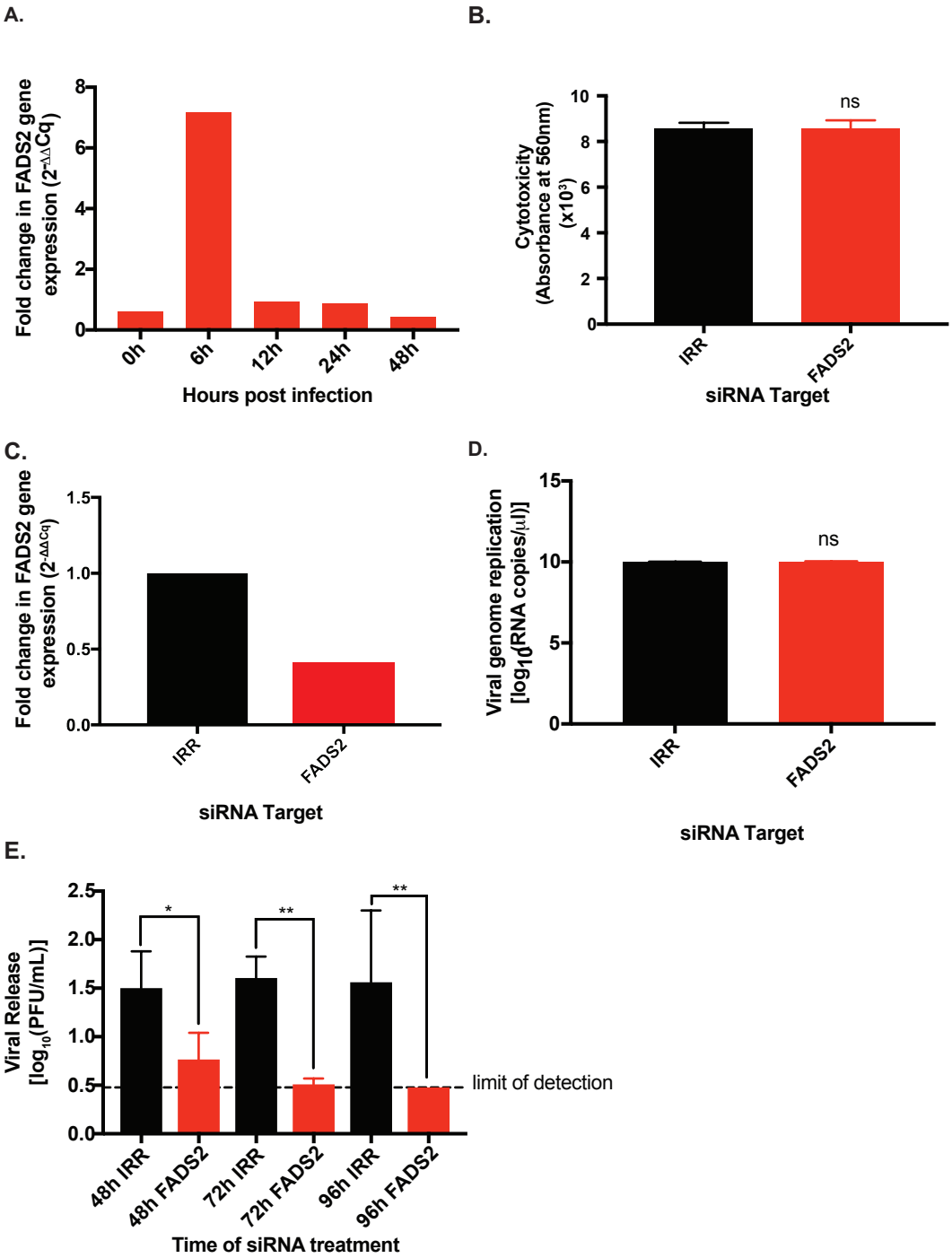

Figure 14 Loss of function of fatty acid desaturase 2 (FADS2) limits DENV2 replication. (A) Huh7 cells were infected with DENV2 (MOI=100) or mock infected and harvested at the indicated time points. FADS2 gene expression was measured by qRT-PCR and the fold change in gene expression compared to mock was calculated with the delta delta ct method (242) using one sample at each time point. (B) FADS2 mRNA was knocked down with a FADS2 specific siRNA and cytotoxicity was measured after 48 hr following knockdown. No significant cytotoxicity was observed compared to controls, DENV2 (siRNA against the viral genome) and IRR (irrelevant/non-specific siRNAs). (C) Huh7 cells were treated

with the indicated siRNAs and subsequently infected with DENV2. Cells were collected and FADS2 gene expression measured compared to RPLPO to confirm knockdown. A 70% decrease in FADS2 mRNA levels was found after 48 hr of siRNA treatment. (D) DENV2 positive strand genome was measured from one sample of these same cells and normalized to RPLPO as in part A. No difference was found in viral genome replication following FADS2 knockdown. (E) Virus containing-supernatants were collected from the same experiment in D and infectious virus was titrated. A significant reduction in infectious virus was found after siRNA treatment for 48, 72 and 96 hr. (*=$p<0.05$, **=$p<0.01$). The results represent 6 biological replicates.

5-Lipoxogenase

To further explore the functional impact of increased PUFA metabolism, we looked at the eicosanoids altered by DENV2 replication (Figure 12). We identified two eicosanoids produced from AA that were increased at peak viral replication (Figure 12). These eicosanoids are produced via the enzyme 5-LOX, which converts AA to 5-HPETE and then rapidly to either 5-HETE or leukotriene A_4. Leukotriene A_4 is then converted to either Leukotriene B_4 or C_4, which act as chemical messengers to other cells. 5-LOX is predominately expressed in bone-marrow derived cells and not in hepatocytes (243), however it can be expressed in many cancerous tissues (244) and has been reported in HepG2 cells (245). Since we observed the two different products of this enzyme in our Huh7 cells we wanted to first confirm its presence in this cell line. Using primers specific to 5-LOX we quantified and confirmed 5-LOX expression in Huh7 cells (Figure 1A).

Given the role of 5-LO in inflammatory processes, inhibitors have been developed against it to treat allergies (246). We took advantage of one such inhibitor to test its impact on DENV2 replication in Huh7 cells. Interestingly, we found a dose-dependent decrease in virus replication at non-cytotoxic concentrations of the inhibitor (Figure 15B). These data suggest that the increased expression of these eicosanoid effectors is likely a pro-viral action in the cell and not merely a general inflammatory response.

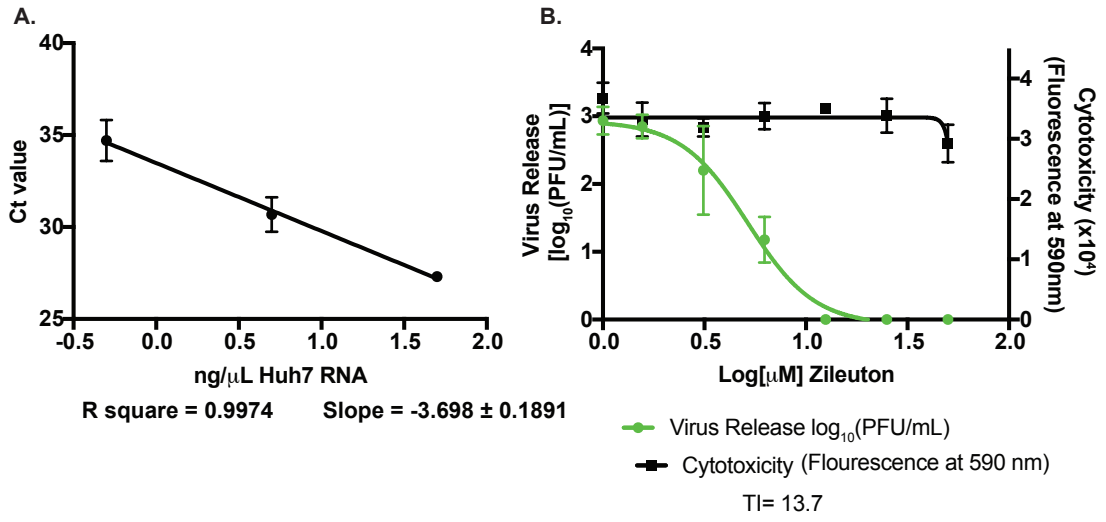

Figure 15 Inhibition of 5-lipoxygenase reduces viral replication. (A) Huh7 cellular RNA was extracted and the concentration was measured. 10-fold dilutions were prepared starting with 50ng/μL to 0.5 ng/μL. Using primers specific for 5-LOX, we measured the amplification (Ct values) of the 5-LOX in the RNA samples with qRT-PCR. (B) Huh7 cells were infected with DENV2 (MOI=0.5) and treated with the indicated concentrations of Zileuton, an FDA approved 5-lipoxygenase inhibitor. After 24 hr, cytotoxicity was measured and virus containing-supernatants were titrated. Therapeutic index was measured as the EC50/CC50. The results represent three biological replicates of a single experiment.

2.3 Discussion

Temporal control of replication is key to successful virion production. Metabolites are potent enhancers or restrictors of viral replication, hence we sought to understand the temporal metabolic changes that occurred during DENV2 infection of human cells to determine how metabolites might temporally control the viral life cycle. Specifically, we carried out a chemo-enrichment approach to analyze metabolomic data acquired during a time course of infection with DENV2 followed by mechanistic investigations of specific pathways that were highlighted by the data.

Pathway analysis over time

Our use of a chemo-enrichment approach (*mummichog*) is a distinct advancement in the field of untargeted metabolomics. The use of network connectivity enhances the likelihood that we have correctly annotated the features and removes the bias of manual annotation [reviewed in (232)]. Using this approach, we have identified biochemical pathways that are enriched in the indicated comparisons and identified where they are shared or remain distinct between treatments. We reasoned that pathways enriched in both DENV2 vs. mock and DENV2 vs. UVI-virus exposure must play an important role in viral replication. Certainly, all the pathways enriched in DENV2 vs. mock are likely involved in viral replication, but when these are shared with the DENV2 vs. UVI-comparison, it increases the likelihood that they are impacted by viral replication specifically, as opposed to viral attachment or entry. We noticed that many of these pathways were involved in fatty acid biosynthesis or metabolism confirming previous observations that fatty acids are important points of control during DENV2 infection (90).

We then looked at the shared pathways attributed to DENV2 replication enriched at each distinct time point of replication, we observed a disturbance in anabolic cellular processes (amino acid synthesis) at early and peak replication time points with a switch to catabolic processes (TCA and glycolysis) at late infection. This switch in cellular metabolism was also observed in HCV infected cells indicating a common energetic need (234). The disturbances in anabolic biochemical pathways were geared towards the production of amino acids and nucleotides at 6 hpi. Early control of these substrates is not surprising given the need for the virus to rapidly translate and replicate its genome. However, we observed a general decrease in metabolites involved in tryptophan metabolism. We did observe an early increase in tetrahydrobiopterin (BH_4) in DENV2-infected cells. BH_4 is a cofactor for tryptophan

hydroxylase, which metabolizes tryptophan on the pathway to serotonin. BH_4 is widely distributed and acts as a co-factor for multiple amino acid hydroxylase enzymes and nitric oxide (NO) synthases and is sensitive to degradation by reactive oxygen species (247). Accumulation of BH_4 along with depletion of certain amino acids (Figure 9A) may indicate that amino acid synthesis is primarily downregulated early during infection or that the virus is depleting substrates too rapidly for the cell to keep up. Others have hypothesized that BH_4 is depleted in severe dengue diseases due to oxidative stress leading to accumulation of phenylalanine (202). Perhaps the early increase in BH_4 coupled to the decrease in advanced infections is a by-product of the time-dependence of oxidative stress in DENV2 infection, which plays a pro-viral role in genome replication (204).

Fatty acid synthesis

Following the early disturbance of nucleotide and amino acid synthesis, we observed changes in fatty acid synthesis at peak viral replication. This time point is when cellular membranes are actively expanding to support viral replication (227). Fatty acids are key substrates for these membranes hence the regulation of FAS by DENV2 (90). However, the fatty acid substrates made by FAS are clearly not sufficient for the required membrane expansion, since we observed accumulation of longer chain unsaturated fatty acids in DENV2 infected cells. The ELOVL family of enzymes are rate-limiting in elongating fatty acids, which is accomplished in a four enzyme cycle to add two carbons to an elongating fatty acid chain (140). ELOVL7 is critical for infectious virion production of human cytomegalovirus (HCMV) (248). Since we observed an increase in oleic acid at 18 hpi, we hypothesized that ELOVL6 and SCD1 are utilized by the virus to synthesize these fatty acids. We demonstrated that reduction of ELOVL6 and SCD1 reduces viral replication. We also observed increases in docosahexanoic acid

(although not statistically significant) and hypothesized that ELOVL2 and FADS2 would be utilized to synthesize these fatty acids. Thus, we demonstrated that reduction of ELOVL2 and FADS2 reduced viral replication. Taken together, our studies here provide biochemical and mechanistic evidence that fatty acid synthesis and elongation are essential for DENV2 replication.

Given the clear importance of phospholipids (PL) during flavivirus infection we measured the levels of PLs over the course of DENV infection. The decrease in PC in DENV2 infected cells was surprising given our previous findings in mosquito cells and midguts (92,106). The extensive membrane expansion in virus-infected cells implies that PL abundance should be increased. However, others have also reported that PC is increased by other positive strand viruses but not by DENV2 (249). Thus, we hypothesize that PCs must be recycled or remodeled throughout the cell to provide alternate lipids for membrane expansions in Huh7 cells. Given this variation, it is clear that DENV2 interacts in a diverse manner with different cell types to modulate the lipid repertoire. Furthermore, as an arbovirus DENV2 has to toggle between mosquito and human hosts, infecting even more diverse cell types. Hence, this ability to metabolically modulate dissimilar cell types depending on its needs is required.

Arachidonic acid biosynthesis and downstream metabolism

At 18 hr and 30 hr of viral replication we found enriched essential fatty acid synthesis and metabolism. Specifically, linoleate synthesis leading to AA metabolism was enhanced, implying a virally triggered increase in its uptake, retention, or reduced degradation. Therefore, we explored the downstream metabolism of linoleate, specifically its conversion to AA.

As an n-6 fatty acid, AA is not synthesized entirely *de novo* in mammalian cells due to a lack of specific enzymes. It is primarily synthesized in the cell from a linoleic acid precursor

rather than directly absorbed from the environment. Hence, modulation of linoleic acid metabolism could be a way to control AA levels. Based on our observations from the metabolomic studies, we chose to analyze the rate-limiting enzyme in AA synthesis, FADS2, the Δ4, Δ6 and Δ8 desaturase. We found a time-dependent increase in FADS2 gene expression similar to SCD1, the Δ9 desaturase (Chapter 3). siRNA knockdown of FADS2 resulted in a significant decrease in DENV2 virion production but had no impact on genome replication suggesting that PUFAs generated by FADS2 may be critical for post-genome replication steps in the viral life cycle.

After AA is synthesized it is stored in PLs by lyso-acyltransferases, until it is cleaved by phospholipase (PLA_2) enzymes. DENV2 triggers apoptosis in neuroblastoma cells by activating PLA_2 to cleave AA, which leads to the generation of superoxide anions and the activation of NF-κB leading to apoptosis (239). Hence the increase in AA that we see may be a result of a cellular response to control infection. However, others have recently demonstrated that WNV uses PLA_2 to cleave PLs for the production of lysoPLs that contribute to the negative curvature required for membrane rearrangements that facilitate viral replication (94). Hence the release of AA could have a strong proviral effect as well.

We observed that inhibition of 5-LOX in Huh7 cells resulted in a dose-dependent decrease in viral replication (Figure 15). Others have found that DENV2 exposure to neutrophils results in increased Leukotriene B_4 production through 5-LOX, but did not demonstrate the effect of 5-LOX inhibition on viral replication (240). Our observations indicate that the inflammatory metabolite products of 5-LOX could also be pro-viral. Interestingly, others have demonstrated that leukotriene A_4 produced by 5-LOX stimulates fatty acid synthase (FAS) expression via SREBP-1 and that inhibition of 5-LOX results in a decrease of FAS in HepG2

cells (245). The significance of FAS for flavivirus replication is clear (90,93,250). If this regulatory mechanism holds true for Huh7 cells, it could indicate why the eicosanoid products of AA via 5-LOX are critical for DENV2 infection and how their inhibition negatively impacts viral replication. In this scenario DENV2 takes advantage of a complex metabolic regulatory mechanism whereby PUFA metabolism produces eicosanoids to stimulate FAS, which in turn the virus utilizes to build replication compartments. Taken together, we see viral control of both AA synthesis through FADS2 as well as its release from PLs by PLA_2 and its further metabolism into eicosanoid effectors (Figure 13).

Thus, DENV2 accomplishes a metabolic reprogramming that favors anabolic processes early and *de novo* fatty acid synthesis at peak viral replication. Then, at later time points during infection when cells are experiencing significant levels of stress, the virus activates catabolic and energy producing processes to sustain a low level of cellular function that serves to continue progeny virion production before cell death proceeds. For example, we observed changes in the TCA cycle and glycolysis at 48 hpi where downstream metabolites in glycolysis were accumulating, indicating an anapleurotic role of upstream glycolytic intermediates (77) leading to overall energy production and cell survival. Hence viral control of cellular metabolic processes in indeed a well-timed phenomenon that serves the changing viral needs during the course of its journey in a cell.

2.4 Materials and Methods

Cells lines:

The cell lines used for this study are as follows: BHK-21, Clone 15 (ATCC CCL-10), and Huh7 (from Dr. Charles Rice, (251)). Huh7 cells were maintained in Dulbecco's Modified Eagle Medium (DMEM) (Gibco, LifeTech), while BHK were maintained in Minimum Essential Media

(MEM) (Gibco, LifeTech), both were supplemented with 0.1 mM nonessential amino acids, and 0.1 mM L- glutamine, and 10% Fetal Bovine Serum (Atlas Biologicals) at 37°C with 5% CO_2.

Viruses:

DENV2 (16681) (252) passaged in C6/36 cells was used for this study. Virus titers were quantified by plaque assay on BHK cells as described previously (253). Approximately, $4x10^6$ Huh7 cells were infected with DENV2 strain 16681 at a MOI = 10. Infection of cells was carried out at 4°C for one hour to allow virus adsorption. Virus was then removed, cells were rinsed with ice-cold 1XPBS 2 times, overlayed with the indicated media and transferred to the 37°C incubator for the indicated periods of time.

To generate UV-inactivated (UVI) DENV2 stocks, we used the same stock of DENV2 (16681) and exposed it to 4000 mj of UV light in a stratalinker for 1.5 mins. The virus was then titrated on BHK cells to ensure no infectious virus was present.

Metabolite extraction

For the metabolomics experiments 5 biological replicates were used for each time point and treatment. Cells were harvested at the indicated time point and metabolites were extracted from an equal number ($3.4x10^6$) of cells per sample. A mixture of 1:1 chloroform:methanol were added to the cells. Specifically, 500µl of methanol (containing 2,6-Di-tert-butyl-4-methylphenol) and 180µl of dH_2O was added to the cell pellet, vortexed vigorously, and then 500µl of chloroform and 180µl of dH2O was added and vortexing repeated. To standardize the metabolite extraction process 20µl of a 100µg/ml stock of 17C-ceramide was added as a standard for the non-polar phase metabolites, and a similar amount of a di-peptide, ALAL was added as a standard for the polar phase metabolites. The samples were then centrifuged at 16,000 rpm in a microcentrifuge for 10min at 4°C, and the polar and non-polar fractions separated and dried

under a vacuum. To prevent degradation of metabolites, samples were processed on ice or at 4°C throughout the process. Samples from aqueous and organic phases were dried separately by speed-vacuum centrifugation and were stored at -80°C for LC-MS/MS analyses.

LC/MS

An LTQ Orbitrap XL instrument (Thermo Scientific, Waltham, MA) was used to analyze each sample. It was coupled to an Agilent 1100 series LC (Agilent Technologies, Santa Clara, CA) equipped with a refrigerated well plate auto sampler and binary pumping device. Reverse-phase liquid chromatography was used to analyze the samples in both phases.

Polar metabolites:

An Atlantis T3 column (Waters Corp., Milford, MA) with 2.1x 150 mm, 5.0 µm dimensions was used for the separation. Solvent A consisted of water + 0.1 % formic acid. Solvent B consisted of acetonitrile + 0.1 % formic acid. The flow rate was 300 µL/minute. A volume of 10 µL was loaded onto the column. The gradient was as follows: time 0 minutes, 0% B; time 1 minutes, 0% B; time 41 minutes, 95% B; time 46 minutes, 95% B; time 50 minutes, 0% B; time 60 minutes 0% B. We ran the LC-MS analysis twice, using positive and negative polarity electrospray ionization (ESI). Data were acquired using data dependent scanning mode. FTMS resolution of 60,000 with a mass range of 50–1100 was used for full scan analysis.

Non-polar metaboplites:

An Xterra C18 column (Waters Corp., Milford, MA) with 2.1 x 150 mm, 5.0 µm dimensions was used for the separation of the non-polar metabolites. Solvent A consisted of water + 10mM ammonium acetate + 0.1% formic acid. Solvent B was acetonitrile/isopropyl alcohol (50/ 50 v/v) + 10mM ammonium acetate + 0.1% formic acid. The flow rate was 300 µL/minute. A sample volume of 10 µL was loaded onto the column. The gradient was as follows:

time 0 minutes, 35% B; time 10 minutes, 80% B; time 20 minutes, 100% B; time 32 minutes, 100% B; time 35 minutes, 35% B; time 40 minutes 35% B. The LC-MS analysis was run twice, with both positive and negative polarity ESI. The acquired data were evaluated with Thermo XCalibur software (version 2.1.0).

MS data processing and analysis

To analyze the mass spec data we converted the raw data to mzXML format with msConvert (254). Much of the downstream analysis used R according to published methods. Peak picking was accomplished with the XCMS package using the centWave (255–257) algorithm and a Gaussian fit for peak-picking, and the OBI-Warp method for retention time correction and alignment (258). Parameters used for XCMS were optimized using the IPO package (259). Features were removed if their retention time was outside of acceptable limits: 2–34 minutes for nonpolar modes and 2–48 minutes for polar modes. Intensities for peaks were determined and normalized using the median fold change method (260,261). Missing values for samples where less than half of the group has the feature clearly identified were assumed to be below the lower limit of detection and imputed with one-half the overall minimum intensity value. Groups with values for at least half of the samples in that group were imputed with the fillPeaks function of XCMS and normalized with previously calculated normalizing constants (262). Where fillPeaks results in zero intensity, we are assuming the intensity is below the lower limit of detection, and we use one-half the overall minimum value. These abundance values were used for pathway analysis described below.

Each of the four chemical and analytical modes (polar/non-polar and negative/positive mode) were processed and analyzed separately. To test for dysregulation of metabolites among the 12 biological groups, we used the limma package in R (228). This approach fits linear models

to the data using an empirical Bayes approach. The Venn diagrams summarize the differences among groups, where absolute log fold changes were at least 1 and adjusted *p*-values were less than 0.005. A low *p*-value is used because of the large number of comparisons that are looked at simultaneously in this study.

Pathway analysis

We used a student's t-test on the imputed abundances for all the features at each time point with each treatment generating 12 different comparisons of features in negative mode and 12 comparisons of features in the positive mode. Network analysis and metabolic pathway analysis was performed using the *mummichog* software version 2.0 (233). This platform tests the enrichment of input features against random data resampled from the reference list and produced an empirical *P* value for each pathway. Input metabolites were then annotated as empirical compounds and the significant one ($p<0.05$) were mapped onto metabolic pathways. They were also linked in a network figure by known metabolic reactions and visualized in Cytoscape version 3.6.0 (263) (Supplemental Figures 3-6). Representative features in arachidonic acid metabolism were plotted with abundance versus time and displayed in a metabolic pathway for Figure 12.

RNA extraction and qRT-PCR:

RNA was extracted from cells using Trizol (ThermoFisher) and from virus in supernatant using Trizol LS (ThermoFisher). A one-step qRT-PCR kit with SYBR green from Agilent was used. Reactions were set up according to the manufacturer's protocol and run on a LightCycler 96 real-time PCR machine (Roche). The cycling parameters were: 20 mins at 50°C for reverse transcription, then 5 mins at 95°C followed by 45 two-step cycles of 95°C for 5 seconds and 60°C for 60 seconds. This was followed by a melt curve starting at 65°C and ending at 97°C.

DENV2 primers (264) were used to quantify viral RNA copies by comparing to a standard curve of *in vitro* transcribed viral RNA from a DENV2 cDNA subclone (265). Copies of viral RNA in the cell as well as copies of cellular mRNA transcripts were both normalized to Ribosomal Protein Lateral Stalk Subunit P0 (RPLPO) RNA using the delta delta ct method (242). For this method: the fold change in gene expression = 2^[-{Infected samples((Ct value of gene of interest) – (Ct value of control gene))}–{Uninfected samples ((Ct value of gene of interest) – (Ct value of control gene))}].

Primers:

DENV2:

Forward: ACAAGTCGAACAACCTGGTCCAT Reverse: GCCGCACCATTGGTCTTCTC

FADS2:

Forward: GGCACTACGCTGGAGAAGATG Reverse: AGTGATCTTTGAGTTCTTGCCGT

RPLPO:

Forward: AGATGCAGCAGATCCGCAT Reverse: GGATGGCCTTGCGCA

5-lipoxygenase (ALOX5):

Forward: GGATGGACGCGCAAAGTTGG Reverse: CCTTGTGGCATTTGGCATCG

Inhibitor and siRNA treatments and confirmation:

The siRNAs used were a scrambled siRNA control with no targets in the mammallian genome (IRR) and an endonuclease prepared FADS2 specific siRNA pool (Sigma, esiRNA). Cells were transfected with siRNAs using RNAiMax (Invitrogen) similar to previous experiments (90) and incubated for 48 hr to allow for sufficient knockdown. Cells were then infected with DENV2 or collected for cytotoxicity tests (described below). Virus was collected and titrated by plaque assay. To confirm knockdown of mRNA transcripts, RNA was extracted

and qRT-PCR performed to measure FADS2 levels relative to RPLPO with FADS2 specific siRNA treated samples and compared to IRR treated samples using the delta delta ct method (242) described above. Cytotoxicity was measured with alamar blue (ThermoFisher) diluted 1:10 in DMEM incubated on cells for 2-4 hr and read on a Victor 1420 Multilabel plate reader (Perkin Elmer) with excitation at 560 nM and emission at 590 nM.

The inhibitor of 5-LOX used was Zileuton (Sigma-Aldrich). It was diluted in DMSO and further diluted in DMEM before being added to cells. Huh7 cells were infected with virus as described above and overlayed with the indicated concentrations diluted in DMEM. Supernatants were collected at 24 hr and plaque assays performed. Cytotoxicity was measured with alamar blue (ThermoFisher) diluted 1:10 in DMEM incubated on cells for 2-4 hr and read on a Victor 1420 Multilabel plate reader (Perkin Elmer) with excitation at 560 nM and emission at 590 nM.

CHAPTER 3. STEAROYL-COA DESATURASE 1 IS A METABOLIC SWITCH THAT DEFINES EARLY AND ADVANCED DENGUE VIRUS INFECTIONS AND DETERMINES VIRUS PARTICLE INFECTIVITY

3.1 Introduction

Phospholipids are critical for membrane structure, function and stability of eukaryotic cells. Specific distributions of lipids within these membranes define their characteristics such as curvature, fluidity, leakiness and the interactions between membranes and membrane-bound protein complexes. A key approach to alter the architecture of a membrane is to incorporate unsaturated fatty acyl chains, to induce curvature and fluidity in a lipid bilayer, altering its functional capacity (97,266). Unsaturated fatty acids (UFA) are generated in the cytoplasm and after their initial desaturation they are further elongated, desaturated and shunted towards triglyceride, cholesterol ester or phospholipid synthesis. This initial desaturation event is the rate-limiting step in UFA biosynthesis and is catalyzed at the Δ9 position in the carbon chain by stearoyl CoA desaturase (SCD) (267,268). In humans, it has two isoforms: SCD1 is ubiquitously expressed and preferentially converts stearic and palmitic acids into oleic and palmitoleic acids, respectively. SCD5, is restricted to the brain and pancreas (176). SCD1 is a 40 kD integral membrane protein in the endoplasmic reticulum (ER) and is highly conserved from bacteria to mammals (175). It regulates the balance between saturated and monounsaturated fatty acids (MUFA) in the cell.

Flaviviruses are obligate intracellular pathogens that hijack lipid metabolic pathways for their energy and substrate requirements. As enveloped viruses, they rely heavily on host phospholipid membranes at every stage of their life cycle and alter the architecture and composition of these membranes to fit their replicative needs (29,249,269,270). Specifically, flaviviruses target

membranes of the ER to generate a scaffold for the assembly of viral protein complexes, concentrate substrates required for genome replication, and protect the double-stranded RNA replicative intermediates from detection by the cellular immune response (226). As a result, the architecture of the ER membrane is altered to form structures known as convoluted membranes (CM), vesicles (Ve) and vesicle packets (Vp) (29,65,271). The CM are considered to be sites for viral protein translation. The Vp/Ve are sites for viral RNA replication (65). Additionally, these viruses co-opt the ER membrane as a structural component of the virus particle (envelope) and use the ER for virus particle assembly and egress. Embedded in this ER-derived lipid envelope are the viral transmembrane glycoproteins, pre-membrane (prM) and envelope (E). Structural transitions between these proteins are critical for virion maturation and infectivity.

Flaviviral dependence on cellular membranes is reflected in alterations in cellular fatty acid metabolism during infection (90,92). This has also been observed for other viruses (272–275). The specific physiochemical properties of the required fatty acids and their influence on specific steps of the flaviviral life cycle are not known. In this study, we investigated the importance of fatty acid desaturation on the flavivirus life cycle. We evaluated required enzymes in the UFA pathway using an siRNA library and identified key restrictions that reduced replication of the flavivirus, dengue virus type 2 (DENV2). The enzymatic activity of SCD1 in particular, was required for viral replication and was regulated in a time-dependent manner. SCD1 protein expression levels were inversely correlated with the concentration of viral dsRNA (Replicative Intermediate, RI) in the cell. This modulation of SCD1, coinciding with the stage of viral replication, highlighted its function as a ‘metabolic switch’ that controls alternate lipid requirements during early and advanced infections. Loss of function of this enzyme adversely

altered the maturation and infectivity of released virions. This study highlights the importance of the UFA biosynthesis pathway in flaviviral genome replication and virion infectivity.

3.2 Results

Bottlenecks in the UFA biosynthesis pathway control DENV2 replication

We hypothesized that enzymes in the UFA biosynthesis pathway are important for the DENV2 lifecycle and interrogated this pathway with siRNAs (Supplemental Table 3) to determine effects of their transient knock-down on viral replication (Figures 16, 17). An irrelevant siRNA (IRR) controlled for off-target effects of siRNA treatment, while an siRNA targeting the DENV2 genome was a positive control for reduction in viral replication. We identified two enzymes in this pathway that represent host-viral interaction points, SCD1 and peroxisomal trans-2-enoyl-coA reductase (PECR) (Figure 16A). These observations were made in two human cell lines (Huh7 and A549), yielding similar effects on viral replication (Figure 16, Figure 17A, 17B). Cytotoxic effects of siRNA treatment were not significant (Figure 17C-E).

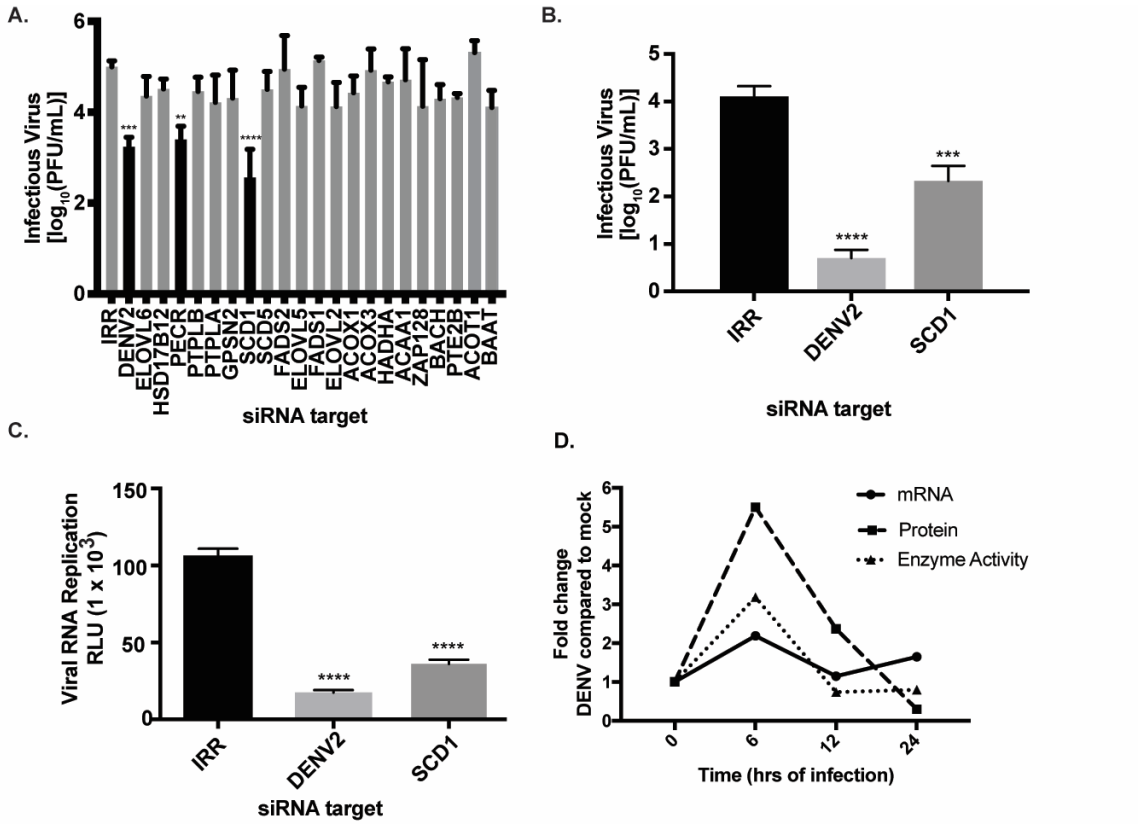

Figure 16 siRNA screen of the UFA biosynthesis pathway indicates that the rate-limiting enzyme is key for DENV2 replication. (A) Huh7 cells were transfected with pools of four siRNAs targeting each gene and infected with DENV2. Infectious virus release was measured by plaque assay. (B) Validation of results in A using a single siRNA targeting SCD1 as well as indicated controls. (C) siRNAs were electroporated into Huh7 cells along with a luciferase-expressing DENV2 replicon. Viral RNA replication was measured by luciferase expression. (D) Huh7 cells were infected with DENV2 (MOI=10) and cells were harvested at indicated time points and processed for gene expression, protein levels or enzymatic activity. Fold change in SCD1 mRNA in virus-infected cells compared to mock-infected cells. qRT-PCR results are normalized to GAPDH. The same cells were flash frozen to preserve active enzymes. Cytoplasmic extracts were prepared and run on a western blot, probed with SCD normalized to actin and TLC was carried out to measure conversion of ^{14}C-labeled Stearoyl-CoA to ^{14}C-labeled-oleic acid. The quantification of these 3 assays is shown here. The data are representative of 3 independent biological replicates. SCD1: stearoyl CoA desaturase, IRR: irrelevant siRNA (without a biological target for the siRNA sequence), DENV2: siRNA against dengue virus, serotype 2 genome. (**=$p<0.05$, ***=$p<0.001$, ****=$p<0.0005$, A-D: one-way ANOVA with multiple comparisons tests, and E: a two-tailed t-test).

We found that knockdown of SCD1 expression significantly reduced DENV2 replication in all cell lines and conditions tested when compared to an irrelevant siRNA (Figure 16A-C, and Figure 17A, B). Since the initial screen was carried out with a pool of four siRNAs against SCD1, we also validated the results with a single siRNA against SCD1 and showed a similar reduction

in virion release (Figure 16B). This siRNA was further tested against a luciferase expressing DENV2 replicon (90), and we found that viral RNA replication was significantly reduced (Figure 16C). Therefore, the effect of SCD1 knockdown on the release of infectious virus is at least partly mediated at the RNA replication step. We confirmed that siRNA treatments were effective at reducing SCD1 mRNA and protein levels using qRT-PCR and western blot analyses. The SCD1 mRNA expression was reduced by 90% and protein levels were below the level of detection (Figure 17F and 17G). These data suggest that UFA synthesis is critical for DENV2 replication.

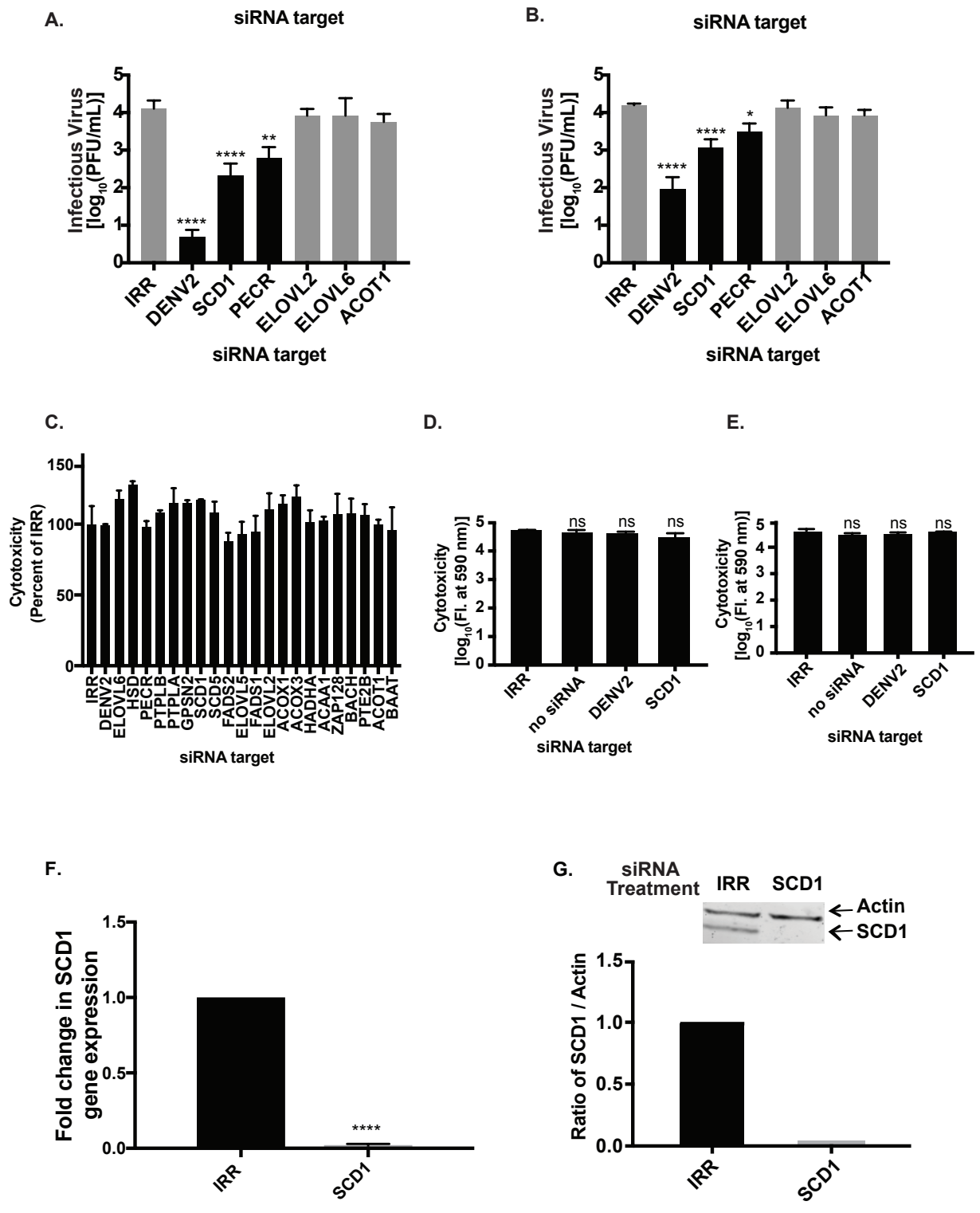

Figure 17 siRNA screen of the human UFA biosynthesis pathway (cytotoxicity and validation). Multiple cell types were transfected with single siRNAs targeting enzyme "hits" initially identified in the pooled siRNA screen of the pathway. Infectious virus release from siRNA treated cells and controls was measured. (A) Huh7 cells, (B) A549 cells. A one-way ANOVA with multiple comparisons was done. (C).

Cytotoxicity of the siRNAs (in Figure 16) was measured by the fluorescence of the reduction of resazurin to resorufin. A one-way ANOVA with multiple comparisons was done; none of the treatments were significantly cytotoxic. Cytotoxicity of the single siRNAs in Huh7 cells are shown in (D) without virus addition and (E) with virus addition. (F) qRT-PCR analysis to confirm knockdown of SCD1 gene expression. (G) Western blot analysis to confirm knockdown of SCD1 protein using antibodies against SCD1 and Actin. Signal intensities are quantified One-way ANOVA indicated no significant difference. (ns=not significant, *=p=0.05, **=p<0.001, ****=p<0.0001 compared to IRR)

SCD1 gene expression and activity are elevated early post-DENV2 infection

Based on the above observations, we hypothesized that DENV2 requires a stable or increased level of the SCD1 enzyme and its products to regulate the cellular lipid repertoire for its replicative advantage, and that the activity of this enzyme may be controlled by viral infection. Since SCD1 expression is regulated at the transcriptional level (276), we first examined SCD1 mRNA levels in infected cells and found them to be increased at early time-points post infection compared to mock-infected cells (Figure 16D). To ensure that the protein is translated and active during viral replication, we quantitatively examined the enzymatic activity of SCD1 in DENV2-infected cells over time. Consistent with the mRNA expression profile at early time points, we found that cells infected with DENV2 had an initial increase in SCD1 activity, as measured by the conversion of radiolabeled stearic acid to oleic acid, as early as 6 hr post infection (Figure 16D). This coincides with early replication and translation of the viral genome. Also, consistent with changes in its mRNA profile, later during infection we found a decrease in SCD1 expression and activity. SCD1 is the only enzyme that can produce oleic acid. Our observations suggest that DENV2 infection specifically up-regulates SCD1 activity early in infection to expand the pool of MUFAs available for its replicative needs.

SCD1 in found within early centers of viral replication

Previous studies with DENV2 have shown that lipid biosynthetic enzymes (such as fatty acid synthase, FAS) are recruited to viral replication complexes, to increase local synthesis of lipids at sites of viral RNA replication and virus assembly (90). Since SCD1 is immediately downstream

of FAS in the biosynthetic pathway, we investigated whether SCD1 was also re-localized to viral replication complexes during DENV2 infection. We processed mock-infected or DENV2-infected cells at 6, 9 and 24 hr for immunofluorescence studies, using antibodies against DENV2 NS3, dsRNA (RI) and human SCD1 (Figure 18). Interestingly, unlike what we previously observed for FAS in Huh7 cells (90), there is a temporal progression in marker distribution (best observed in Figure 18A, 24 hr dsRNA and SCD1 panel). Uninfected cells show normal SCD1 signal (Figure 18A and Figure 19C), while cells with a low level (early) infection show that SCD1 can be found within viral replication complexes. Using Manders co-localization values (277,278), we can see a strong correlation between RI and SCD1 in all infected cells (Figure 18B). However, cells high levels of RI (late infection) show very low levels of SCD1 (Figure 18C). Quantification of the mean fluorescent intensity in a representative image of these cells demonstrated an inverse correlation between levels of SCD1 and viral markers (Figure 18D, E). These data correspond with our findings of SCD1 expression and enzymatic activity, where Huh7 cells with high levels of RI at late time points of infection have reduced levels of SCD1. The initial spike in SCD1 activity from its localization around viral replication and assembly sites early during infection likely generates concentrations of oleic acid sufficient for the metabolic needs throughout replication. The specificity of the SCD1 antibody was tested in SCD1 siRNA-treated cells (Figure 19B, C). We did not see this distribution of SCD1 in DENV-infected A549 or human embryonic lung (HEL) cells. Rather we see a uniform co-localization of SCD1 and NS3 (Figure 19D, E). This suggests that changes in SCD1 expression levels are cell-type specific.

A.

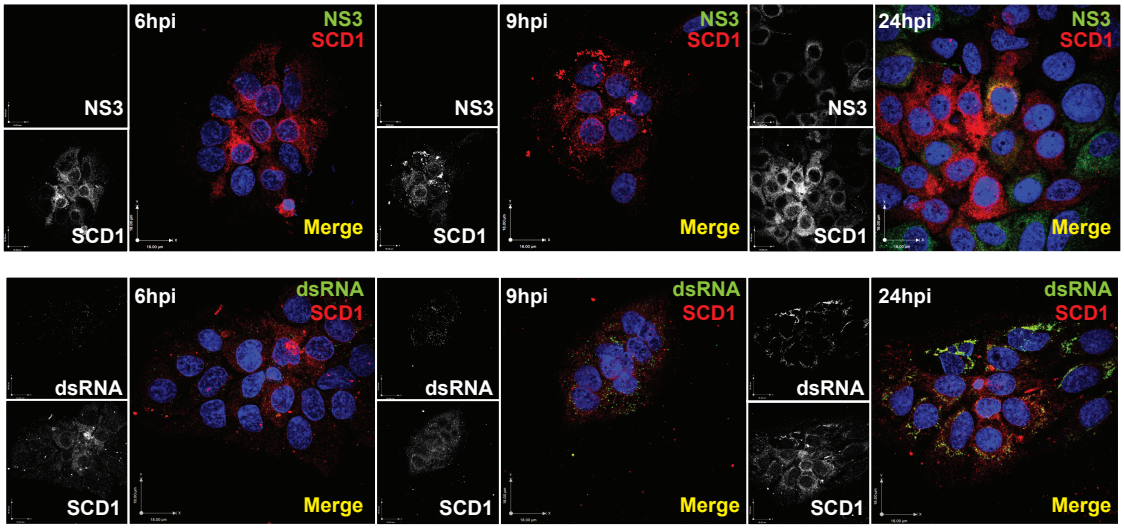

B.

	Cells with high RI	Cells with low RI	Uninfected
dsRNA intensity	11.099	1.854	0.259
SCD1 intensity	26.477	78.054	232.247
Pearsons Correlation	0.271	-0.0555	-0.0088
Colocalization of SCD1 with dsRNA (Manders 1)	0.156	0.0031	0.0005
Colocalization of dsRNA with SCD1 (Manders 2)	0.72	0.675	0.189

C.

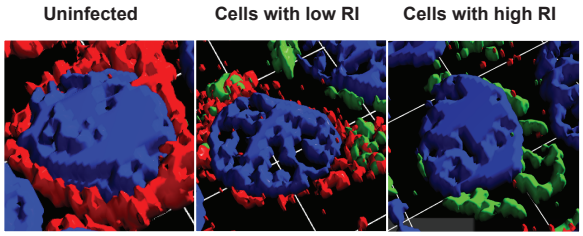

D.

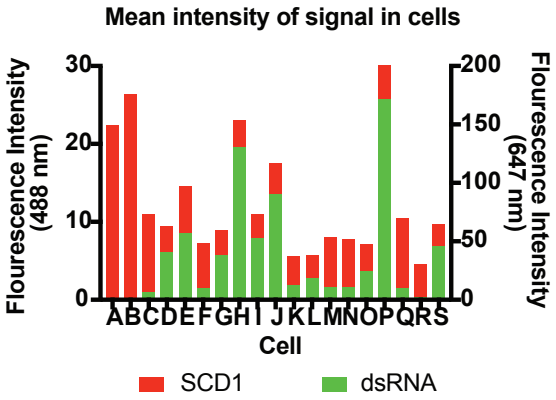

E.

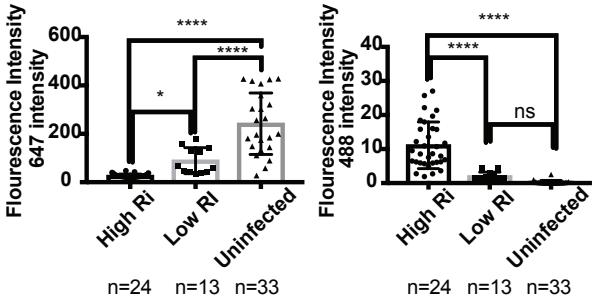

Figure 18 SCD1 protein expression is modulated with viral load. (A) Immunofluorescence analysis of Huh7 cells uninfected or infected with DENV2 at three time points. Viral protein NS3 or dsRNA (488nm, green), SCD1 (647nm, red). (B) Cells were classified as uninfected, low viral load or high viral load based on their dsRNA (488 nm, green) signal. A summary of the mean intensities of dsRNA and SCD1 in the 3 cell populations with co-localization coefficients: Pearsons global correlation and Manders correlation M1 and M2. (C) 3-D reconstructions of 3 representative cells at 24 hr showing dsRNA and SCD1. (D) Mean fluorescent intensity of dsRNA and SCD1 signals was measured in each cell of a representative image frame at 24 hr. (E) Mean fluorescent intensity of each cell in multiple images was averaged. The average 488 nm (dsRNA, green) signal and 647 nm (SCD1, red) signal for each group of

cells are plotted here. (ns=not significant, **=p<0.005, ***=p<0.001, ****=p<0.0001, from a one-way ANOVA with a multiple comparisons tests), hpi: hours post-infection.

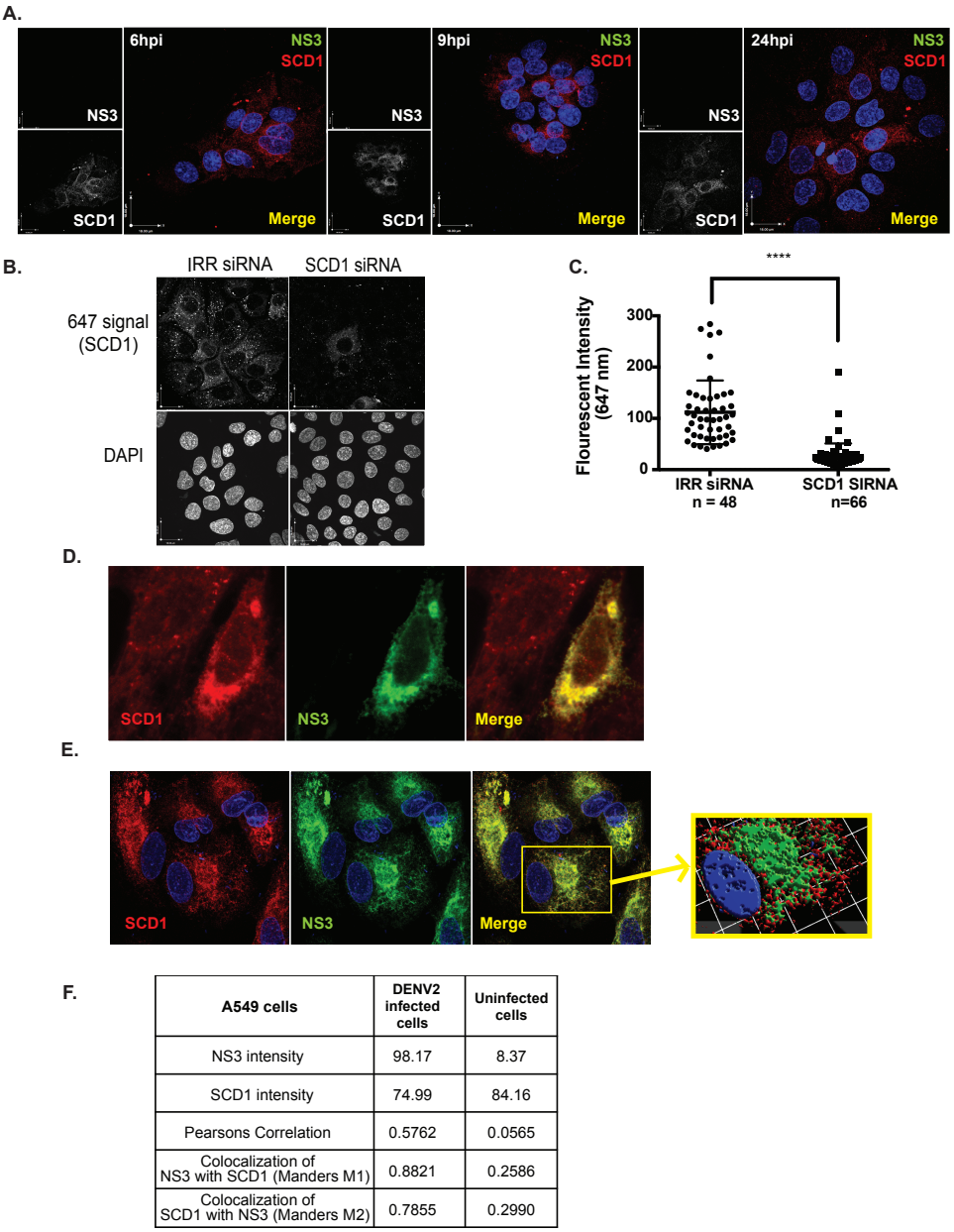

F.

A549 cells	DENV2 infected cells	Uninfected cells
NS3 intensity	98.17	8.37
SCD1 intensity	74.99	84.16
Pearsons Correlation	0.5762	0.0565
Colocalization of NS3 with SCD1 (Manders M1)	0.8821	0.2586
Colocalization of SCD1 with NS3 (Manders M2)	0.7855	0.2990

Figure 19 NS3 co-localizes with SCD1 in certain cell types. (A) Huh7 cells were mock infected and fixed in ice-cold methanol at the indicated time points. Cells were permeabilized and probed with the indicated antibodies. (B) Huh7 cells on cover slips were transfected with an irrelevant (IRR) siRNA or one specific for SCD1 and fixed after 48 hr to ensure complete degradation of SCD1 mRNAs and turnover of the SCD1 protein. Cells were then permeabilized and probed for SCD1 with an Alexafluor 647 secondary antibody. The 647 signal is shown in the top two panels with DAPI in the bottom panels. (C) The signals from these cells were quantified and we see less 647 signal in cells treated with the SCD1 siRNA. An unpaired t-test showed a significant difference with p<0.05. (D) and (E) Human embryonic lung (HEL) cells and A549 cells were infected with DENV for 36 and 24 hr respectively and processed similarly to A. Inset shows a 3-D reconstruction of a infected A549 cell. (F) Quantification of signals and

co-localization coefficients of A549 cells. In both cell types uninfected cells show expression of SCD1, but infected cells show accumulation at perinuclear sites. (****=p<0.0001), hpi: hours post-infection

Inhibition of SCD1 disrupts replication of all DENV serotypes and other enveloped viruses

We used a pharmacological inhibitor to characterize the enzymatic requirement for SCD1 during DENV2 replication. The piperidine-aryl urea-based inhibitor, A939572, which we will refer to as the SCD1 inhibitor, has been shown to be effective (279). We tested the SCD1 inhibitor in our activity assay and found that it abolished the formation of oleic acid (Figure 20A). In DENV-infected cells, SCD1 inhibition resulted in a dose-dependent reduction in viral titers (up to 2 logs) without toxicity (Figure 20B). Analysis of the effectiveness of the SCD1 inhibitor as an antiviral compound gave a therapeutic index of 2.1. The SCD1 inhibitor was also effective against DENV2 replication in A549 cells but it had no effect on mosquito cells (Figure 21A, B), suggesting that the Δ9 desaturase in arthropods may differ from the mammalian version.

Inhibition of SCD1 halts the desaturation of stearic acid (C18:0), acid leading to a decrease in cellular concentrations of oleic acid (C18:1). Oleic acid is a key building block for more complex phospholipids, cholesterol esters and triglycerides that function as constituents of cellular and virus-induced membranes. We hypothesized that addition of exogenous oleic acid would rescue the effect of SCD1 inhibition on virus replication. To accomplish this we added oleic acid conjugated to BSA in serum free medium combined with the SCD1 inhibitor and measured viral replication. We found that addition of oleic acid restored viral replication, implying that the product of SCD1 enzymatic activity is critical for DENV2 replication (Figure 20C). The rescue was not complete, likely because exogenous fatty acids have many destinations in the cell and are often shunted to β-oxidation (280). Therefore, they may be minimally incorporated into the ER where they could be used for virus replication.

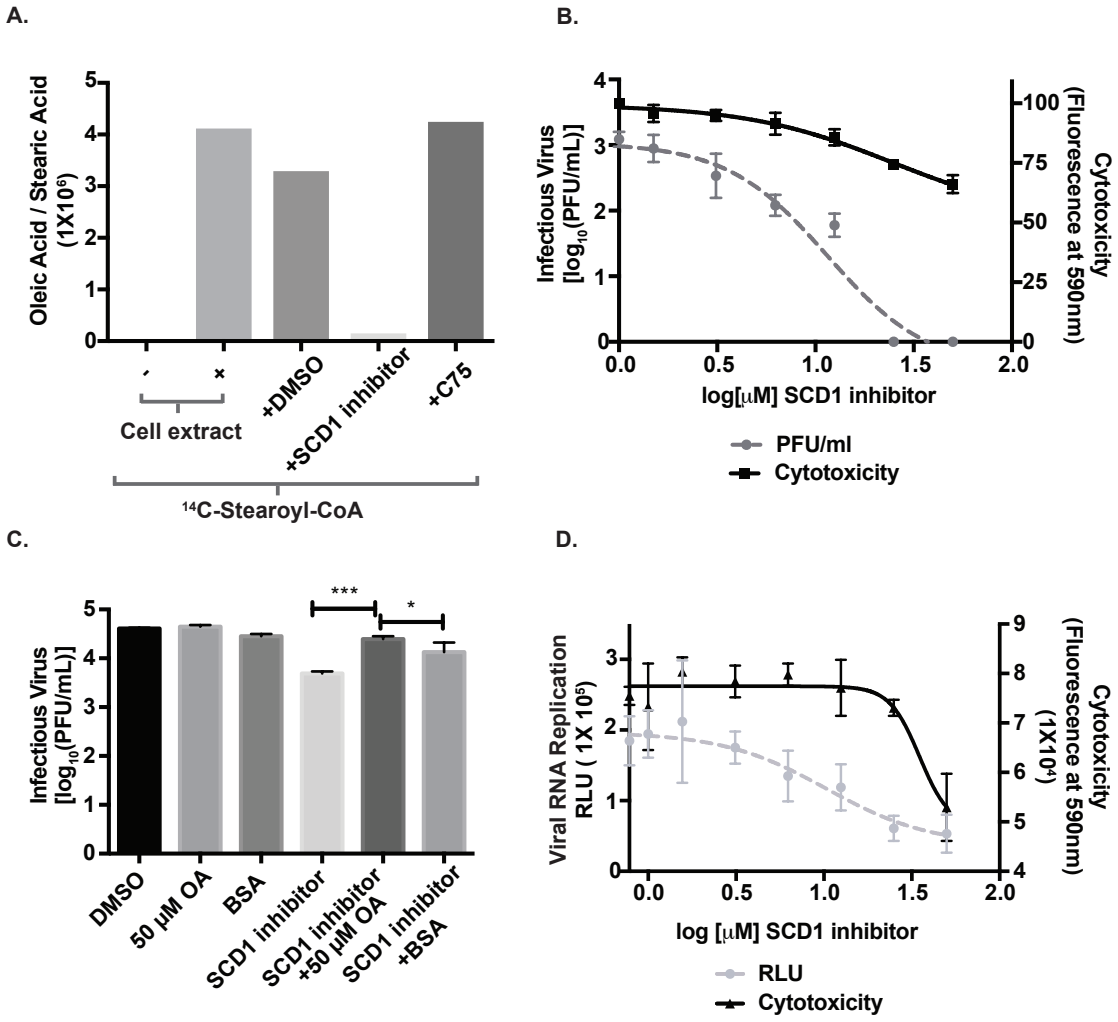

Figure 20 Oleic Acid supplementation following inhibition of SCD1 rescues viral replication. (A) The production of ^{14}C-labeled oleic acid and stearic acid in uninfected cell extracts were quantified and compared across indicated conditions. (B) Infectious virus release from Huh7 cells infected with DENV2 (MOI=0.5) and treated with the indicated concentrations of the SCD1 inhibitor for 24 hr. Cytotoxicity was also measured. (C) Huh7 cells were infected with DENV and treated with 10 μM SCD1 inhibitor and 50 μM oleic acid conjugated to BSA or indicated controls. At 24 hr post infection virus was collected and titrated by plaque assay. (D) Huh7 cells were electroporated with RNA from a DENV2 luciferase-expressing replicon and treated with the indicated concentrations of the SCD1 inhibitor. RLU and cytotoxicity was measured at 24 hr. (*=p=0.05, ***=p<0.001, from a one-way ANOVA with a multiple comparisons test).

Next, we tested the SCD1 inhibitor for its effects on the replication of other enveloped, mosquito-borne viruses. We used a non-cytotoxic concentration that was effective against DENV2 and found that the replication of all other DENV serotypes and Kunjin virus (KUNV),

yellow fever virus (YFV), Zika virus (ZIKV) and Sindbis virus (SINV) was significantly reduced (Figure 22A-D, I). To confirm that this was not due to off-target effects of the inhibitor, we knocked down SCD1 with siRNA and found similar effects on viral replication (Figure 22E-H, I). These data indicate a common need for SCD1 enzymatic activity and incorporation of MUFAs into complex lipid species to aid in the replication of enveloped viruses.

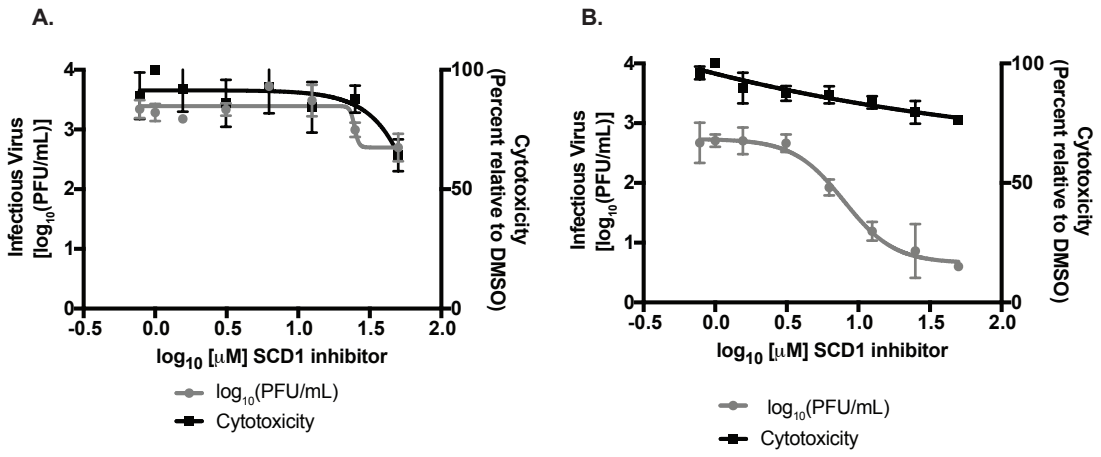

Figure 21 Inhibition of SCD1 in other cell types. A dose response curve of SCD1 inhibition of DENV2 replication in C6/36 cells (A) and A549 (B). Cells were infected with DENV2 (MOI=0.5) and treated with the indicated concentrations of the SCD1 inhibitor. Virus supernatant was collected at 24 hpi and quantified by plaque assay. Cytotoxicity was measured by the fluorescence of the reduction of resazurin to resorufin.

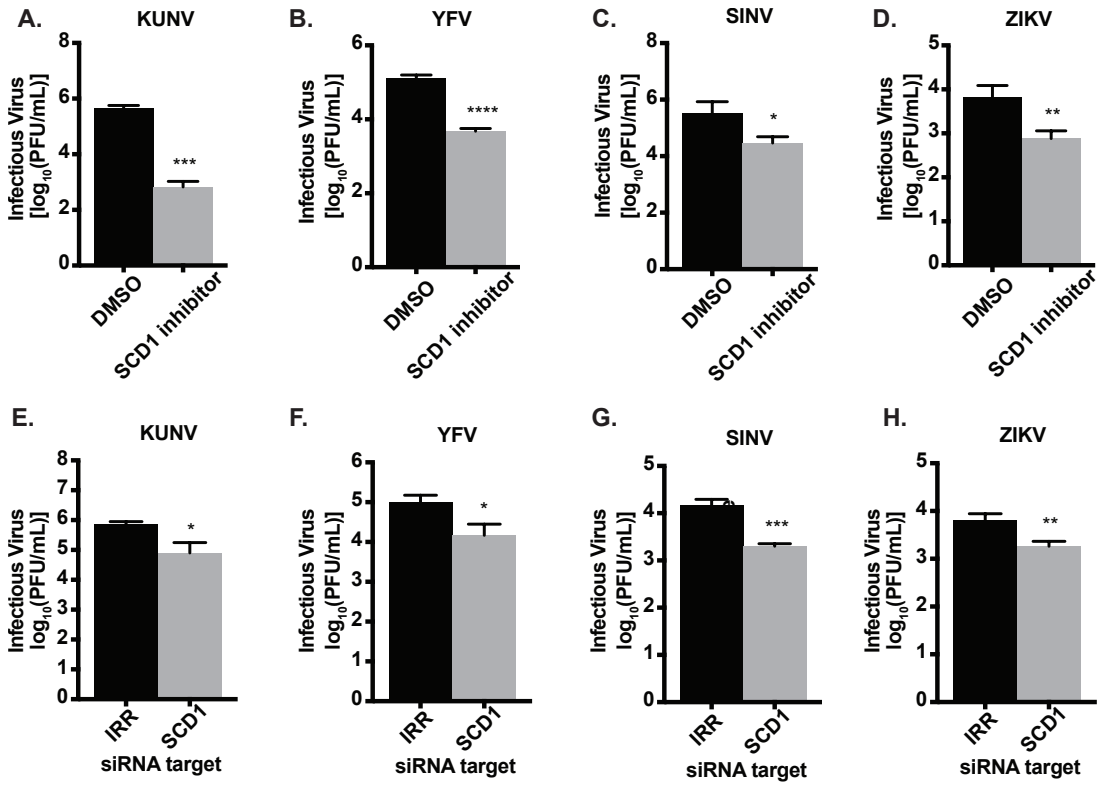

I.

	DENV1	DENV3	DENV4
Fold reduction with inhibitor	19.94	172.86	9.34
p value	0.0049	0.0015	0.0191
Fold reduction with siRNA	12.25	12.00	9.46
p value	0.0056	0.0032	0.0003

Figure 22 Inhibition and knockdown of SCD1 reduces replication of multiple enveloped viruses. Huh7 cells were infected with (A). KUNV (MOI=0.1), (B). YFV (MOI=0.1), (C). SINV (MOI=0.01) or (D). ZIKV (MOI=0.5) and treated with 10μM of the SCD1 inhibitor or DMSO. (E-H). Huh7 cells were transfected with IRR or SCD1 specific siRNA and infected after 48 hr of knockdown with (E). KUNV (MOI=0.1), (F). YFV (MOI=0.1), (G). SINV (MOI=0.01) or (H). ZIKV (MOI=0.5). Supernatants were collected at 24 hr post infection for KUNV, YFV and ZIKV, and at 8 hr post infection for SINV according to the time point for maximum viral replication. Virus release was quantified by plaque assay on BHK cells. I. Summary of results for DENV serotypes 1, 3 and 4. Inhibitor and siRNA analyses were done similar to the previous experiments. Unpaired t-tests were performed for all experiments indicating significant reduction in viral replication with inhibition or knockdown of SCD1. (*=$p<0.05$, ***=$p<0.0005$, ****=$p<0.0001$) compared to control)

SCD1 activity is critical for infectious virus release

Having determined that SCD1 is important for the DENV2 life cycle, we investigated its requirement at specific stages of viral replication. Using a viral replicon, we found that inhibition of SCD1 reduced DENV2 RNA replication (Figure 20D). Viral RNA replication and assembly are tightly coordinated (281). We examined the release of infectious virus particles by quantifying the intra- and extracellular virus at 24 and 48 hr post infection and found that intra- and extracellular virus from untreated cells had equivalent titers at 24 hr with an increase in extracellular virus titer at 48 hr (Figure 23A). However, virus grown in the presence of SCD1 inhibitor lagged in release of extracellular infectious virus compared to intracellular virus at 24 hr. Titers reached equivalence at 48 hr but were below those of untreated controls (Figure 23A). Three-way ANOVA confirmed a significant interaction between inhibitor treatment and intracellular vs. extracellular virus location (Figure 23B; $p=1.600e-06$ for the interaction term). These analyses indicate that inhibition of SCD1 affects the release of infectious virus.

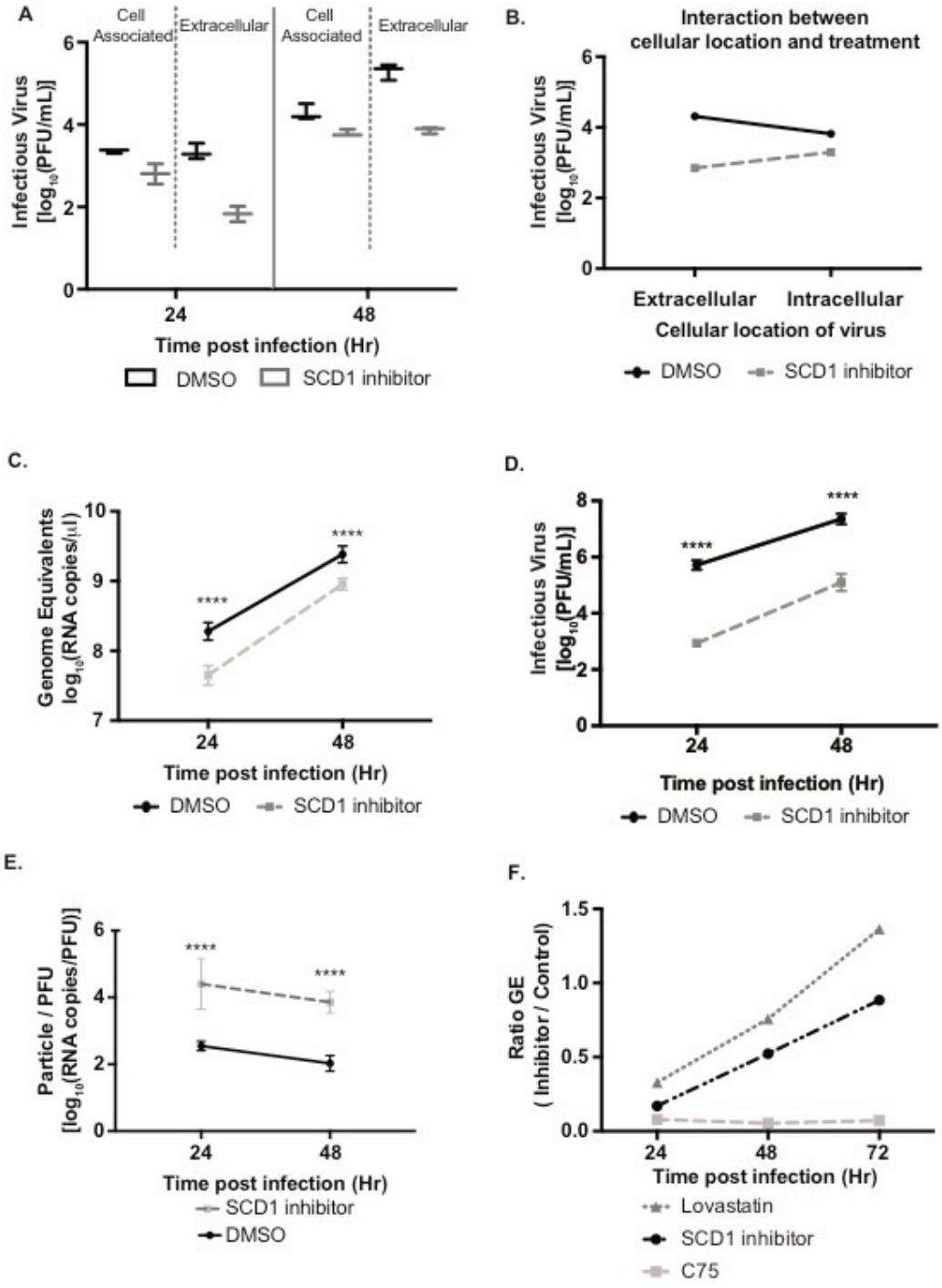

Figure 23 Inhibition of SCD1 impacts viral particle infectivity. Huh7 cells were infected with DENV2, MOI=1 and treated with SCD1 inhibitor or DMSO. (A) Virus in supernatants (extracellular) and cell-associated virus were collected at 24 and 48 hr and quantified by plaque assay. (B) Statistical interaction plot of data from A. The non-parallel lines indicate interaction between the cellular location of the virus and the treatment. A three-way ANOVA confirmed this interaction with a p=1.600e-06. C-E. Huh7 cells

were infected with DENV2 and treated with the SCD1 inhibitor or DMSO. Supernatants were collected at 24 and 48 hr. Virus was quantified by plaque assay. Virus RNA was extracted from the same samples for qRT-PCR analysis. (C) GE were determined by qRT-PCR using a standard curve of viral RNA copies. (D) The titer of the viruses at each time point as determined by plaque assay. (E) The particle:pfu ratio was calculated by dividing the RNA copies/mL by the PFU/mL from C and D. (F) Comparison of GE in cells treated with the SCD1 inhibitor to those treated with lipid synthesis inhibitors, C75 and Lovastatin. [Inhibitor: (Genome equivalents/mL) / DMSO: (Genome equivalents/mL)]. (****=$p<0.0001$). GE: Genome equivalents.

We next investigated the effect of SCD1 inhibition on the ratio of infectious and non-infectious virus particles released. We measured the ratio of total particles released to infectious-particles released (the specific infectivity) for virus grown in cells exposed to the SCD1 inhibitor compared to untreated cells. We found a small but significant reduction in total particles released from SCD1-inhibited cells as measured by genome equivalents (GE) (Figure 23C). However, the titer of infectious particles (as measured by plaque assay) was reduced at both time points by almost 100-fold, similar to our previous results (Figure 23D), and indicated a reduction in the specific infectivity of virus released from inhibitor-treated cells (Figure 23E). Hence, when cells are treated with the SCD1 inhibitor, the total numbers of viral particles released was only slightly lowered compared to control cells, but fewer of these viral particles were infectious (Figure 23C-E). Similar results were observed for Zika virus released from Huh7 cells treated with the SCD1 inhibitor (data not shown). This was not observed in C6/36 mosquito cells treated with SCD1 inhibitor (Figure 24A). The DENV2 GE in virus particles released from SCD1 inhibitor-treated Huh7 cells were compared to GE from cells treated with two other lipid synthesis inhibitors, C75 (inhibits FAS) and Lovastatin (inhibits cholesterol synthesis) (Figure 23F), that had previously been shown to be effective against DENV2 (90,92,117).

We observed a defect in the release of infectious particles with all treatments (Figure 24B and C), however, C75 treatment resulted in a larger decrease in the GE ratio compared to the other treatments (Figure 23F and compare 24D to 24E). FAS activity is critical for DENV2

genome replication (90), while cholesterol (altered by Lovastatin) is critical for maturation of DENV2 and generation of infectious particles (282). Inhibition of SCD1 was similar to inhibition of cholesterol biosynthesis (Figure 23 and 24), further demonstrating its significance in the virus life cycle.

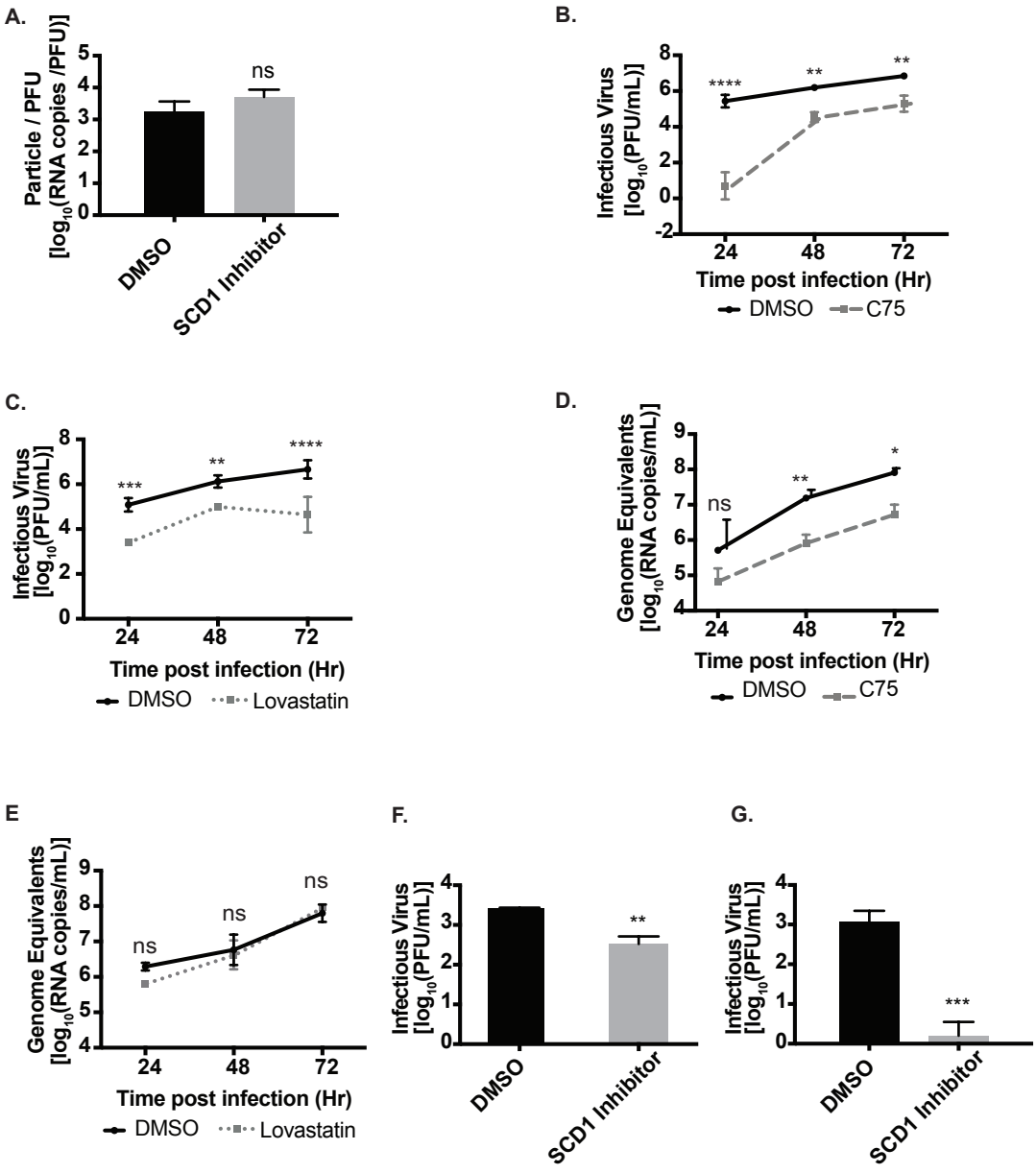

Figure 24 DENV2 treated with SCD1 inhibitor has a defect in infectivity in human cells but not mosquito cells. (A). C636 cells were infected with DENV2 and treated with the SCD1 inhibitor for 24 hr. Supernatant was collected and quantified by plaque assay. RNA was extracted and genome copies measured by qRT-PCR. (B-E). Huh7 cells were infected with DENV2 (MOI=0.5) and treated with C75 or

DMSO (B, D) or Lovastatin or DMSO (C, E). Supernatants were collected at the indicated time points and viral titer determined by plaque assay (B, C) or RNA was extracted and genome equivalents measured by qRT-PCR (D, E). (F) and (G). Cells were infected with DENV2 (MOI=3) and treated with 10μM SCD1 inhibitor. This virus was collected at 24 hr and subsequently used to re-infect new cells at MOI=0.1 in the absence of inhibitor. Supernatant was collected at 24 hr and viral titer determined by plaque assay. (F). Experiments in Huh7 cells. (G). Experiments in A549 cells. (ns=not signficant, *=$p<0.05$, **=$p<0.005$, ***=$p<0.0005$, ****=$p<0.0001$ compared to control)

Virion infectivity is altered following SCD1 inhibition

We evaluated the virions released from inhibitor-treated cells for defects in infectivity. DENV2 was passaged in Huh7 cells in the presence of the SCD1 inhibitor or DMSO, and released virus particles were collected, titrated, and used to infect new Huh7 cells in the absence of inhibitor (Figure 25A). During adsorption, the same concentration of inhibitor (10μM) was added to control supernatants to mimic remaining, un-metabolized inhibitor in the treated-cell supernatant. Virus isolated from inhibitor-treated cells had reduced infectivity compared to virus from control cells as determined by intracellular viral RNA (Figure 25B) and a reduction in released infectious virus (Figure 24F). This was confirmed in A549 cells (Figure 24G). To control for possible interference by defective particles in drug-treated cell supernatants, we UV-inactivated virus in supernatants from drug-treated and control cells and added it to equal titers of untreated virus stock to observe possible inhibition of infection. We found no difference in the resulting production of infectious virus, indicating that defective particles from cells treated with the SCD1 inhibitor did not interfere with subsequent virus infection (Figure 25C). Therefore, the defect in initiating a second round of infection is unique to virus particles released from cells lacking SCD1 activity.

We examined the early kinetics of viral infection with the virus from inhibitor-treated cells versus virus from control cells. We used a viral entry assay to determine the amount of virus internalized or endocytosed at given time points after attachment. Virus still external to the cell was inactivated at the indicated time point. The virus from cells treated with SCD1 inhibitor was

slower to enter new cells (0.133 PFU/min versus 0.243 PFU/min for the control virus; Figure 25D). This defect was found both in the rate at which virus entered cells as well as the number of virus particles that entered the cells at equal titer of infection. Inhibition of SCD1 lowers the quantity of and changes the characteristics of infectious particles. These data indicate that there is an attachment or fusion defect that is generated in cells with decreased SCD1 enzymatic activity.

To determine if the defect was in the physical structure of the virus particle (either the prM/E glycoprotein shell or virion lipid envelope) or in the genome encapsidated within virus particles released from SCD-inhibited cells, we isolated and transfected the RNA from these virus particles into BHK cells and measured the ability of the RNA to initiate infection. We found that both viral RNA populations were able to initiate infections with the same efficiency (Figure 25E).

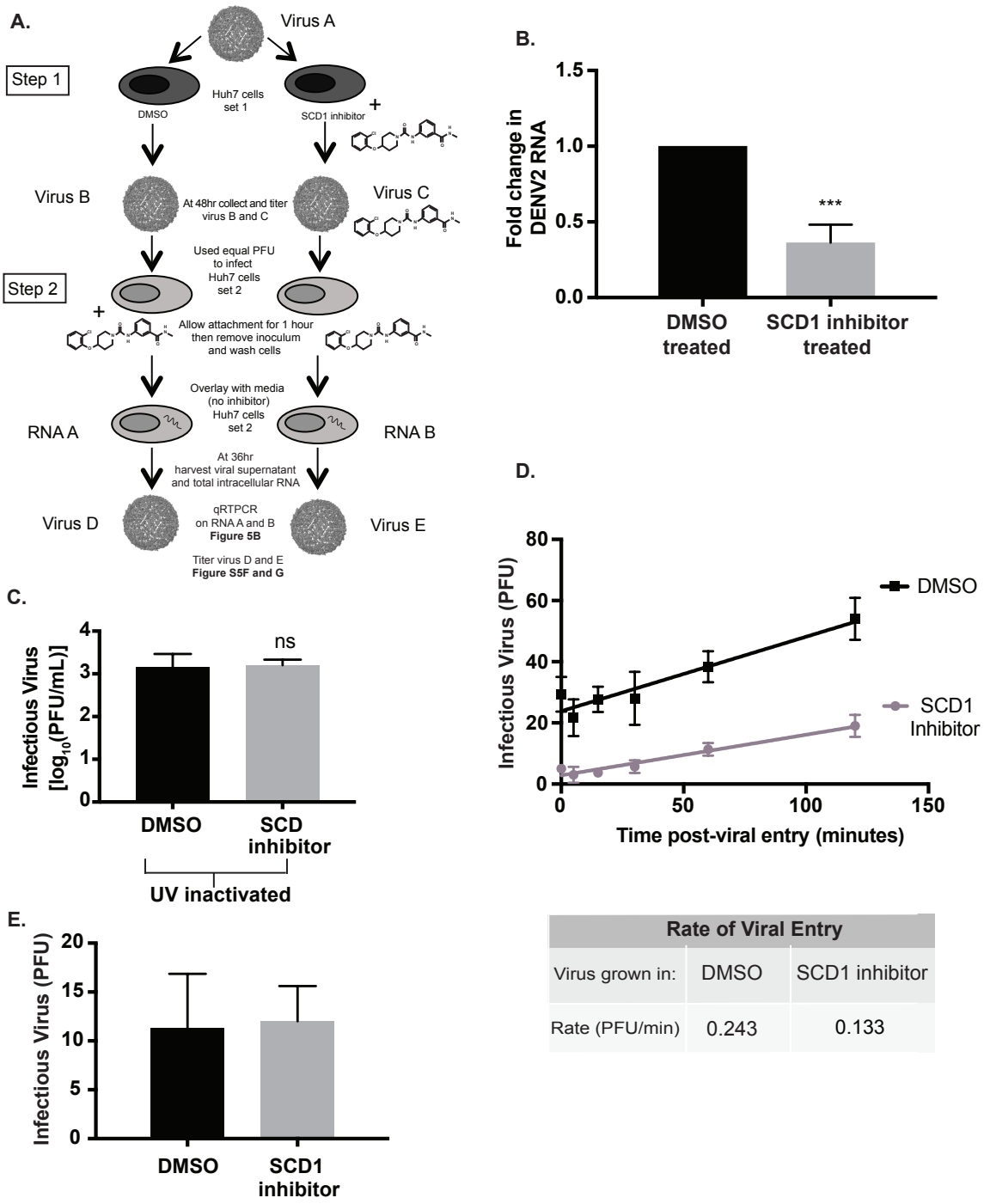

Rate of Viral Entry		
Virus grown in:	DMSO	SCD1 inhibitor
Rate (PFU/min)	0.243	0.133

Figure 25 Infectious particles grown in the presence of the SCD1 inhibitor are slower to infect new cells. (A) Schematic of the experimental design: Step 1: Huh7 cells (set 1) were infected with DENV2, MOI=3 (Virus A) and treated with DMSO or the SCD1 inhibitor. At 48 hr the virus was titrated (Virus B and C). Step 2: This virus was used to infect naïve Huh7 cells (set 2) at a MOI of 0.1. The concentration of inhibitor remaining in viral supernatant C was mimicked by adding inhibitor to viral supernatant B during attachment. Cells were washed and overlaid with media without inhibitor and incubated for 36 hr. Total RNA (RNA A and B) and virus supernatant (Virus D and E) were collected. (B) Viral RNA copies (RNA A and B) from Huh7 cells (set 2) were measured by qRT-PCR. The fold change of viral RNA

copies in RNA B compared to RNA A is shown. (C) Supernatants were collected from DENV-infected cells with or without the inhibitor and UV-inactivated. WT DENV2 was then diluted in these UV-treated supernatants and used to infect new cells with an equal MOI. (D) Virus grown with the SCD1 inhibitor was again titrated and used to infect BHK cells with 100pfu/well. Attachment was allowed to occur at 4°C for 2 hr, the temperature was shifted to 37°C and the cells were treated with acid glycine at the indicated time points after infection to inactivate un-internalized virus. Cells were overlayed with agarose and plaques were counted at 6 days. A linear regression was performed. The slope of the entry of the virus grown in the presence of the SCD1 inhibitor was 0.133 PFU/min and DMSO was 0.243 PFU/min. (E) Huh7 cells were infected with DENV2 (MOI=3) and treated with SCD1 inhibitor or DMSO. Supernatants were collected at 48 hr, RNA was extracted, viral RNA copies were measured by qRT-PCR. Equal RNA copies were transfected into BHK cells to allow plaques to form. (ns=not significant, ***=$p<0.001$, from a two-tailed t-test).

Inhibition of SCD1 results in release of immature virions

These data suggest that there is a change to the physical structure of the virion when it is released from cells lacking SCD1 activity. We initially tested if the virions were less thermally stable when grown in the presence of the SCD1 inhibitor compared to controls. The virus from SCD1-inhibitor treated and control-infected cells were diluted to the same infectious virus concentration, heated to the indicated temperatures (Figure 26A), and titrated. Nonlinear regression demonstrated that the control virus lost infectivity at 44.03°C and the SCD1 inhibitor-treated virus lost infectivity at 43°C. An F-test to determine the difference between the two models indicated no significant difference (Figure 26A). We also carried out freeze/thaw cycles on virus samples and measured infectivity and found that control virus maintained its infectivity for 6 or more freeze/thaw cycles, but virus grown in the presence of the SCD1 inhibitor lost its infectivity after 3 freeze/thaw cycles (Figure 26B). This effect was also observed with Zika virus grown in the presence of the SCD1 inhibitor (data not shown). We limited the defect in SCD1 inhibitor-treated virus infectivity to the structure of the virion envelope, which is more susceptible to freeze-thaw transitions than the control.

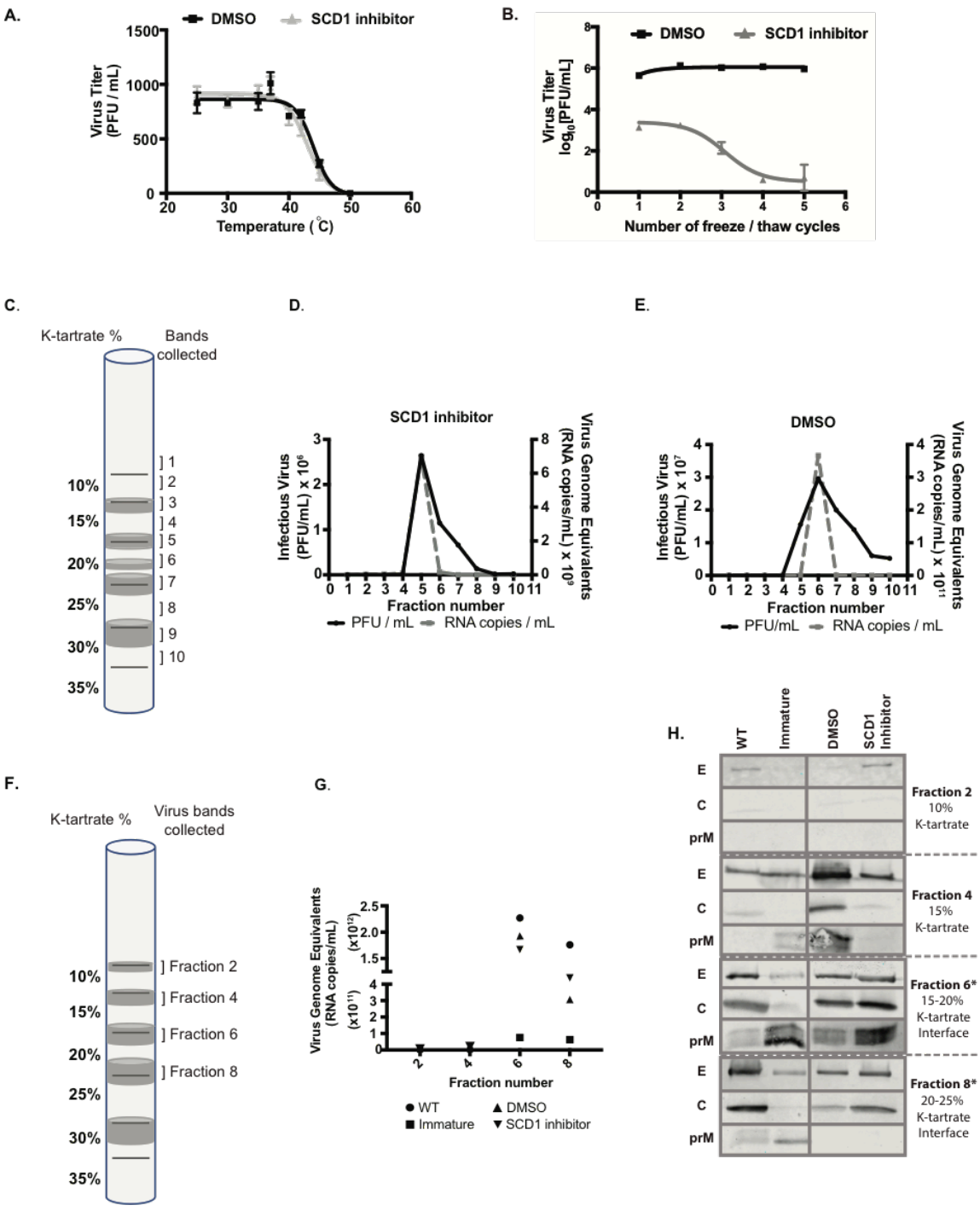

Figure 26 Characterization of virus grown in the presence of SCD1 inhibitor. Huh7 cells were infected with DENV2 and treated with the SCD1 inhibitor or vehicle. Supernatant was collected at 24 hr and the viral titer quantified by plaque assay. (A) The virus was then diluted to 1000 pfu/ml and subjected to the indicated temperature for 15 minutes. The virus was allowed to recover at room temperature and then used to infect BHK cells. Plaques were counted and the PFU/mL was calculated. (B) The indicated virus samples were subjected to freeze/thaw cycles. Virus was thawed, titrated on BHK cells and returned to -80°C until frozen. This cycle was repeated 5 times. A linear regression was performed and the control

samples yielded a slope of 0.06 that was not significantly different from zero, while the SCD1 inhibitor samples yielded a slop of -0.75 that significantly deviated from zero with p=0.02. (C-H). Huh7 cells were infected with DENV2 and left untreated (WT), treated with 20mM NH4Cl (immature), 10mM SCD1 inhibitor or vehicle (DMSO). (C-E). Virus grown with the SCD1 inhibitor or DMSO was collected at 24 hr, concentrated through a sucrose cushion and run on a K-tartrate gradient. (C). Ten fractions were collected (labeled 1-10). Distinct bands observed are shown in grey. The virus in each fraction from DMSO (D) or SCD1 inhibitor treated samples (E) was titrated (black) and RNA from each fraction was extracted to measure genome equivalents (grey). (F-H). Virus supernatant was also collected at 72 hpi, PEG precipitated, concentrated through a sucrose cushion, and purified on a K-tartrate gradient. (F). Distinct bands (fractions 2, 4, 6 and 8) where virus was observed (grey) were concentrated, and buffer exchanged. (G). RNA was extracted from these bands to measure genome equivalents and (H). Western blots performed to probe for envelope, capsid and prM viral proteins. *These data (for fractions 6 and 8) were also shown in Figure 27.

During infection, cells produce a range of structurally diverse particles with varying levels of infectivity. The main structural classes are immature, partially mature or fully mature and they are defined by the amount of uncleaved prM protein retained on the virion (283,284). Although the precise role of these various particles in the infectious cycle and immune modulation is not well understood, we sought to determine whether virions grown in the presence of the SCD1 inhibitor had uncleaved prM protein similar to immature virus. We purified viruses from Huh7 cells infected with DENV2 at an MOI=3 under four conditions: untreated (WT), immature virus (treated with 20mM NH_4Cl), and virus from cells treated with the SCD1 inhibitor or with vehicle (DMSO). Virus from DMSO or SCD1 inhibitor-treated cells at 24 hpi were pelleted through a sucrose cushion and purified by sedimentation velocity in a potassium tartrate step gradient. Visible bands (Figure 26C) were analyzed for viral RNA and infectious virus. A majority of the viral RNA and infectivity from both treatments sedimented in fractions 5-7 (Figure 26D and 26E). To characterize the physical properties of the virus particles in each gradient we collected and similarly processed cell culture supernatants from all four conditions at 72 hpi, a time-point with sufficient virus for purification and analysis. The bands observed in gradients for all samples were similar to those obtained from the gradient analysis of virus harvested at 24 hr with the exception of the top band (fraction 2 at the top of the 10%

interface) that was more prominent after 72 hr, indicating the presence of low molecular weight material (Figure 26F). We collected each band separately and characterized them for viral RNA (Figure 26G), prM, capsid and envelope proteins (Figure 27A, B, and 26H). Quantification of the western blots is shown in Figure 27C-F. The WT virus primarily sedimented at the 15-20% interface (fraction 6) and the 20-25% interface (fraction 8). Both of these fractions had similar levels of viral RNA. Typically, DENV2 purified from mosquito cells sediments in the 20-25% fraction, which was the primary fraction previously used for structure elucidation (37). DENV2 produced in Huh7 cells show differences in sedimentation profiles. Immature virus sedimented at the same densities as WT virus (fractions 6 and 8) and showed the expected enrichment in prM protein compared to envelope protein (Figure 27C and D, fraction 6), but had less capsid protein compared to the WT virus. The virus isolated from SCD1 inhibitor-treated cells showed similar patterns of enrichment of the prM protein as the immature virus, and this enrichment was confined to the virus population in fraction 6 (Figure 26F and H). The virus population that sedimented in fraction 8 had no detectable prM. The virus isolated from vehicle-treated (DMSO) cells that sedimented in fraction 6 had a similar protein content to WT virus, but there was a prominent population that sedimented in fraction 4 that did not have high GE (Figure 26G). Based on these analyses, the fractions with the highest GE (fractions 6 and 8) demonstrated the clearest differences between the four conditions. The virus isolated from SCD1 inhibitor-treated cells was similar to immature virus in prM content and was distinctly different from WT virus.

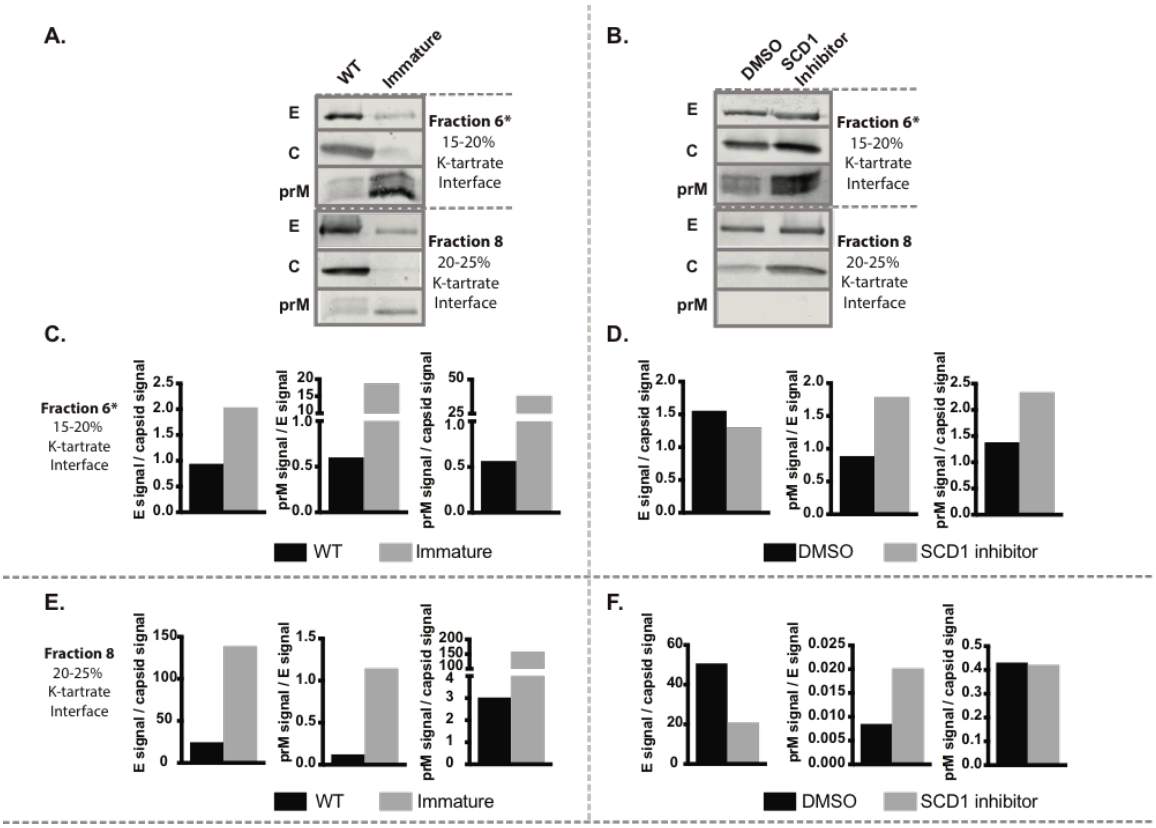

Figure 27 Inhibition of SCD1 Impairs viral maturation. Huh7 cells were infected with DENV2 and left untreated (WT), treated with 20 mM NH_4Cl (immature), 10 μM SCD1 inhibitor, or vehicle (DMSO). (A) and (B). At 72 hpi virus purified by density gradient sedimentation. Bands (fractions 6 and 8) where the highest concentration of genomes were observed (and previously known to have virus particles) were buffer-exchanged, concentrated and processed by western blot with antibodies for envelope, capsid and prM proteins. (C-F) The relative quantification of the viral glycoproteins prM and E in fractons 6 and 8.

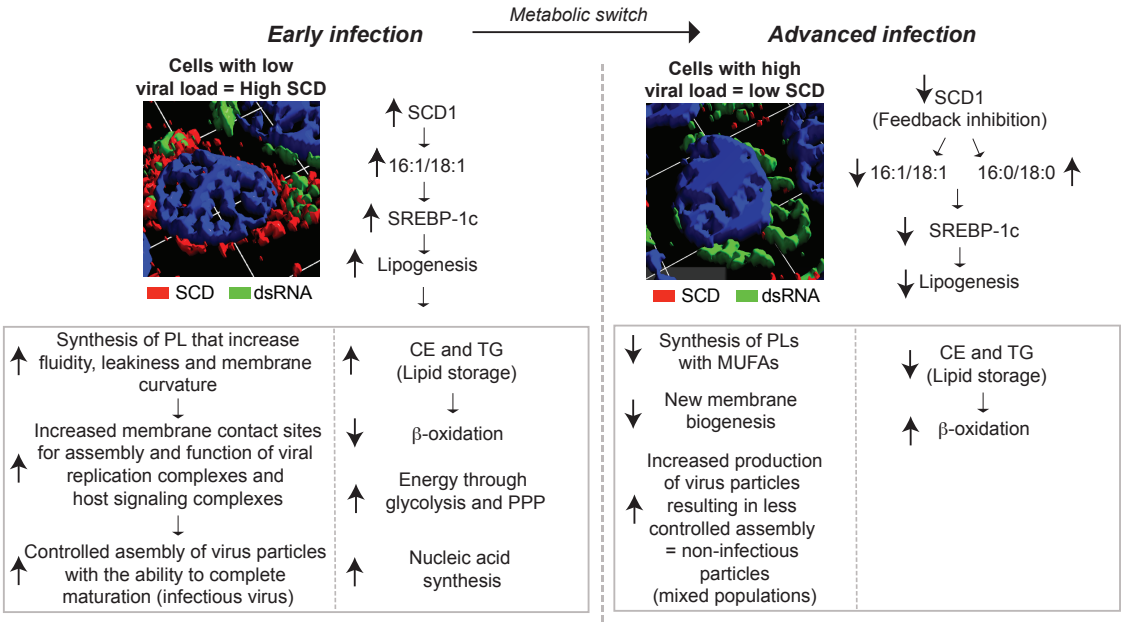

Figure 28 Stearoyl-CoA desaturase 1 is a metabolic switch that defines early and advanced dengue virus infections. A proposed model for a 'metabolic switch' involving SCD1 that differentiates the metabolic state in early versus advanced DENV2 infections. E: envelope protein, c: capsid protein, prM: pre-membrane protein, CE: cholesterol Esters, TG: triglycerides

3.3 Discussion

Previously we showed that lipid biosynthesis was upregulated in DENV-infected cells through the activation and relocalization of fatty acid synthase (FAS), an enzyme critical to the production of palmitic and stearic acids that are structural components of complex lipids (90). Here, we investigated the next step following FAS-catalyzed fatty acid production in the lipid biosynthesis pathway and demonstrated that desaturation of these fatty acids plays a critical role in the viral life cycle. Specifically, DENV2 infection resulted in upregulated monounsaturated fatty acid (MUFA) biosynthesis, catalyzed by SCD1 at early time points post-infection. Inhibition of this process impaired virion maturation and particle infectivity and stability.

Two distinct scenarios were observed (quantitatively and visually) in this study: early during infection when low levels of viral RNA and protein were present, SCD1 transcripts, protein and enzymatic activity levels were elevated. However, late during infection, when high concentrations of viral RNA were present, SCD1 mRNA, protein and activity levels declined. As summarized in Figure 28, we hypothesize that the metabolic environment required to progress from early to advanced infections changes and SCD1 activity could function as a 'metabolic switch' to modulate these changes. For instance, at early stages of viral RNA replication, increased amount of fatty acids, specifically MUFAs, are generated (through activity of SCD1) for construction of virus replication compartments. The unique architecture of positive-strand RNA virus replication compartments likely requires certain lipid components that can induce membrane curvature to provide extensive membrane contact sites and increased fluidity and leakiness to acquire substrates for genome replication (29,272–274). Energy and lipid substrates are provided by increased glycolysis and activation of the pentose-phosphate pathway (76). Increased SCD1 activity also results in the build-up of storage lipids, which reduces levels of β-

oxidation. The high content of MUFAs in the membranes (resulting from SCD1 activity) also ensures appropriate assembly and maturation of the virus particles being released during early infection. However, during advanced infections, when viral RNA replication is at maximum efficiency, the cell has excess complex fatty acids that feed back to inhibit SCD1 expression (285). By the time this occurs, the virus has already constructed its replication compartments and sites of assembly and does not require synthesis of new components by SCD1. At this later time point, the focus is on producing a massive explosion of virus particles from the already assembled viral replication factories. This massive output of virus compromises quality control and increases the probability of producing mixed populations (structurally diverse) of virus particles. In these advanced infections, the decrease in MUFAs through the inhibition of SCD1 negatively influences virus particle quality, resulting in the production of higher ratios of non-infectious particles.

Viral replication compartments are tightly coordinated with sites of virion assembly. For flaviviruses, only replicated viral RNA is packaged into newly assembled virions (286). Therefore, the lipid membrane environment surrounding viral RNA replication complexes and that involved in virion assembly must be physically coordinated to transfer newly replicated viral genomes to sites of virion assembly (29). Essentially, any lipid alterations that occur in these complex, virus-induced membranes must retain the capacity to support multiple functions. This is especially important since intracellular membranes become structural component of virus particles (virion envelope) that require assembly of a specific stoicheometry of viral glycoproteins. Conformational transitions that occur between these glycoproteins in lipid membranes define the state of maturation and infectivity of virus particles. Accordingly, we found that virion infectivity decreased when SCD1 was inhibited early in infection. At the given

dose of the SCD1 inhibitor, DENV2 was able to replicate and produce particles with intact genomes, however a higher proportion of these particles were non-infectious. We and others have provided evidence that SCD1 inhibition results in lowering MUFAs in cellular membranes. Our observations suggest that the physical properties of the virus envelope influenced by the proportion of MUFAs may be critical for virus infectivity.

DENV2 populations grown in the presence of the SCD1 inhibitor were found to be as stable to increased temperature as control virus, however, when the virus was subjected to multiple freeze-thaw cycles, it lost its infectivity faster than untreated virus. Inhibition of SCD1 results in changes in lipid content of the ER, resulting in an increase in saturated fatty acids (287,288). At lower temperatures, saturated fatty acids pack together tightly, forming a rigid membrane (289–291). Rigid membranes are not able to curve well and this may impair interactions with the trans-membrane glycoproteins (289,291). Hence we observed a greater loss of functionality or infectivity of viral particles from SCD1-inhibited cells when transitioning from freezing to ambient temperature versus transitioning from higher temperatures, where lipids may achieve greater fluidity (292).

The defect in infectivity of virus particles from SCD1-inhibited cells apparently resulted from incomplete particle maturation. After acquiring its ER-derived lipid envelope with inserted, stoicheometrically assembled prM and E glycoprotein heterodimers, the newly formed virions traverse the Golgi apparatus to complete a maturation process prior to exiting the cell. Maturation includes pH-dependent conformational transitions between the prM and E glycoproteins embedded in the envelope that are pre-requisite for the cleavage of the prM protein to M protein in mature virions by a Golgi-resident furin protease. If the conformational changes are inhibited or incomplete, furin cannot access the cleavage site on prM to complete the

maturation process. This results in prM retention on the virions; these virions are non-infectious. Based on our observations in this study, the virus requires MUFAs in its lipid envelope to allow the necessary structural transitions for virion maturation. SCD1 inhibition results in decreased proportions of MUFAs in intracellular membranes destined to become virion envelopes, resulting in impaired conformational shifts necessary for maturation and increased release of prM containing virions. We demonstrated that virions with higher prM content were defective in viral entry in subsequent infections. This establishes for the first time that lipids incorporated into the virion envelope are critical for particle infectivity.

Enveloped viruses must acquire their lipid envelope from a specific organelle membrane (120,122,293,294). Our data suggest that DENV2 assembly may occur preferentially and successfully at ER-membrane regions with a high content of MUFAs. Future research will explore the content of specific lipid species at sites of viral assembly and the consequences of their alterations. The lipid composition of the DENV2 virion is currently undetermined, thus the content of MUFAs in the infectious virion envelope is unknown. Studies of the lipid composition of other enveloped viruses have focused on lipid classes such as phospholipids and sphingolipids but have not looked at fatty acid content or saturation levels. However, it is clear that certain lipid species are enriched in viral envelopes and are functionally relevant for virion infectivity (1,100,124,125,295).

This study provides insights on how fatty acid biosynthesis, specifically unsaturated fatty acids impact flavivirus genome replication and assembly of infectious viral particles in human cells. It sheds light on host metabolic pathways that enhance viral replication success and provides a unique avenue for antiviral intervention.

3.4 Materials and Methods

Cells Lines:

The cell lines used were as follows: Human embryonic Lung epithelial cells (HEL 299) (ATCC CCL-137, male), adenocarcinomic human alveolar basal epithelial cells (A549) (ATCC CRM-CCL-185, male), C636 (ATCC CRL-1660, larva, sex unknown), Clone 15 (ATCC CCL-10) of the Baby Hampster Kidney Clone 21 cells (BHK-21), and Human hepatoma (Huh7) (From Dr. Charles Rice, sex unknown, (251). Huh7, HEL and A549 cells were maintained in Dulbecco's Modified Eagle Medium (DMEM) (Gibco, LifeTech), while BHK and C636 were maintained in Minimum Essential Media (MEM) (Gibco, LifeTech), both supplemented with 0.1 mM nonessential amino acids, and 0.1 mM L- glutamine, and 10% Fetal Bovine Serum (Atlas Biologicals) at 37°C with 5% CO_2.

Viruses:

The virus strains used are as follows: DENV1 (16007) (296), DENV2 (16681) (252,296), DENV3 (16562) (297–299), DENV4 (1036) (297), YFV 17D (300), and KUNV (301) these viruses were passaged in C6/36 cells. Additionally, ZIKA (PRVABC59) (302) was passaged in African Green Monkey Kidney Epithilial cells from the Vero lineage (Vero). A DENV luciferase reporter replicon containing only the nonstructural proteins was also used (90). Virus titers were determined by plaque assay on BHK cells as described previously (253). Infection of cells was carried out at room temperature for one hour to allow virus to adhere to cells. Virus was then removed, cells rinsed with 1XPBS, overlayed with the indicated media and transferred to the 37°C incubator for required periods of time.

RNA extraction and qRT-PCR:

RNA was extracted from cells using Trizol (ThermoFisher) and from virus in supernatant using Trizol LS (ThermoFisher). A one-step qRT-PCR kit with SYBR green from Agilent was used. Reactions were set up according to the manufacturer's protocol and run on a LightCycler 96 real-time PCR machine (Roche). The cycling parameters were: 20 mins at 50°C for reverse transcription, then 5 mins at 95°C followed by 45 two-step cycles of 95°C for 5 seconds and 60°C for 60 seconds. This was followed by a melt curve starting at 65°C and ending at 97°C. DENV primers (264) were used to quantify viral RNA copies in the supernatant as well as in cells. A standard curve of *in vitro* transcribed viral RNA from a DENV2 cDNA subclone was generated and used to quantify the genome copies in the supernatant (265). Copies of viral RNA in the cell as well as copies of SCD mRNA transcripts were both normalized to glyceraldehyde 3-phosphate dehydrogenase (GAPDH) RNA using the delta delta ct method (242). For this method: the fold change in gene expression = 2^(-(Infected samples((Ct value of gene of interest) – (Ct value of control gene)))–(Uninfected samples ((Ct value of gene of interest) – (Ct value of control gene)))). The Ct values were generated from the Light Cycler software and the gene of interest was either SCD1 or DENV and the control gene was GAPDH.

siRNA treatments and confirmation:

Cells were transfected with siRNAs using RNAiMax (Invitrogen) similar to previous experiments (90) and allowed to incubate for 48 hr. Cells were then infected with DENV2, or collected for knockdown confirmation or cytotoxicity tests (described below). Virus was collected and titrated with plaque assays. To confirm knockdown of mRNA transcripts RNA was extracted and qRT-PCR performed to measure SCD1 levels relative to GAPDH in SCD1 siRNA treated samples and compared to IRR treated samples using the delta delta ct method (242)

described above. To confirm knockdown of protein levels cellular protein was collected in radioimmunoprecipitation assay buffer (RIPA) [150 mM sodium chloride, 1.0% NP-40, 0.5% sodium deoxycholate, 0.1% SDS (sodium dodecyl sulfate), 50 mM Tris, pH 8.0]. and separated by electrophoresis on an SDS-Page gel. They were then transferred to a nitrocellulose membrane (Bio-Rad), blocked in 5% milk and probed with SCD N-20 (Santa Cruz Biotechnology) and β-actin (Cell Signaling Technology). Secondary antibodies were IRDye 680RD and IRDye 800CW (Li-Cor). The blot was imaged on an Odyssey IR Imaging system (Li-Cor) and quantification of the signals measured with Image Studio 5.2 (Li-Cor).

Inhibitors and fatty acid treatments:

The inhibitors used were A939572 (the SCD1 inhibitor, MedChem Express), C75 (Cayman Chemicals) and Lovastatin (Sigma-Aldrich). Each was diluted in DMSO, added to DMEM and filtered through a 0.2μM filter before being added to cells. Oleic acid was acquired from Sigma and came dissolved in bovine serum albumin (BSA) at 200mM. It was further diluted in 1% fatty acid free BSA (Gold Biotechnology) in 1x phosphate buffered saline (PBS) to 50 μM. Huh7 cells were infected with virus as described above and overlayed with the indicated treatments diluted in DMEM. Supernatants were collected at 24 hr and plaque assays performed. Cytotoxicity was measured with alamar blue (ThermoFisher) diluted 1:10 in DMEM incubated on cells for 2-4 hr and read on a Victor 1420 Multilabel plate reader (Perkin Elmer) with excitation at 560 nM and emission at 590 nM.

Re-infection Experiments:

Virus that was used for re-infection and entry assays was grown in Huh7 cells at an MOI of 3 in 10 μM SCD1 inhibitor or DMSO (0.02%). The virus samples were titrated by plaque assay and diluted to equivalent titers. The SCD1 inhibitor was added to the DMSO sample and

the virus samples (equivalent pfu/ml) were allowed to attach to new cells for 1 hr at room temperature before being removed. The cells were then washed with 1xPBS and incubated with DMEM + 2% FBS for the indicated times at 37°C.

Assay for viral entry:

Each virus was diluted to 1000 pfu/ml in DMEM. The SCD inhibitor was added to the virus that was grown in DMSO (0.02%) at 10 μM and then filtered. Virus was allowed to attach to BHK cells in 6 well plates for 2 hr at 4°C. The virus was then aspirated and cells were rinsed with 1XPBS to remove any unbound virus. The cells were then overlayed with MEM with 10% FBS and transferred to 37°C. At given time points after the temperature shift, cells were removed from the incubator rinsed with 1XPBS and treated with acid-glycine (8 g of NaCl, 0.38 g of KCl, 0.1 g of $MgCl_2$ $6H_2O$, 0.1 g of $CaCl_2$ $2H_2O$, and 7.5g of glycine/L, pH adjusted to 3 with HCl) for 1 minute at room temperature to inactivate any extracellular virus. The cells were again rinsed with 1XPBS and overlayed with 1% agarose and MEM with 5% FBS, plaques were counted at 6 days.

Immunofluorescence Assay:

Cells were grown on a sterilized cover slip and maintained in 10% DMEM. Cells were infected with DENV2 (M0I=100) or mock infected (1XPBS). Cells were fixed in ice-cold methanol (Fisher Chemical) at room temperature and permeabilized with 0.1% TritonX (Fisher Chemical) in 1XPBS with 1% BSA (GoldBiotech) at room temperature and blocked with 0.01% TritonX in 1XPBS with 1% BSA overnight at 4°C. Cells were then probed with the indicated primary antibodies including dsRNA (English and Scientific Consulting Bt.), NS3 (gifted by Richard Kuhn, Purdue University) and SCD N-20 (Santa Cruz Biotechnology). Secondary antibodies were Alexa-fluor 488 or 647. The coverslips were fixed to slides with FluoroSave

(Calbiochem) and imaged on an Olympus inverted IX81 FV1000 (Olympus) confocal laser scanning microscope with a 100x oil objective using FV10-ASW 4.2 (Olympus). Digital images were processed with Volocity 6.3 (Perkin Elmer) and colocalization coefficients calculated by encircling each individual cell and using the measurement function with internal thresholds. Values represent averages of at least 30 cells from different image frames of the same slide.

SCD Activity Assay:

The indicated cell samples were collected at given time points and prepared in order to preserve enzymatic activity (303). Briefly, cells were washed in the wash buffer (35 mM Hepes, pH 7.4, 146 mM NaCl, 11 mM glucose) 3 times, then incubated in a hypotonic solution (20 mM Hepes pH 7.4, 10 mM KCl, 1.5 mM MgOAc, 1mM DTT) for 20 minutes to allow the cells to swell. Then they were passed through the dounce homogenizer 25 times to break apart the membranes. A post lysis buffer (20 mM Hepes pH 7.4, 120 mM KOAc, 4mM MgOAc, 5 mM DTT) was added. Nuclei were spun down at 1000xg for 5 minutes at 4°C and the cytoplasmic extract was flash frozen in liquid N_2. Protein content was measured by BCA (Pierce) and equal protein content was used for activity assays. Activity assays were performed similar to previous studies (304). Briefly, 1.5 mg/ml protein was incubated with 0.01 μCi of stearoyl [1-14C]-coA (American RadioLabled Chemicals, 55mCi/mM) at 37°C for 5 minutes. The reactions were stopped by adding 150 μL of methanolic HCl (Sigma-Aldrich) for 1 hour at 72°C, which generated fatty acid methyl esters that were extracted from the samples in 1 mL of chloroform. One aliquot of these samples was measured on a Beckman LS 6500 liquid scintillation counter (Beckman) and equal counts were spotted on a 0.5% $AgNO_3$ impregnated normal phase thin layer chromatography plate. Fatty acids were separated by a mobile phase of hexane : acetone (50:1). Plates were exposed on a phosphoimager screen and scanned on a Typhoon Trio 9400

(GE Healthcare). Pixel intensity was measured with ImageQuant TL(GE Health Care) software. Standards were sprayed with 5% phosphomolibic acid in 100% ethanol and heated to visualize fatty acids.

Virus purification:

Virus purification and identification of prM were carried out similar to previous studies (37,305). Briefly, Huh7 cells were infected with DENV (MOI=3) and left untreated, treated with 10 μM of the SCD inhibitor or DMSO similar to other experiments presented here. The supernatant was collected at the indicated time points and was replaced with fresh DMEM plus the indicated treatment. At 24 hr after infection 20mM NH_4Cl was added to generate the immature virus samples. The supernatants from the SCD inhibitor and DMSO samples were collected at 24 hr. Cellular debris was removed from the supernatant and the virus was run through a 22% sucrose cushion at 32,000 xg for 2 hr at 4°C in a Sorvell WX ultracentrifuge (Thermo Fisher Scientific). The pellet was loaded onto a potassium-tartrate step gradient consisting of 10, 15, 20, 25, 30 and 35% potassium-tartrate in TNE buffer (50 mM Tris–HCl (pH 7.4), 100 mM NaCl, 0.1 mM EDTA) and spun at 32,000 xg for 2 hr at 4°C in a Sorvell WX ultracentrifuge (Thermo Fisher Scientific). Ten different fractions were collected from each gradient and used to titrate the virus and quantify viral genomes similar to other experiments. At 72 hr virus from all 4 samples were collected, cellular debris removed and virus was PEG precipitated at 4°C. The virus was then run through a 22% sucrose cushion and loaded onto a potassium-tartrate gradient same as mentioned above. Visible band of virus were noted in the gradients and the 4 fractions were collected and buffer exchanged with TNE buffer. Viral genome copies were measured with qRT-PCR. Protein content was measure with BCA (Pierce/Thermo Fisher) and equal amounts of protein were loaded on an SDS-page gel and

transferred to a PVDF membrane and probed for prM, capsid and E. Blots were imaged on an Odyssey and densitometric measurements were made. Western blots for each fraction (ie: fraction 6) had equal total protein loaded for the four conditions. Conditions between fractions cannot be compared due to differences in protein sedimentation between fractions (ie: total protein in fraction 6 cannot be compared to total protein in fraction 8).

Quantification and statistical analysis:

Results were expressed as mean values with standard deviation. The statistical details are noted in the figures and/ or in the corresponding figure legends. Statistical significance was primarily determined using either an unpaired Student's t-test or a one or two way Analysis of Variance (ANOVA) with a Bonferroni, Dunnets or Tukey's multiple-comparison depending on the experimental design in the GraphPad Prism version 7.00 for Mac OS x (GraphPad Software, La Jolla California USA). Drug inhibition studies were analyzed with a non-linear regression using GraphPad Prism version 7.00 for Mac OS x (GraphPad Software, La Jolla California USA) to calculate an IC50. The assay for viral release (Figure 23A) was analyzed with a 3-way ANOVA and included an interaction term for each. This was performed in R studio version 1.0.136 (306). Finally, the nonlinear regression models for the thermostability of the viruses (Figure 16A, B) was also performed in R studio version 1.0.136 (306). The model used was y=a+((b-a)/((1+10^((c-temp)*d))). An F-test was used to determine the difference between the curves with the formula $F=((SS_{total}-SS_{pooled}) / ((m+1)(K-1))) / (SS_{pooled}/df_{pooled})$. Each study shown is representative of at least two independent experiments.

Additional key resources are included in Supplementary Table 4.

CHAPTER 4. DEVELOPMENT OF A METABOLIC BIOSIGNATURE TO DIFFERENTIATE SEVERE AND NON-SEVERE DENGUE DISEASE AND CHIKUNGUNYA INFECTIONS

4.1 Introduction

Currently there are an estimated 400 million DENV infections each year (2,307). The diseases caused by dengue virus infection vary significantly; however, initial presentation is similar and clinically impossible to distinguish from other febrile illnesses (2,11,308,309). Diseases range from a mild febrile illness, dengue fever (DF), to advanced diseases such as dengue hemorrhagic fever (DHF) and dengue shock syndrome (DSS) (10,11). The recent emergence in the western hemisphere of chikungunya virus (CHIKV), an alphavirus transmitted by the same mosquito vector, has been an additional burden on health care systems (310). Initial presentation with CHIKV infection is indistinguishable from dengue diseases, yet it can progress to an advanced arthralgia (311).

Traditional diagnostic tools for dengue diseases involve virus isolation and serology. While state of the art, these techniques take time, give very little indication of disease severity and are not meeting the current needs (4,11,312). Predicting disease outcomes is a persistent challenge in health care, particularly in resource poor settings where allocation of limited resources is difficult, yet crucial to saving lives (313). Hence, broader diagnostic and prognostic tools are needed to deliver a clear assessment of the care needed. This will aid in proper allocation of limited resources for complex diseases.

Metabolites are the front line phenotypic indicators of underlying pathology. The accurate measurement of these molecules through techniques such as LC-MS/MS, can identify patterns of metabolites that unlock the mysteries of acute infections. In fact, metabolomics demonstrates promise in identifying small molecules associated with a variety of disease states (314).

The application of metabolomics to the field of dengue diseases is not new. Indeed, our group and others have identified many biomarkers with utility in predicting disease outcome (198,206,223,315–318). However, the field has yet to achieve consensus on a specific set of biomarkers and currently nothing is standardized nor used clinically. Much of this is due to the difficulty in rigorously narrowing down a specific set of metabolites that collectively can predict a disease outcome. Similar analysis and metabolite sets have been used in other fields to predict disease states (314,319).

Here we follow up our previous work profiling the serum metabolome of dengue patients (206). We have significantly expanded our sample size and identified a discrete set of well-defined metabolites capable of predicting disease in these patient samples. We used reverse phase-LC/MS to retrospectively characterize the serum metabolome of patients diagnosed as DF, DHF or DSS and compared the results to patient serum with CHIKV and non-dengue (ND) febrile diseases. We used least absolute shrinkage and selection operator (LASSO) predictive models to identify specific sets of metabolites that can distinguish severe dengue disease from non-severe as well as dengue diseases from non-dengue febrile diseases, and finally a set that can distinguish CHIKV from dengue. For each of these comparisons, we identified a discrete and manageable list of features, smaller than found in other studies. This is promising, since our ultimate goal is to translate small molecule biomarkers (SMB) to a clinical setting in a cost-effective manner. Furthermore, we used an integrated pathway and network analysis platform to annotate features and identify biochemical pathways dysregulated in these diseases. These sets of metabolites are a significant step forward in this field and show real promise for both understanding dengue disease pathology and allocating resources for effective treatment.

4.2 Results

Clinical Samples

For this study 535 serum samples were retrospectively obtained from 2 different well-established studies in Managua, Nicaragua (Table 5). One set was from a cohort study with over 3,000 initially healthy well-characterized children between the ages of 6 months and 15 years old. These patients were enrolled, followed over time and monitored for development of febrile diseases. To complement these samples, we also used serum samples from patients that presented at the Hospital Infantil Manuel de Jesús Rivera, the National Pediatric Reference Hospital in Nicaragua, with a fever or history of fever for <7 days and one or more of the following signs and symptoms: headache, arthralgia, myalgia, retro-orbital pain, positive tourniquet test, petechiae, or signs of bleeding. Patients who met the 1997 WHO case definition for dengue were used in our analysis (320). There was an outbreak of CHIKV in this area during the 2014-15 season. Therefore, we used serum samples from these patients to develop a biosignature that differentiates DENV from CHIKV disease. Additionally, we retrospectively tested the dengue negative samples from 2012-15 for CHIKV to ensure that samples were properly identified. Hereafter, we will use non-dengue (ND) for patients who had an undifferentiated fever and tested negative for dengue and CHIKV (if collected from 2012-2015).

Table 5 Serum specimens from two studies in Nicaragua used for metabolomics analysis.

Study	Days of fever			Sex		Clinical Diagnosis					Serotype		
	Total	Mean	range	Males	Females	DF	DHF	DSS	CHIKV	ND	1	2	3
Cohort	122	0.9	0-3	52(42.6%)	70(57.4%)	33	1	0	0	88	29	2	3
Hospital	413	2.7	0-6	226 (54.7%)	187 (45.3%)	152	43	22	47	149	73	88	27

All samples used for this study were collected during the acute stage of disease (0-6 days of fever). Diagnostic testing was carried out with RT-PCR and serology testing to identify dengue cases and when possible the serotype. All dengue positive cases were also classified with both the 1997 and 2009 WHO case definitions for dengue diseases. Here we use the 1997 definition of DF, DHF and DSS. Thus, our sample set was composed of 257 females and 278 males,185 DF, 44 DHF, 22 DSS, 47 CHIKV, and 237 ND patients from 2005- 2015 (Table 5). Details of DENV serotype and season are in Tables 6 and 7.

Table 6 The number of patient samples collected each year from 2005-2015 and their disease etiology.

Season	ND	DF	DHF	DSS	CHIKV	TOTAL
2005	11	8	3	1	0	23
2006	13	3	5	8	0	29
2007	1	8	3	11	0	23
2008	0	4	2	0	0	6
2009	1	4	0	0	0	5
2010	8	0	0	0	0	8
2011	9	0	0	0	0	9
2012	100	92	12	1	0	205
2013	78	66	10	1	0	155
2014	11	0	2	0	23	36
2015	5	0	7	0	24	36
TOTAL	**237**	**185**	**44**	**22**	**47**	**535**

Table 7 Dengue disease patients samples classified by serotype and dengue disease diagnosis.

Serotype	DF	DHF	DSS	TOTAL
1	91	10	1	102
2	45	24	21	90
3	23	7	0	30
NR	26	3	0	29
TOTAL	185	44	22	251

Biosignature Development

For the discovery phase of our analysis we used untargeted LC/MS data to characterize the global metabolic changes occurring with each disease state. Features were rigorously filtered for

robustness, and missing values were imputed using random forest imputation, with details given in the methods section. Our workflow to characterize these changes and identify a key set of metabolites is shown in Figure 29. For the statistical comparisons, we used linear models, implemented in the R package 'limma' (228,321), to compare molecular features (MFs) found in one disease group versus another with p-values adjusted to control false discovery rate at 0.05. The log fold change for each of these features was calculated and used as an initial portrayal of the data. MFs found in only one group were discarded for this initial discovery phase. Thus, we generated a list of 1493 significant (adjusted $p < 0.005$) molecular features differentiating ($\geq$ 2fold change in relative abundance) DEN and ND. Comparison of DF to ND, we found 27 features that increased, 15 that decreased and 1451 that remained unchanged. Comparing DHF cases to ND cases we found 28 features increased, 336 that decreased and 1129 that remained unchanged. Finally, comparing DSS to ND there were 169 features that increased, 1169 that decreased and 155 that remained unchanged (Figure 30). We see more features differing between the more severe form of dengue compared to ND, while the milder forms are metabolically very similar to ND diseases. A principle component analysis (PCA) demonstrates the ability of the significant features to separate the three diseases; the first two components accounted for 81.42% of variation in the data (Figure 31A).

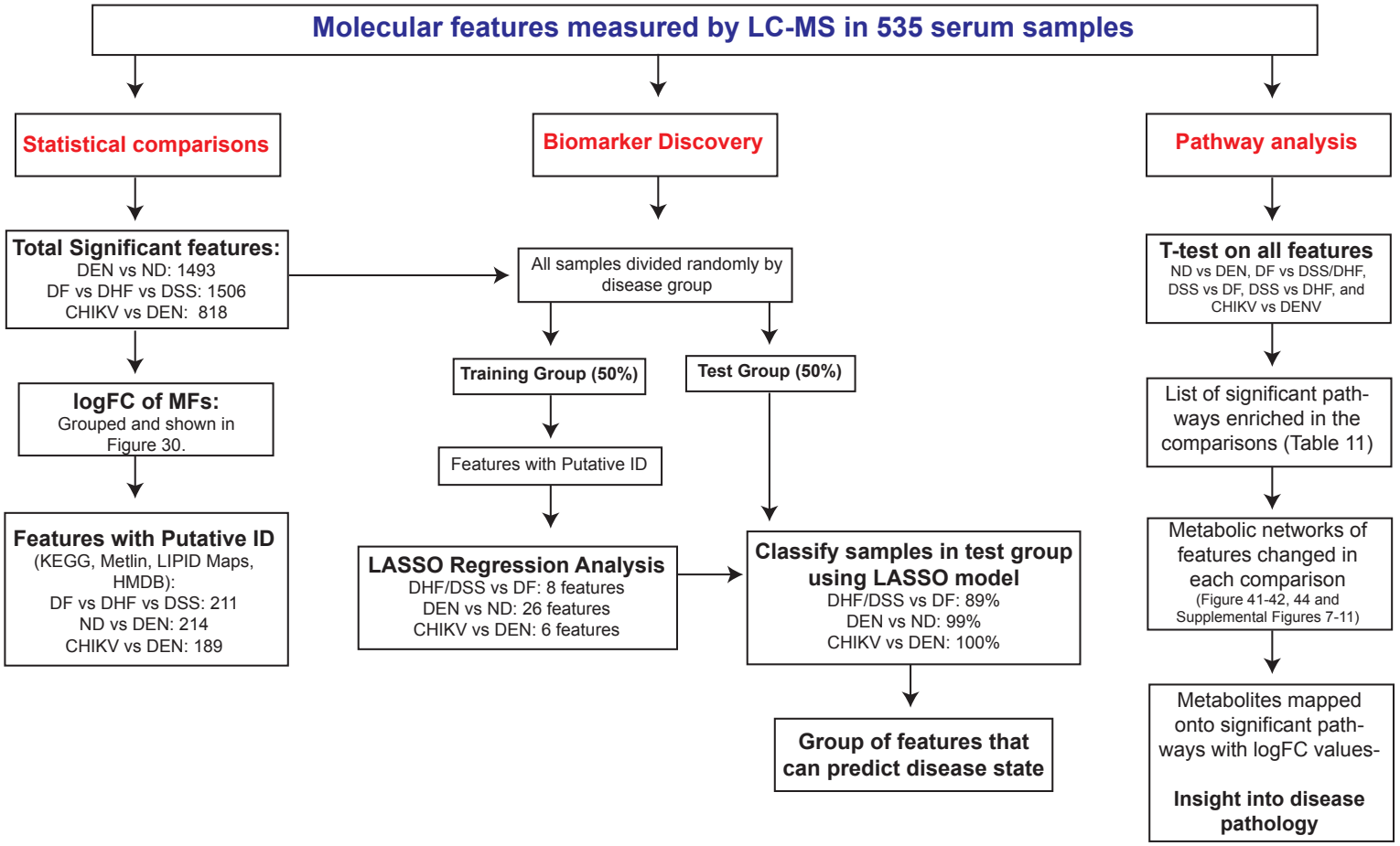

Figure 29 Workflow to discover and test serum biomarkers of dengue diseases, chikungunya and undifferentiated febrile diseases. We used untargeted metabolomics to identify biomarkers in 535 serum samples from febrile patients in Nicaragua. We used statistical comparisons to determine the overall dysregulation of the metabolome in the various diseases. We then built a diagnostic model using LASSO regression and tested it on our samples. Finally, we used pathway analysis to identify biochemical pathways perturbed in the different diseases that have implications for disease pathology.

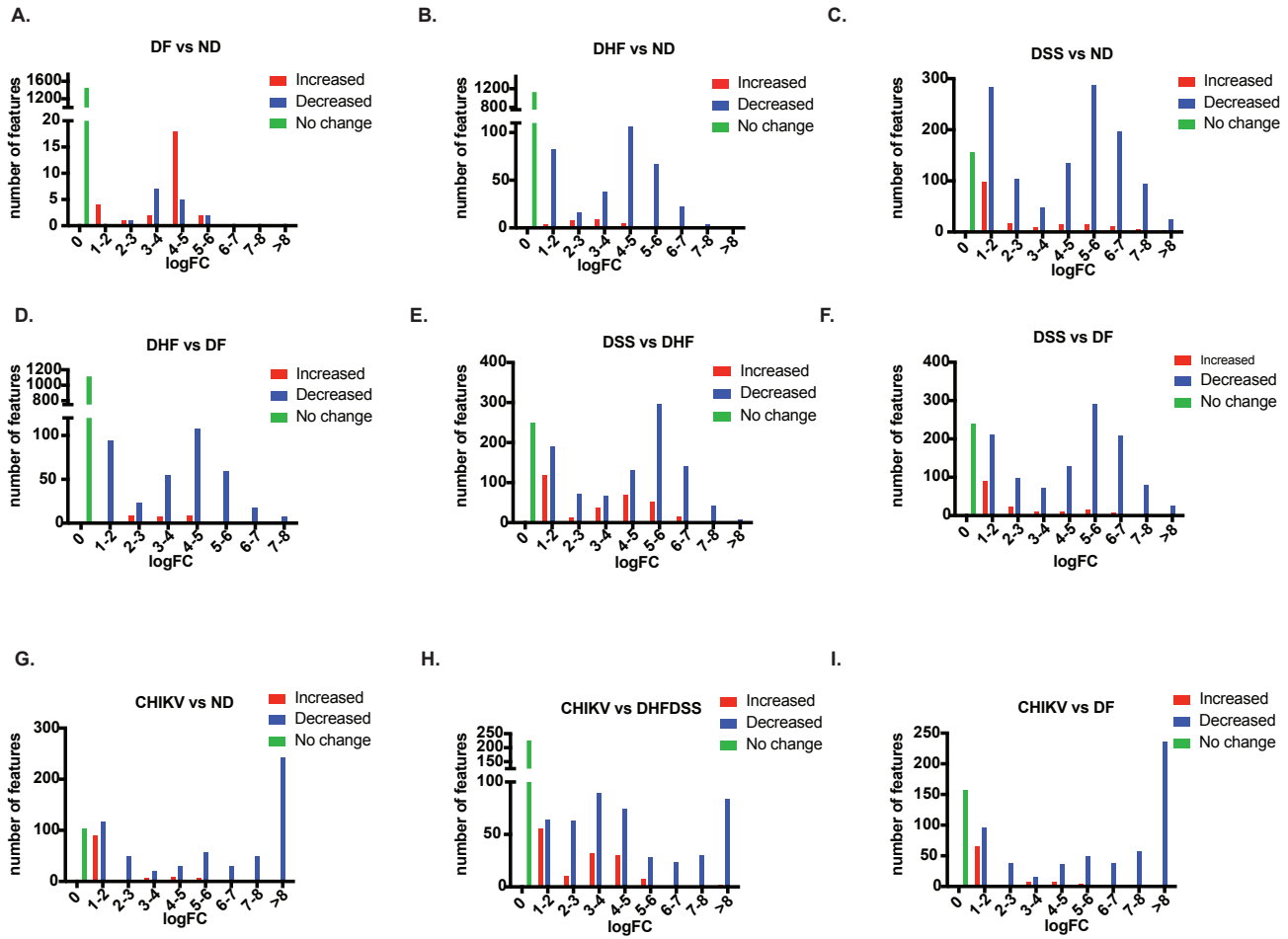

Figure 30 Dysregulation of metabolites in the 9 different comparisons. (A-I) We measured the log fold changes (log(FC)) in each measured molecular feature between the indicated groups. The number of features that remained unchanged, increased (log(FC)>0) or decreased (log(FC)<0) in abundance were counted and divided into groups depending on the degree of change and plotted.

Presumptive chemical identification was performed on all of the molecular features in each comparison group interrogating the monoisotopic mass [+/- 20 parts per million (ppm)] of each molecular feature against the Metlin, HMDB, KEGG and LipidMaps databases (322). For DEN vs. ND, 642 molecular features were assigned a putative chemical structure with an MSI of 3. These features were further filtered to 214 reliable and relevant metabolites. The metabolites were classified and divided into 7 categories. We found 60 glycerophospholipids, 9 glycerolipids, 8 sphingolipids, 47 fatty acids, 27 sterol lipids, 8 prenol lipids, and 55 other organic compounds. The fold change in each glycerophospholipid species comparing each DEN disease to ND comparisons is plotted to observe changes in their expression (Figure 31B).

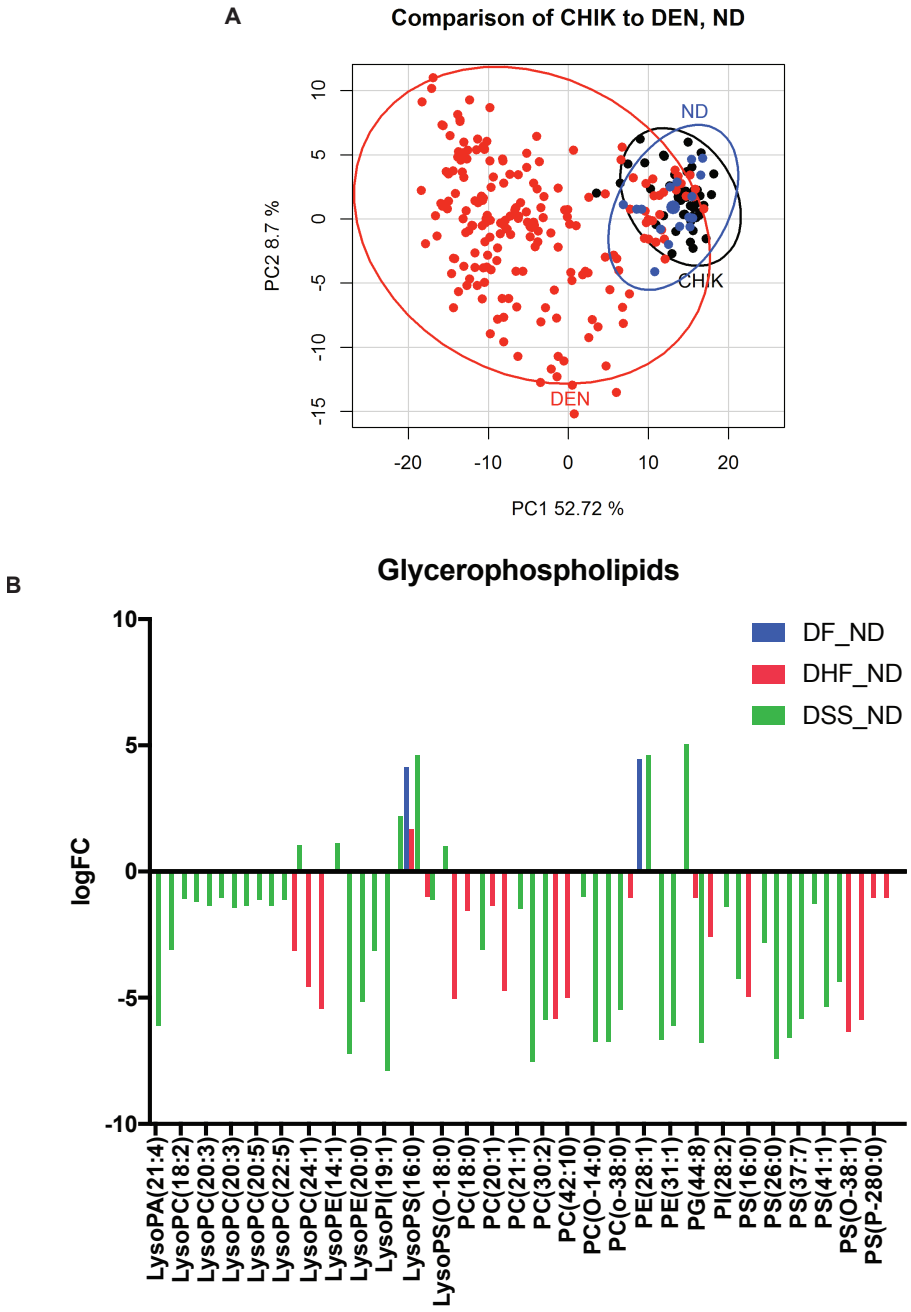

Figure 31 Global metabolome changes and dysregulation of glycerophospholipids. (A) We ran a principle component analysis (PCA) on all of the samples using all of the significantly different molecular features. In red are DEN samples, black are CHIKV samples, and in blue are ND samples. (B) In our linear model to test for overall dysregulation we calculated the log FC for all features. These features were putatively identified (MSI level = 3) and the features tentatively classified as glycerophospholipids were plotted here. The log FC values are plotted to show which features increase or decrease in the indicated comparisons. PC; phosphatidylcholine, PE; phosphatidylethanolamine, PS; phosphatidylserine, PA; phosphatidic acid, PG; phosphatidylglycerol.

Similar analysis was performed comparing DEN samples with each other. We found 1506 MFs that differed significantly (adjusted $p < 0.05$) with ≥ 2 fold change in relative abundance between DF, DHF and DSS. A principle component analysis (PCA) demonstrates the ability of the significant features to separate the three dengue diseases moderately; the first two components accounted for 54% of variation in the data (Figure 32). Of these features 310 displayed increased abundance, 946 decreased and 250 unchanged in DSS vs. DHF (Figure 30). Similar numbers were found when we compared DF, CHIKV and ND cases, indicating a unique serum metabolome profile in each disease state. Overall, we see more features decreased than increased in more severe forms of dengue disease.

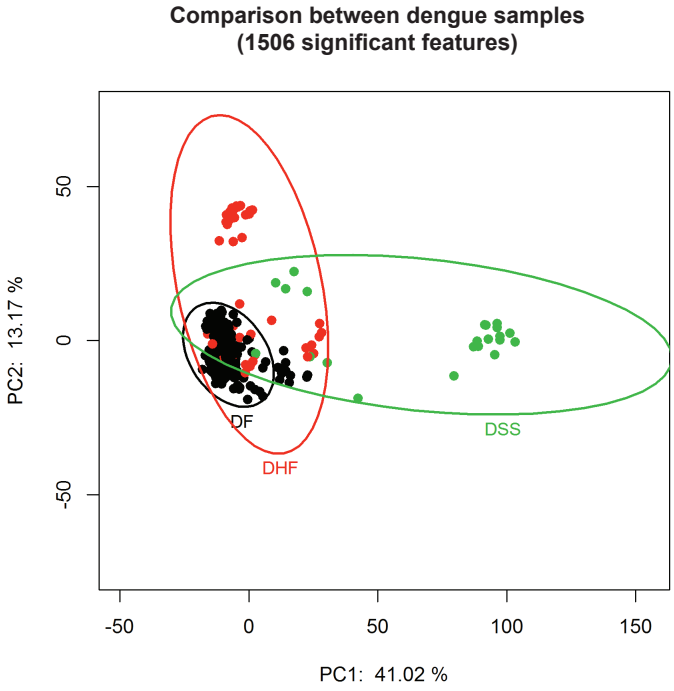

Figure 32 Global metabolome changes in dengue diseases. We ran a principle component analysis (PCA) on all of the dengue disease samples using the 1506 molecular features that were found to be significantly different between dengue diseases. In black are DF samples, in red are DHF samples and in green are DSS samples.

When comparing DF, DHF and DSS a putative chemical structure was assigned to 657 features. These features were further down-selected to 211 reliable and relevant metabolites. The

metabolites were tentatively classified and divided into 7 categories. We found 63 glycerophospholipids, 10 glycerolipids, 6 sphingolipids, 48 fatty acids, 27 sterol lipids, 8 prenol lipids, and 48 other organic compounds identified at MSI level 3. The fold change in each putative glycerophospholipid species amongst the DEN comparisons is plotted to observe changes in their abundances (Figure 33). While the DSS vs. DHF has some features with increased abundance, DHF vs. DF and DSS vs DF predominately display decreased abundance of glycerophsopholipid species.

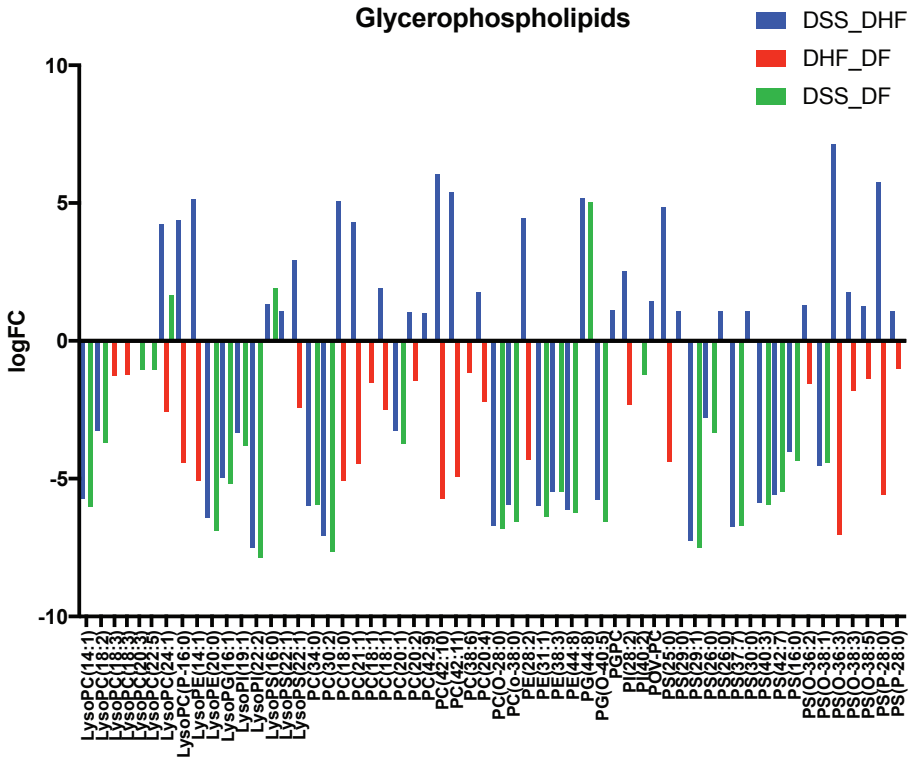

Figure 33 Dysregulation of glycerophospholipids in dengue diseases. In our linear model to test for overall dysregulation we calculated the log FC for all features. These features were putatively identified (MSI level = 3) and the features tentatively classified as glycerophospholipids were plotted here. Their log FC values are plotted to show which features increase or decrease in the indicated comparisons. PC; phosphatidylcholine, PE; phosphatidylethanolamine, PS; phosphatidylserine, PA; phosphatidic acid, PG; phosphatidylglycerol.

Finally, we compared the CHIKV patient samples to DF and DHF/DSS and ND samples from 2012-2015 to achieve an adequate sample size. We found 818 significant (adjusted p<

0.005) molecular features different (>= 2fold change in relative abundance). Of these features 96 were increased, 565 were decreased and 157 remained unchanged in CHIKV vs. DF. Comparing CHIKV to severe dengue (DSS and DHF) we found 137 features increased, 455 decreased and 226 remained unchanged. Finally, we compared CHIKV to ND and found 119 features increased with 595 decreased and 104 that remained unchanged (Figure 30). Overall, CHIKV displays a different metabolic profile to both dengue diseases and non-dengue diseases with a trend towards decreased expression of many of the molecular features.

We were able to assign a putative chemical structure (MSI = 3) to 466 molecular features in the dataset comparing DEN and CHIKV cases. These features were further filtered to 189 reliable and relevant metabolites. The metabolites were tentatively classified and divided into categories. We found 57 glycerophospholipids, 6 glycerolipids, 6 sphingolipids, 37 fatty acids, 23 sterol lipids, 7 prenol lipids, and 53 other organic compounds. The fold change in each glycerophospholipid species amongst the CHIKV comparisons is plotted (Figure 34). Aside from one lysoPL species, all features were downregulated in CHIKV compared to ND, DF or DHF/DSS.

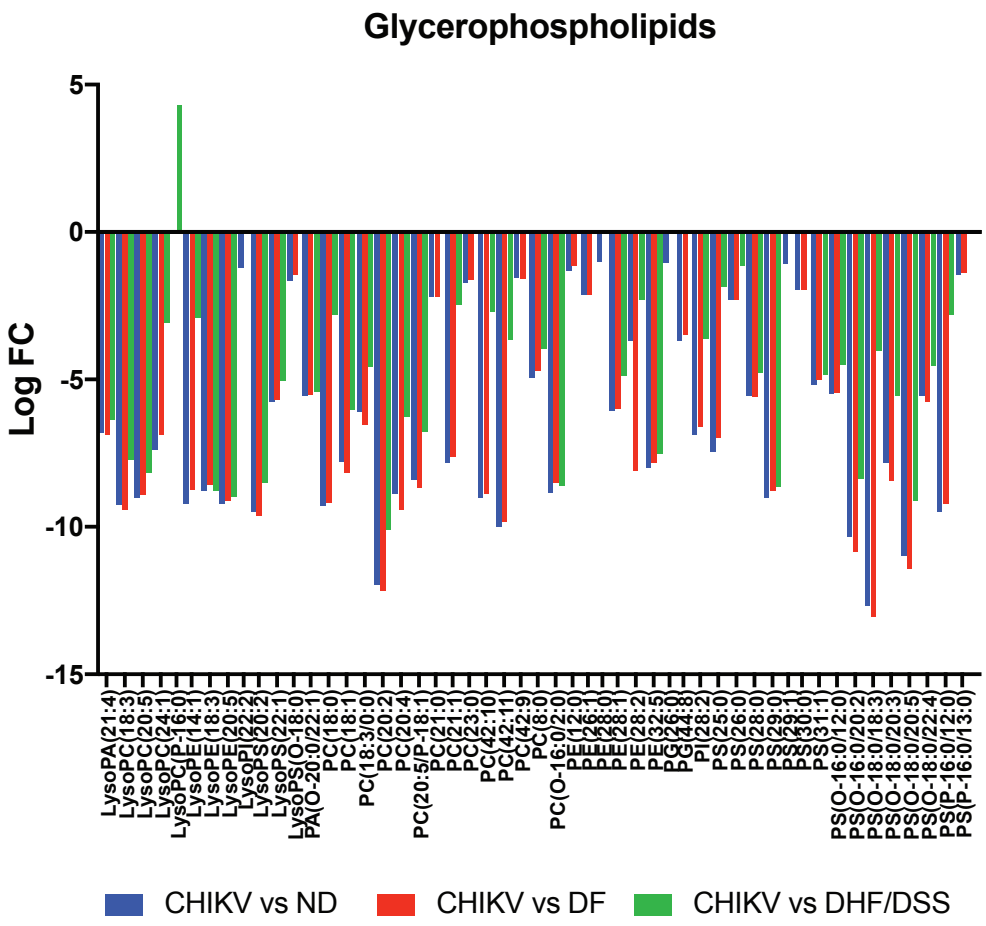

Figure 34 Dysregulation of glycerophospholipids in CHIKV vs. DEN. In our linear model to test for overall dysregulation we calculated the log FC for all features. These features were putatively identified (MSI level = 3) and the features tentatively classified as glycerophospholipids were plotted here. Their log FC values are plotted to show which features increase or decrease in the indicated comparisons. PC; phosphatidylcholine, PE; phsphatidylethanolamine, PS; phosphatidylserine, PA; phosphatidic acid, PG; phosphatidylglycerol.

Diagnostic Classification

A LASSO classification model was built to determine if a subset of the significant features identified in each comparison could differentiate one disease state from another. Training and test groups were randomly selected splitting 50% of the samples from each disease into the two groups. For the purpose of comparing dengue diseases we grouped them as severe (DHF and DSS) or not severe (DF) in order to obtain sufficient sample size. Furthermore, for the CHIKV

vs. DEN model we used all DEN samples exclusively from 2012-2015 to compare with CHIKV cases representing a similar time frame and excluded all non-dengue samples.

The training groups were exclusively used to train the models, while the test group was exclusively used to test the accuracy of the models. We first developed linear models on the features in training groups to identify 'significant' features with a log fold change ≥ 1 and adjusted p-value < 0.05 within the training set alone. Metabolomics data sets such as ours currently have many unidentifiable features (229–231) and thus irrelevant in developing a useful diagnostic model. Therefore, from the list of significant features, we retained only the presumptively identifiable features with ppm <=20 in our training group to build the model.

We developed a filtered list of features and fit a LASSO model to compare all DEN cases to ND cases. The training group (126 DEN; 119 ND) for this comparison built a model composed of 26 molecular features that was used to identify samples in the test group and performed on the test set (n = 243) with a combined accuracy of 99.2% with a sensitivity and specificity of 0.99 (Figure 35A, B). A PCA of these features separated samples well and accounted for 93.7% of the variation (Figure 35C). The features were assigned putative identifications (MSI level = 3) yielding 1 acyl carnitine, 5 fatty acids, 1 glycerolipid, 3 glycerophospholipids, 5 peptides, 2 sterol lipids and 9 other organic compounds (Table 8). The abundances of these features in all DEN and ND samples are plotted and the misdiagnosed samples indicated with a star (Figure 36).

A.

	DEN	ND
DEN	124	1
ND	1	117

B.

	Performance
Sensitivity	0.99
Specificity	0.99
Positive predicitve value	0.99
Negative predicitve value	0.99
Balanced accuracy	0.99

C.

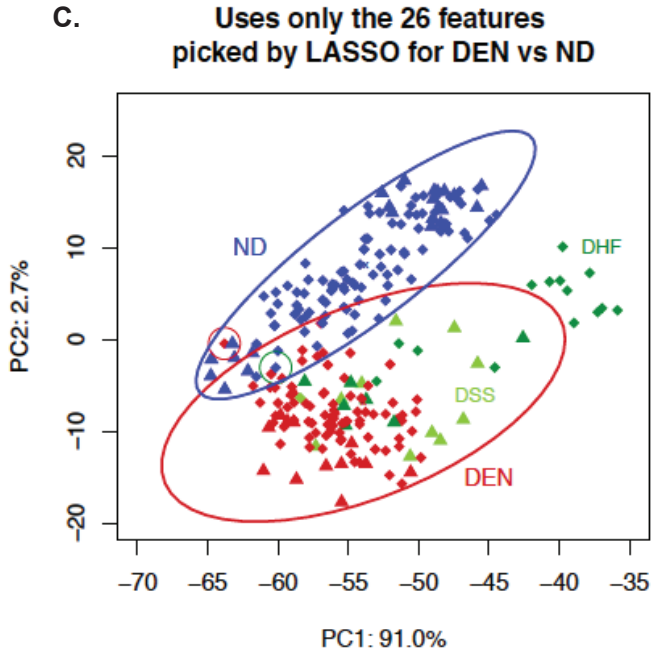

Figure 35 Results of LASSO analysis on DEN vs. ND disease. (A) Results of LASSO predicted classes for the test set. Observed classes are given in columns, predicted classes in rows (B) Measures of performance for the LASSO model predictions on the test set. Balanced accuracy takes into account errors in classification. (C) Principal components for samples in the test set, using the 26 chosen features. Samples that were misclassified are circled. All DEN samples were modeled as a single group; the points are colored according to disease severity. The group of outlying points outside the 95% confidence ellipse to the right are DHF samples collected in season 2012 and later.

Table 8 Features selected by LASSO to differentiate ND from DEN with putative identifications.

Feature ID	m/z	RT	logFC_DF_ND	adj.P.Val_DF_ND	logFC_DHF_ND	adj.P.Val_DHF_ND	logFC_DSS_ND	adj.P.Val_DSS_ND
MZ139.1116_10.11	139.1115933	606.686	NA	NA	-4.596528111	2.86E-48	NA	NA
MZ231.0838_1.51	231.0837671	90.3325	-4.771866308	8.09E-24	-5.049329284	8.28E-11	NA	NA
MZ256.0752_3.51	256.0752024	210.411	4.561001314	8.39E-40	4.773611897	2.15E-18	4.780019476	3.98E-11
MZ289.1504_1.7	289.1504065	101.813	NA	NA	-4.71635685	1.29E-43	-6.497435708	2.57E-45
MZ297.0833_13.46	297.0833213	807.848	NA	NA	-5.662048683	1.43E-107	-6.1181968	2.30E-81
MZ319.2282_9.55	319.228196	572.979	4.442148634	3.84E-24	NA	NA	6.833943318	6.16E-13
MZ325.2354_10.76	325.2354036	645.796	NA	NA	-5.33383612	1.16E-33	-5.160244495	3.78E-19
MZ334.1413_3	334.1413003	180.117	NA	NA	-4.960487257	5.11E-54	-6.83869307	3.30E-56
MZ335.1376_4.83	335.1376275	289.797	NA	NA	-5.864825802	6.15E-73	-7.700570618	4.53E-71
MZ339.1605_12.33	339.1605467	739.747	2.930929833	1.72E-26	3.421051578	2.09E-14	3.56945027	1.82E-09
MZ342.2649_12.13	342.2648991	727.722	4.165239733	3.83E-25	NA	NA	4.667401269	7.73E-08
MZ352.1699_5.03	352.1699209	301.794	NA	NA	-1.065560652	1.24E-05	-6.206647986	2.71E-68
MZ359.2217_9.34	359.2217304	560.244	5.288987846	2.54E-35	NA	NA	7.856789872	5.63E-18
MZ366.0599_1.7	366.0599336	101.733	4.566697344	5.88E-28	NA	NA	-2.39725648	0.009591868
MZ367.247_10.02	367.2470438	601.077	NA	NA	-5.509706552	6.27E-41	NA	NA
MZ369.2337_6.95	369.2336685	417.299	-3.903960794	5.87E-31	-4.210852571	9.81E-15	NA	NA
MZ387.182_8.91	387.1819989	534.434	-5.564100082	5.88E-39	NA	NA	NA	NA
MZ389.2141_5.45	389.2141418	326.916	4.28537066	1.45E-33	4.84133641	1.67E-17	NA	NA
MZ419.3503_10.02	419.3503113	601.091	NA	NA	-5.662048683	1.43E-107	-6.1181968	2.30E-81
MZ471.133_1.4	471.1330169	83.7155	NA	NA	NA	NA	-7.328793922	4.82E-91
MZ539.1133_8.65	539.1133251	519.072	-3.040638734	2.82E-33	NA	NA	NA	NA
MZ580.3676_13.74	580.3675985	824.1385	4.151393791	1.73E-29	1.706664679	0.008322311	4.628351566	4.59E-09
MZ591.3191_6.18	591.3191189	370.863	-4.100127813	9.29E-30	NA	NA	NA	NA
MZ614.7782_2.05	614.7782139	122.856	1.790463134	6.68E-05	2.591751273	0.000248899	9.251428831	5.00E-24
MZ632.4251_13.33	632.4251417	800.016	4.47563814	2.75E-30	NA	NA	4.611193779	3.73E-08
MZ811.592_4.99	811.5920402	299.145	NA	NA	-1.044568791	3.54E-06	-6.79170267	9.93E-86

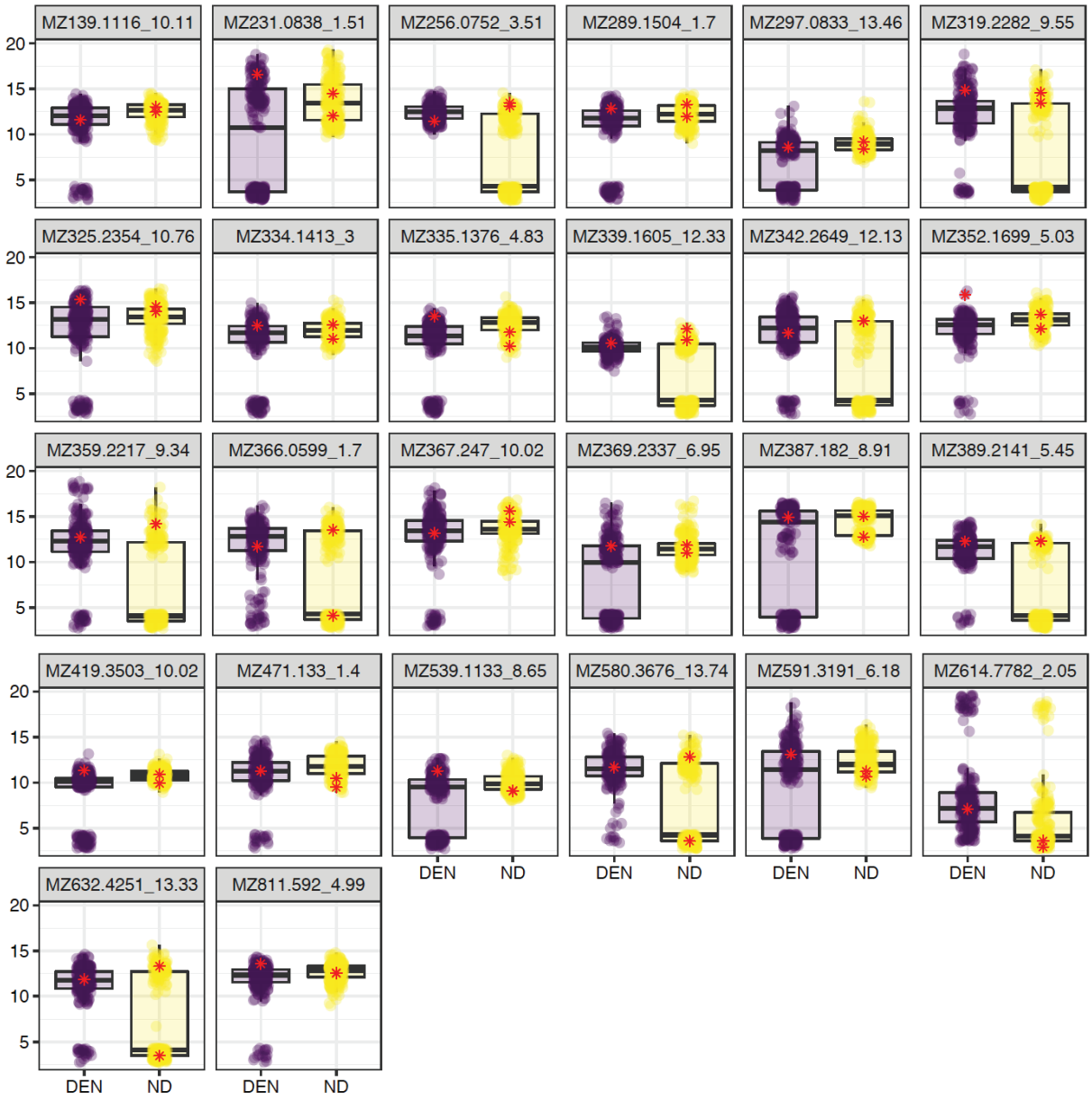

Figure 36 Abundances of the 26 features chosen by the LASSO predictive model to distinguish dengue from non-dengue. Each feature is labeled with MZ value and RT in minutes. Each dot represents a sample; samples that were misclassified are indicated by a red star. The abundance for each feature in all DEN and ND samples are included here.

A LASSO model trained on 126 dengue patient samples (93 DF; 33 DHF/DSS) identified 8 molecular features that distinguish between dengue disease states. When tested on the test set (92 DF; 33 DHF/DSS) this model performed with a combined accuracy of 89% with a sensitivity of 1.00 and a specificity of 0.79 (Figure 37). A PCA of these features separated the DEN samples

moderately and accounted for 75.06% of the variation (Figure 37C). Based on putative identifications (MSI level = 3), the model was composed of 2 peptides, 1 fatty acid, 2 sterol lipids, 1 eicosanoid, 1 triglyceride and 1 glyceride (Table 9). The abundances of these features in all DEN samples are plotted and the misdiagnosed samples indicated with a star (Figure 38).

A.

	DF	DHF/DSS
DF	92	7
DHF/DSS	0	26

B.

	Performance
Sensitivity	1.00
Specificity	0.79
Positive predicitve value	0.93
Negative predicitve value	1.00
Balanced accuracy	0.89

C.

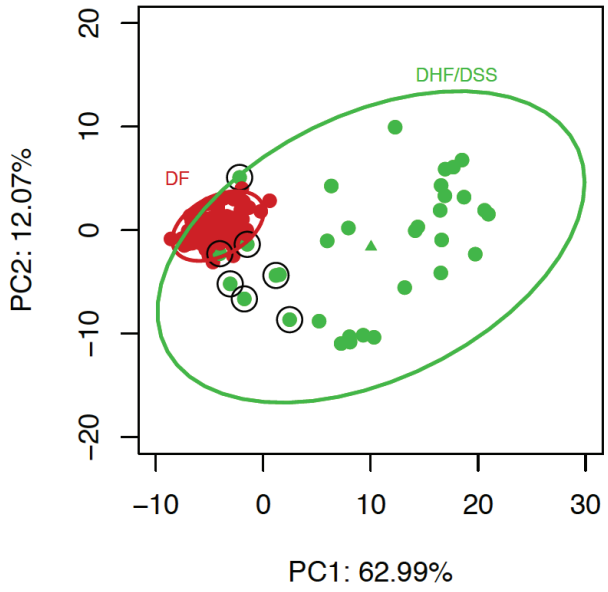

Figure 37 Results of LASSO analysis on severe vs. non-severe dengue diseases. (A) Results of LASSO predicted classes for the test set. Observed classes are given in columns and predicted classes in rows. (B) Measures of performance for the LASSO model predictions on the test set. Balanced accuracy takes into account errors in classification. (C) Principal components for samples in the test set, using the 8 chosen features. Samples that were misclassified are circled.

Table 9 Features selected by LASSO to differentiate severe vs. non-severe dengue diseases with putative identifications.

Feature ID	m/z	RT	logFC_DSS_DHF	adj.P.Val_DSS_DHF	logFC_DHF_DF	adj.P.Val_DHF_DF	logFC_DSS_DF	adj.P.Val_DSS_DF
MZ213.1229_1.38	213.1229093	83.098	-1.49838	0.00931	-4.76231	4.09E-33	-6.26069	4.40E-33
MZ231.1697_2.89	231.1697485	173.493	-2.14924	0.001441	-5.53453	5.37E-32	-7.68377	1.44E-34
MZ283.1652_2.67	283.1651672	160.304	NA	NA	-5.45959	1.30699E-29	-5.44795	3.47014E-19
MZ293.2455_14.96	293.2455223	897.621	NA	NA	-5.7489	1.2056E-33	-6.87966	2.78178E-29
MZ397.2367_10.57	397.2367051	634.348	NA	NA	-7.41981	2.15E-28	-7.04546	6.94E-17
MZ407.2422_9.62	407.2422066	577.3645	5.89971	3.31E-16	-5.18167	4.81E-26	NA	NA
MZ419.3503_10.02	419.3503113	601.091	NA	NA	-5.26116	1.00E-53	-5.71731	1.18E-42
MZ551.4992_4.66	551.4992051	279.7855	1.993834	0.002692	-4.8816	1.96E-27	-2.88777	1.86E-07

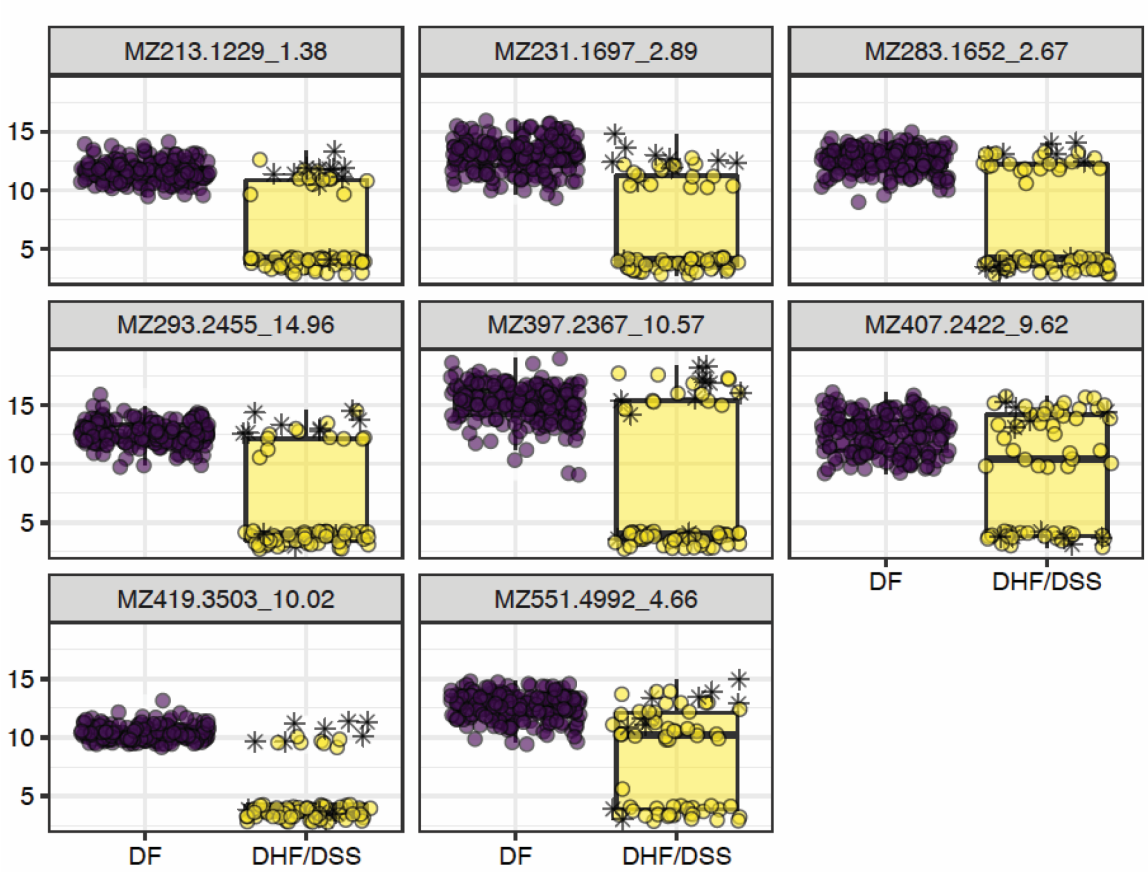

Figure 38 Abundances of the 8 features chosen by the LASSO predictive model to distinguish severe vs. non-severe dengue disease. Each feature is labeled with MZ value and RT in minutes. Each dot represents a sample; samples that were misclassified are indicated by a star. For the most part, misclassified samples had higher levels of the features than did severe dengue samples that were not misclassified. Samples from the entire dataset are included. The higher/lower levels of abundance in DHF/DSS samples do not have an obvious relationship to sex, serotype, age, season of collection, days of illness, or batch.

Finally, to distinguish CHIKV vs. DEN we used 238 patient samples from 2012-2015. The training group (96 DEN; 24 CHIK) for this comparison built a model composed of 6 molecular features that were able to identify samples in the test group (n = 118) with a combined accuracy of 100% with a specificity and sensitivity of 1.00 (Figure 39). A PCA of these features separated the DEN samples very well and accounted for 96.76% of the variation (Figure 39C). Putative identifications (MSI level = 3) were assigned yielding 2 phospholipids, 1 fatty acid, 1 sterol lipids and 2 other organic compounds (Table 10). Their abundances are plotted for all CHIKV and DEN samples displaying clear separation between CHIKV and DEN samples (Figure 40).

A.

	CHIK	DEN
CHIK	23	0
DEN	0	95

B.

	Performance
Sensitivity	1.00
Specificity	1.00
Positive predicitve value	1.00
Negative predicitve value	1.00
Balanced accuracy	1.00

C.

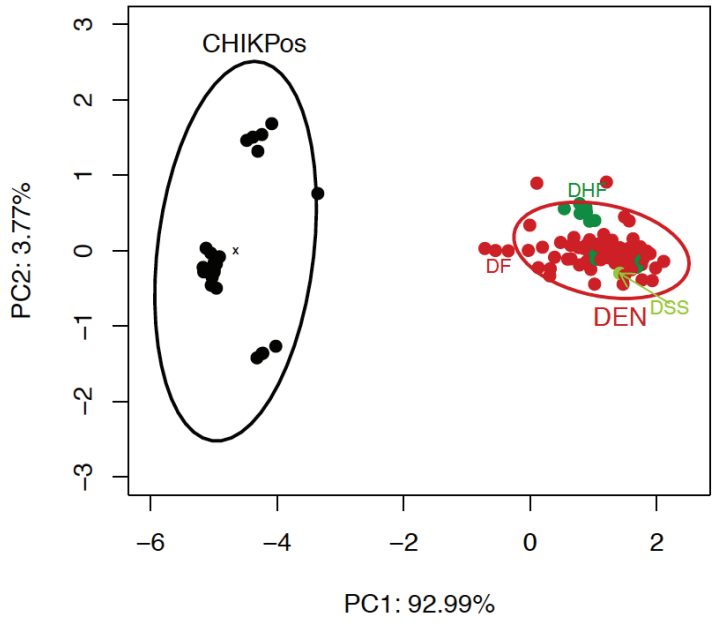

Figure 39 Results of LASSO analysis on CHIKV vs. DEN. (A) Results of LASSO predicted classes for the test set. Observed classes are given in columns, predicted classes in rows. (B) Measures of performance for the LASSO model predictions on the test set. Balanced accuracy takes into account errors in classification. (C) Principal components for samples in the test set, using the 6 chosen features. All DEN samples were modeled as a single group but are colored for different degrees of severity.

Table 10 Features selected by LASSO to differentiate CHIKV from DEN with putative identifications.

Feature ID	m/z	RT	logFC_CHIK_DF	adj.P.Val_CHIK_DF	logFC_CHIK_DHFDSS	adj.P.Val_CHIK_DHFDSS	logFC_CHIK_ND	adj.P.Val_CHIK_ND
MZ153.1272_10.98	153.1271745	659.042	-8.51404	1.1481E-189	-8.82191	3.3739E-146	-8.94755	3.3665E-201
MZ193.123_11.17	193.1230365	670.493	-9.23481	1.5214E-200	-9.09365	1.4028E-148	-9.43625	1.456E-207
MZ391.2476_11.23	391.2476197	674.084	-10.0722	4.3674E-192	-9.59068	1.6589E-136	-10.2804	3.7232E-199
MZ432.2775_16	432.2774608	959.8765	-6.91603	3.3354E-125	-7.15212	1.98731E-89	-7.24299	1.2393E-134
MZ500.2799_9.11	500.2798756	546.3955	-9.0926	1.5214E-200	-8.98387	8.669E-149	-9.19068	4.6143E-206
MZ542.3242_8.83	542.3241606	529.933	-8.91888	1.9957E-130	-8.14311	5.30373E-80	-9.0076	6.8828E-135

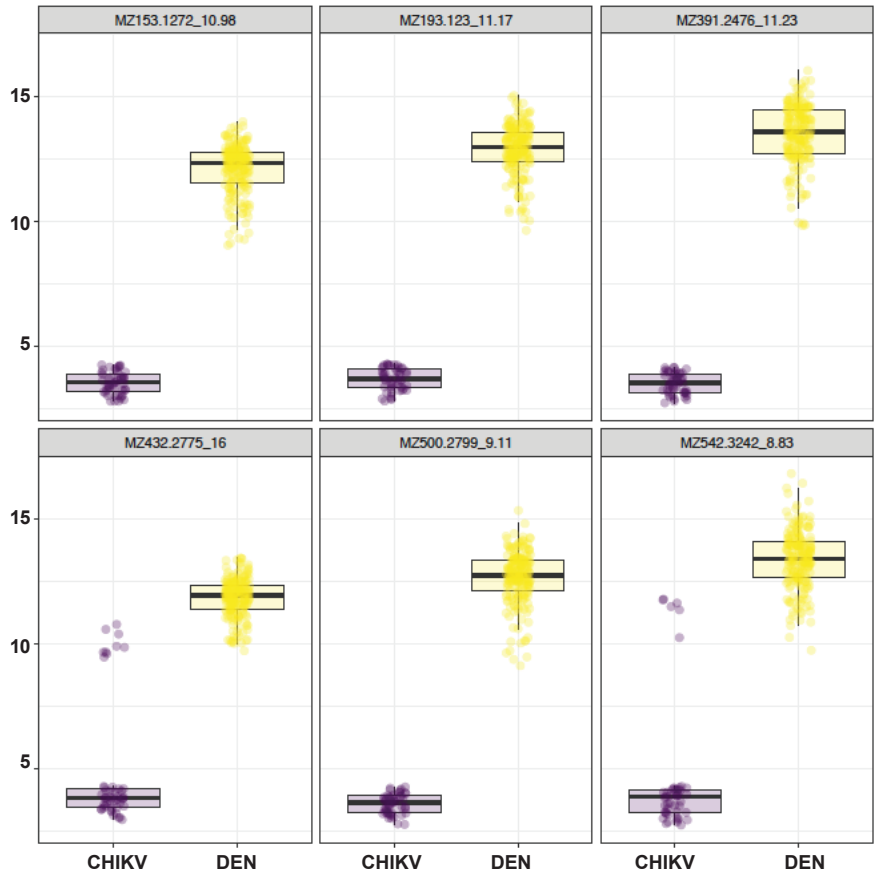

Figure 40 Abundances of the 6 features chosen by the LASSO predictive model to distinguish DEN from CHIKV. Each feature is labeled with MZ value and RT in minutes. Each dot represents a sample. Abundance for each feature in all CHIKV and all DENV samples are shown here. The features shown were present in all dengue samples, but absent or with low abundance in the majority of CHIKV infected samples (which therefore had low median imputed abundance).

The accuracy of the LASSO models with the small number of metabolites required to differentiate the disease groups suggest that metabolic profiling of patient serum can be developed to accurately classify patients in these critical disease groups.

Pathway analysis

In addition to diagnostic and prognostic tools, there is a need for better understanding of arbovirus disease pathology for the development of antivirals. As such, we probed further into our metabolomics data set to identify biochemical pathways disturbed in each of these diseases.

As described in Chapter 2 using integrated pathway and network analysis to analyze untargeted mass spectrometry data is a superior approach to achieve accurate annotation of features, while removing human bias and identifying perturbed biochemical pathways. As such, we again utilized the *mummichog* analytical platform to determine connectivity and find enriched pathways (233). We used two-way comparisons to feed data into the software. These comparisons were DEN vs. ND, DHF/DSS vs. DF (all severe disease), and for further granularity we also separated these into: DSS vs. DHF, and DSS vs. DF, and finally to compare to alphavirus infection: CHIKV vs. DEN. These comparisons and the enriched pathways are outlined in Figure 29 and Table 11.

Table 11 Pathways significantly enriched in each comparison (pathways in bold will be discussed further).

DEN vs ND	DF vs DHF/DSS	DSS vs DF	DSS vs DHF	CHIKV vs DEN
Carnitine shuttle	**Vitamin A (retinol) metabolism**	**De novo fatty acid biosynthesis**	**Linoleate metabolism**	**C21-steroid hormone biosynthesis and metabolism**
Valine, Leucine, and Isoleucine degradation	**De novo FA biosynthesis**	**Arachidonic acid metabolism**	**Arachidonic acid metabolism**	Putative anti-inflammatory metabolites formation from EPA
Leukotriene metabolism	**Leukotriene metabolism**	Fatty acid activation	Fatty acid activation	Drug metabolism-cytochrome P450
Drug metabolism-cytochrome P450	**Arachidonic acid metabolism**	**Leukotriene metabolism**	**De novo fatty acid biosynthesis**	**Leukotriene metabolism**
Propanoate metabolism		**Fatty Acid Metabolism**	**Leukotriene metabolism**	
		Linoleate metabolism	Glycerophospholipid metabolism	
		Vitamin A (retinol) metabolism	Omega-3 fatty acid metabolism	
			Aspartate and asparagine metabolism	
			Xenobiotics metabolism	
			Butanoate metabolism	

We generated a metabolic map for each comparison that shows the upregulated or downregulated metabolites (nodes on the map) in each comparison and how they connect via enzymatic reactions (edges on the map). The color and size of the node represents whether it is

increased or decreased in the indicated comparison (see legends). The network for DEN vs. ND in shown in Supplementary Figure 7. We see enrichment of multiple eicosanoids in the DEN samples. We also observed down-regulation of multiple carnitine species in compared to ND. Since carnitines were the top pathway hit for DEN vs. ND (Table 11), metabolites (nodes) connected to L-carnitine were pulled out in the sub-network for enhanced visualization (Figure 41A).

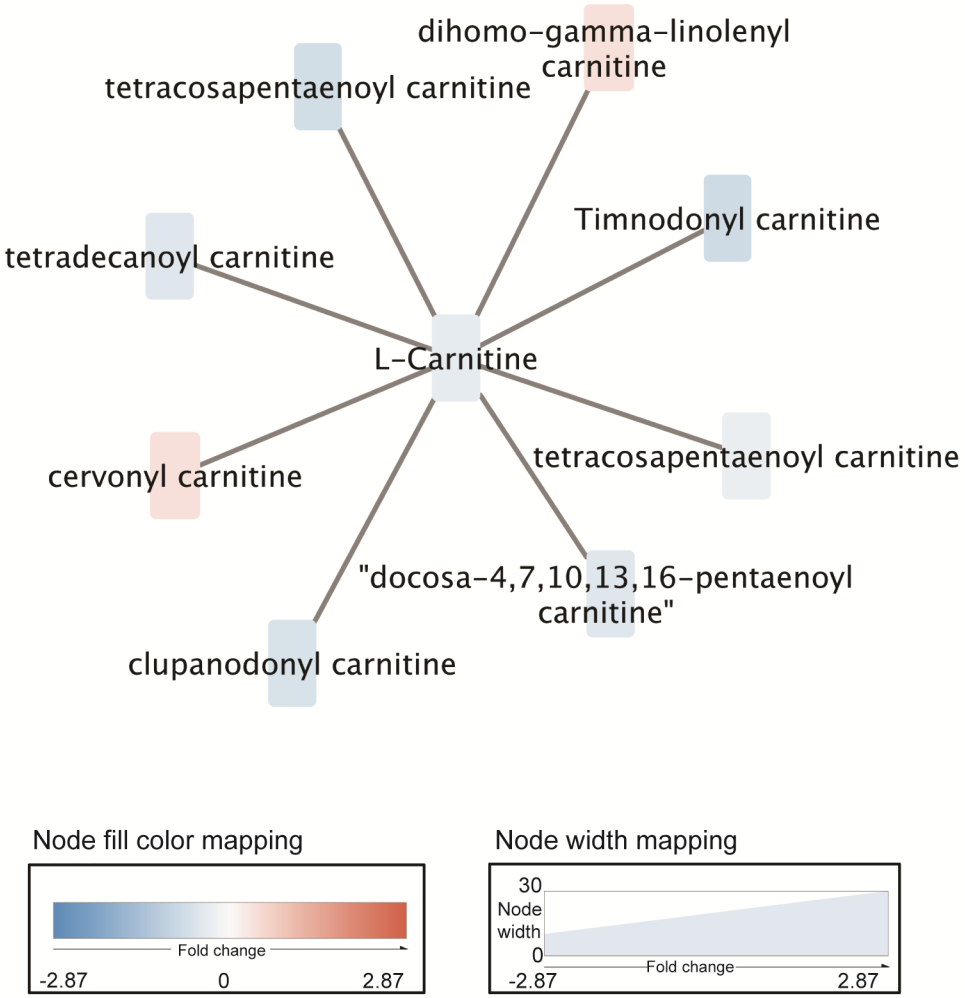

Figure 41 Metabolic sub-network of DEN vs. ND samples. Metabolites annotated by network analysis that are found when comparing DEN to ND samples. The node size and color are determined by the statistical differences between the samples with the values noted in the legend. The large nodes in red are metabolites that are upregulated in dengue samples and the small blue nodes are metabolites that are decreased in DEN (increased in ND). The edges connecting the nodes represent enzymatic reactions that

connect the metabolites and their length has no significance. This is a sub-network of all features connected to L-carnitine. The legend indicates values of size and color for the nodes.

Initially we compared all severe dengue samples (DSS/DHF) to DF samples (Supplementary Figure 8). We observed dysregulation in retinol metabolism (Table 11), thus we pulled out the sub-network of features connected to retinol and retinoate (Figure 42A) and saw that some of these features were upregulated in DHF/DSS compared to DF, while others appeared downregulated. However, when we pulled apart the three diseases and plotted their normalized abundances, we see that the features, particularly cis-9-retinoic acid, displayed an increase in abundance in DSS (Figure 43).

One strength of our study is that we have a large sample size of DSS patients (22 samples) compared to most studies. To take advantage of this, we wanted to increase our understanding of the pathways changed in this unique severe form of dengue. Hence, we compared DSS to either DHF or DF individually to identify metabolic pathways that were altered. The metabolic map for each of these comparisons are quite similar (Supplementary Figure 9 and 10), likely indicating that the changes seen in DHF/DSS vs. DF (Supplementary Figure 8) can largely be attributed to the DSS samples given the similarities between DHF and DF. Overall, there were numerous pathways in fatty acid synthesis and metabolism dysregulated in DSS (Table 11) and their eicosanoid products were upregulated in the networks (Supplementary Figure 9 and 10). Thus, we enhanced the sub-network for one eicosanoid: prostaglandin, comparing DSS to DHF (Figure 42B). The linoleate and leukotriene sub-networks were enhanced for the DSS vs. DF network (Figure 42C). Overall, we see that linoleate metabolism to arachidonic acid and the production of eicosanoid effectors (prostaglandins and leukotrienes) are increased in DSS (Figure 42C).

A.

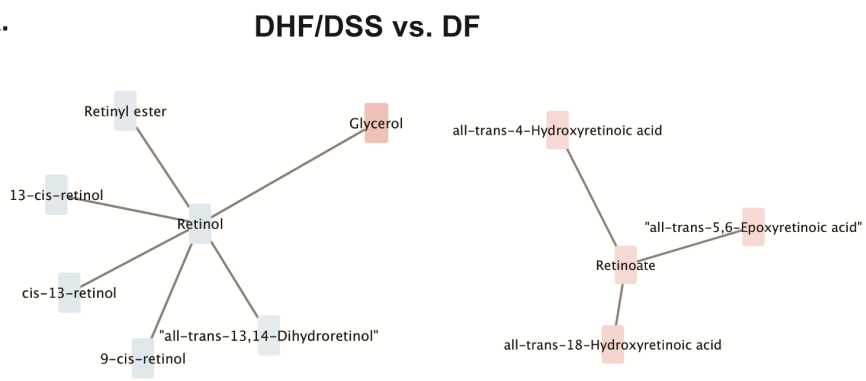
DHF/DSS vs. DF
Retinyl ester
Glycerol
13-cis-retinol
Retinol
cis-13-retinol
"all-trans-13,14-Dihydroretinol"
9-cis-retinol
all-trans-4-Hydroxyretinoic acid
"all-trans-5,6-Epoxyretinoic acid"
Retinoate
all-trans-18-Hydroxyretinoic acid

B.

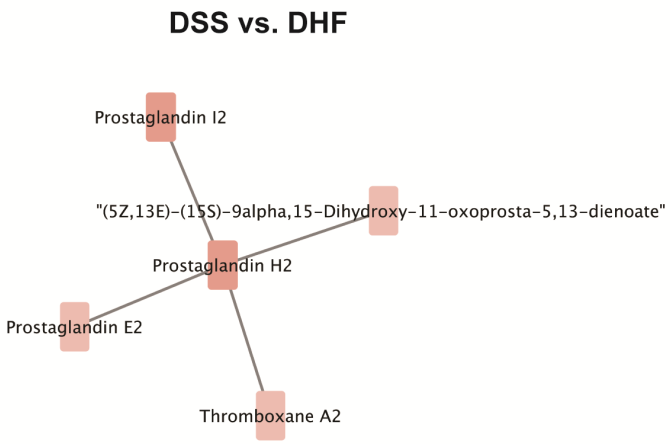
DSS vs. DHF
Prostaglandin I2
"(5Z,13E)-(15S)-9alpha,15-Dihydroxy-11-oxoprosta-5,13-dienoate"
Prostaglandin H2
Prostaglandin E2
Thromboxane A2

C.

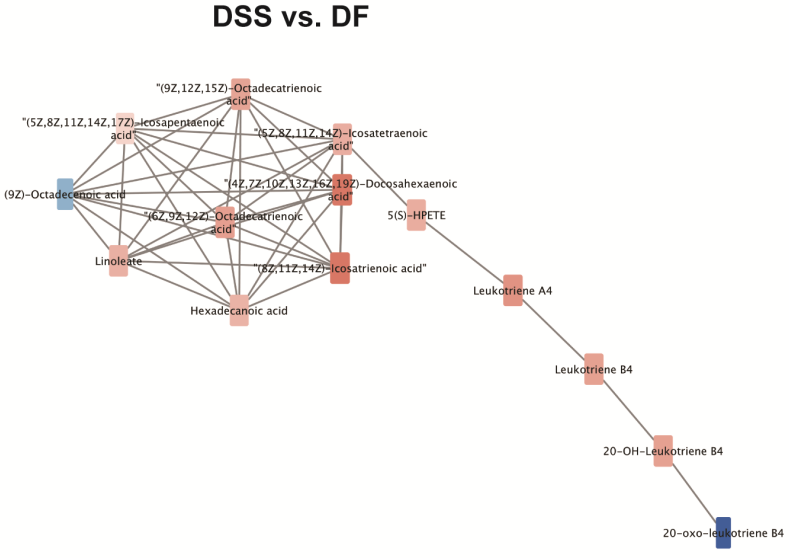
DSS vs. DF
"(9Z,12Z,15Z)-Octadecatrienoic acid"
"(5Z,8Z,11Z,14Z,17Z)-Icosapentaenoic acid"
"(5Z,8Z,11Z,14Z)-Icosatetraenoic acid"
(9Z)-Octadecenoic acid
"(4Z,7Z,10Z,13Z,16Z,19Z)-Docosahexaenoic acid"
"(6Z,9Z,12Z)-Octadecatrienoic acid"
5(S)-HPETE
Linoleate
"(8Z,11Z,14Z)-Icosatrienoic acid"
Hexadecanoic acid
Leukotriene A4
Leukotriene B4
20-OH-Leukotriene B4
20-oxo-leukotriene B4

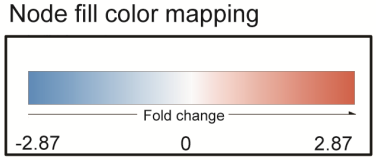
Node fill color mapping
Fold change
-2.87
0
2.87

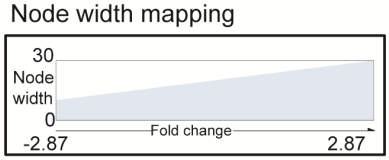
Node width mapping
30
Node width
0
Fold change
-2.87
2.87

Figure 42 Metabolic sub-networks of DEN disease samples. Metabolites were annotated by network analysis. The node size and color are determined by the statistical differences between the samples with the values noted in the legend. (A) The sub-network of all features connected to retinol and retinoate. The large nodes in red are metabolites that are upregulated in DHF/DSS samples and the small blue nodes are metabolites that are decreased in DHF/DSS samples (increased in DF). The edges connecting the nodes represent enzymatic reactions that connect the metabolites and their length has no significance. (B) The a sub-network of all features connected to Prostaglandin H2. The large nodes in red are metabolites that are upregulated in DSS samples and the small blue nodes are metabolites that are decreased in DSS samples (increased in DHF). The edges connecting the nodes represent enzymatic reactions that connect the metabolites and their length has no significance. (C) The sub-network of all features in linoleate metabolism and leukotriene production. The large nodes in red are metabolites that are upregulated in DSS samples and the small blue nodes are metabolites that are decreased in DSS samples (increased in DF). The edges connecting the nodes represent enzymatic reactions that connect the metabolites and their length has no significance. The legend indicates values for colors and width of nodes.

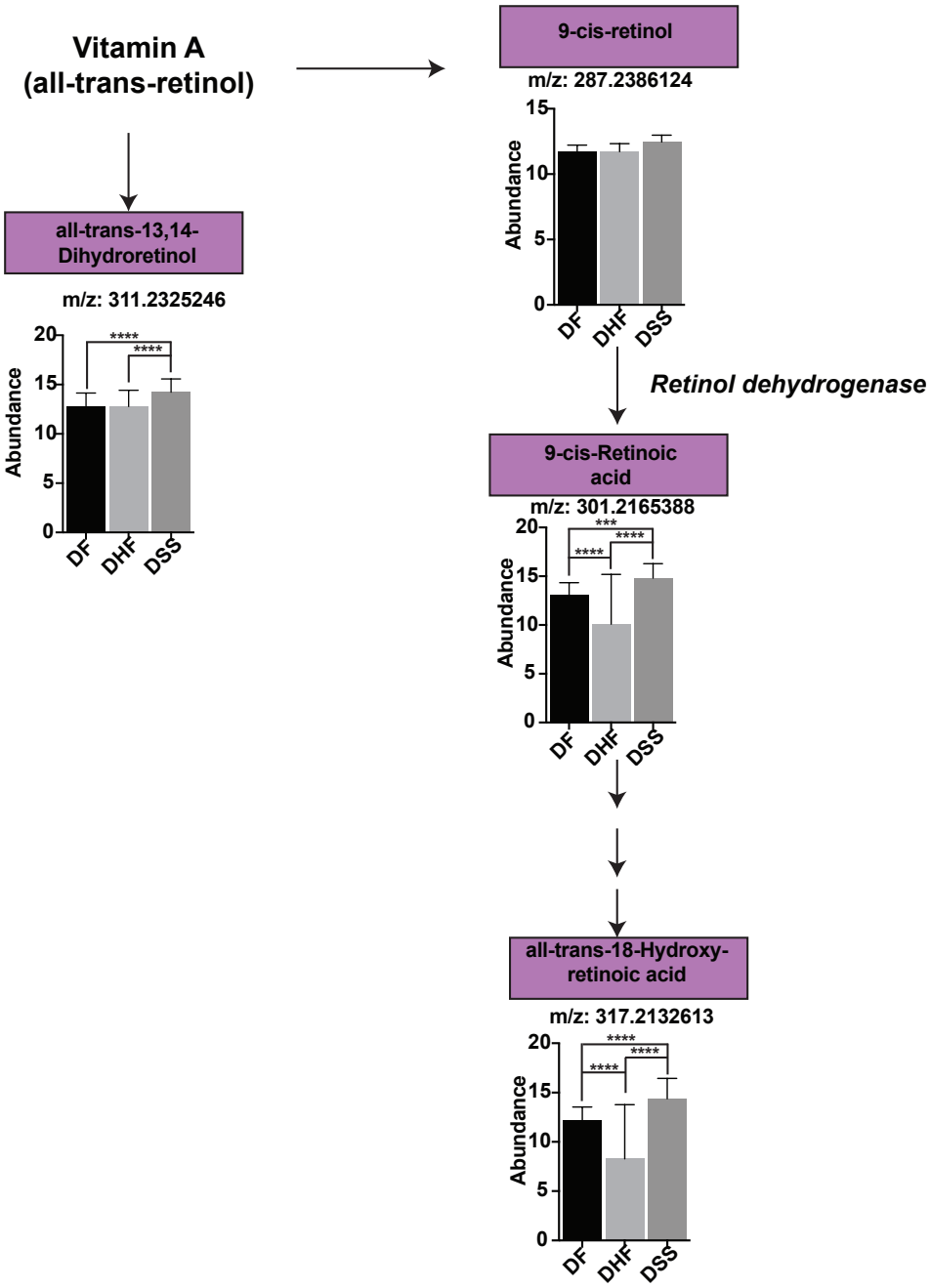

Figure 43 Retinol metabolism is disturbed in severe DEN. The normalized abundance in each disease state is plotted for the annotated features. The common name of the metabolite is noted in purple and the m/z value measured is below. The features were mapped onto a portion of the KEGG (235) pathway for retinol metabolism. Statistical significance comes from our linear model taking all features into account and controlling for false discovery. *=p<0.05, **=p<0.01, ***=p<0.005, ****=p<0.001,

To compare these pathological findings to another arbovirus we compared CHIKV samples to all dengue samples (DEN) from 2012-2015. We observed a strong disturbance in C21-steroid

hormone metabolism (Table 11). A common treatment protocol for CHIKV infection is steroids, due to the inflammatory nature of the disease. Thus, we confirmed that none of these patients had received steroids prior to sample collection. Hence, the perturbations in this pathway are unique to the infection with CHIKV compared to DENV. Interestingly, we observed an overall down-regulation of many of the metabolites in the network of CHIKV compared to DEN (Supplementary Figure 11). Furthermore, most of the features in the steroid hormone biosynthesis sub-network were also strongly downregulated (Figure 44B).

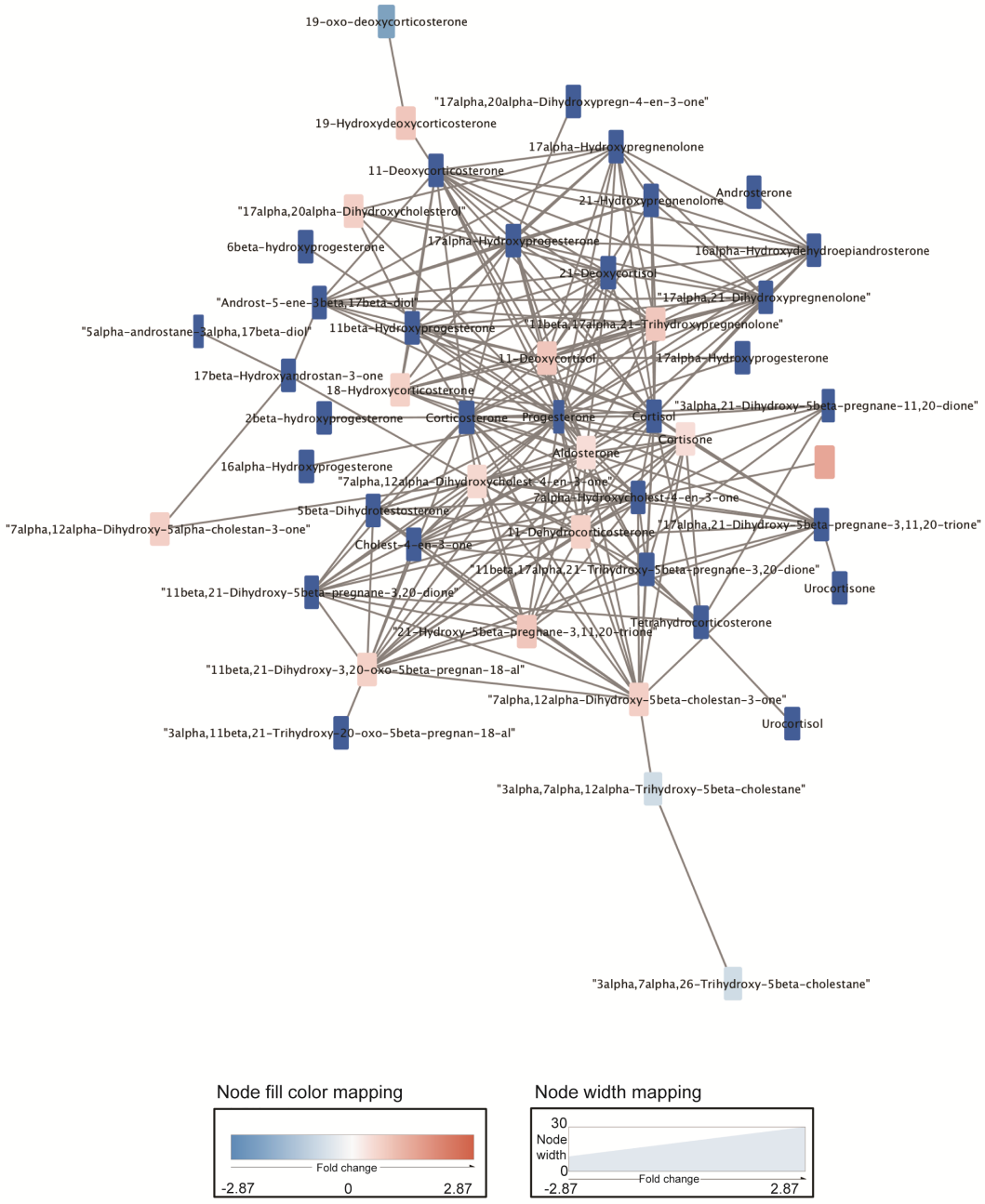

Figure 44 Metabolic sub-network of CHIKV vs. DEN samples. Metabolites annotated by network analysis that are found when comparing CHIKV to DEN samples. The node size and color are determined by the statistical differences between the samples with the values noted in the legend. The large nodes in red are metabolites that are upregulated in CHIKV samples and the small blue nodes are metabolites that are decreased in CHIKV samples (increased in DEN). The edges connecting the nodes represent enzymatic reactions that connect the metabolites and their length has no significance. (A) A sub-network of features in steroid hormone biosynthesis. The legend indicates values for colors and width of nodes.

Given the disturbances in fatty acid synthesis and metabolism amongst the dengue disease comparisons (Table 11) we wanted to look in more detail at these metabolites. The *mummichog*

software annotates input m/z values based on their connectivity to other m/z values and uses sets of m/z values with different adducts to enhance the likelihood of the annotation. As such, it generates a set of features with higher degree of certainty called empirical features, in addition to all of the annotated features that are plotted on our metabolic maps (Supplementary Figures 7-11). Using the empirical features, we measured in the DSS vs. DF comparison, we mapped features onto the *de novo* fatty acid biosynthesis pathway (Figure 45). The common name is displayed in green with the m/z value for that feature below. The normalized abundance for each feature is plotted in DF, DHF and DSS samples. The significance levels result from our linear model adjusted for multiple comparisons (described in the methods section). We see a decrease in the carbon precursor to fatty acids, malonyl-CoA, in severe dengue diseases. Then in DSS we see a clear increase in the fatty acids, palmitic acid and oleic acid, likely indicating increased flux through the pathway.

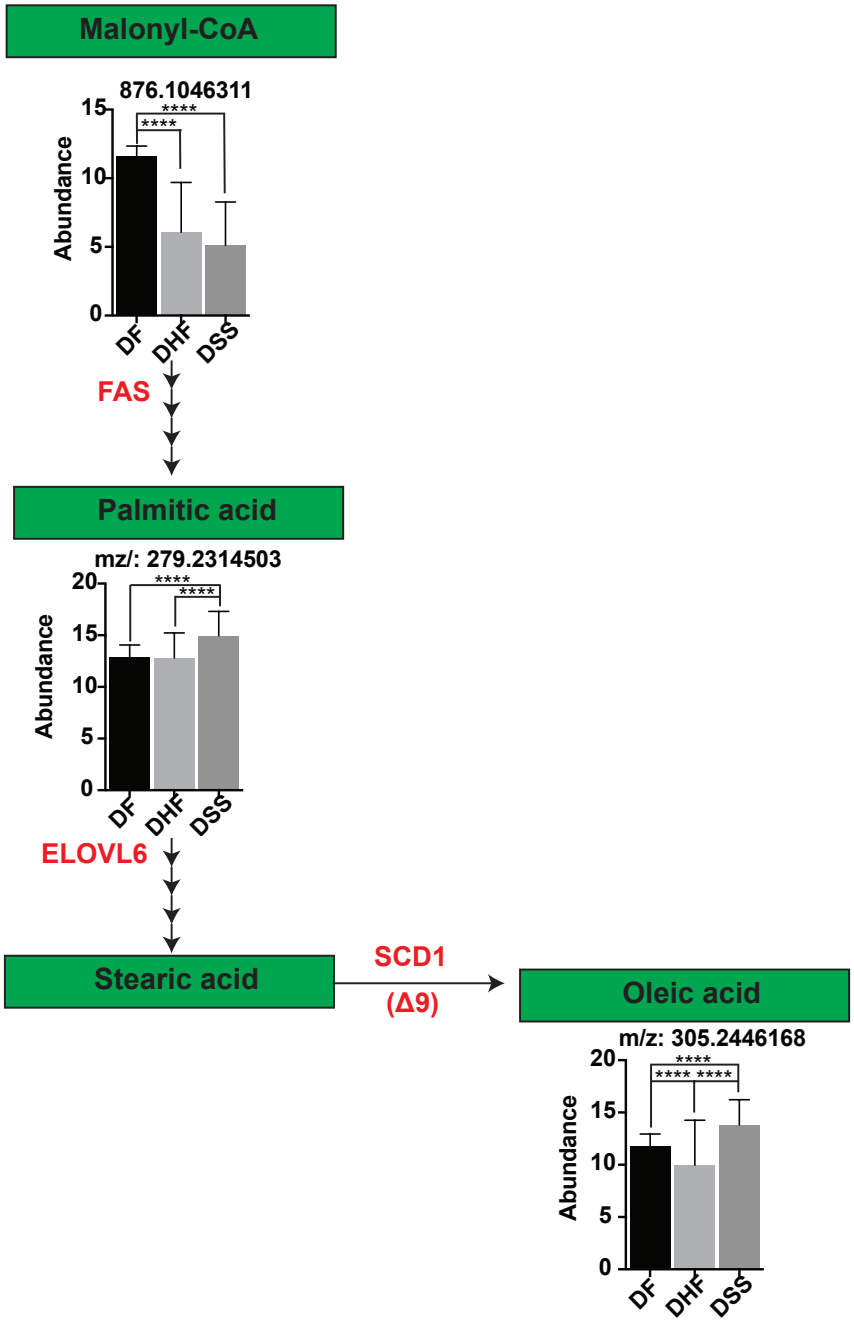

Figure 45 *De Novo* fatty acid biosynthesis in DEN samples. We mapped the measured features in *de novo* fatty acid biosynthesis onto the KEGG(235) pathway. The common name for each feature is in green with the measured m/z value below it. The rate-limiting enzyme at each step is labeled in red. We found a significant reduction of the malonyl-CoA precursor to FA synthesis in severe dengue samples compared to DF samples. Significant increases in the down-stream fatty acids was seen in DSS samples. Statistical significance comes from our linear model taking all features into account and controlling for false discovery. (*=p<0.05, **=p<0.01, ***=p<0.005, ****=p<0.001)

We then used the same process to map empirical features onto the arachidonic acid (AA) synthesis (linoleate metabolism) and AA metabolism pathways (Figure 46). Again, the common name is highlighted in red with the m/z value below, and the normalized abundance plotted. After synthesis, AA is stored in membrane phospholipids by lyso-acyltransferase enzymes, and when activated AA is released from PC by PLA_2 (323,324). Then it is oxygenated, either randomly by reactive oxygen species or enzymatically by three main classes of enzymes and others that vary depending on tissue. Interestingly, we again see clear increases in the precursors to AA in DSS samples compared to both DF and DHF. We also see increases in three eicosanoids products of AA: leukotriene A_4, prostaglandin E_2 and hepoxilin A_3 that were all significantly increased in DSS serum samples compared to both DF and DHF. This suggests a specific or enhanced inflammatory response in DSS that is absent in DHF and DF.

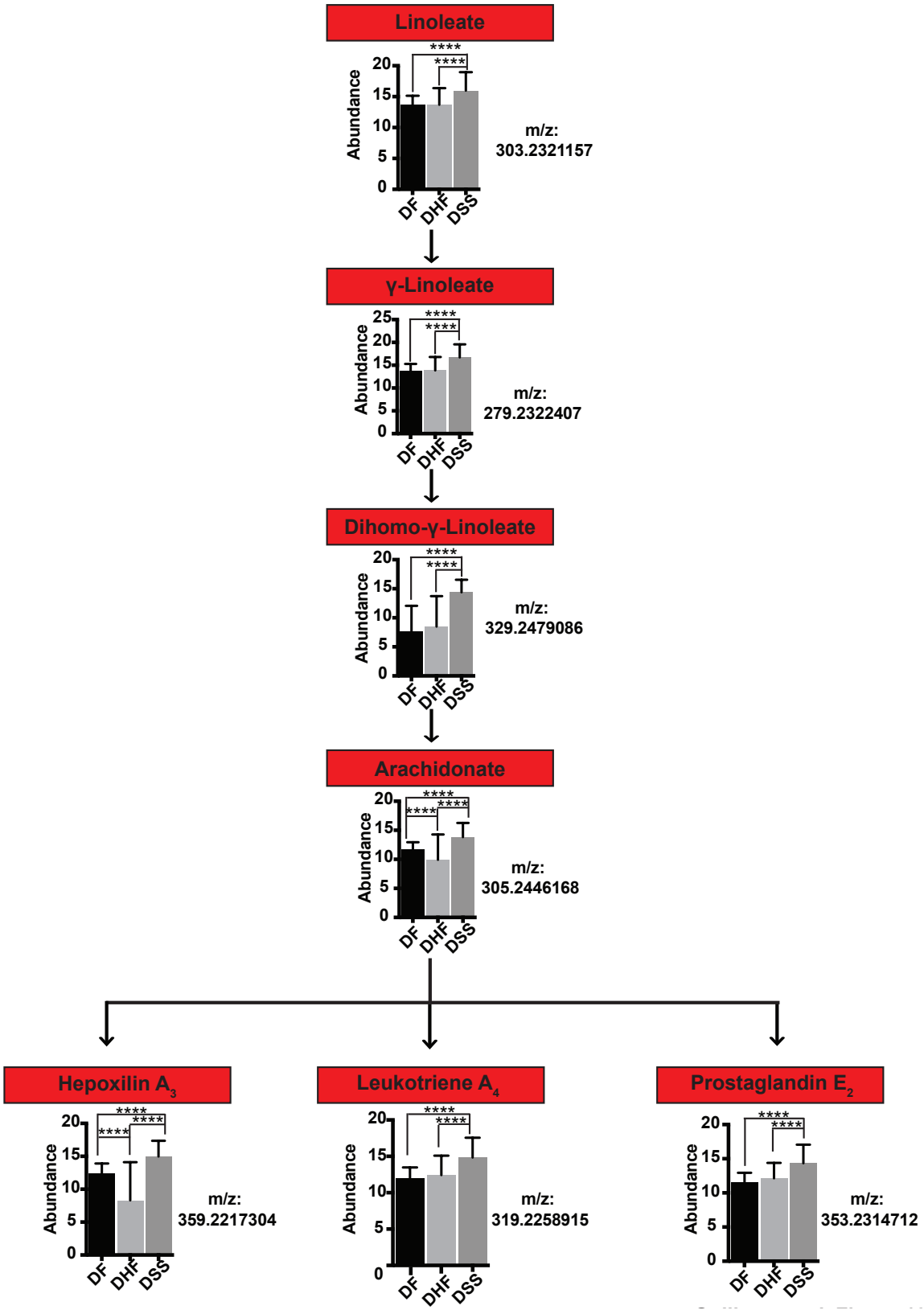
Linoleate
Abundance
m/z:
303.2321157
DF
DHF
DSS
γ-Linoleate
m/z:
279.2322407
Dihomo-γ-Linoleate
m/z:
329.2479086
Arachidonate
m/z:
305.2446168
Hepoxilin A3
m/z:
359.2217304
Leukotriene A4
m/z:
319.2258915
Prostaglandin E2
m/z:
353.2314712

Figure 46 Arachidonic acid synthesis and metabolism in dengue samples. We mapped the measured features in linoleic acid and arachidonic acid metabolism onto the KEGG(235) pathway. The common name for each feature is in red with the measured m/z value below it. We found the features in AA synthesis (linoleic acid metabolism) to be consistently, significantly increased in DSS samples compared to DF and DHF. We also found increases in three different eicosanoid products of AA in DSS samples. Statistical significance comes from our linear model taking all features into account and controlling for false discovery. (*=$p<0.05$, **=$p<0.01$, ***=$p<0.005$, ****=$p<0.001$)

4.3 Discussion

Many diseases present initially with common symptoms of fever and malaise yet can be self-limiting or progress to a severe disease or death. Accurate diagnosis and early care is absolutely critical to saving lives. However, when resources are limited, it is difficult to allocate them appropriately. Hence, new tools are necessary to address this knowledge gap. Here we analyzed acute phase serum of patients with DF, DHF, DSS, CHIKV or an undiagnosed febrile disease [non-dengue, non-CHIKV (ND)]. Our aim was first to identify small molecule biomarkers that characterized one disease state or another in acute phase serum with the potential to predict disease outcomes. Our second aim was to use network analysis to accurately annotate features combined with pathway analysis to identify biochemical perturbations linked to disease pathology. Here we present correlative data that when tested, accurately predicts patient disease status, and biochemical features that may be responsible for dengue disease symptoms. These small and reliable sets of metabolites should be tested against other sample sets to confirm their current potential as diagnostic tools.

Despite multiple metabolomic studies of dengue infection (198,206,223,224), the field has yet to achieve consensus on a specific set of biomarkers. There are many factors indicating why it has been difficult to identify a core set of metabolites (325). Here we have addressed some of these elements by using a considerably larger sample size than most metabolomics studies (325), using multiple patient cohorts, and expanding our previous metabolite set by using a complementary chromatography platform. We have followed up our previous work with patients

from the same genetic background and observed similar profiles of changing metabolites, thereby strengthening our findings and lending credence to this approach.

Our use of rigorous unbiased statistical techniques has enabled us to identify a specific set of serum metabolites that can predict dengue disease outcome. In fact, when tested our refined diagnostic bio-signature performed extremely well. This demonstrated the power of such an approach both in the accuracy of the tests as well as the limited number of features used for the models. This makes future applications of these markers much more feasible for use in a clinical setting.

Not only did our diagnostic biosignature perform strongly in correctly identifying our test group, it also identified features of biological relevance that have been observed in other studies. Thus, similar trends in metabolites can be identified across chromatography platforms and studies. This further indicates that our diagnostic panel and disturbed pathways have real biological significance as well as potential utility as prognostic biomarkers.

By profiling acute serum samples, we have identified an early shift in the metabolic profile that differs between these diseases. We also found changes in lipid metabolism indicative of pathology. It is well characterized that lipid metabolism is disturbed in dengue virus infection (29,90,92,106), however the precise role in disease pathology is not entirely clear. Interestingly, we found that serum glycerophospholipids were predominately decreased in severe vs. non-severe dengue diseases. A similar decrease in serum phospholipids was seen also seen in other studies (198). This may indicate a retention of these lipids intracellularly, which may play a role in viral replication and production.

Using an integrated pathway and network analysis platform we observed metabolites that are altered between each comparison and determined their connectivity. We have also identified

biochemical pathways that are significantly disturbed between the indicated comparisons demonstrating explicit physiological changes. More specifically, many of these pathways are related first to liver damage, second the inflammatory response and third, may be implicated in vascular permeability.

First, we identified that retinoic acid metabolism is disturbed in DSS/DHF vs. DF and in DSS vs. DF. Retinoic acid is released into circulation when there is damage to the liver and it serves to regulate metabolic gene expression through ligand dependent transcription factors (326). In particular, we observed an increase in 9-cis-retinoic acid in DSS samples, which is a ligand for both retinoic acid receptors (RARs) and retinoid X receptors (RXRs), key nuclear transcription factors (327). The increase in retinoic acid we observed may be due to the liver damage caused in severe dengue diseases. Dysregulation of this transcription factor has broad implications for the perturbation of other metabolic pathways and the overall response to infection.

Second, we observed disturbances in fatty acid biosynthesis and metabolism in all of the dengue disease comparisons (DFvsDHF/DSS, DSSvsDHF and DSSvsDF). Disturbed fatty acids, including many of the long and very–long chain species we found, have been shown in many of the dengue disease serum metabolomics studies thus far (198,202,206). Many fatty acids act as signaling molecules to mediate inflammation, which is common to all of these diseases but is particularly increased in DSS. FAS activity is known to be increased in DENV infection in cell culture (90). Perhaps the increase in fatty acids we observed may represent increased viral replication in severe dengue disease, causing an increase in FAS and an accumulation of intermediate fatty acid species in the serum. Or it may be indicative of the cellular inflammatory response to infection. However, we did not observe increased fatty acids in CHIKV samples,

rather they were decreased compared to DEN samples. Thus, the increase in fatty acids may be a specific feature of DENV infection that is not a general inflammatory response.

Furthermore, we observed disturbances in linoleate metabolism in DSS vs. DHF and DSS vs. DF. Linoleate is an essential n-6 fatty acid that is metabolized into arachidonic acid (AA) or other very-long chain fatty acids. We observed significant increases in the metabolites in this pathway in DSS compared to DHF and DF. Further demonstrating that the synthesis and metabolism of fatty acids is perturbed in severe dengue diseases.

Third, enhanced linoleate metabolism serves to increase pools of AA, which is a potent inflammatory molecule when it is transformed into eicosanoids. With our empirical features, we measured 3 different eicosanoids: leukotriene A_4, prostaglandin E_2 and hepoxilin A_3. These features may have implications for the vascular permeability observed in DSS. The leukotriene species we observed are produced by the action of 5-lipoxygenase (5-LOX). Initially 5-LOX generates 5-hydroperoxyeicosatetraenoic acid (5-HPETE), which is unstable and rapidly converted to 5-hydroxyeicosatetraenoic acid (5-HETE) or to LTA_4 another unstable intermediate that is converted to LTB_4 or LTC_4. 5-LOX is primarily expressed in leukocytes where it produces multiple cysteinyl leukotrienes (cLT) such as LTB_4, a polymorphonuclear leukocyte (PMN) chemoattractant involved in anaphylaxis (323,328). Furthermore, LTC_4 serves to increase vascular permeability and plasma leakage (329,330).

In this data set we didn't observe LTC_4, however we measure LTA_4 reliably and LTB_4 was observed in some of our networks. Previous studies have also observed an increase in plasma leukotriene B_4 during the febrile stage of DEN patients (240). Additionally, cell culture of human derived neutrophils revealed that exposure to DENV, both infectious and heat–inactivated,

caused an increase in LTB_4. Inhibition of 5-LO attenuated LTB_4 production, but the effect on viral replication was not demonstrated (240).

Prostaglandins are produced from AA through the action of cyclooxygenase (COX) isoenzymes. Here, we observed prostaglandin E_2 (PGE_2) increased in DSS samples. PGE_2 is the most abundant prostaglandin produced in mammals and it is significantly increased during inflammation (331). Additionally, it causes increased microvascular permeability during an inflammatory event (331,332). Hence, it may also play a role in the vascular permeability observed in DSS. Others have demonstrated a role for COX-2 in DENV replication in cell culture (333), implying a virally-induced phenomenon that may be at play as well.

The third eicosanoid we observed was hepoxilin A_3 (HxA3). This is a non-canonical eicosanoid that is produced when AA is converted to 12S-HpETE through the action of 12S-LOX, which is then converted into HxA3. Hepoxilins are considered a novel type of inflammation that is not as well understood. They are formed in neutrophils where they promote chemotaxis and cause skin vascular permeability (334,335). During a general inflammatory event, vasodilation occurs to allow for an increase in blood flow to an injured site along with controlled vascular permeability to allow for plasma to leak into the injured tissue (334). This permeability event is likely mediated by hepoxilins (334,336). Hence the increase of hepoxilins during DENV infection may also be responsible for the vascular permeability in severe disease.

Mast cells (MCs) are well known to produce leukotrienes and other vasoactive factors such as prostaglandins, proteases, VEGF and TNF. MCs line blood vessels and when activated, release these factors to induce vascular permeability. These cells have been implicated in the vascular permeability that occurs with DENV infection (213). In particular, chymase produced by mast cells acting at the site of virus infection induced vascular leakage in mice and was

elevated in serum from human patients with DENV infection. Additionally, inhibition of leukotriene receptors in the mouse model reduced virus-induced vascular leakage (213). Hence, there are likely multiple factors that work together to induce vascular leakage.

Clearly all of these features are involved in inflammation and it is not surprising to measure them in the diseases comprising our sample set. Their increase in DSS is interesting, which may simply be due to general increased inflammation. However, each of these features have specific mechanisms of action that may be influential in the symptoms we observe. Their unique abundance in DSS compared to DF and DHF implies that they are not a general inflammatory response, but a specific response to this severe form of DENV infection. Clearly this study can only demonstrate associations and speculate about causes, but the features we measured are worthy of follow up studies to identify mechanisms.

The field of metabolomics has been slow to move forward with applicable biomarkers, for many reasons. The study we present here is a feasible application of metabolomic biomarker discovery because we are proposing a system where a known diagnostic (PCR/ serology) is coupled to a discrete panel of metabolites at relative ratios that predict disease severity. Importantly, this panel does not overlap with the other disease states used in our study, rather different metabolic profiles were observed to predict these similar yet distinctly different phenotypes. Thus, despite the clinical difficulties in early diagnosis of febrile patients, we demonstrate that these diseases are in fact clearly distinguishable when using distinct changes in the serum metabolome. Rapid and accurate measurement in a cost-effective manner of these metabolites has real therapeutic potential. Naturally, this particular set of metabolites needs to be tested in further sets of patient serum, both patients from different genetic backgrounds as well as patients in different age ranges and from different seasons of dengue outbreaks. Additionally,

this particular set of features could be tweaked in the case of metabolites that may be more difficult to measure in a cost-effective manner. These features could be replaced with other metabolites that show additional promise. A rigorous iterative approach is required to improve upon the diagnostic sets we propose here to make them more clinically applicable.

We submit that a paradigm shift is needed for the development of prognostic tools and metabolomic profiling is key to this end. We have demonstrated an improved approach to biomarker discovery applied to dengue disease prognosis. With further testing this can be applied to clinical settings.

4.4 Materials and Methods

Patients and Serum sampling and handling

Acute-phase serum samples were obtained from patients who had been diagnosed as ND, DF, DHF, DSS, or CHIKV. The days of fever ranged from 0-3 for cohort patients and 0-6 for hospital patients (Table 5). These cohort patients presented to the study clinic Centro de Salud Sócrates Flores Vivas and met the 1997 WHO case definition for dengue (320) or presented with undifferentiated fever. The hospital patients presented to the Hospital Infantil Manuel de Jesús Rivera, the National Pediatric Reference Hospital. All dengue patients presented with a fever or history of fever <7 days and one or more of the following signs and symptoms: headache, arthralgia, myalgia, retro-orbital pain, positive tourniquet test, petechiae, or signs of bleeding. All the samples were from pediatric patients, <15 years of age, and 52% of the samples were from male and 48% from female patients (Table 5). Cases were laboratory-confirmed for DENV infection by detection of DENV RNA by RT-PCR, isolation of DENV, seroconversion of DENV-specific IgM antibody titers observed by MAC-ELISA in paired acute- and convalescent-phase samples, and/or a ≥4-fold increase in anti-DENV antibody titer measured using inhibition

ELISA in paired acute and convalescent samples. Diseases severity was diagnosed by computerized algorithms based on the 1997 WHO schema were used to classify cases (13,312,320).

Metabolite extraction.

Samples were prepared in a randomized order. 5µL (0.08 ug/ml) of D5 L-tryptophan (Cambridge Isotope Laboratories) was added to 20µL of serum as an internal standard. Samples were extracted with 100µL of cold methanol and vortexed for 30 s. To precipitate proteins, the samples were incubated for 12 h at -80 ºC, followed by 30 min centrifugation at 18,000*xg*. The supernatant was transferred to a new tube and dried in a vacuum concentrator. Extracted samples were resuspended in 25µl 50% methanol, let stand at room temperature for 15 m, vortexed for 20 s, and centrifuged 30 m at 18,000*xg* to remove insoluble debris. The supernatant was transferred to HPLC vials and directly submitted for LC/MS analysis.

Untargeted LC/MS analysis.

Sample order for injection, including technical triplicates, was randomized. 10µL of each sample were injected on an Agilent 1290 HPLC system coupled to an Agilent 6224 time-of-flight mass spectrometer [Santa Clara, CA, USA]. Samples were run in positive ion mode. An XBridge BEH C18 column (2.5 µm particle size, 2.1x100mm, Waters Millford, MA, USA) at a flow rate of 250 µL/min was used. A linear gradient elution from 0% to 98% B (0-13 min) and 98% B (13-14 min) was applied. The mobile phase was composed of A= water plus 0.1% formic acid and B= 95% acetonitrile with 0.1% formic acid. ESI source conditions were set as follows: gas temperature 325 ºC, drying gas 5 L/min, nebulizer 20psi, fragmentor 120 V, skimmer 50 V, and capillary voltage 4000 V. Mass spectral data were collected in profile and

centroid mode. The instrument ran in 2 GHz extended dynamic range mode with a range of 85 to 1700 *m/z* at a scan rate of 2 spectra/s. Samples were run in six batches.

Data processing

Peak Identification

The raw data files were processed for peak detection using ProteoWizard MS Convert version 3.0.6478 64 bit. Retention-time correction, chromatogram alignment and metabolite feature annotation were performed using XCMS software version 1.46 in R version 3.2.2 (255–257).

Preprocessing

All data analyses were conducted in R version 3.4.2 (337). Features were first filtered to remove any that failed to meet the following criteria: 1) present in at least 20% of all samples as a whole; 2) present in at least 75% of all pooled QC samples; 3) present in at least 70% of at least one group (ND, DF, DHF, DSS, CHIK+, CHIK-); 4) eluting within the gradient time, i.e. ≤14.5 minutes).

Normalization was conducted step-wise. First, within each batch separately, features that were not present in at least 80% of pooled QC in that batch were removed. Features were then normalized using a tobit regression (left-censored at the minimum value for each batch) fitted to the pooled QC samples, implemented in the R package 'AER' version 1.2.5 (Kleiber and Zeileis 2008). Batches were then combined, retaining only those features present in all batches, and normalized feature-wise over all batches by the ratio of pooled QC mean batch abundance to pooled QC overall mean abundance.

We found that the season of collection had a large effect on the presence of some features, suggesting that length of storage and/or methods of collection and handling may be influencing

the results. Therefore, features were removed if found to be present (in ≥50% of all samples, irrespective of group) only in samples collected in the 2005-2009 seasons, or only in samples collected in the 2001-2015 seasons. However, if the feature thus identified appeared to be specific to a single serotype (i.e. found in >50% of samples of that serotype, and <50% of samples from other serotypes), then the feature was retained. Finally features that had a coefficient of variation >30% in pooled QC samples after combining and normalizing batches were deemed unreliable and removed prior to analysis. Abundances were transformed by taking the log2 prior to further analysis. Missing values were imputed using a random forest algorithm implemented in the R package missForest version 1.4 (338,339).

Statistical Analyses

Abundance variance was calculated for each feature across all samples, and features in the lowest quartile were excluded from analysis (340). Prior to further analyses, the subset of samples to be compared was randomly divided into training and test sets. Test sets were used only to test predictions from fitted models. Linear models with empirical Bayes statistics were applied feature-wise using the package limma version 3.32.10 (228,321). Features were considered to be significant based on log2 fold change of ≥1 and p-value< 0.05 after adjustment for false discovery rate (341). From the list of significant features, those compounds for which putative identification was available were used to build predictive LASSO models implemented in the R package 'glmnet' version 2.0.13 (342,343) using a tuning parameter chosen by cross-validation. Transformed feature abundances were centered and scaled prior to principal components analysis.

Feature Annotation

Molecular features were assigned putative annotations first by running mass per charge ratios (m/z) through the Purdue omics Discovery Pipeline (322). $[M+H]^+$ and $[M+Na]^+$ adducts were accounted for in the neutral mass calculation of the positive ionization mode data. Annotations with mass accuracy <20 ppm error were further classified into molecular classes. The features that were classified as glycerophospholipids were retained and their fold change values (described above) were graphed in Figures 31B and 33. The features that were selected from the LASSO regression analysis were further annotated with the Human Metabolome Database (HMDB) and LIPID Metabolites and Pathways Strategy (LIPID MAPS) to identify the most likely annotation based on RT values and biological relevance.

Pathway analysis

We used a student's t-test on the imputed abundances for all the features in each disease group comparison in negative ionization mode and positive ionization mode. Network analysis and metabolic pathway analysis was performed using the *mummichog* software version 2.0 with default parameters (233). This platform tests the enrichment of input features against random data resampled from the reference list and produced an empirical *P* value for each pathway. Input metabolites were then annotated as empirical compounds and the significant features ($p<0.05$) were mapped onto biochemical pathways. They were also linked in a network figure by known metabolic reactions and visualized in Cytoscape version 3.6.0 (263). Representative features in retinol metabolism, *de novo* fatty acid biosynthesis, and arachidonic acid metabolism were plotted with abundance in each disease state and displayed in metabolic pathways based on KEGG pathways (235).

CHAPTER 5. CONCLUSIONS

In this thesis, we present insight into how DENV2 temporally perturbs cellular metabolism in an *in vitro* human infection model, Huh7 and decipher commonalities to metabolic alterations observed during dengue disease progression in human patients. Specifically, we discuss changes in the Huh7 cellular metabolome induced by DENV2 replication over time; provide mechanistic detail of the changes observed in unsaturated fatty acid biosynthesis and the implications for virion formation and demonstrate the applicability of these metabolic changes to disease prognosis.

Throughout these different systems we see three main consistent themes. First, host cellular metabolism changes with time to cater to viral replicative needs. This is observed both in cell culture models as well as human disease models. Second, multiple arms of fatty acid biosynthesis are perturbed by viral replication, presumably for the construction of viral replication complexes and particle assembly. Third, downstream metabolism of these fatty acids produces signaling molecules that may contribute to and exacerbate the signs of severe disease.

DENV2 induced metabolomic changes in human hepatoma cells

We have previously profiled the metabolome of DENV2 infected mosquito cells and mosquito midguts and described global changes caused by virus infection as well as changes to specific biochemical pathways (92,106). To complement these findings, we comprehensively profiled metabolic changes in the human hepatoma cell line (Huh7 cells) following DENV2 infection. Given that flaviviruses significantly alter cellular membranes in a consistent time-dependent manner (227), we hypothesized that temporal control of specific metabolic pathways

must occur to cater to changing needs as infection progresses. These temporal changes can be used as a tipping point to alter the outcomes of infection.

To test this hypothesis, we used a comprehensive approach by profiling both polar and non-polar metabolites in both negative and positive ionization modes. We infected cells with DENV2 virus and collected samples at 6, 18, 30 and 48 hours post infection. For controls, we included mock-infected cells and UV-inactivated-DENV2 that can attach to and enter cells but is unable to replicate. This allows us to distinguish changes in the metabolome caused by exposure to virus from the actual replication of the genome and production of viral proteins. Thus, we identified global dysregulation of metabolites caused by the effects of time, virus exposure and virus replication. Here, we highlighted those changes due to virus replication.

We also used an integrated network and pathway analysis platform to annotate metabolites and identify significantly perturbed biochemical pathways. We specifically identified that there is a disturbance in anabolic pathways during early viral replication, with a shift towards catabolic pathways at late viral replication. During peak viral replication we found disturbances in fatty acid biosynthesis and metabolism. In particular we found that linoleic acid (n-3) metabolism was increased at peak viral replication. We measured an increase in each metabolic intermediate along the pathway from linoleic acid to arachidonic acid. The rate-limiting enzyme for this pathway is fatty acid desaturase 2 (FADS2). We observed a reduction in infectious virus released from cells with FADS2 knockdown. This implies that the virus specifically up regulates this biosynthetic pathway to stimulate production of PUFAs for completion of its life cycle and production of infectious virions. Furthermore, we observed an increase in two key eicosanoids: leukotriene A_4 and 5-HETE at peak viral replication. We

demonstrated that inhibition of the rate-limiting enzyme for their production, 5-lipoxygenase (5-LOX), also reduced viral replication.

This is the first comprehensive profiling of global metabolic changes in DENV2 infected Huh7 cells. We have identified vast changes and highlighted a few trends here. Further analysis of this data set will provide deeper insight into other biochemical pathways and lipid molecules changed by DENV2 infection in Huh7 cells.

Future directions:

We found it quite surprising that phospholipid species were decreased in DENV2 infected Huh7 cells. This is in direct opposition to what we have previously demonstrated with mosquito cells and midguts with DENV2 infection (92,106). However, we hypothesized that since Huh7 cells are a liver hepatoma cell line, they already have extensive ER networks and stores of lipids. Instead of increasing the abundance of PLs, perhaps the virus alters the localization of PLs in the cell in order rearrange the ER membranes and form replication platforms. Additionally, we measured increases in certain lysophospholipid species, which may reflect the decrease in total PLs. Perhaps, AA is being cleaved from numerous PC species to be processed into eicosanoids and the virally induced membranes are primarily comprised of LysoPC species. Further characterization of these lipid species and their localization to various cellular compartments during DENV2 replication in Huh7 cells will provide insight into the changing needs of the virus as it toggles between its human and mosquito host.

Stearoyl-CoA desaturase 1 is a metabolic switch that defines early and advanced dengue virus infections and determines virus particle infectivity

It had previously been demonstrated that the DENV2 NS3 protein recruits fatty acid synthase (FAS) to viral replication complexes and increases its activity.(90) This causes localized production of saturated fatty acids. Unsaturated fatty acids (UFAs) play a key role in cellular membrane fluidity. Flaviviruses are dependent on these membranes, particularly ER membranes, for multiple stages of their life-cycle. Thus, we hypothesized that disruption of UFA biosynthesis through the rate-limiting enzyme stearoyl-CoA desaturase 1 (SCD1) would impact virus genome replication and virion formation and function. We assumed that SCD1 would behave similarly to FAS, displaying a re-localization and increase in activity in DENV2 infected cells. However, we found instead two key results. First, SCD1 expression and activity is time-dependent, displaying an early increase in activity followed by a late decrease. This is likely because SCD1 is primarily transcriptionally regulated and sensitive to excess PUFA generation. Second, we found that while inhibition of SCD1 causes a moderate decrease in viral genome replication, it has a much greater impact on infectious particle formation. In fact, we determined that inhibition of SCD impacted the virion maturation process, causing enhanced production of immature particles.

This is the first demonstration that unsaturated fatty acid biosynthesis impacts virion maturation. Furthermore, we have significantly contributed to the understanding of flaviviral control of cellular metabolism, with mechanistic detail. We have done so by demonstrating cell-to-cell variation in a key metabolic enzyme that is dependent on the degree of viral replication. We have built on the previous literature of the role of FAS in DENV2 replication and demonstrated the role of SCD1 in both viral replication and virion production. To accomplish

this, we have taken observations from our metabolomics data set (Chapter 2), showing enhanced unsaturated fatty acid (UFA) biosynthesis, and demonstrated the mechanistic role for SCD1 in this process. Furthermore, we have demonstrated that SCD1 is critical for the replication of all DENV serotypes, other flaviviruses of medical interest and an alphavirus. This demonstrates a shared need for unsaturated fatty acid species for the generation of membranous platforms for positive-strand RNA virus replication and virion assembly.

Future directions:

We remain curious about the destination of newly synthesized UFAs in the virus infected cell. We hypothesize that they are incorporated into phospholipid (PL) species for the expansion of ER membranes, but this may vary by cell type. Surprisingly, we observed decreases in PLs (discussed above) in our metabolomics data set, indicating that this hypothesis may be incorrect for Huh7 cells. Alternative destinations for newly synthesized FAs include cholesterol esters or triglycerides. Favoring one of these options would represent a shift towards FA storage that could be exploited at advanced time-points of viral infection for energy production. This could keep the cell alive as the virus continues to multiply and produce virions.

As such we have screened acyltransferase enzymes involved in the transfer of newly synthesized fatty acids to either phospholipid, cholesterol ester or triglyceride species. Results of this screen will provide insights into the channeling of FAs throughout the cell during DENV2 infection. We will also pair knockdown of the enzymes of interest with SCD1 knockdown to further confirm channeling and destinations of *de novo* FAs. Such an approach may shed light on potential protein-protein interactions of SCD1 with other metabolic enzymes to accomplish

FA channeling and its impact on virus replication. Additionally, it will provide insight into the energetic needs of the virus and will have broad implications for other metabolic changes upon SCD1 inhibition.

Development of a metabolic biosignature to differentiate severe and non-severe dengue disease and chikungunya infections

Infection with dengue viruses manifests as multiple disease types with a range of outcomes, including dengue fever (DF), dengue hemorrhagic fever (DHF) and dengue shock syndrome (DSS). It is difficult to accurately distinguish these diseases at initial presentation and properly allocate resources. We hypothesizde that the earliest signs of pathological manifestations of disease can be identified using metabolic biosignatures related to a specific etiology and disease state. These biosignatures can be exploited for prognosis or diagnosis. Many attempts have been made to identify metabolic biomarkers to diagnose or prognose various diseases. Metabolomics studies have been carried out in a variety of patient populations infected with dengue viruses and numerous metabolites have been proposed as biomarkers (198,199,202,206,344). However, consensus has yet to be achieved and none of these have made it to the clinic. Hence, we aimed to characterize the acute-phase serum metabolome of patients with dengue diseases, chikungunya infection or an undifferentiated fever. By expanding on previous work from our group (206) using a complementary analytical platform, expanding our sample size and using statistical analyses not previously applied to these types of data sets, we have contributed to and enhanced this field.

Through the use of rigorous statistical analyses we have developed discrete models of metabolites that can accurately predict disease states in our data set. These models can

distinguish between DEN vs. non-dengue (ND) patients, DHF/DSS vs. DF, and CHIKV vs. DEN, where DEN refers to all three phenotypes, DF, DHF and DSS.

Furthermore, through the use of integrated network and pathway analysis we have identified biochemical pathways disturbed by these various disease states. We found disturbances in fatty acid synthesis and metabolism in DEN vs. ND and between DHF/DSS vs. DF. We also found a disturbance in steroid hormone biosynthesis when comparing CHIKV and DEN. Since these patients were not treated with steroids, we assume that this is a virally induced phenomenon and may play a role in the different disease symptoms caused by these unique viruses.

We were particularly interested in the disturbances to fatty acid metabolism caused by severe dengue diseases and the production of eicosanoids. We identified two eicosanoid species, leukotriene A_4 and prostaglandin E_2, which have previously been observed in DEN diseases. This demonstrates the reproducibility of DEN disease metabolomics studies and the feasibility for applications of these findings. We also observed an increase in a novel eicosanoid, hepoxilin A_3, not previously observed in DENV infections. This demonstrates the strength of our data set for novel discovery with comprehensive data analyses, as well as the benefit to utilizing multiple chromatography platforms for biomarker discovery. These eicosanoid features further demonstrate potential mechanisms of the vascular permeability observed in DSS and are worthy of mechanistic exploration.

Future directions:

Metabolomics studies have unfortunately been slow to identify useful biomarkers that have been applied in a clinical setting. However, we submit that DENV infection is a useful

model for this type of approach because we are proposing a system where a known diagnostic (PCR/ serology) is coupled to a discrete panel of metabolites at relative ratios that predict disease severity.

In order to accomplish this, there is a need for multi-center coordinated efforts between research groups. Samples from multiple genetic backgrounds and age-ranges need to be analyzed on multiple analytical platforms to identify consistently reproducible biomarkers. Furthermore, these biomarkers need to be tested in well-designed randomized trials.

To further define these diagnostic sets of metabolites and their applicability to severe DEN diseases, we have since re-run the LASSO analysis comparing DSS to DF and DSS to DHF, rather than the pooled severe vs. non-severe dengue classification that we have included in this dissertation. We have improved on this new analysis by running the model 500 times to identify the frequency at which each metabolite is included in the model to predict a given disease state. From this analysis we have observed that metabolites tend to behave in groups. For example, certain sets of metabolites tend to always have increased abundance in DSS and are predictive, while other sets of metabolites tend to be decreased and are also predictive. This makes sense biologically, as metabolites that belong to similar pathways or have shared function tend to display similar behavior when metabolic flux increases uniformly. Consequently, certain groups of metabolites may be interchangeable as biomarkers.

Given variations in human metabolism particularly from varying genetic backgrounds and behaviors, we submit that the application of metabolomic biomarker discovery may one day need to be personalized, however this is likely in the distant future. In the meantime, prognostic tests could take the form of "choose your own adventure" where specific serum metabolites are measured and the levels of one class of metabolites are used to determine which metabolites to

measure next and in what relative ratios etc. This approach is also extremely complex, but the application of advanced mathematical models and testing of large numbers of patient samples may advance this idea to a more feasible option.

Concluding thoughts:

Using multiple analytical platforms including global profiling, hypothesis driven mechanistic discovery and application to patient samples we have characterized DENV2 metabolic alterations in the human host. We have also identified consistent themes, including temporal control of metabolism, viral induced up-regulation of fatty acid biosynthesis and the production of eicosanoids that may mediate severe disease outcomes.

We found it particularly interesting that DENV2 induced a shift in disturbed pathways over time. This is not surprising given the changing needs of the virus with time as it completes genome replication, translation and production of infectious virions. Further understanding of each metabolic pathway perturbed will allow for specific connections to be made between metabolic changes and impact on stages of the virus life-cycle. For example, in Chapter 3 we connected *de novo* unsaturated fatty acid metabolism to infectious virion production. This type of mechanistic connection can be made for each of these metabolic pathways that the virus perturbs for distinct stages of its life-cycle.

This is particularly important when we think about developing host-targeted antivirals. Host-targeted antivirals are a feasible approach for treating acute flavivrus infections since they are taken for short periods of time and thus minimize side effects. Also, they may exert less evolutionary pressure on the virus thus reducing the likelihood of resistance (345). With thorough understanding of viral induced metabolic changes, this can be accomplished in a targeted fashion leading to more effective antivirals. For example, host-targeted antivirals that

alter metabolism to impact earlier stages of the virus life-cycle may be more effective at preventing progression of viral replication. However, targeting these stages may put more evolutionary pressure on the virus to develop resistance. Meanwhile targeting later stages may impact virion formation, leading to decreased spread throughout a host. Nonetheless, the formation of immature particles may enhance the host response, causing more severe disease (346). Of course, metabolic changes at early and late time points of infection are intricately tied as we have demonstrated in Chapter 3. Teasing apart these stages into more discrete events may allow for targeted drug discovery.

Furthermore, dissecting the cellular response from viral induced mechanisms, particularly to cellular stress and signaling pathways, is still unclear. While NS3 has been demonstrated to play a distinct role in the re-localization of FAS (90), we have not identified a viral protein responsible for changes in SCD1. Nor have viral proteins been identified for many of the metabolic changes we discussed in Chapter 1. Furthermore, others have demonstrated that UVI virus can induce changes in cellular metabolic pathways in a similar manner to infectious virus (89,347). We also observed changes in metabolic pathways caused by UVI; many, but not all, were distinct from viral infection.

The fact that attachment and entry alone may serve as a control point whereby the virus induces changes in the host to prepare for its eventual entry and replication is an intriguing concept. Clearly, it is difficult to distinguish this process from a general host response to receptor-mediated endocytosis. Perhaps inclusion of specific non-viral proteins or synthetic beads that could undergo receptor-mediated endocytosis compared to UVI would tease apart these steps in the virus life-cycle.

We also saw a consistent increase in the synthesis of multiple types of fatty acids in each of our various systems. The increase in n-6 fatty acid abundances led to increased arachidonic acid and an increase in its eicosanoid products. In our cell culture system, we demonstrated that inhibition of 5-LOX resulted in reduced viral replication, implying that this enzyme may be activated by or at least important for viral replication. However, it is also possible that leukotriene production is simply a secondary effect of increased fatty acid metabolism and oxidative stress caused by virus infection. Cells don't tolerate excess fatty acids very well, thus it makes sense that the cell would further metabolize or store them. Perhaps too many of them are shunted towards AA resulting in eicosanoid production.

Each of the eicosanoids that we measured in our serum samples could individually be responsible for the vascular permeability observed in DSS. However, we measured multiple species, implying that there are multiple cell types involved in this process. Is this a result of infection of multiple cell types that are all triggered and cause leakage? Or just an overreaction of the immune system that activates too many different cells? Does each eicosanoid enhance the action of another to induce permeability or are they independent events? The coordinated efforts of all them would be difficult to pull apart, but necessary to really understand the causes of these extreme disease symptoms. Understanding the role of the virus in activating particular metabolic pathways and enzymes to produce eicosanoids as well as a more thorough characterization of the infected cell population will shed light on the mechanism of this phenomenon.

In summary, we have advanced our understanding of viral induced changes in cellular metabolism and provided a practical application of these findings to human health. While metabolism is easy to perturb, biological systems seek homeostasis. Thus, the long-lasting and consistent changes that we see in cellular metabolism upon viral infection represent significant

events with far reaching impacts. Further integration of viral perturbation of pathways directly with stages of viral replication will represent that next major steps in this field.

REFERENCES

1. Callens N, Brügger B, Bonnafous P, Drobecq H, Gerl MJ, Krey T, et al. Morphology and Molecular Composition of Purified Bovine Viral Diarrhea Virus Envelope. PLOS Pathog. 2016 Mar 3;12(3):e1005476.
2. Simmons CP, Farrar JJ, van Vinh Chau N, Wills B. Dengue. N Engl J Med. 2012 Apr 12; 366(15):1423–32.
3. Halstead SB. Dengue haemorrhagic fever--a public health problem and a field for research. Bull World Health Organ. 1980;58(1):1–21.
4. WHO. WHO | Dengue haemorrhagic fever: diagnosis, treatment, prevention and control. 2nd edition. Geneva : World Health Organization. WHO. 2015.
5. Halstead SB. Pathogenesis of dengue: challenges to molecular biology. Science. 1988 Jan 29;239(4839):476–81.
6. Holmes EC, Twiddy SS. The origin, emergence and evolutionary genetics of dengue virus. Infect Genet Evol. 2003 May 1;3(1):19–28.
7. Wang E, Ni H, Xu R, Barrett AD, Watowich SJ, Gubler DJ, et al. Evolutionary relationships of endemic/epidemic and sylvatic dengue viruses. J Virol. 2000 Apr 1;74(7):3227–34.
8. Hotta S. Experimental Studies on Dengue: I. Isolation, Identification and Modification of the Virus. J Infect Dis. 1952 Jan 1;90(1):1–9.
9. Messina JP, Brady OJ, Scott TW, Zou C, Pigott DM, Duda KA, et al. Global spread of dengue virus types: mapping the 70 year history. Trends Microbiol. 2014 Mar 1;22(3):138–46.
10. Halstead SB. Dengue. Lancet. 2007 Nov 10 ;370(9599):1644–52.
11. Yacoub S, Wills B. Predicting outcome from dengue. BMC Med . 2014 Dec 4;12(1):147.
12. WHO. Dengue guidelines for diagnosis, treatment, prevention and control treatment, prevention and control treatment, prevention and control. WHO. 2009.

13. Narvaez F, Gutierrez G, Pérez MA, Elizondo D, Nuñez A, Balmaseda A, et al. Evaluation of the Traditional and Revised WHO Classifications of Dengue Disease Severity. Hirayama K, editor. PLoS Negl Trop Dis. 2011 Nov 8;5(11):e1397.

14. Sabchareon A, Wallace D, Sirivichayakul C, Limkittikul K, Chanthavanich P, Suvannadabba S, et al. Protective efficacy of the recombinant, live-attenuated, CYD tetravalent dengue vaccine in Thai schoolchildren: a randomised, controlled phase 2b trial. Lancet. 2012 Nov 3;380(9853):1559–67.

15. Halstead S. Dengue vaccine development: a 75% solution? Elsevier. 2012.

16. Halstead SB. Critique of World Health Organization Recommendation of a Dengue Vaccine. J Infect Dis. 2016 Dec 15;214(12):1793–5.

17. van der Schaar HM, Rust MJ, Chen C, van der Ende-Metselaar H, Wilschut J, Zhuang X, et al. Dissecting the Cell Entry Pathway of Dengue Virus by Single-Particle Tracking in Living Cells. Farzan M, editor. PLoS Pathog. 2008 Dec 19;4(12):e1000244.

18. Meertens L, Carnec X, Lecoin MP, Ramdasi R, Guivel-Benhassine F, Lew E, et al. The TIM and TAM families of phosphatidylserine receptors mediate dengue virus entry. Cell Host Microbe. 2012 Oct 18;12(4):544–57.

19. Lozach P-Y, Burleigh L, Staropoli I, Navarro-Sanchez E, Harriague J, Virelizier J-L, et al. Dendritic Cell-specific Intercellular Adhesion Molecule 3-grabbing Non-integrin (DC-SIGN)-mediated Enhancement of Dengue Virus Infection Is Independent of DC-SIGN Internalization Signals. J Biol Chem. 2005 Jun 24

20. Miller JL, deWet BJM, Martinez-Pomares L, Radcliffe CM, Dwek RA, Rudd PM, et al. The Mannose Receptor Mediates Dengue Virus Infection of Macrophages. PLoS Pathog. 2008;4(2):e17.

21. Tassaneetrithep B, Burgess TH, Granelli-Piperno A, Trumpfheller C, Finke J, Sun W, et al. DC-SIGN (CD209) Mediates Dengue Virus Infection of Human Dendritic Cells. J Exp Med. 2003 Apr 7

22. van der Schaar HM, Rust MJ, Chen C, van der Ende-Metselaar H, Wilschut J, Zhuang X, et al.

Dissecting the Cell Entry Pathway of Dengue Virus by Single-Particle Tracking in Living Cells. Farzan M, editor. PLoS Pathog. 2008 Dec 19;4(12):e1000244.

23. Acosta EG, Castilla V, Damonte EB. Functional entry of dengue virus into Aedes albopictus mosquito cells is dependent on clathrin-mediated endocytosis. J Gen Virol. 2008 Feb 1;89(2):474–84.

24. van der Schaar HM, Rust MJ, Chen C, van der Ende-Metselaar H, Wilschut J, Zhuang X, et al. Dissecting the Cell Entry Pathway of Dengue Virus by Single-Particle Tracking in Living Cells. Farzan M, editor. PLoS Pathog. 2008 Dec 19;4(12):e1000244.

25. Nour AM, Li Y, Wolenski J, Modis Y. Viral membrane fusion and nucleocapsid delivery into the cytoplasm are distinct events in some flaviviruses. PLoS Pathog. 2013 Jan;9(9):e1003585.

26. Harrison SC. The pH sensor for flavivirus membrane fusion. J Cell Biol. 2008 Oct 20;183(2):177–9.

27. Stiasny K, Fritz R, Pangerl K, Heinz FX. Molecular mechanisms of flavivirus membrane fusion. Amino Acids. 2011 Nov 1;41(5):1159–63.

28. Mukhopadhyay S, Kuhn RJ, Rossmann MG. A structural perspective of the flavivirus life cycle. Nat Rev Microbiol. 2005 Jan 1;3(1):13–22.

29. Perera R, Kuhn RJ. Host Metabolism and its Contribution in Flavivirus Biogenesis. In: Arboviruses: Molecular Biology, Evolution and Control. Caister Academic Press; 2016. p. 45–60.

30. Chambers TJ, Hahn CS, Galler R, Rice CM. Flavivirus Genome Organization, Expression, and Replication. Annu Rev Microbiol. 1990 Oct;44(1):649–88.

31. Zhang Y, Kostyuchenko VA, Rossmann MG. Structural analysis of viral nucleocapsids by subtraction of partial projections. J Struct Biol. 2007 Feb 1;157(2):356–64.

32. Colpitts TM, Barthel S, Wang P, Fikrig E. Dengue Virus Capsid Protein Binds Core Histones and Inhibits Nucleosome Formation in Human Liver Cells. Ooi EE, editor. PLoS One. 2011 Sep 1;6(9):e24365.

33. Sangiambut S, Keelapang P, Aaskov J, Puttikhunt C, Kasinrerk W, Malasit P, et al. Multiple

regions in dengue virus capsid protein contribute to nuclear localization during virus infection. J Gen Virol. 2008 May 1;89(5):1254–64.

34. Netsawang J, Noisakran S, Puttikhunt C, Kasinrerk W, Wongwiwat W, Malasit P, et al. Nuclear localization of dengue virus capsid protein is required for DAXX interaction and apoptosis. Virus Res. 2010;147(2):275–83.

35. Jones CT, Ma L, Burgner JW, Groesch TD, Post CB, Kuhn RJ. Flavivirus capsid is a dimeric alpha-helical protein. J Virol. 2003 Jun;77(12):7143–9.

36. Patkar CG, Jones CT, Chang Y, Warrier R, Kuhn RJ. Functional requirements of the yellow fever virus capsid protein. J Virol. 2007 Jun 15;81(12):6471–81.

37. Kuhn RJ, Zhang W, Rossmann MG, Pletnev S V., Corver J, Lenches E, et al. Structure of Dengue Virus Implications for Flavivirus Organization, Maturation, and Fusion. Cell. 2002 Mar 8;108(5):717–25.

38. Guirakhoo F, Heinz FX, Mandl CW, Holzmann H, Kunz C. Fusion activity of flaviviruses: comparison of mature and immature (prM-containing) tick-borne encephalitis virions. J Gen Virol. 1991 Jun 1;72(6):1323–9.

39. Guirakhoo F, Bolin RA, Roehrig JT. The Murray Valley encephalitis virus prM protein confers acid resistance to virus particles and alters the expression of epitopes within the R2 domain of E glycoprotein. Virology. 1992 Dec;191(2):921–31.

40. Allison SL, Schalich J, Stiasny K, Mandl CW, Heinz FX. Mutational Evidence for an Internal Fusion Peptide in Flavivirus Envelope Protein E. J Virol. 2001 May;75(9):4268–75.

41. Plevka P, Battisti AJ, Sheng J, Rossmann MG. Mechanism for maturation-related reorganization of flavivirus glycoproteins. J Struct Biol. 2014 Jan;185(1):27–31.

42. Mukhopadhyay S, Kim B-S, Chipman PR, Rossmann MG, Kuhn RJ. Structure of West Nile virus. Science. 2003 Oct 10;302(5643):248.

43. Dowd KA, Mukherjee S, Kuhn RJ, Pierson TC. Combined effects of the structural heterogeneity and dynamics of flaviviruses on antibody recognition. J Virol. 2014 Oct 1;88(20):11726–37.

44. Lindenbach BD, Rice CM. Genetic interaction of flavivirus nonstructural proteins NS1 and NS4A as a determinant of replicase function. J Virol. 1999 Jun;73(6):4611–21.

45. Muller DA, Young PR. The flavivirus NS1 protein: Molecular and structural biology, immunology, role in pathogenesis and application as a diagnostic biomarker. Antiviral Res. 2013 May;98(2):192–208.

46. Beatty PR, Puerta-Guardo H, Killingbeck SS, Glasner DR, Hopkins K, Harris E. Dengue virus NS1 triggers endothelial permeability and vascular leak that is prevented by NS1 vaccination. Sci Transl Med. 2015;

47. Puerta-Guardo H, Glasner DR, Harris E. Dengue Virus NS1 Disrupts the Endothelial Glycocalyx, Leading to Hyperpermeability. Kuhn RJ, editor. PLOS Pathog. 2016 Jul 14;12(7):e1005738.

48. Akey DL, Brown WC, Dutta S, Konwerski J, Jose J, Jurkiw TJ, et al. Flavivirus NS1 structures reveal surfaces for associations with membranes and immune system. Science (80-). 2014;

49. Edeling MA, Diamond MS, Fremont DH. Structural basis of Flavivirus NS1 assembly and antibody recognition. Proc Natl Acad Sci U S A. 2014 Mar 18;111(11):4285–90.

50. Xie X, Zou J, Puttikhunt C, Yuan Z, Shi P-Y. Two Distinct Sets of NS2A Molecules Are Responsible for Dengue Virus RNA Synthesis and Virion Assembly. Beemon KL, editor. J Virol. 2015 Jan 15;89(2):1298–313.

51. Patkar CG, Kuhn RJ. Yellow Fever virus NS3 plays an essential role in virus assembly independent of its known enzymatic functions. J Virol. 2008 Apr 1;82(7):3342–52.

52. Khadka S, Vangeloff AD, Zhang C, Siddavatam P, Heaton NS, Wang L, et al. A physical interaction network of dengue virus and human proteins. Mol Cell Proteomics. 2011 Dec;10(12):M111.012187.

53. Aguirre S, Maestre AM, Pagni S, Patel JR, Savage T, Gutman D, et al. DENV Inhibits Type I IFN Production in Infected Cells by Cleaving Human STING. Diamond MS, editor. PLoS Pathog. 2012 Oct 4;8(10):e1002934.

54. Stabell AC, Meyerson NR, Gullberg RC, Gilchrist AR, Webb KJ, Old WM, et al. Dengue viruses

cleave STING in humans but not in nonhuman primates, their presumed natural reservoir. Elife. 2018 Mar 20;7.

55. Miller S, Kastner S, Krijnse-Locker J, Bühler S, Bartenschlager R. The Non-structural Protein 4A of Dengue Virus Is an Integral Membrane Protein Inducing Membrane Alterations in a 2K-regulated Manner. J Biol Chem. 2007 Mar 23;282(12):8873–82.

56. Roosendaal J, Westaway EG, Khromykh A, Mackenzie JM. Regulated Cleavages at the West Nile Virus NS4A-2K-NS4B Junctions Play a Major Role in Rearranging Cytoplasmic Membranes and Golgi Trafficking of the NS4A Protein. J Virol. 2006 May 1;80(9):4623–32.

57. Zou J, Xie X, Wang Q-Y, Dong H, Lee MY, Kang C, et al. Characterization of Dengue Virus NS4A and NS4B Protein Interaction. Dermody TS, editor. J Virol. 2015 Apr 1;89(7):3455–70.

58. Muñoz-Jordan JL, Sánchez-Burgos GG, Laurent-Rolle M, García-Sastre A. Inhibition of interferon signaling by dengue virus. Proc Natl Acad Sci U S A. 2003 Nov 25;100(24):14333–8.

59. Munoz-Jordan JL, Laurent-Rolle M, Ashour J, Martinez-Sobrido L, Ashok M, Lipkin WI, et al. Inhibition of Alpha/Beta Interferon Signaling by the NS4B Protein of Flaviviruses. J Virol. 2005 Jul 1;79(13):8004–13.

60. Issur M, Geiss BJ, Bougie I, Picard-Jean F, Despins S, Mayette J, et al. The flavivirus NS5 protein is a true RNA guanylyltransferase that catalyzes a two-step reaction to form the RNA cap structure. RNA. 2009 Dec;15(12):2340–50.

61. Geiss BJ, Thompson AA, Andrews AJ, Sons RL, Gari HH, Keenan SM, et al. Analysis of Flavivirus NS5 Methyltransferase Cap Binding. J Mol Biol. 2009 Feb 6;385(5):1643–54.

62. Choi KH, Groarke JM, Young DC, Kuhn RJ, Smith JL, Pevear DC, et al. The structure of the RNA-dependent RNA polymerase from bovine viral diarrhea virus establishes the role of GTP in de novo initiation. Proc Natl Acad Sci. 2004 Mar 30;101(13):4425–30.

63. Johansson M, Jans DA, Vasudevan SG, Brooks AJ. A small region of the dengue virus-encoded RNA-dependent RNA polymerase, NS5, confers interaction with both the nuclear transport receptor importin-β and the viral helicase, NS3. J Gen Virol. 2001 Apr 1;82(4):735–45.

64. Welsch S, Miller S, Romero-Brey I, Merz A, Bleck CKE, Walther P, et al. Composition and three-dimensional architecture of the dengue virus replication and assembly sites. Cell Host Microbe. 2009 Apr 23;5(4):365–75.

65. Gillespie LK, Hoenen A, Morgan G, Mackenzie JM. The endoplasmic reticulum provides the membrane platform for biogenesis of the flavivirus replication complex. J Virol. 2010 Oct;84(20):10438–47.

66. Khromykh AA, Varnavski AN, Sedlak PL, Westaway EG. Coupling between Replication and Packaging of Flavivirus RNA: Evidence Derived from the Use of DNA-Based Full-Length cDNA Clones of Kunjin Virus. J Virol. 2001 May 15;75(10):4633–40.

67. Sanchez EL, Lagunoff M. Viral activation of cellular metabolism. Virology. 2015 May ;479–480:609–18.

68. Gack MU, Diamond MS. Innate immune escape by Dengue and West Nile viruses. Curr Opin Virol. 2016 Oct 1;20:119–28.

69. Vastag L, Koyuncu E, Grady SL, Shenk TE, Rabinowitz JD. Divergent Effects of Human Cytomegalovirus and Herpes Simplex Virus-1 on Cellular Metabolism. Lagunoff M, editor. PLoS Pathog. 2011 Jul 14;7(7):e1002124.

70. Sanchez EL, Lagunoff M. Viral activation of cellular metabolism. Virology. 2015;

71. Vander Heiden MG, Cantley LC, Thompson CB. Understanding the Warburg Effect: The Metabolic Requirements of Cell Proliferation. Science (80-). 2009;324.

72. WARBURG O. On respiratory impairment in cancer cells. Science. 1956 Aug 10;124(3215):269–70.

73. WARBURG O. On the origin of cancer cells. Science. 1956 Feb 24;123(3191):309–14.

74. Ramière C, Rodriguez J, Enache LS, Lotteau V, André P, Diaz O. Activity of hexokinase is increased by its interaction with hepatitis C virus protein NS5A. J Virol. 2014 Mar 15 ;88(6):3246–54.

75. Ripoli M, D'Aprile A, Quarato G, Sarasin-Filipowicz M, Gouttenoire J, Scrima R, et al. Hepatitis

C virus-linked mitochondrial dysfunction promotes hypoxia-inducible factor 1 alpha-mediated glycolytic adaptation. J Virol. 2010 Jan 1;84(1):647–60.

76. Fontaine KA, Sanchez EL, Camarda R, Lagunoff M. Dengue virus induces and requires glycolysis for optimal replication. J Virol. 2015 Feb 15;89(4):2358–66.

77. Fernandes-Siqueira LO, Zeidler JD, Sousa BG, Ferreira T, Da Poian AT. Anaplerotic Role of Glucose in the Oxidation of Endogenous Fatty Acids during Dengue Virus Infection. Fernandez-Sesma A, editor. mSphere. 2018 Jan 31;3(1):e00458-17.

78. Tiwari SK, Dang J, Qin Y, Lichinchi G, Bansal V, Rana TM. Zika virus infection reprograms global transcription of host cells to allow sustained infection. Emerg Microbes Infect. 2017 Apr 26;6(4):e24–e24.

79. Uldry M, Thorens B. The SLC2 family of facilitated hexose and polyol transporters. Pflgers Arch Eur J Physiol. 2004 Feb 1;447(5):480–9.

80. Allonso D, Andrade IS, Conde JN, Coelho DR, Rocha DCP, da Silva ML, et al. Dengue Virus NS1 Protein Modulates Cellular Energy Metabolism by Increasing Glyceraldehyde-3-Phosphate Dehydrogenase Activity. J Virol. 2015 Dec;89(23):11871–83.

81. Fernandes-Siqueira LO, Zeidler JD, Souza BG, Ferreira T, Da Poian AT. Anaplerotic role of glucose in the oxidation of endogenous fatty acids during dengue virus.

82. Heaton NS, Randall G. Dengue virus-induced autophagy regulates lipid metabolism. Cell Host Microbe. 2010 Nov 18;8(5):422–32.

83. Barbier V, Lang D, Valois S, Rothman AL, Medin CL. Dengue virus induces mitochondrial elongation through impairment of Drp1-triggered mitochondrial fission. Virology. 2017 Jan 1;500:149–60.

84. Chatel-Chaix L, Cortese M, Romero-Brey I, Bender S, Neufeldt CJ, Fischl W, et al. Dengue Virus Perturbs Mitochondrial Morphodynamics to Dampen Innate Immune Responses. Cell Host Microbe. 2016 Sep 14;20(3):342–56.

85. El-Bacha T, Midlej V, Pereira da Silva AP, Silva da Costa L, Benchimol M, Galina A, et al.

Mitochondrial and bioenergetic dysfunction in human hepatic cells infected with dengue 2 virus. Biochim Biophys Acta. 2007;1772(10):1158–66.

86. Al-alimi AA, Ali SA, Al-Hassan FM, Idris FM, Teow S-Y, Mohd Yusoff N. Dengue Virus Type 2 (DENV2)-Induced Oxidative Responses in Monocytes from Glucose-6-Phosphate Dehydrogenase (G6PD)-Deficient and G6PD Normal Subjects. Guzman MG, editor. PLoS Negl Trop Dis. 2014 Mar 13;8(3):e2711.

87. Chao Y-C, Huang C-S, Lee C-N, Chang S-Y, King C-C, Kao C-L. Higher Infection of Dengue Virus Serotype 2 in Human Monocytes of Patients with G6PD Deficiency. Gregson A, editor. PLoS One. 2008 Feb 13;3(2):e1557.

88. Roe B, Kensicki E, Mohney R, Hall WW. Metabolomic Profile of Hepatitis C Virus-Infected Hepatocytes. Jhaveri R, editor. PLoS One. 2011 Aug 11;6(8):e23641.

89. Diamond DL, Syder AJ, Jacobs JM, Sorensen CM, Walters K-A, Proll SC, et al. Temporal proteome and lipidome profiles reveal hepatitis C virus-associated reprogramming of hepatocellular metabolism and bioenergetics. PLoS Pathog. 2010 Jan 8;6(1):e1000719.

90. Heaton NS, Perera R, Berger KL, Khadka S, Lacount DJ, Kuhn RJ, et al. Dengue virus nonstructural protein 3 redistributes fatty acid synthase to sites of viral replication and increases cellular fatty acid synthesis. Proc Natl Acad Sci U S A. 2010 Oct 5;107(40):17345–50.

91. Merino-Ramos T, Vázquez-Calvo Á, Casas J, Sobrino F, Saiz J-C, Martín-Acebes MA. Modification of the Host Cell Lipid Metabolism Induced by Hypolipidemic Drugs Targeting the Acetyl Coenzyme A Carboxylase Impairs West Nile Virus Replication. Antimicrob Agents Chemother. 2016 Oct 26;60(1):307–15.

92. Perera R, Riley C, Isaac G, Hopf-Jannasch AS, Moore RJ, Weitz KW, et al. Dengue virus infection perturbs lipid homeostasis in infected mosquito cells. Heise MT, editor. PLoS Pathog. 2012 Jan;8(3):e1002584.

93. Martín-Acebes MA, Blázquez A-B, Jiménez de Oya N, Escribano-Romero E, Saiz J-C, Murray K, et al. West Nile Virus Replication Requires Fatty Acid Synthesis but Is Independent on

Phosphatidylinositol-4-Phosphate Lipids. Wang T, editor. PLoS One. 2011 Sep 20;6(9):e24970.

94. Liebscher S, Ambrose RL, Aktepe TE, Mikulasova A, Prier JE, Gillespie LK, et al. Phospholipase A2 activity during the replication cycle of the flavivirus West Nile virus. Kuhn RJ, editor. PLOS Pathog. 2018 Apr 30;14(4):e1007029.

95. Royle J, Donald CL, Merits A, Kohl A, Varjak M. Differential effects of lipid biosynthesis inhibitors on Zika and Semliki Forest viruses. Vet J. 2017 Oct 19;

96. Vance JE. Phospholipid Synthesis and Transport in Mammalian Cells. Traffic. 2015 Jan;16(1):1–18.

97. McMahon HT, Gallop JL. Membrane curvature and mechanisms of dynamic cell membrane remodelling. Nature. 2005 Dec 1;438(7068):590–6.

98. van Meer G. Dynamic transbilayer lipid asymmetry. Cold Spring Harb Perspect Biol. 2011 May;3(5).

99. Fagone P, Jackowski S. Membrane phospholipid synthesis and endoplasmic reticulum function. J Lipid Res. 2009 Apr;50 Suppl(Suppl):S311-6.

100. Martín-Acebes MA, Merino-Ramos T, Blázquez A-B, Casas J, Escribano-Romero E, Sobrino F, et al. The composition of West Nile virus lipid envelope unveils a role of sphingolipid metabolism in flavivirus biogenesis. J Virol. 2014 Oct;88(20):12041–54.

101. Melo CFOR, de Oliveira DN, Lima E de O, Guerreiro TM, Esteves CZ, Beck RM, et al. A Lipidomics Approach in the Characterization of Zika-Infected Mosquito Cells: Potential Targets for Breaking the Transmission Cycle. Lanz-Mendoza H, editor. PLoS One. 2016 Oct 10;11(10):e0164377.

102. Zhang J, Zhang Z, Chukkapalli V, Nchoutmboube JA, Li J, Randall G, et al. Positive-strand RNA viruses stimulate host phosphatidylcholine synthesis at viral replication sites. Proc Natl Acad Sci U S A. 2016 Feb 23;113(8):E1064-73.

103. Melo CFOR, de Oliveira DN, Lima E de O, Guerreiro TM, Esteves CZ, Beck RM, et al. A Lipidomics Approach in the Characterization of Zika-Infected Mosquito Cells: Potential Targets

for Breaking the Transmission Cycle. PLoS One. 2016;11(10):e0164377.

104. Lopane C, Agosti P, Gigante I, Sabbà C, Mazzocca A. Implications of the lysophosphatidic acid signaling axis in liver cancer. Biochim Biophys Acta - Rev Cancer. 2017 Aug 1;1868(1):277–82.

105. Rivera R, Chun J. Biological effects of lysophospholipids. In: Reviews of Physiology Biochemistry and Pharmacology. Berlin, Heidelberg: Springer Berlin Heidelberg; 2006. p. 25–46.

106. Chotiwan N, Andre BG, Sanchez-Vargas I, Islam MN, Grabowski JM, Hopf-Jannasch A, et al. Dynamic remodeling of lipids coincides with dengue virus replication in the midgut of Aedes aegypti mosquitoes. Cherry S, editor. PLOS Pathog. 2018 Feb 15;14(2):e1006853.

107. Merrill AH, Wang MD, Park M, Sullards MC. (Glyco)sphingolipidology: an amazing challenge and opportunity for systems biology. Trends Biochem Sci. 2007 Oct;32(10):457–68.

108. Hannun YA, Obeid LM. The Ceramide-centric Universe of Lipid-mediated Cell Regulation: Stress Encounters of the Lipid Kind. J Biol Chem. 2002 Jul 19;277(29):25847–50.

109. Ohanian J, Ohanian V. Sphingolipids in mammalian cell signalling. Cell Mol Life Sci. 2001 Dec;58(14):2053–68.

110. Holthuis JCM, Pomorski T, Raggers RJ, Sprong H, Van Meer G. The Organizing Potential of Sphingolipids in Intracellular Membrane Transport. Physiol Rev. 2001 Jan 10 ;81(4):1689–723.

111. Hannun YA, Obeid LM. Sphingolipids and their metabolism in physiology and disease. Nat Rev Mol Cell Biol. 2017 Nov 22;19(3):175–91.

112. Gault CR, Obeid LM, Hannun YA. An overview of sphingolipid metabolism: from synthesis to breakdown. Adv Exp Med Biol. 2010;688:1–23.

113. Aktepe TE, Pham H, Mackenzie JM. Differential utilisation of ceramide during replication of the flaviviruses West Nile and dengue virus. Virology. 2015 Oct;484:241–50.

114. Pike LJ. Lipid rafts: bringing order to chaos. J Lipid Res. 2003 Apr 1;44(4):655–67.

115. Deng Y, Almsherqi ZA, Ng MML, Kohlwein SD. Do viruses subvert cholesterol homeostasis to induce host cubic membranes? Trends Cell Biol. 2010 Jul;20(7):371–9.

116. Soto-Acosta R, Mosso C, Cervantes-Salazar M, Puerta-Guardo H, Medina F, Favari L, et al. The

increase in cholesterol levels at early stages after dengue virus infection correlates with an augment in LDL particle uptake and HMG-CoA reductase activity. Virology. 2013;442(2):132–47.

117. Rothwell C, LeBreton A, Young Ng C, Lim JYH, Liu W, Vasudevan S, et al. Cholesterol biosynthesis modulation regulates dengue viral replication. Virology. 2009;389(1):8–19.

118. Li C, Deng Y-Q, Wang S, Ma F, Aliyari R, Huang X-Y, et al. 25-Hydroxycholesterol Protects Host against Zika Virus Infection and Its Associated Microcephaly in a Mouse Model. Immunity. 2017 Mar 21;46(3):446–56.

119. Mackenzie JM, Khromykh AA, Parton RG. Cholesterol Manipulation by West Nile Virus Perturbs the Cellular Immune Response. Cell Host Microbe. 2007 Oct;2(4):229–39.

120. Campbell SM, Crowe SM, Mak J. Lipid rafts and HIV-1: From viral entry to assembly of progeny virions. In: Journal of Clinical Virology. 2001. p. 217–27.

121. Nayak D, Shivakoti S, Balogun RA, Lee G, Zhou ZH. Structure, disassembly, assembly, and budding of influenza viruses. In: Textbook of Influenza. 2013. p. 35–56.

122. Rossman JS, Lamb RA. Influenza virus assembly and budding. Virology. 2011;411(2):229–36.

123. Liao Z, Graham DR, Hildreth JEK. Lipid Rafts and HIV Pathogenesis: Virion-Associated Cholesterol Is Required for Fusion and Infection of Susceptible Cells. AIDS Res Hum Retroviruses. 2003 Aug;19(8):675–87.

124. Huarte N, Carravilla P, Cruz A, Lorizate M, Nieto-Garai JA, Kräusslich H-G, et al. Functional organization of the HIV lipid envelope. Sci Rep. 2016 Sep 28;6:34190.

125. Richard AS, Zhang A, Park S-J, Farzan M, Zong M, Choe H. Virion-associated phosphatidylethanolamine promotes TIM1-mediated infection by Ebola, dengue, and West Nile viruses. Proc Natl Acad Sci U S A. 2015 Nov 24;112(47):14682–7.

126. Callens N, Brügger B, Bonnafous P, Drobecq H, Gerl MJ, Krey T, et al. Morphology and Molecular Composition of Purified Bovine Viral Diarrhea Virus Envelope. Kuhn RJ, editor. PLOS Pathog. 2016 Mar 3;12(3):e1005476.

127. Tautz N, Tews BA, Meyers G. The Molecular Biology of Pestiviruses. Adv Virus Res. 2015 Jan 1;93:47–160.

128. Merz A, Long G, Hiet M-S, Brügger B, Chlanda P, Andre P, et al. Biochemical and morphological properties of hepatitis C virus particles and determination of their lipidome. J Biol Chem. 2011 Jan 28;286(4):3018–32.

129. Smit JM, Moesker B, Rodenhuis-Zybert I, Wilschut J. Flavivirus cell entry and membrane fusion. Viruses. 2011 Feb;3(2):160–71.

130. Möbius W, van Donselaar E, Ohno-Iwashita Y, Shimada Y, Heijnen HFG, Slot JW, et al. Recycling compartments and the internal vesicles of multivesicular bodies harbor most of the cholesterol found in the endocytic pathway. Traffic. 2003 Apr;4(4):222–31.

131. Schulze H, Kolter T, Sandhoff K. Principles of lysosomal membrane degradation. Biochim Biophys Acta - Mol Cell Res. 2009 Apr;1793(4):674–83.

132. Stiasny K, Koessl C, Heinz FX. Involvement of lipids in different steps of the flavivirus fusion mechanism. J Virol. 2003 Jul;77(14):7856–62.

133. Phalen T, Kielian M. Cholesterol is required for infection by Semliki Forest virus. J Cell Biol. 1991 Feb 15;112(4):615–23.

134. Zhu Y-Z, Cao M-M, Wang W-B, Wang W, Ren H, Zhao P, et al. Association of heat-shock protein 70 with lipid rafts is required for Japanese encephalitis virus infection in Huh7 cells. J Gen Virol. 2012 Jan 1;93(1):61–71.

135. Haid S, Pietschmann T, Pécheur E-I. Low pH-dependent hepatitis C virus membrane fusion depends on E2 integrity, target lipid composition, and density of virus particles. J Biol Chem. 2009 Jun 26;284(26):17657–67.

136. Corver J, Ortiz A, Allison SL, Schalich J, Heinz FX, Wilschut J. Membrane Fusion Activity of Tick-Borne Encephalitis Virus and Recombinant Subviral Particles in a Liposomal Model System. Virology. 2000 Mar 30;269(1):37–46.

137. Zaitseva E, Yang S-T, Melikov K, Pourmal S, Chernomordik L V. Dengue virus ensures its fusion

in late endosomes using compartment-specific lipids. PLoS Pathog. 2010 Jan;6(10):e1001131.

138. André P, Komurian-Pradel F, Deforges S, Perret M, Berland JL, Sodoyer M, et al. Characterization of low- and very-low-density hepatitis C virus RNA-containing particles. J Virol. 2002 Jul 15;76(14):6919–28.

139. Carro AC, Damonte EB. Requirement of cholesterol in the viral envelope for dengue virus infection. Virus Res. 2013 Jun;174(1–2):78–87.

140. Guillou H, Zadravec D, Martin PGP, Jacobsson A. The key roles of elongases and desaturases in mammalian fatty acid metabolism: Insights from transgenic mice. Prog Lipid Res. 2010 Apr 1;49(2):186–99.

141. Jump DB. Mammalian fatty acid elongases. Methods Mol Biol. 2009;579:375–89.

142. Bond LM, Miyazaki M, O'Neill LM, Ding F, Ntambi JM. Fatty Acid Desaturation and Elongation in Mammals. In: Biochemistry of Lipids, Lipoproteins and Membranes. Elsevier; 2016. p. 185–208.

143. Leonard AE, Kelder B, Bobik EG, Chuang L-T, Lewis CJ, Kopchick JJ, et al. Identification and expression of mammalian long-chain PUFA elongation enzymes. Lipids. 2002 Aug;37(8):733–40.

144. Alsaleh A, Maniou Z, Lewis FJ, Hall WL, Sanders TAB, O'Dell SD. ELOVL2 gene polymorphisms are associated with increases in plasma eicosapentaenoic and docosahexaenoic acid proportions after fish oil supplement. Genes Nutr. 2014 Jan;9(1):362.

145. Aulchenko YS, Ripatti S, Lindqvist I, Boomsma D, Heid IM, Pramstaller PP, et al. Loci influencing lipid levels and coronary heart disease risk in 16 European population cohorts. Nat Genet. 2009 Jan;41(1):47–55.

146. Yamashita Y, Nishiumi S, Kono S, Takao S, Azuma T, Yoshida M. Differences in elongation of very long chain fatty acids and fatty acid metabolism between triple-negative and hormone receptor-positive breast cancer. BMC Cancer. 2017 Aug 29;17(1):589.

147. Boot A, Oosting J, van Eendenburg JDH, Kuppen PJK, Morreau H, van Wezel T. Methylation associated transcriptional repression of ELOVL5 in novel colorectal cancer cell lines. Suzuki H, editor. PLoS One. 2017 Sep 20;12(9):e0184900.

148. Matsuzaka T, Shimano H, Yahagi N, Kato T, Atsumi A, Yamamoto T, et al. Crucial role of a long-chain fatty acid elongase, Elovl6, in obesity-induced insulin resistance. Nat Med. 2007 Oct 30;13(10):1193–202.

149. Moon Y-A, Horton JD. Identification of two mammalian reductases involved in the two-carbon fatty acyl elongation cascade. J Biol Chem. 2003 Feb 28;278(9):7335–43.

150. Rantakari P, Lagerbohm H, Kaimainen M, Suomela J-P, Strauss L, Sainio K, et al. Hydroxysteroid (17β) Dehydrogenase 12 Is Essential for Mouse Organogenesis and Embryonic Survival. Endocrinology. 2010 Apr 1;151(4):1893–901.

151. Sakurai N, Miki Y, Suzuki T, Watanabe K, Narita T, Ando K, et al. Systemic distribution and tissue localizations of human 17beta-hydroxysteroid dehydrogenase type 12. J Steroid Biochem Mol Biol. 2006 Jun;99(4–5):174–81.

152. Nagasaki S, Suzuki T, Miki Y, Akahira J -i., Kitada K, Ishida T, et al. 17 -Hydroxysteroid Dehydrogenase Type 12 in Human Breast Carcinoma: A Prognostic Factor via Potential Regulation of Fatty Acid Synthesis. Cancer Res. 2009 Feb 3;69(4):1392–9.

153. Szajnik M, Szczepanski MJ, Elishaev E, Visus C, Lenzner D, Zabel M, et al. 17β hydroxysteroid dehydrogenase type 12 (HSD17B12) is a marker of poor prognosis in ovarian carcinoma. Gynecol Oncol. 2012 Dec;127(3):587–94.

154. Ikeda M, Kanao Y, Yamanaka M, Sakuraba H, Mizutani Y, Igarashi Y, et al. Characterization of four mammalian 3-hydroxyacyl-CoA dehydratases involved in very long-chain fatty acid synthesis. Vol. 582, FEBS Letters. 2008.

155. Sawai M, Uchida Y, Ohno Y, Miyamoto M, Nishioka C, Itohara S, et al. The 3-hydroxyacyl-CoA dehydratases HACD1 and HACD2 exhibit functional redundancy and are active in a wide range of fatty acid elongation pathways. J Biol Chem. 2017 Sep 15 ;292(37):15538–51.

156. Wang B, Pelletier J, Massaad MJ, Herscovics A, Shore GC. The yeast split-ubiquitin membrane protein two-hybrid screen identifies BAP31 as a regulator of the turnover of endoplasmic reticulum-associated protein tyrosine phosphatase-like B. Mol Cell Biol. 2004 Apr 1;24(7):2767–78.

157. Kohlwein SD, Eder S, Oh C-S, Martin CE, Gable K, Bacikova D, et al. Tsc13p Is Required for Fatty Acid Elongation and Localizes to a Novel Structure at the Nuclear-Vacuolar Interface inSaccharomyces cerevisiae. Mol Cell Biol. 2001 Jan 1;21(1):109–25.

158. Abe K, Ohno Y, Sassa T, Taguchi R, Çalışkan M, Ober C, et al. Mutation for Nonsyndromic Mental Retardation in the *trans* -2-Enoyl-CoA Reductase *TER* Gene Involved in Fatty Acid Elongation Impairs the Enzyme Activity and Stability, Leading to Change in Sphingolipid Profile. J Biol Chem. 2013 Dec 20;288(51):36741–9.

159. Paton CM, Ntambi JM. Biochemical and physiological function of stearoyl-CoA desaturase. Am J Physiol Endocrinol Metab. 2009 Jul 1;297(1):E28-37.

160. Miyazaki M, Ntambi JM. Fatty acid desaturation and chain elongation in mammals. In: Biochemistry of Lipids, Lipoproteins and Membranes. Elsevier; 2008. p. 191–211.

161. Murakami M, Yamamoto K, Miki Y, Murase R, Sato H, Taketomi Y. The Roles of the Secreted Phospholipase A2 Gene Family in Immunology. Adv Immunol. 2016 Jan 1;132:91–134.

162. Mouchlis VD, Dennis EA. Membrane and inhibitor interactions of intracellular phospholipases A2. Adv Biol Regul. 2016;61:17–24.

163. Nakamura MT, Nara TY. Essential fatty acid synthesis and its regulation in mammals. Prostaglandins, Leukot Essent Fat Acids. 2003 Feb 1;68(2):145–50.

164. Monteiro J, Leslie M, Moghadasian MH, Arendt BM, Allard JP, Ma DWL. The role of n − 6 and n − 3 polyunsaturated fatty acids in the manifestation of the metabolic syndrome in cardiovascular disease and non-alcoholic fatty liver disease. Food Funct. 2014 Feb 26;5(3):426.

165. Leslie MA, Cohen DJA, Liddle DM, Robinson LE, Ma DWL. A review of the effect of omega-3 polyunsaturated fatty acids on blood triacylglycerol levels in normolipidemic and borderline hyperlipidemic individuals. Lipids Health Dis. 2015 Dec 6;14(1):53.

166. Oscarsson J, Hurt-Camejo E. Omega-3 fatty acids eicosapentaenoic acid and docosahexaenoic acid and their mechanisms of action on apolipoprotein B-containing lipoproteins in humans: a review. Lipids Health Dis. 2017 Dec 10;16(1):149.

167. Casas R, Sacanella E, Estruch R. The immune protective effect of the Mediterranean diet against chronic low-grade inflammatory diseases. Endocr Metab Immune Disord Drug Targets. 2014;14(4):245–54.

168. Chowdhury R, Stevens S, Gorman D, Pan A, Warnakula S, Chowdhury S, et al. Association between fish consumption, long chain omega 3 fatty acids, and risk of cerebrovascular disease: systematic review and meta-analysis. BMJ. 2012 Oct 30;345:e6698.

169. Myhrstad MCW, Retterstøl K, Telle-Hansen VH, Ottestad I, Halvorsen B, Holven KB, et al. Effect of marine n-3 fatty acids on circulating inflammatory markers in healthy subjects and subjects with cardiovascular risk factors. Inflamm Res. 2011 Apr;60(4):309–19.

170. Wolters M, Dering C, Siani A, Russo P, Kaprio J, Risé P, et al. The role of a FADS1 polymorphism in the association of fatty acid blood levels, BMI and blood pressure in young children—Analyses based on path models. Palmer ND, editor. PLoS One. 2017 Jul 21;12(7):e0181485.

171. Guo H, Zhang L, Zhu C, Yang F, Wang S, Zhu S, et al. A Single Nucleotide Polymorphism in the FADS1 Gene is Associated with Plasma Fatty Acid and Lipid Profiles and Might Explain Gender Difference in Body Fat Distribution. Lipids Health Dis. 2017 Dec 31;16(1):67.

172. Li S-W, Wang J, Yang Y, Liu Z-J, Cheng L, Liu H-Y, et al. Polymorphisms in FADS1 and FADS2 alter plasma fatty acids and desaturase levels in type 2 diabetic patients with coronary artery disease. J Transl Med. 2016 Dec 22;14(1):79.

173. Vaittinen M, Walle P, Kuosmanen E, Männistö V, Käkelä P, Ågren J, et al. *FADS2* genotype regulates delta-6 desaturase activity and inflammation in human adipose tissue. J Lipid Res. 2016 Jan;57(1):56–65.

174. Sampath H, Ntambi JM. Role of stearoyl-CoA desaturase-1 in skin integrity and whole body energy balance. J Biol Chem. 2014 Jan 31;289(5):2482–8.

175. Bené H, Lasky D, Ntambi JM. Cloning and characterization of the human stearoyl-CoA desaturase gene promoter: transcriptional activation by sterol regulatory element binding protein and repression by polyunsaturated fatty acids and cholesterol. Biochem Biophys Res Commun. 2001 Jun 29;284(5):1194–8.

176. Ntambi JM, Miyazaki M, Dobrzyn A. Regulation of stearoyl-CoA desaturase expression. Lipids. 2004 Nov;39(11):1061–5.

177. Ntambi JM, Miyazaki M, Stoehr JP, Lan H, Kendziorski CM, Yandell BS, et al. Loss of stearoyl-CoA desaturase-1 function protects mice against adiposity. Proc Natl Acad Sci U S A. 2002 Aug 20;99(17):11482–6.

178. Tillander V, Alexson SEH, Cohen DE. Deactivating Fatty Acids: Acyl-CoA Thioesterase-Mediated Control of Lipid Metabolism. Trends Endocrinol Metab. 2017 Jul 1; 28(7):473–84.

179. Xia C, Dong R, Chen C, Wang H, Wang DW. Cardiomyocyte specific expression of Acyl-coA thioesterase 1 attenuates sepsis induced cardiac dysfunction and mortality. Biochem Biophys Res Commun. 2015 Dec 25;468(4):533–40.

180. Yang S, Chen C, Wang H, Rao X, Wang F, Duan Q, et al. Protective Effects of Acyl-coA Thioesterase 1 on Diabetic Heart via PPARα/PGC1α Signaling. Peng T, editor. PLoS One. 2012 Nov 30;7(11):e50376.

181. Moffat C, Bhatia L, Nguyen T, Lynch P, Wang M, Wang D, et al. Acyl-CoA thioesterase-2 facilitates mitochondrial fatty acid oxidation in the liver. J Lipid Res. 2014 Dec 1;55(12):2458–70.

182. Hunt MC, Tillander V, Alexson SEH. Regulation of peroxisomal lipid metabolism: The role of acyl-CoA and coenzyme A metabolizing enzymes. Biochimie. 2014 Mar 1;98:45–55.

183. Yamada J. Long-chain acyl-CoA hydrolase in the brain. Amino Acids. 2005 May 2;28(3):273–8.

184. Forwood JK, Thakur AS, Guncar G, Marfori M, Mouradov D, Meng W, et al. Structural basis for recruitment of tandem hotdog domains in acyl-CoA thioesterase 7 and its role in inflammation. Proc Natl Acad Sci U S A. 2007 Jun 19;104(25):10382–7.

185. Varanasi U, Chu R, Chu S, Espinosa R, LeBeau MM, Reddy JK. Isolation of the human peroxisomal acyl-CoA oxidase gene: organization, promoter analysis, and chromosomal localization. Proc Natl Acad Sci U S A. 1994 Apr 12;91(8):3107–11.

186. Abe Y, Honsho M, Nakanishi H, Taguchi R, Fujiki Y. Very-long-chain polyunsaturated fatty acids accumulate in phosphatidylcholine of fibroblasts from patients with Zellweger syndrome and acyl-CoA oxidase1 deficiency. Biochim Biophys Acta - Mol Cell Biol Lipids. 2014 Apr 4;1841(4):610–9.

187. Zha S, Ferdinandusse S, Hicks JL, Denis S, Dunn TA, Wanders RJ, et al. Peroxisomal branched chain fatty acid ?-oxidation pathway is upregulated in prostate cancer. Prostate. 2005 Jun 1;63(4):316–23.

188. Das AK, Uhler MD, Hajra AK. Molecular Cloning and Expression of Mammalian Peroxisomal *trans* -2-Enoyl-coenzyme A Reductase cDNAs. J Biol Chem. 2000 Aug 11 ;275(32):24333–40.

189. Gloerich J, Ruiter JPN, van den Brink DM, Ofman R, Ferdinandusse S, Wanders RJA. Peroxisomal *trans* -2-enoyl-CoA reductase is involved in phytol degradation. FEBS Lett. 2006 Apr 3;580(8):2092–6.

190. Yan H, Li Z, Shen Q, Wang Q, Tian J, Jiang Q, et al. Aberrant expression of cell cycle and material metabolism related genes contributes to hepatocellular carcinoma occurrence. Pathol - Res Pract. 2017 Apr 1;213(4):316–21.

191. Kases BF, Bjorkhemq I. The Journal Of Biological Chemistry Peroxisomal Bile Acid-CoA:Amino-Acid N-Acyltransferase in Rat Liver. 1989;264(16):9220–3.

192. Hunt MC, Siponen MI, Alexson SEH. The emerging role of acyl-CoA thioesterases and acyltransferases in regulating peroxisomal lipid metabolism. Biochim Biophys Acta - Mol Basis Dis. 2012 Sep 1;1822(9):1397–410.

193. Carpenter K, Pollitt RJ, Middleton B. Human liver long-chain 3-hydroxyacyl-coenzyme a dehydrogenase is a multifunctional membrane-bound beta-oxidation enzyme of mitochondria. Biochem Biophys Res Commun. 1992 Mar 16;183(2):443–8.

194. Choi JH, Yoon HR, Kim GH, Park SJ, Shin YL, Yoo HW. Identification of novel mutations of the HADHA and HADHB genes in patients with mitochondrial trifunctional protein deficiency. Int J Mol Med. 2007 Jan 1;19(1):81–7.

195. Zhao Z, Lu J, Han L, Wang X, Man Q, Liu S. Prognostic significance of two lipid metabolism enzymes, HADHA and ACAT2, in clear cell renal cell carcinoma. Tumor Biol. 2016 Jun 29;37(6):8121–30.

196. Amako Y, Munakata T, Kohara M, Siddiqui A, Peers C, Harris M. Hepatitis C virus attenuates mitochondrial lipid β-oxidation by downregulating mitochondrial trifunctional-protein expression. J Virol. 2015 Apr 15;89(8):4092–101.

197. Sumner LW, Amberg A, Barrett D, Beale MH, Beger R, Daykin CA, et al. Proposed minimum reporting standards for chemical analysis. Metabolomics. 2007 Sep 19;3(3):211–21.

198. Cui L, Lee YH, Kumar Y, Xu F, Lu K, Ooi EE, et al. Serum Metabolome and Lipidome Changes in Adult Patients with Primary Dengue Infection. Michael SF, editor. PLoS Negl Trop Dis. 2013 Aug 15;7(8):e2373.

199. Cui L, Lee YH, Thein TL, Fang J, Pang J, Ooi EE, et al. Serum Metabolomics Reveals Serotonin as a Predictor of Severe Dengue in the Early Phase of Dengue Fever. Rothman AL, editor. PLoS Negl Trop Dis. 2016 Apr 7;10(4):e0004607.

200. Walther DJ, Peter J-U, Winter S, Höltje M, Paulmann N, Grohmann M, et al. Serotonylation of Small GTPases Is a Signal Transduction Pathway that Triggers Platelet α-Granule Release. Cell. 2003 Dec 26;115(7):851–62.

201. Blankfield A. A Brief Historic Overview of Clinical Disorders Associated with Tryptophan: The Relevance to Chronic Fatigue Syndrome (CFS) and Fibromyalgia (FM). Int J Tryptophan Res. 2012;5:27–32.

202. Cui L, Pang J, Lee YH, Ooi EE, Ong CN, Leo YS, et al. Serum metabolome changes in adult patients with severe dengue in the critical and recovery phases of dengue infection. Harris E, editor. PLoS Negl Trop Dis. 2018 Jan 24;12(1):e0006217.

203. Chen T-H, Tang P, Yang C-F, Kao L-H, Lo Y-P, Chuang C-K, et al. Antioxidant defense is one of the mechanisms by which mosquito cells survive dengue 2 viral infection. Virology. 2011 Feb 20;410(2):410–7.

204. Gullberg RC, Jordan Steel J, Moon SL, Soltani E, Geiss BJ. Oxidative stress influences positive strand RNA virus genome synthesis and capping. Virology. 2015 Jan;475:219–29.

205. Cui L, Hou J, Fang J, Lee YH, Costa VV, Wong LH, et al. Serum Metabolomics Investigation of Humanized Mouse Model of Dengue Virus Infection. J Virol. 2017 Jul 15;91(14).

206. Voge N V., Perera R, Mahapatra S, Gresh L, Balmaseda A, Loroño-Pino MA, et al. Metabolomics-Based Discovery of Small Molecule Biomarkers in Serum Associated with Dengue Virus Infections and Disease Outcomes. Simmons CP, editor. PLoS Negl Trop Dis. 2016 Feb 25;10(2):e0004449.

207. Møller S, Laigaard F, Olgaard K, Hemmingsen C. Effect of 1,25-dihydroxy-vitamin D3 in experimental sepsis. Int J Med Sci. 2007 Jul 10;4(4):190–5.

208. El-Bacha T, Struchiner CJ, Cordeiro MT, Almeida FCL, Marques ET, Da Poian AT, et al. 1H Nuclear Magnetic Resonance Metabolomics of Plasma Unveils Liver Dysfunction in Dengue Patients. J Virol. 2016 Aug 15;90(16):7429–43.

209. Biswas HH, Gordon A, Nuñez A, Perez MA, Balmaseda A, Harris E. Lower Low-Density Lipoprotein Cholesterol Levels Are Associated with Severe Dengue Outcome. Halstead SB, editor. PLoS Negl Trop Dis. 2015 Sep 3;9(9):e0003904.

210. Tollinger CD, Vreman HJ, Weiner MW. Measurement of acetate in human blood by gas chromatography: effects of sample preparation, feeding, and various diseases. Clin Chem. 1979 Oct;25(10):1787–90.

211. Newsholme P, Curi R, Pithon Curi TC, Murphy CJ, Garcia C, Pires de Melo M. Glutamine metabolism by lymphocytes, macrophages, and neutrophils: its importance in health and disease. J Nutr Biochem. 1999 Jun;10(6):316–24.

212. Beatty PR, Puerta-Guardo H, Killingbeck SS, Glasner DR, Hopkins K, Harris E. Dengue virus NS1 triggers endothelial permeability and vascular leak that is prevented by NS1 vaccination. Sci Transl Med. 2015 Sep 9;7(304):304ra141.

213. St John AL, Rathore AP, Raghavan B, Ng M-L, Abraham SN, Putvatana R. Contributions of mast cells and vasoactive products, leukotrienes and chymase, to dengue virus-induced vascular leakage. Elife. 2013 Apr 30;2:e00481.

214. Tramontini Gomes de Sousa Cardozo F, Baimukanova G, Lanteri MC, Keating SM, Moraes Ferreira F, Heitman J, et al. Serum from dengue virus-infected patients with and without plasma leakage differentially affects endothelial cells barrier function in vitro. Jin D-Y, editor. PLoS One. 2017 Jun 6;12(6):e0178820.

215. Myers RM, Carey DE. Concurrent isolation from patient of two arboviruses, Chikungunya and dengue type 2. Science. 1967 Sep 15;157(3794):1307–8.

216. Villamil-Gómez WE, Rodríguez-Morales AJ, Uribe-García AM, González-Arismendy E, Castellanos JE, Calvo EP, et al. Zika, dengue, and chikungunya co-infection in a pregnant woman from Colombia. Int J Infect Dis. 2016 Oct 1;51:135–8.

217. Zambrano H, Waggoner JJ, Almeida C, Rivera L, Benjamin JQ, Pinsky BA. Zika Virus and Chikungunya Virus CoInfections: A Series of Three Cases from a Single Center in Ecuador. Am J Trop Med Hyg. 2016 Oct 5;95(4):894–6.

218. Dupont-Rouzeyrol M, O'Connor O, Calvez E, Daurès M, John M, Grangeon J-P, et al. Co-infection with Zika and dengue viruses in 2 patients, New Caledonia, 2014. Emerg Infect Dis. 2015 Feb;21(2):381–2.

219. Waggoner JJ, Gresh L, Vargas MJ, Ballesteros G, Tellez Y, Soda KJ, et al. Viremia and Clinical Presentation in Nicaraguan Patients Infected With Zika Virus, Chikungunya Virus, and Dengue Virus. Clin Infect Dis. 2016 Dec 15;63(12):1584–90.

220. Furuya-Kanamori L, Liang S, Milinovich G, Soares Magalhaes RJ, Clements ACA, Hu W, et al. Co-distribution and co-infection of chikungunya and dengue viruses. BMC Infect Dis. 2016 Dec 3;16(1):84.

221. Melo CFOR, Delafiori J, de Oliveira DN, Guerreiro TM, Esteves CZ, Lima E de O, et al. Serum Metabolic Alterations upon Zika Infection. Front Microbiol. 2017 Oct 10;8:1954.

222. Shrinet J, Shastri JS, Gaind R, Bhavesh NS, Sunil S. Serum metabolomics analysis of patients with chikungunya and dengue mono/co-infections reveals distinct metabolite signatures in the three disease conditions. Sci Rep. 2016 Nov 15;6(1):36833.

223. Cui L, Fang J, Ooi EE, Lee YH. Serial Metabolome Changes in a Prospective Cohort of Subjects with Influenza Viral Infection and Comparison with Dengue Fever. J Proteome Res. 2017 Jul 7;16(7):2614–22.

224. Shahfiza N, Osman H, Thean Hock T, Zaki Abdel-Hamid A-H. Metabolomics approach for multibiomarkers determination to investigate dengue virus infection in human patients. 2017.

225. Birungi G, Chen SM, Loy BP, Ng ML, Fong S, Li Y. Metabolomics Approach for Investigation of Effects of Dengue Virus Infection Using the EA . hy926 Cell Line research articles. 2010;6523–34.

226. Uchida L, Espada-Murao LA, Takamatsu Y, Okamoto K, Hayasaka D, Yu F, et al. The dengue virus conceals double-stranded RNA in the intracellular membrane to escape from an interferon response. Sci Rep. 2014 Jan 10;4:7395.

227. Junjhon J, Pennington JG, Edwards TJ, Perera R, Lanman J, Kuhn RJ. Ultrastructural characterization and three-dimensional architecture of replication sites in dengue virus-infected mosquito cells. J Virol. 2014 May 1;88(9):4687–97.

228. Ritchie ME, Phipson B, Wu D, Hu Y, Law CW, Shi W, et al. limma powers differential expression analyses for RNA-sequencing and microarray studies. Nucleic Acids Res. 2015 Apr 20;43(7):e47–e47.

229. Wishart DS, Feunang YD, Marcu A, Guo AC, Liang K, Vázquez-Fresno R, et al. HMDB 4.0: the human metabolome database for 2018. Nucleic Acids Res. 2018 Jan 4;46(D1):D608–17.

230. da Silva RR, Dorrestein PC, Quinn RA. Illuminating the dark matter in metabolomics. Proc Natl Acad Sci U S A. 2015 Oct 13;112(41):12549–50.

231. Dias D, Jones O, Beale D, Boughton B, Benheim D, Kouremenos K, et al. Current and Future Perspectives on the Structural Identification of Small Molecules in Biological Systems. Metabolites. 2016 Dec 15;6(4):46.

232. Xia J. Computational Strategies for Biological Interpretation of Metabolomics Data. In Springer, Cham; 2017. p. 191–206.

233. Li S, Park Y, Duraisingham S, Strobel FH, Khan N, Soltow QA, et al. Predicting Network Activity from High Throughput Metabolomics. Ouzounis CA, editor. PLoS Comput Biol. 2013 Jul 4;9(7):e1003123.

234. Diamond DL, Syder AJ, Jacobs JM, Sorensen CM, Walters K-A, Proll SC, et al. Temporal Proteome and Lipidome Profiles Reveal Hepatitis C Virus-Associated Reprogramming of Hepatocellular Metabolism and Bioenergetics. Luo GG, editor. PLoS Pathog. 2010 Jan 8;6(1):e1000719.

235. Kanehisa M, Goto S. KEGG: kyoto encyclopedia of genes and genomes. Nucleic Acids Res. 2000 Jan 1;28(1):27–30.

236. Jump DB. Mammalian fatty acid elongases. Methods Mol Biol. 2009;579:375–89.

237. Dennis EA, Cao J, Hsu Y-H, Magrioti V, Kokotos G. Phospholipase A 2 Enzymes: Physical Structure, Biological Function, Disease Implication, Chemical Inhibition, and Therapeutic Intervention. Chem Rev. 2011 Oct 12;111(10):6130–85.

238. Dennis EA, Norris PC. Eicosanoid storm in infection and inflammation. Nat Rev Immunol. 2015 Aug;15(8):511–23.

239. Jan J-T, Chen B-H, Ma S-H, Liu C-I, Tsai H-P, Wu H-C, et al. Potential Dengue Virus-Triggered Apoptotic Pathway in Human Neuroblastoma Cells: Arachidonic Acid, Superoxide Anion, and NF-kappa B Are Sequentially Involved. J Virol. 2000 Sep 15;74(18):8680–91.

240. Loke W, Chow A, Lam Mok Sing K, Lee C-YJ, Halliwell B, Lim EC, et al. Augmentation of 5-lipoxygenase activity and expression during dengue serotype-2 infection. Virol J. 2013 Oct 30;10(1):322.

241. Caputo M, De Rosa MC, Rescigno T, Zirpoli H, Vassallo A, De Tommasi N, et al. Binding of polyunsaturated fatty acids to LXRα and modulation of SREBP-1 interaction with a specific SCD1 promoter element. Cell Biochem Funct. 2014 Dec;32(8):637–46.

242. Livak KJ, Schmittgen TD. Analysis of Relative Gene Expression Data Using Real- Time Quantitative PCR and the 2 ΔΔC T Method. METHODS. 2001;25:402–8.

243. Shimada K, Navarro J, Goeger DE, Mustafa SB, Weigel PH, Weinman SA. Expression and regulation of leukotriene-synthesis enzymes in rat liver cells. Hepatology. 1998 Nov 1;28(5):1275–81.

244. Xu X-M. 5-Lipoxygenase contributes to the progression of hepatocellular carcinoma. Mol Med Rep. 2011 Aug 8.

245. Wang Q, Zhang W, Liu Q, Zhang X, Lv N, Ye L, et al. A mutant of hepatitis B virus X protein (HBxDelta127) promotes cell growth through a positive feedback loop involving 5-lipoxygenase and fatty acid synthase. Neoplasia. 2010 Feb;12(2):103–15.

246. Bell RL, Young PR, Albert D, Lanni C, Summers JB, Brooks DW, et al. The discovery and development of zileuton: an orally active 5-lipoxygenase inhibitor. Int J Immunopharmacol. 1992 Apr;14(3):505–10.

247. Shi W, Meininger CJ, Haynes TE, Hatakeyama K, Wu G. Regulation of Tetrahydrobiopterin Synthesis and Bioavailability in Endothelial Cells. Cell Biochem Biophys. 2004;41(3):415–34.

248. Purdy JG, Shenk T, Rabinowitz JD. Fatty Acid Elongase 7 Catalyzes Lipidome Remodeling Essential for Human Cytomegalovirus Replication. Cell Rep. 2015 Mar 3;10(8):1375–85.

249. Zhang J, Zhang Z, Chukkapalli V, Nchoutmboube JA, Li J, Randall G, et al. Positive-strand RNA viruses stimulate host phosphatidylcholine synthesis at viral replication sites. Proc Natl Acad Sci. 2016 Feb 23;113(8):E1064–73.

250. Tang W-C, Lin R-J, Liao C-L, Lin Y-L. Rab18 Facilitates Dengue Virus Infection by Targeting Fatty Acid Synthase to Sites of Viral Replication. J Virol. 2014 Jun 15;88(12):6793–804.

251. Blight KJ, McKeating JA, Rice CM. Highly permissive cell lines for subgenomic and genomic hepatitis C virus RNA replication. J Virol. 2002 Dec;76(24):13001–14.

252. Kinney RM, Butrapet S, Chang G-JJ, Tsuchiya KR, Roehrig JT, Bhamarapravati N, et al. Construction of Infectious cDNA Clones for Dengue 2 Virus: Strain 16681 and Its Attenuated Vaccine Derivative, Strain PDK-53. Virology. 1997 Apr 14;230(2):300–8.

253. Dulbecco R, Vogt M. Some problems of animal virology as studied by the plaque technique. Cold Spring Harb Symp Quant Biol. 1953;18:273–9.

254. RC T. R: A language and environment for statistical computing. Vienna, Austria. 2015; http://www.r-project.org/.

255. Tautenhahn R, Bottcher C, Neumann S. Highly sensitive feature detection for high resolution LC/MS. BMC Bioinformatics. 2008 Nov 28;9(1):504.

256. Benton HP, Want EJ, Ebbels TMD. Correction of mass calibration gaps in liquid chromatography–mass spectrometry metabolomics data. Bioinformatics. 2010 Oct 1;26(19):2488–9.

257. Colin A. Smith, Elizabeth J. Want, Grace O'Maille, Ruben Abagyan and, Siuzdak* G. XCMS: Processing Mass Spectrometry Data for Metabolite Profiling Using Nonlinear Peak Alignment, Matching, and Identification. 2006.

258. and JTP, Marcotte* EM. Chromatographic Alignment of ESI-LC-MS Proteomics Data Sets by Ordered Bijective Interpolated Warping. 2006.

259. Libiseller G, Dvorzak M, Kleb U, Gander E, Eisenberg T, Madeo F, et al. IPO: a tool for automated optimization of XCMS parameters. BMC Bioinformatics. 2015 Dec 16;16(1):118.

260. Weixun Wang †, Haihong Zhou †, Hua Lin, Sushmita Roy, Thomas A. Shaler, Lander R. Hill, et al. Quantification of Proteins and Metabolites by Mass Spectrometry without Isotopic Labeling or Spiked Standards. 2003.

261. Veselkov KA, Vingara LK, Masson P, Robinette SL, Want E, Li J V., et al. Optimized Preprocessing of Ultra-Performance Liquid Chromatography/Mass Spectrometry Urinary Metabolic Profiles for Improved Information Recovery. Anal Chem. 2011 Aug;83(15):5864–72.

262. Tautenhahn R, Patti GJ, Rinehart D, Siuzdak G. XCMS Online: A Web-Based Platform to Process Untargeted Metabolomic Data. Anal Chem. 2012 Jun 5;84(11):5035–9.

263. Shannon P, Markiel A, Ozier O, Baliga NS, Wang JT, Ramage D, et al. Cytoscape: A Software Environment for Integrated Models of Biomolecular Interaction Networks. Genome Res. 2003 Nov 1;13(11):2498–504.

264. Laue T, Emmerich P, Schmitz H. Detection of dengue virus RNA in patients after primary or secondary dengue infection by using the TaqMan automated amplification system. J Clin Microbiol. 1999 Aug;37(8):2543–7.

265. Butrapet S, Kinney RM, Huang CYH. Determining genetic stabilities of chimeric dengue vaccine candidates based on dengue 2 PDK-53 virus by sequencing and quantitative TaqMAMA. J Virol Methods. 2006;131(1):1–9.

266. Zimmerberg J, Kozlov MM. How proteins produce cellular membrane curvature. Nat Rev Mol Cell Biol. 2006 Jan; 7(1):9–19.

267. Paton CM, Ntambi JM. Biochemical and physiological function of stearoyl-CoA desaturase. AJP Endocrinol Metab. 2009 Jul 1;297(1):E28–37.

268. Sampath H, Ntambi JM. Role of stearoyl-CoA desaturase-1 in skin integrity and whole body energy balance. J Biol Chem. 2014 Jan 31;289(5):2482–8.

269. Aktepe TE, Pham H, Mackenzie JM. Differential utilisation of ceramide during replication of the flaviviruses West Nile and dengue virus. Virology. 2015;484:241–50.

270. Xu K, Nagy PD. RNA virus replication depends on enrichment of phosphatidylethanolamine at replication sites in subcellular membranes. Proc Natl Acad Sci U S A. 2015 Mar 25;112(14):E1782-1791.

271. Welsch S, Miller S, Romero-Brey I, Merz A, Bleck CKE, Walther P, et al. Composition and three-dimensional architecture of the dengue virus replication and assembly sites. Cell Host Microbe. 2009 Apr 23;5(4):365–75.

272. Lee WM, Ishikawa M, Ahlquist P. Mutation of host delta9 fatty acid desaturase inhibits brome mosaic virus RNA replication between template recognition and RNA synthesis. J Virol. 2001 Mar 1;75(5):2097–106.

273. Nguyen LN, Lim Y-S, Pham L V, Shin H-Y, Kim Y-S, Hwang SB. Stearoyl coenzyme a desaturase 1 is associated with hepatitis C virus replication complex and regulates viral replication. J Virol. 2014 Nov 13;88(21):12311–25.

274. Lyn RK, Singaravelu R, Kargman S, O'Hara S, Chan H, Oballa R, et al. Stearoyl-CoA desaturase inhibition blocks formation of hepatitis C virus-induced specialized membranes. Sci Rep. 2014 Jan 1;4:4549.

275. Nchoutmboube JA, Viktorova EG, Scott AJ, Ford LA, Pei Z, Watkins PA, et al. Increased long chain acyl-Coa synthetase activity and fatty acid import is linked to membrane synthesis for development of picornavirus replication organelles. PLoS Pathog. 2013 Jan 6;9(6):e1003401.

276. Ntambi JM, Miyazaki M. Regulation of stearoyl-CoA desaturases and role in metabolism. Prog Lipid Res. 2004;43(2):91–104.

277. Dunn KW, Kamocka MM, McDonald JH. A practical guide to evaluating colocalization in biological microscopy. Am J Physiol Cell Physiol. 2011 Apr;300(4):C723-42.

278. Manders Emm, Verbeek Fj, Aten Ja. Measurement of co-localization of objects in dual-colour confocal images. J Microsc. 1993 Mar 1;169(3):375–82.

279. Xin Z, Zhao H, Serby MD, Liu B, Liu M, Szczepankiewicz BG, et al. Discovery of piperidine-aryl urea-based stearoyl-CoA desaturase 1 inhibitors. Bioorg Med Chem Lett. 2008 Aug 1;18(15):4298–302.

280. Liao J, Sportsman R, Harris J, Stahl A. Real-time quantification of fatty acid uptake using a novel fluorescence assay. J Lipid Res. 2005 Mar 1;46(3):597–602.

281. Apte-Sengupta S, Sirohi D, Kuhn RJ. Coupling of replication and assembly in flaviviruses. Curr Opin Virol. 2014 Dec;9:134–42.

282. Carro AC, Damonte EB. Requirement of cholesterol in the viral envelope for dengue virus infection. Virus Res. 2013 Jun;174(1–2):78–87.

283. Plevka P, Battisti AJ, Junjhon J, Winkler DC, Holdaway HA, Keelapang P, et al. Maturation of flaviviruses starts from one or more icosahedrally independent nucleation centres. EMBO Rep. 2011 Jun;12(6):602–6.

284. Yu I-M, Zhang W, Holdaway HA, Li L, Kostyuchenko VA, Chipman PR, et al. Structure of the immature dengue virus at low pH primes proteolytic maturation. Science. 2008 Mar 28;319(5871):1834–7.

285. Landschulz KT, Jump DB, Macdougald OA, Lane MD. Transcriptional Control of the Stearoyl-CoA Desaturase-1 Gene by Polyunsaturated Fatty Acids1. Biochem Biophys Res Commun. 1994 Apr;200(2):763–8.

286. Kümmerer BM, Rice CM. Mutations in the yellow fever virus nonstructural protein NS2A selectively block production of infectious particles. J Virol. 2002 May 15;76(10):4773–84.

287. Peck B, Schug ZT, Zhang Q, Dankworth B, Jones DT, Smethurst E, et al. Inhibition of fatty acid desaturation is detrimental to cancer cell survival in metabolically compromised environments. Cancer Metab. 2016;4(1):297–308.

288. Scaglia N, Igal RA. Inhibition of Stearoyl-CoA Desaturase 1 expression in human lung adenocarcinoma cells impairs tumorigenesis. Int J Oncol. 2008 Oct;33(4):839–50.

289. Hagen RM, Rodriguez-Cuenca S, Vidal-Puig A. An allostatic control of membrane lipid composition by SREBP1. FEBS Lett. 2010 Jun 18;584(12):2689–98.

290. Quinn PJ. A lipid-phase separation model of low-temperature damage to biological membranes. Cryobiology. 1985 Apr 1;22(2):128–46.

291. Spector AA, Yorek MA. Membrane lipid composition and cellular function. J Lipid Res. 1985 Sep 1;26(9):1015–35.

292. Murata N, 10s DA. Membrane Fluidity and Temperature Perception'. Plant Phvsiol. 1997;11(5):875–9.

293. Jose J, Snyder JE, Kuhn RJ. A structural and functional perspective of alphavirus replication and assembly. Future Microbiol. 2009 Sep 1;4(7):837–56.

294. Stephens EB, Compans RW. Assembly Of Animal Viruses At Cellular Membranes. Ann Rev Microbiol;988(42):489–5.

295. Liao Z, Cimakasky LM, Hampton R, Nguyen DH, Hildreth JEK. Lipid Rafts and HIV Pathogenesis: Host Membrane Cholesterol Is Required for Infection by HIV Type 1. AIDS Res Hum Retroviruses. 2001 Jul 20;17(11):1009–19.

296. Huang CY, Butrapet S, Pierro DJ, Chang GJ, Hunt AR, Bhamarapravati N, et al. Chimeric dengue type 2 (vaccine strain PDK-53)/dengue type 1 virus as a potential candidate dengue type 1 virus vaccine. J Virol. 2000 Apr;74(7):3020–8.

297. Jirakanjanakit N, Khin MM, Yoksan S, Bhamarapravati N. Dynamics of susceptibility and transmissibility of the live, attenuated, candidate vaccines dengue-1 PDK13, dengue-3 PGMK30F3, and dengue-4 PDK48 after oral infection in Aedes aegypti. Am J Trop Med Hyg. 1999 Oct;61(4):672–6.

298. Angsubhakorn S, Yoksan S, Pradermwong A, Nitatpattana N, Sahaphong S, Bhamarapravati N. Dengue-3 (16562) PGMK 33 vaccine: neurovirulence, viremia and immune responses in Macaca fascicularis. Southeast Asian J Trop Med Public Health. 1994 Sep;25(3):554–9.

299. Goh KCM, Tang CK, Norton DC, Gan ES, Tan HC, Sun B, et al. Molecular determinants of plaque size as an indicator of dengue virus attenuation. Sci Rep. 2016 Sep 17;6(1):26100.

300. Rice CM, Lenches EM, Eddy SR, Shin SJ, Sheets RL, Strauss JH. Nucleotide sequence of yellow fever virus: implications for flavivirus gene expression and evolution. Science. 1985 Aug 23;229(4715):726–33.

301. Khromykh AA, Westaway EG. Completion of Kunjin virus RNA sequence and recovery of an infectious RNA transcribed from stably cloned full-length cDNA. J Virol. 1994 Jul;68(7):4580–8.

302. Lanciotti RS, Lambert AJ, Holodniy M, Saavedra S, Signor L del CC. Phylogeny of Zika Virus in Western Hemisphere, 2015. Emerg Infect Dis. 2016 May;22(5):933–5.

303. Brown BA, Ehrenfeld E. Translation of poliovirus rna in vitro: Changes in cleavage pattern and initiation sites by ribosomal salt wash. Virology. 1979;97(2):396–405.

304. Miyazaki M, Kim YC, Gray-Keller MP, Attie AD, Ntambi JM. The biosynthesis of hepatic cholesterol esters and triglycerides is impaired in mice with a disruption of the gene for stearoyl-CoA desaturase 1. J Biol Chem. 2000 Sep 29;275(39):30132–8.

305. Junjhon J, Edwards TJ, Utaipat U, Bowman VD, Holdaway HA, Zhang W, et al. Influence of pr-M cleavage on the heterogeneity of extracellular dengue virus particles. J Virol. 2010 Aug;84(16):8353–8.

306. Team RS. RStudio:Integrated Development for R. RStudio Inc, Boston, MA. 2016;URL http://www.rstudio.com/.

307. Bhatt S, Gething PW, Brady OJ, Messina JP, Farlow AW, Moyes CL, et al. The global distribution and burden of dengue. Nature. 2013 Apr 25;496(7446):504–7.

308. Halstead SB. Dengue. Imperial College Press; 2008. 485.

309. Guzman MG, Halstead SB, Artsob H, Buchy P, Farrar J, Gubler DJ, et al. Dengue: a continuing global threat. Nat Rev Microbiol. 2010 Dec 1;8(12):S7–16.

310. Nasci RS. Movement of chikungunya virus into the Western hemisphere. Emerg Infect Dis. 2014 Aug;20(8):1394–5.

311. Zaid A, Gérardin P, Taylor A, Mostafavi H, Malvy D, Mahalingam S. Chikungunya Virus Arthritis: Implications of Acute and Chronic Inflammation Mechanisms on Patient Management. Arthritis Rheumatol. 2017 Dec 29

312. Special Programme for Research & Training in Tropical Diseases (TDR) sponsored by Handbook : Quality Practices In Basic Biomedical Research.

313. Mabey D, Peeling RW, Ustianowski A, Perkins MD. Diagnostics for the developing world. Nat Rev Microbiol. 2004 Mar 1;2(3):231–40.

314. Molins CR, Ashton L V, Wormser GP, Andre BG, Hess AM, Delorey MJ, et al. Metabolic differentiation of early Lyme disease from southern tick-associated rash illness (STARI). Sci Transl Med. 2017 Aug 16;9(403):eaal2717.

315. Cui L, Pang J, Hou Y, Eng L, Ooi E, Nam C, et al. PLOS Neglected Tropical Diseases Serum Metabolome Changes in Adult Patients with Severe Dengue in the Critical and Recovery Phases of Dengue Infection. 2018 Jan 24;12(1):e0006217

316. Cui L, Lee YH, Thein TL, Fang J, Pang J, Ooi EE, et al. Serum Metabolomics Reveals Serotonin as a Predictor of Severe Dengue in the Early Phase of Dengue Fever. PLoS Negl Trop Dis. 2016 Apr;10(4):e0004607.

317. Villamor E, Villar La, Lozano A, Herrera Vm, Herrán Of. Vitamin D serostatus and dengue fever progression to dengue hemorrhagic fever/dengue shock syndrome. Epidemiol Infect. 2017 Oct 14;145(14):2961–70.

318. Giraldo DM, Cardona A, Urcuqui-Inchima S. High-dose of vitamin D supplement is associated with reduced susceptibility of monocyte-derived macrophages to dengue virus infection and pro-inflammatory cytokine production: An exploratory study. Clin Chim Acta. 2018 Mar;478:140–51.

319. Molins CR, Ashton L V., Wormser GP, Hess AM, Delorey MJ, Mahapatra S, et al. Development of a Metabolic Biosignature for Detection of Early Lyme Disease. Clin Infect Dis. 2015 Jun 15;60(12):1767–75.

320. World Health Organization. Dengue haemorrhagic fever : diagnosis, treatment, prevention, and control. World Health Organization; 1997. 84p.

321. Phipson B, Lee S, Majewski IJ, Alexander WS, Smyth GK. Robust Hyperparameter Estimation Protects Against Hypervariable Genes And Improves Power To Detect Differential Expression. Ann Appl Stat. 2016 Jun;10(2):946–63

322. Riley CP, Gough ES, He J, Jandhyala SS, Kennedy B, Orcun S, et al. The Proteome Discovery Pipeline – A Data Analysis Pipeline for Mass Spectrometry-Based Differential Proteomics Discovery. Open Proteomics J. 2010;3:8–19.

323. Borgeat P, Samuelsson B. Arachidonic acid metabolism in polymorphonuclear leukocytes: effects of ionophore A23187. Proc Natl Acad Sci U S A. 1979 May 1;76(5):2148–52.

324. Iversen L, Kragballe K. Arachidonic acid metabolism in skin health and disease. Prostaglandins Other Lipid Mediat. 2000 Nov 1;63(1–2):25–42.

325. Trivedi DK, Hollywood KA, Goodacre R. Metabolomics for the masses: The future of metabolomics in a personalized world. New Horizons Transl Med. 2017 Mar;3(6):294–305.

326. Shirakami Y, Lee S-A, Clugston RD, Blaner WS. Hepatic metabolism of retinoids and disease associations. Biochim Biophys Acta. 2012 Jan;1821(1):124–36.

327. Heyman RA, Mangelsdorf DJ, Dyck JA, Stein RB, Eichele G, Evans RM, et al. 9-cis retinoic acid is a high affinity ligand for the retinoid X receptor. Cell. 1992 Jan 24;68(2):397–406.

328. Lewis RA, Austen KF, Drazen JM, Clark DA, Marfat A, Corey EJ. Slow reacting substances of anaphylaxis: identification of leukotrienes C-1 and D from human and rat sources. Proc Natl Acad Sci U S A. 1980 Jun 1;77(6):3710–4.

329. Dahlén SE, Björk J, Hedqvist P, Arfors KE, Hammarström S, Lindgren JA, et al. Leukotrienes promote plasma leakage and leukocyte adhesion in postcapillary venules: in vivo effects with relevance to the acute inflammatory response. Proc Natl Acad Sci U S A. 1981 Jun 1;78(6):3887–91.

330. Bjork J, Hedqvist P, Arfors K-E. Increase in vascular permeability induced by leukotriene b4 and the role of polymorphonuclear leukocytes. Inflammation. 1982 Jun;6(2):189–200.

331. Ricciotti E, FitzGerald GA. Prostaglandins and inflammation. Arterioscler Thromb Vasc Biol. 2011 May;31(5):986–1000.

332. Funk CD. Prostaglandins and Leukotrienes: Advances in Eicosanoid Biology. Science (80-). 2001 Nov 30;294(5548):1871–5.

333. Lin C-K, Tseng C-K, Wu Y-H, Liaw C-C, Lin C-Y, Huang C-H, et al. Cyclooxygenase-2 facilitates dengue virus replication and serves as a potential target for developing antiviral agents. Sci Rep. 2017 Mar 20;7:44701.

334. Pace-Asciak CR. Pathophysiology of the hepoxilins. Biochim Biophys Acta - Mol Cell Biol Lipids. 2015 Apr 1;1851(4):383–96.

335. Pace-Asciak CR. Hepoxilins in cancer and inflammation—use of hepoxilin antagonists. Cancer Metastasis Rev. 2011 Dec 18;30(3–4):493–506.

336. McCormick BA. Bacterial-induced hepoxilin A_3 secretion as a pro-inflammatory mediator. FEBS J. 2007 Jul;274(14):3513–8.

337. R core team. R: A Language and Environment for Statistical Computing. https://wwwR-project.org/. 2017

338. Stekhoven DJ, Buhlmann P. MissForest--non-parametric missing value imputation for mixed-type data. Bioinformatics. 2012 Jan 1;28(1):112–8.

339. Stekhoven DJ, Bühlmann P. MissForest - nonparametric missing value imputation for mixed-type data. 2011 May 4.

340. Hackstadt AJ, Hess AM. Filtering for increased power for microarray data analysis. BMC Bioinformatics. 2009 Jan 8;10(1):11.

341. Benjamini Y, Hochberg Y. Controlling the False Discovery Rate: A Practical and Powerful Approach to Multiple Testing. Vol. 57, Journal of the Royal Statistical Society. Series B (Methodological). WileyRoyal Statistical Society; 1995. p. 289–300.

342. Tibshirani R. Regression Shrinkage and Selection via the Lasso. Vol. 58, Journal of the Royal Statistical Society. Series B (Methodological). WileyRoyal Statistical Society; 1996. p. 267–88.

343. Friedman J, Hastie T, Tibshirani R. Regularization Paths for Generalized Linear Models via Coordinate Descent. J Stat Softw. 2010;33(1):1–22.

344. Cui L, Fang J, Ooi EE, Lee YH. Serial Metabolome Changes in a Prospective Cohort of Subjects with Influenza Viral Infection and Comparison with Dengue Fever. J Proteome Res. 2017 Jul 7;16(7):2614–22.

345. Plummer E, Buck MD, Sanchez M, Greenbaum JA, Turner J, Grewal R, et al. Dengue Virus Evolution under a Host-Targeted Antiviral. J Virol. 2015 May 15;89(10):5592–601.

346. Rodenhuis-Zybert IA, van der Schaar HM, da Silva Voorham JM, van der Ende-Metselaar H, Lei H-Y, Wilschut J, et al. Immature dengue virus: a veiled pathogen? PLoS Pathog. 2010 Jan;6(1):e1000718.

347. Moser TS, Schieffer D, Cherry S. AMP-Activated Kinase Restricts Rift Valley Fever Virus Infection by Inhibiting Fatty Acid Synthesis. Khromykh A, editor. PLoS Pathog. 2012 Apr 19;8(4):e1002661.

APPENDIX

Supplemental Figures

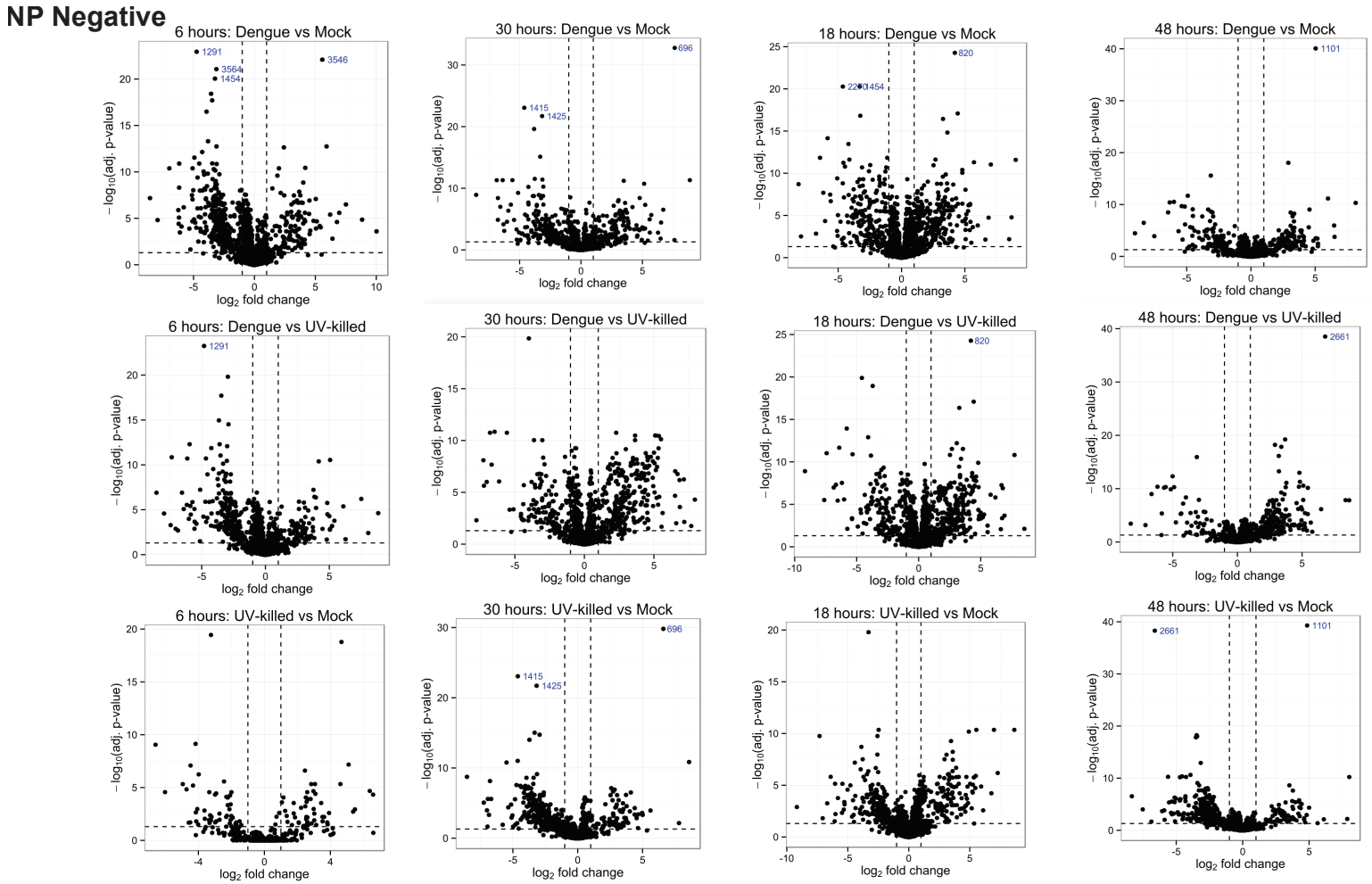

Supplemental Figure 1 Volcano plots of non-polar metabolites in negative mode. All the significantly different metabolites in the non-polar negative samples at the indicated time-points and comparisons are shown for molecular features with altered levels of abundance (|log2 fold change| ≥ 1 and p-value < 0.05). The vertical dashed lines indicate a 2-fold change in abundance and the horizontal dashed line indicates a p-value = 0.05.

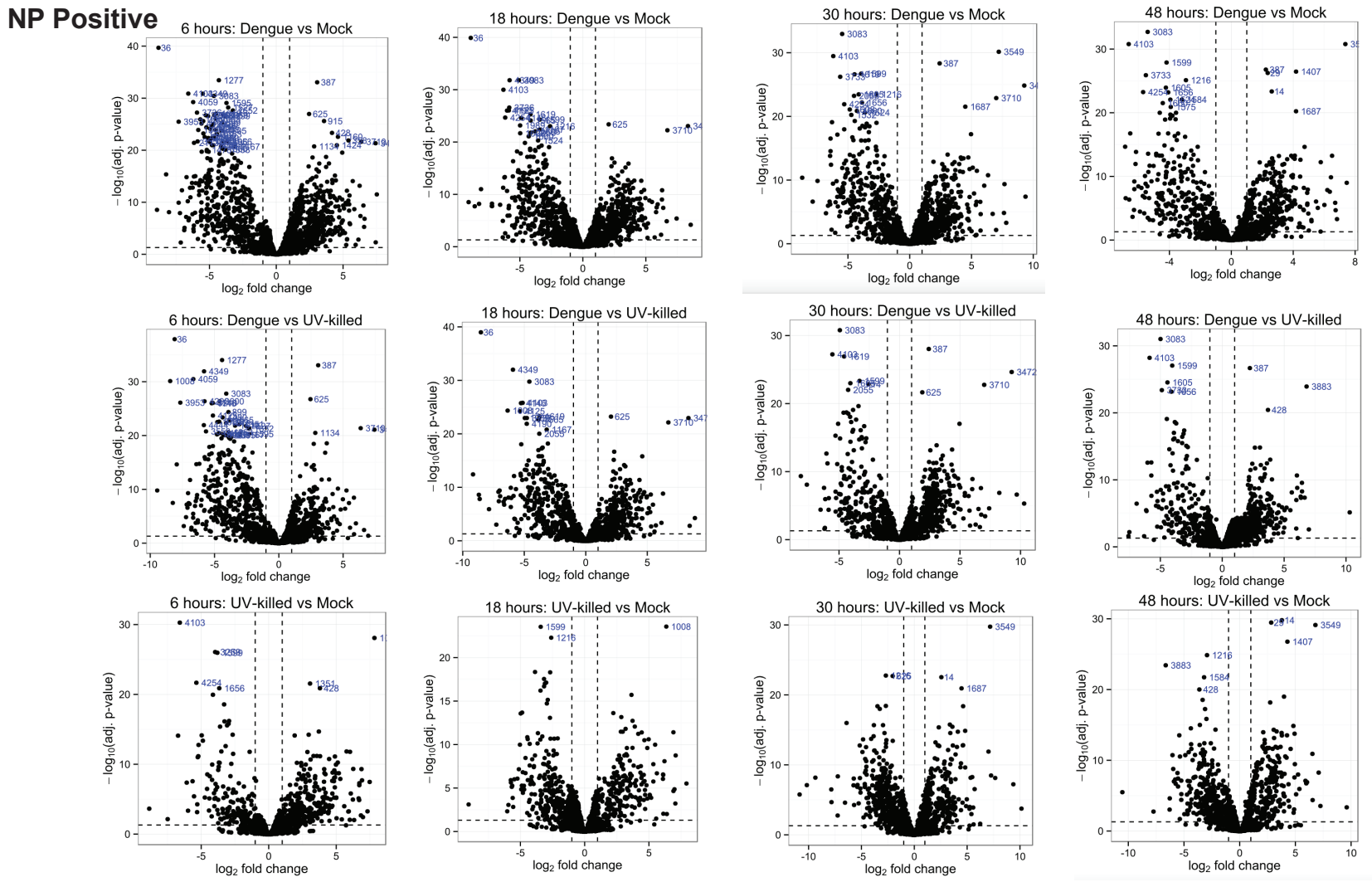

Supplemental Figure 2 Volcano plots of non-polar metabolites in positive mode. All the significantly different metabolites in the non-polar positive samples at the indicated time-points and comparisons are shown for molecular features with altered levels of abundance (|log2 fold change| ≥ 1 and p-value < 0.05). The vertical dashed lines indicate a 2-fold change in abundance and the horizontal dashed line indicates a p-value = 0.05.

Polar Negative

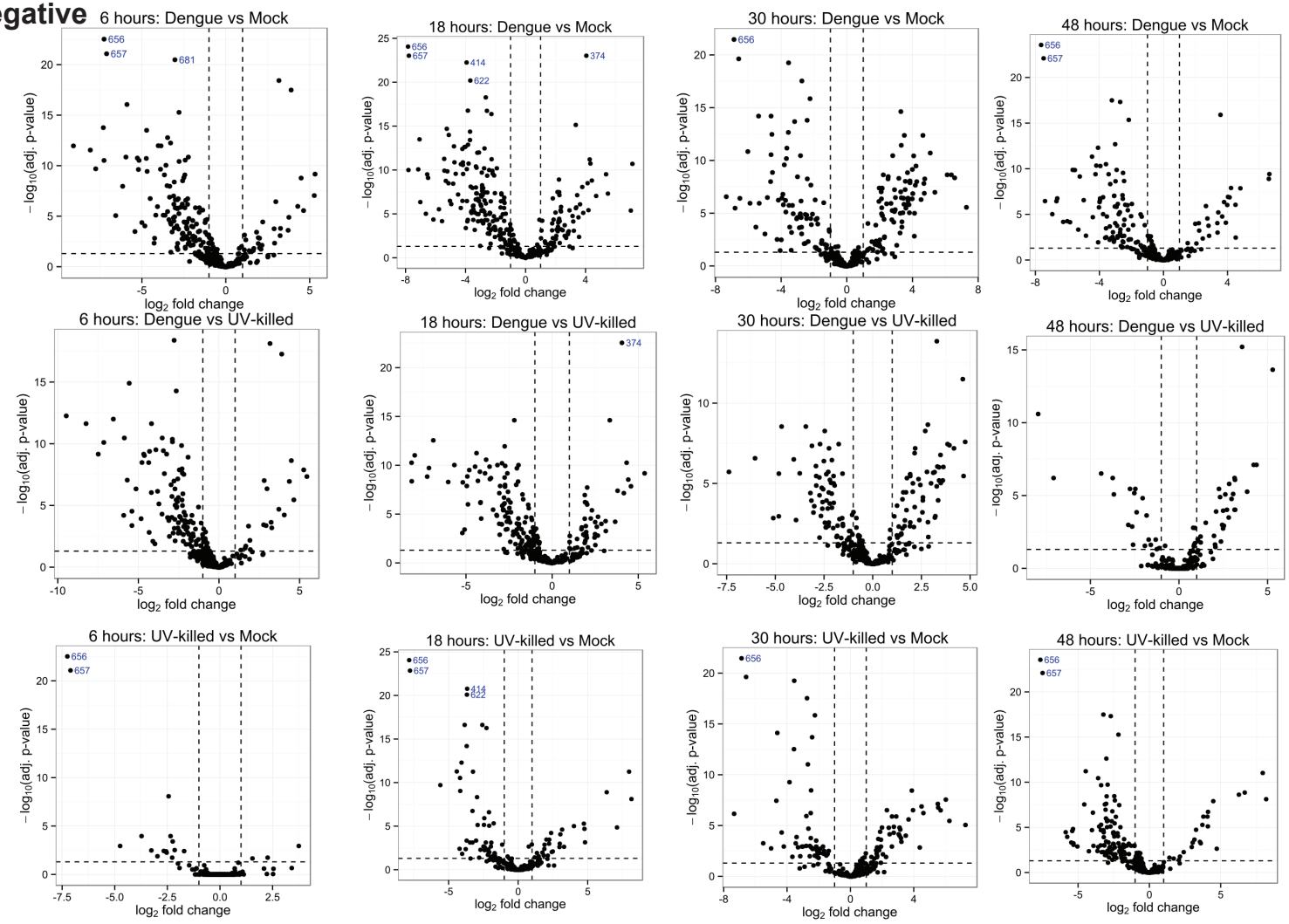

Supplemental Figure 3 Volcano plots of polar metabolites in the negative mode. All the significantly different metabolites at the indicated time-points and comparisons are shown for molecular features with altered levels of abundance (|log2 fold change| ≥ 1 and p-value < 0.05). The vertical dashed lines indicate a 2-fold change in abundance and the horizontal dashed line indicates a p-value = 0.05.

Polar Positive

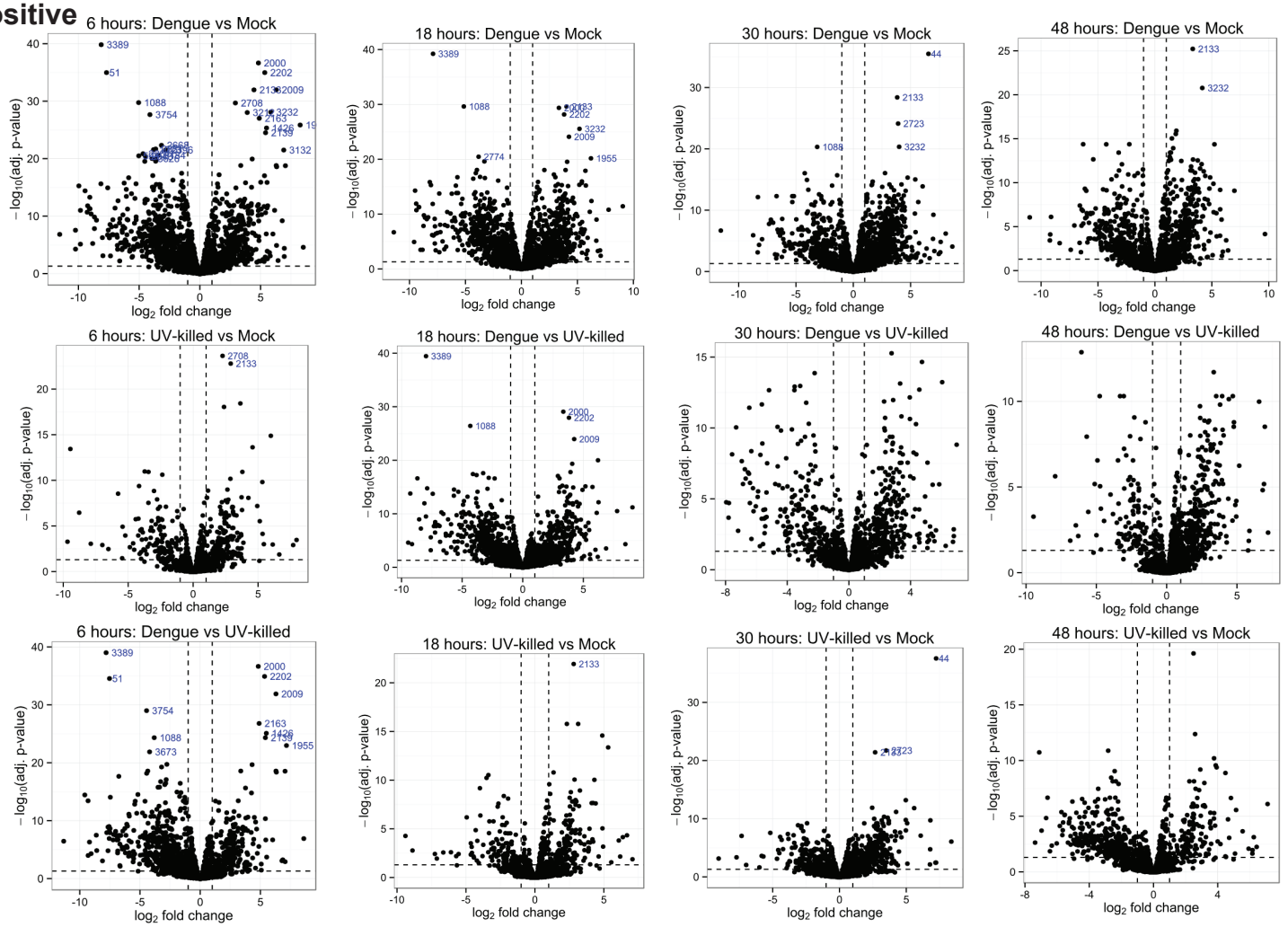

Supplemental Figure 4 Volcano plots of polar metabolites in the positive mode. All the significantly different metabolites at the indicated time-points and comparisons are shown for molecular features with altered levels of abundance (|log2 fold change| ≥ 1 and p-value < 0.05). The vertical dashed lines indicate a 2-fold change in abundance and the horizontal dashed line indicates a p-value = 0.05.

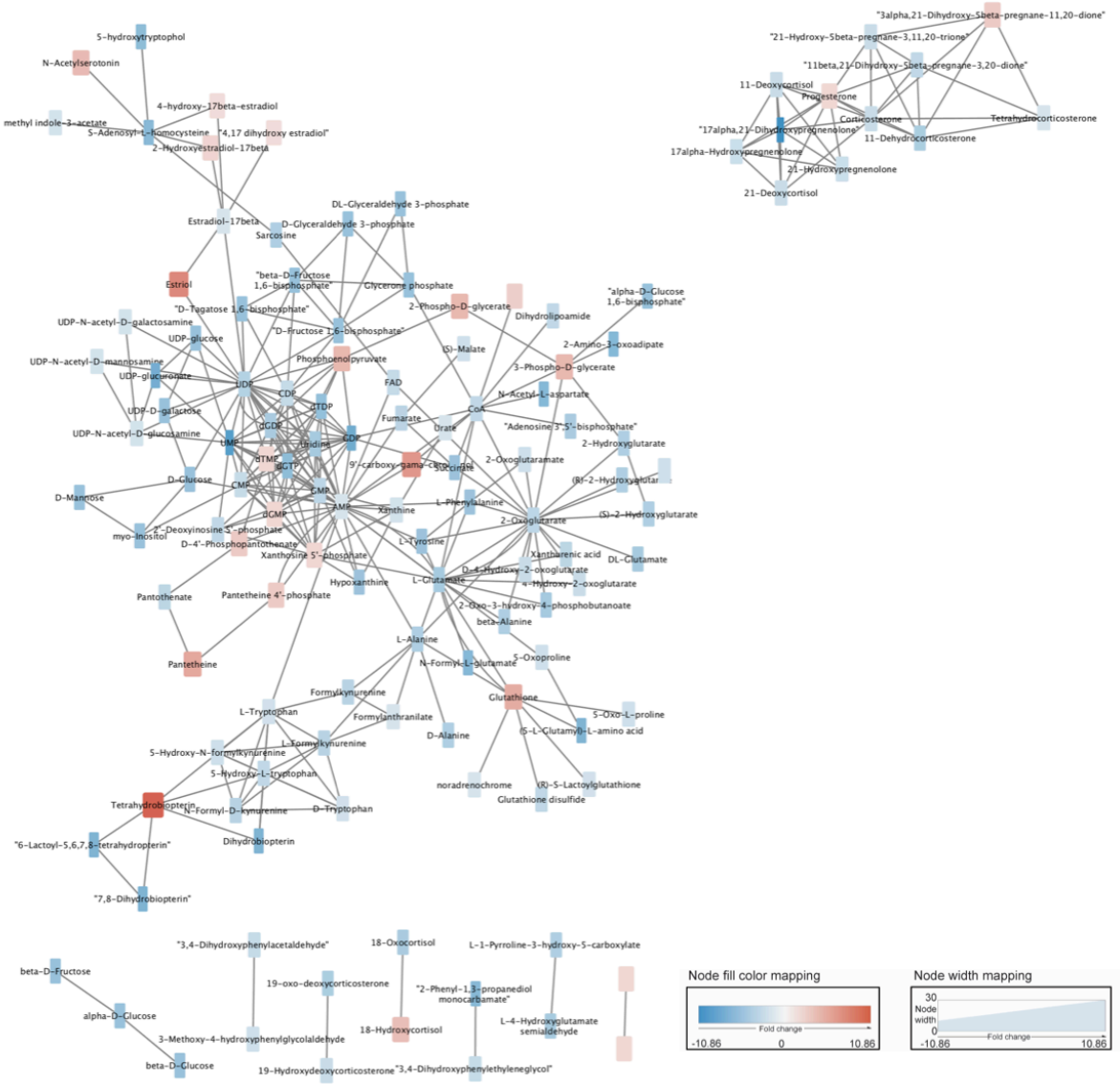
"3alpha,21-Dihydroxy-5beta-pregnane-11,20-dione"
"21-Hydroxy-5beta-pregnane-3,11,20-trione"
"11beta,21-Dihydroxy-5beta-pregnane-3,20-dione"
11-Deoxycortisol
Progesterone
Corticosterone
Tetrahydrocorticosterone
"17alpha,21-Dihydroxypregnenolone"
11-Dehydrocorticosterone
17alpha-Hydroxypregnenolone
21-Hydroxypregnenolone
21-Deoxycortisol
5-hydroxytryptophol
N-Acetylserotonin
4-hydroxy-17beta-estradiol
methyl indole-3-acetate
S-Adenosyl-L-homocysteine
"4,17 dihydroxy estradiol"
2-Hydroxyestradiol-17beta
Estradiol-17beta
DL-Glyceraldehyde 3-phosphate
D-Glyceraldehyde 3-phosphate
Sarcosine
Estriol
"beta-D-Fructose 1,6-bisphosphate"
Glycerone phosphate
"D-Tagatose 1,6-bisphosphate"
2-Phospho-D-glycerate
Dihydrolipoamide
"alpha-D-Glucose 1,6-bisphosphate"
UDP-N-acetyl-D-galactosamine
UDP-glucose
"D-Fructose 1,6-bisphosphate"
(S)-Malate
2-Amino-3-oxoadipate
UDP-N-acetyl-D-mannosamine
Phosphoenolpyruvate
3-Phospho-D-glycerate
UDP-glucuronate
UDP
CDP
FAD
N-Acetyl-L-aspartate
UDP-D-galactose
dTDP
Fumarate
CoA
"Adenosine 3',5'-bisphosphate"
UDP-N-acetyl-D-glucosamine
dUDP
Urate
2-Hydroxyglutarate
UMP
Uridine
GDP
dTMP
dGTP
9'-carboxy-gamma-C...
Succinate
2-Oxoglutaramate
D-Glucose
(R)-2-Hydroxyglutar...
CMP
D-Mannose
L-Phenylalanine
AMP
Xanthine
2-Oxoglutarate
(S)-2-Hydroxyglutarate
dGMP
2'-Deoxyinosine 5'-phosphate
myo-Inositol
L-Tyrosine
D-4'-Phosphopantothenate
Xanthosine 5'-phosphate
Xanthurenic acid
DL-Glutamate
D-4-Hydroxy-2-oxoglutarate
Hypoxanthine
L-Glutamate
4-Hydroxy-2-oxoglutarate
Pantothenate
Pantetheine 4'-phosphate
2-Oxo-3-hydroxy-4-phosphobutanoate
beta-Alanine
L-Alanine
Pantetheine
N-Formyl-L-glutamate
5-Oxoproline
Formylkynurenine
Glutathione
L-Tryptophan
5-Oxo-L-proline
Formylanthranilate
(S-L-Glutamyl)-L-amino acid
D-Alanine
L-Formylkynurenine
5-Hydroxy-N-formylkynurenine
5-Hydroxy-L-tryptophan
noradrenochrome
(R)-S-Lactoylglutathione
Glutathione disulfide
Tetrahydrobiopterin
N-Formyl-D-kynurenine
D-Tryptophan
"6-Lactoyl-5,6,7,8-tetrahydropterin"
Dihydrobiopterin
"7,8-Dihydrobiopterin"
"3,4-Dihydroxyphenylacetaldehyde"
18-Oxocortisol
L-1-Pyrroline-3-hydroxy-5-carboxylate
beta-D-Fructose
19-oxo-deoxycorticosterone
"2-Phenyl-1,3-propanediol monocarbamate"
alpha-D-Glucose
L-4-Hydroxyglutamate semialdehyde
3-Methoxy-4-hydroxyphenylglycolaldehyde
18-Hydroxycortisol
beta-D-Glucose
19-Hydroxydeoxycorticosterone
"3,4-Dihydroxyphenylethyleneglycol"
Node fill color mapping
Fold change
-10.86
0
10.86
Node width mapping
30
Node width
0
Fold change
-10.86
10.86

Supplemental Figure 1 Metabolic map at 6 hpi. Metabolites annotated by network analysis that are found when comparing DENV2 to mock samples at 6 hpi. The node size and color are determined by the statistical differences between DENV2 and mock with the values noted in the legend. The large nodes (red) are metabolites that are upregulated in DENV2 vs. mock and the small nodes (blue) are metabolites that are downregulated in DENV2 vs. mock samples. The edges connecting the nodes represent enzymatic reactions that connect the specific metabolites. Their length has no significance.

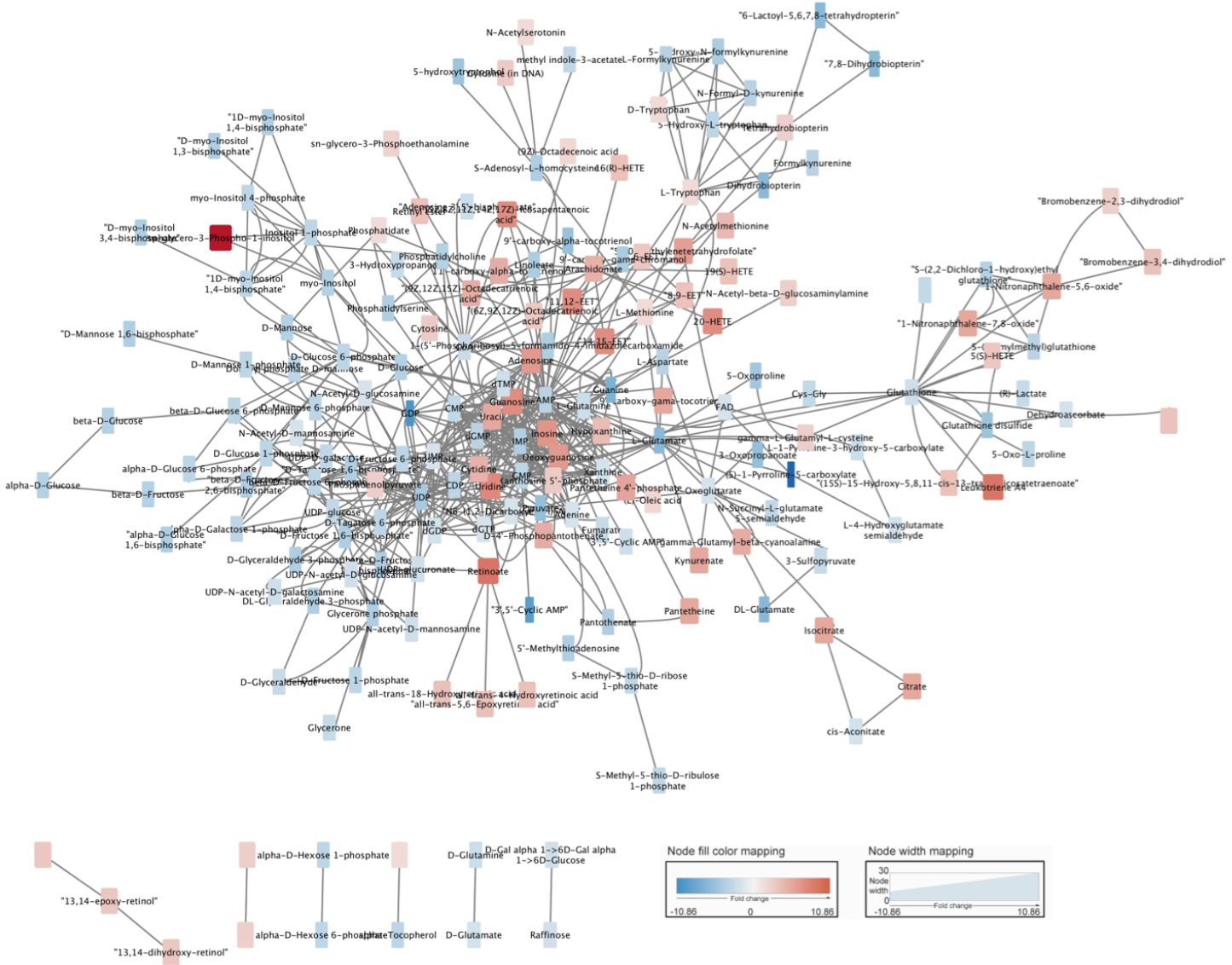
"6-Lactoyl-5,6,7,8-tetrahydropterin"
N-Acetylserotonin
"7,8-Dihydrobiopterin"
methyl indole-3-acetate
L-Formylkynurenine
5-hydroxytryptophol
N-Formyl-D-kynurenine
D-Tryptophan
Tetrahydrobiopterin
"1D-myo-Inositol 1,4-bisphosphate"
"D-myo-Inositol 1,3-bisphosphate"
sn-glycero-3-Phosphoethanolamine
(9Z)-Octadecenoic acid
S-Adenosyl-L-homocysteine
16(R)-HETE
Formylkynurenine
L-Tryptophan
Dihydrobiopterin
myo-Inositol 4-phosphate
"Bromobenzene-2,3-dihydrodiol"
"D-myo-Inositol 3,4-bisphosphate"
Inositol 1-phosphate
Phosphatidate
N-Acetylmethionine
"Bromobenzene-3,4-dihydrodiol"
Phosphatidylcholine
3-Hydroxypropanoate
19(S)-HETE
"1D-myo-Inositol 1,4-bisphosphate"
myo-Inositol
"S-(2,2-Dichloro-1-hydroxyethyl glutathione"
1-Nitronaphthalene-5,6-oxide
"(9Z,12Z,15Z)-Octadecatrienoic acid"
8,9-EET
N-Acetyl-beta-D-glucosaminylamine
Phosphatidylserine
"11,12-EET"
"(6Z,9Z,12Z)-Octadecatrienoic acid"
L-Methionine
20-HETE
"1-Nitronaphthalene-7,8-oxide"
"D-Mannose 1,6-bisphosphate"
D-Mannose
Cytosine
14,15-EET
5-Oxoproline
D-Glucose 6-phosphate
Adenosine
L-Aspartate
Cys-Gly
Glutathione
D-Mannose 1-phosphate
D-Glucose
(R)-Lactate
N-Acetyl-D-glucosamine
Guanine
FAD
Dehydroascorbate
beta-D-Glucose
beta-D-Glucose 6-phosphate
D-Mannose 6-phosphate
Guanosine
AMP
L-Glutamine
Glutathione disulfide
CMP
Uracil
N-Acetyl-D-mannosamine
dGMP
Inosine
Hypoxanthine
L-Glutamate
gamma-L-Glutamyl-L-cysteine
D-Glucose 1-phosphate
IMP
3-Oxopropanoate
5-Oxo-L-proline
alpha-D-Glucose 6-phosphate
Cytidine
Deoxyguanosine
(S)-1-Pyrroline-5-carboxylate
alpha-D-Glucose
beta-D-Fructose
"beta-D-Fructose 6-phosphate"
2,6-bisphosphate"
CDP
Uridine
Xanthine
Pantetheine 4'-phosphate
"(15S)-15-Hydroxy-5,8,11-cis-13-trans-eicosatetraenoate"
Leukotriene A4
2-Oxoglutarate
(Z)-Oleic acid
UDP
N-Succinyl-L-glutamate
5'-semialdehyde
UDP-glucose
Adenine
L-4-Hydroxyglutamate semialdehyde
"alpha-D-Galactose 1-phosphate
D-Tagatose 6-phosphate
"alpha-D-Glucose 1,6-bisphosphate"
D-Fructose 1,6-bisphosphate
dGDP
dGTP
D-4'-Phosphopantothenate
3',5'-Cyclic AMP
gamma-Glutamyl-beta-cyanoalanine
Kynurenate
3-Sulfopyruvate
D-Glyceraldehyde 3-phosphate
D-Fructose
Retinoate
UDP-N-acetyl-D-glucosamine
UDP-N-acetyl-D-galactosamine
DL-Glyceraldehyde 3-phosphate
"3',5'-Cyclic AMP"
Pantetheine
DL-Glutamate
Isocitrate
Glycerone phosphate
Pantothenate
UDP-N-acetyl-D-mannosamine
5'-Methylthioadenosine
S-Methyl-5-thio-D-ribose 1-phosphate
D-Glyceraldehyde
D-Fructose 1-phosphate
Citrate
all-trans-18-Hydroxyretinoic acid
"all-trans-5,6-Epoxyretinoic acid"
Glycerone
cis-Aconitate
S-Methyl-5-thio-D-ribulose 1-phosphate
"13,14-epoxy-retinol"
alpha-D-Hexose 1-phosphate
D-Glutamine
D-Gal alpha 1->6D-Gal alpha 1->6D-Glucose
"13,14-dihydroxy-retinol"
alpha-D-Hexose 6-phosphate
alpha-Tocopherol
D-Glutamate
Raffinose
Node fill color mapping
Fold change
-10.86
0
10.86
Node width mapping
30
Node width
0
Fold change
-10.86
10.86

Supplemental Figure 2 Metabolic map at 18 hpi. Metabolites annotated by network analysis that are found when comparing DENV2 to mock samples at 18 hpi. The node size and color are determined by the statistical differences between DENV2 and mock with the values noted in the legend. The large nodes (red) are metabolites that are upregulated in DENV2 vs. mock and the small nodes (blue) are metabolites that are downregulated in DENV2 vs. mock samples. The edges connecting the nodes represent enzymatic reactions that connect the specific metabolites. Their length has no significance.

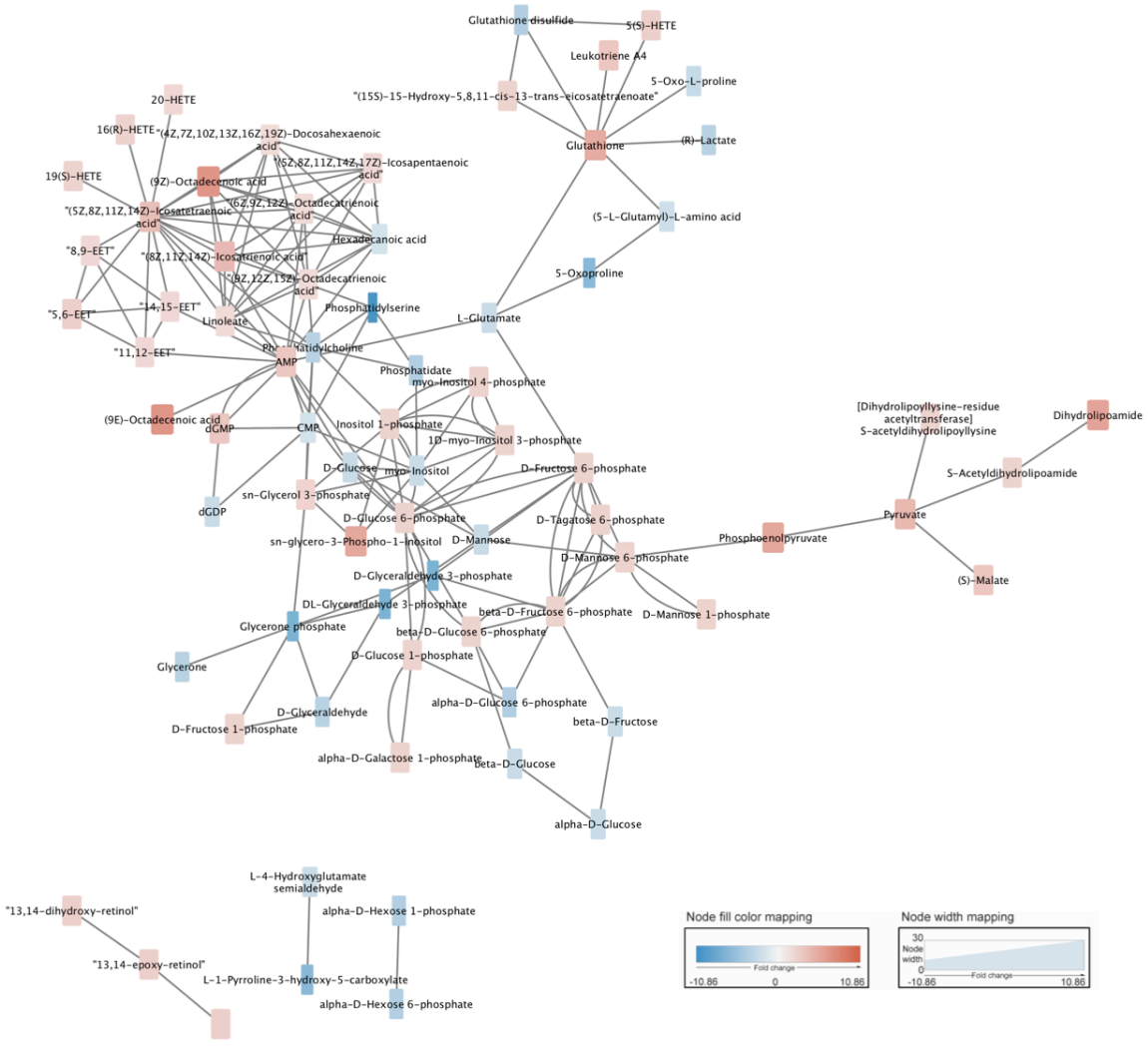

Supplemental Figure 3 Metabolic map at 30 hpi. Metabolites annotated by network analysis that are found when comparing DENV2 to mock samples at 30 hpi. The node size and color are determined by the statistical differences between DENV2 and mock with the values noted in the legend. The large nodes (red) are metabolites that are upregulated in DENV2 vs. mock and the small nodes (blue) are metabolites that are downregulated in DENV2 vs. mock samples. The edges connecting the nodes represent enzymatic reactions that connect the specific metabolites. Their length has no significance.

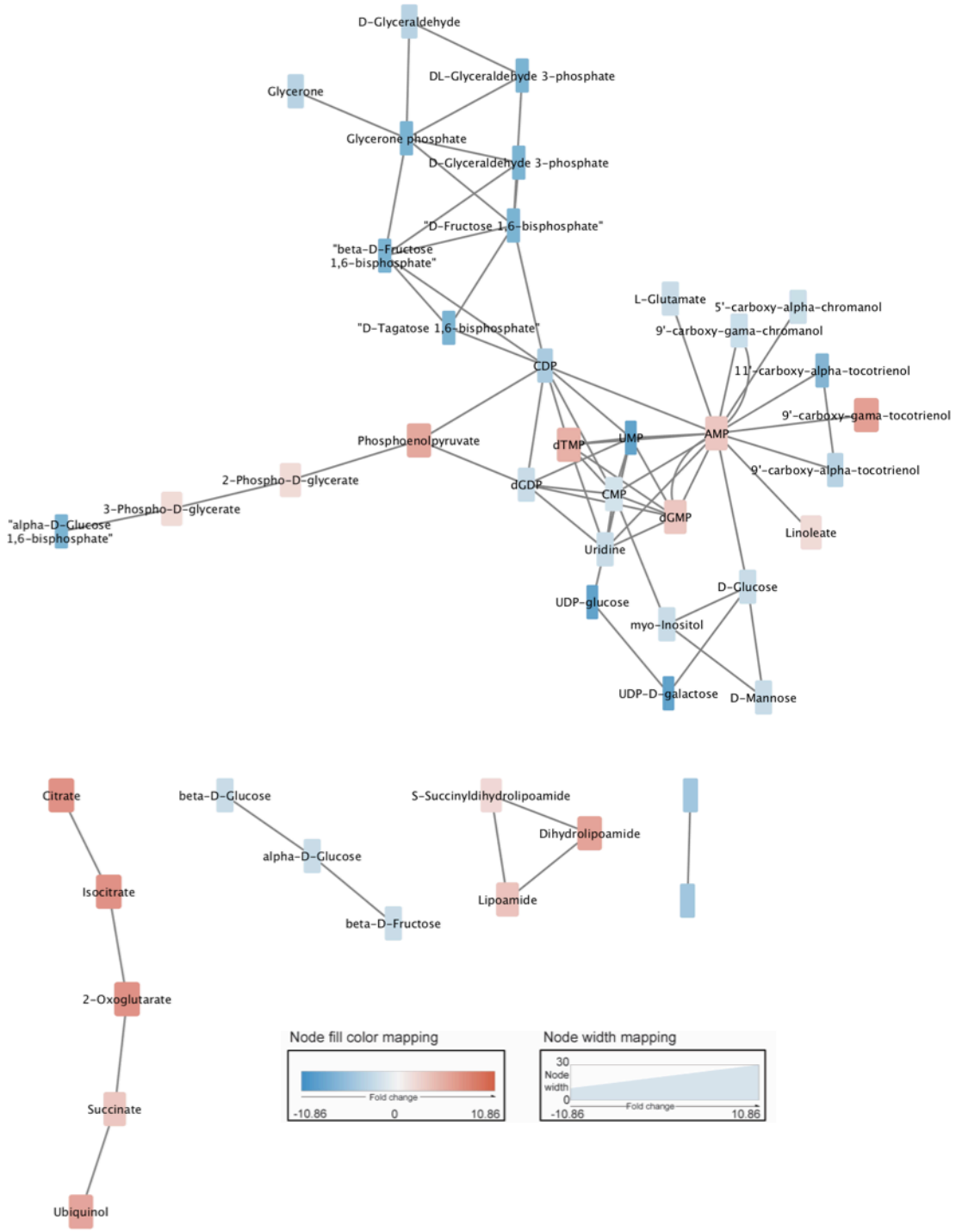

Supplemental Figure 4 Metabolic map at 48 hpi. Metabolites annotated by network analysis that are found when comparing DENV2 to mock samples at 48 hpi. The node size and color are determined by the statistical differences between DENV2 and mock with the values noted in the legend. The large nodes (red) are metabolites that are upregulated in DENV2 vs. mock and the small nodes (blue) are metabolites that are downregulated in DENV2 vs. mock samples. The edges connecting the nodes represent enzymatic reactions that connect the specific metabolites. Their length has no significance.

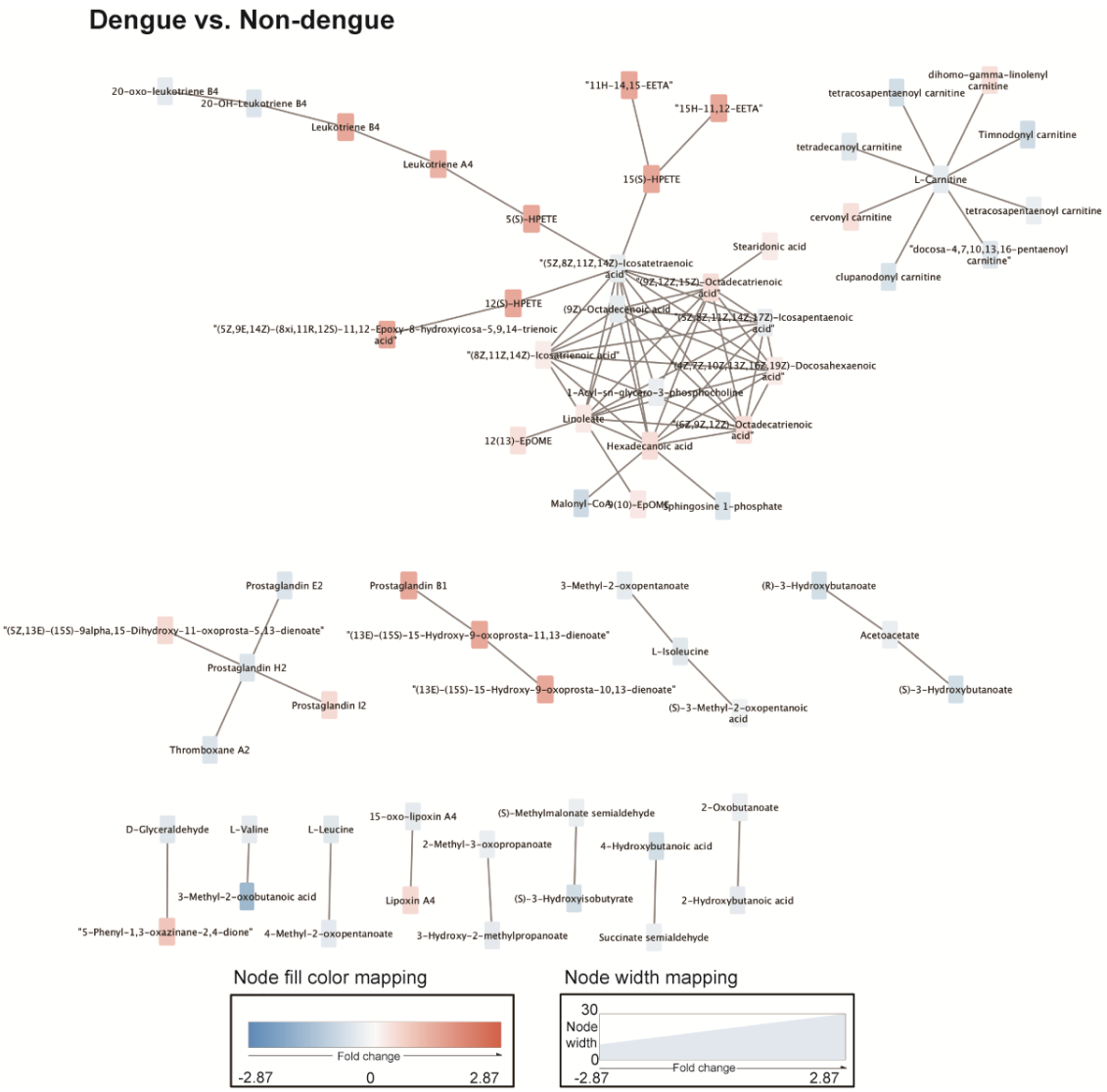

Supplemental Figure 5 Metabolic map of dengue vs. non-dengue samples. Metabolites annotated by network analysis that are found when comparing dengue to non-dengue samples. The node size and color are determined by the statistical differences between the samples with the values noted in the legend. The large nodes in red are metabolites that are upregulated in dengue samples and the small nodes in blue are metabolites that are decreased in dengue samples (increased in non-dengue). The edges connecting the nodes represent enzymatic reactions that connect the metabolites and their length has no significance.

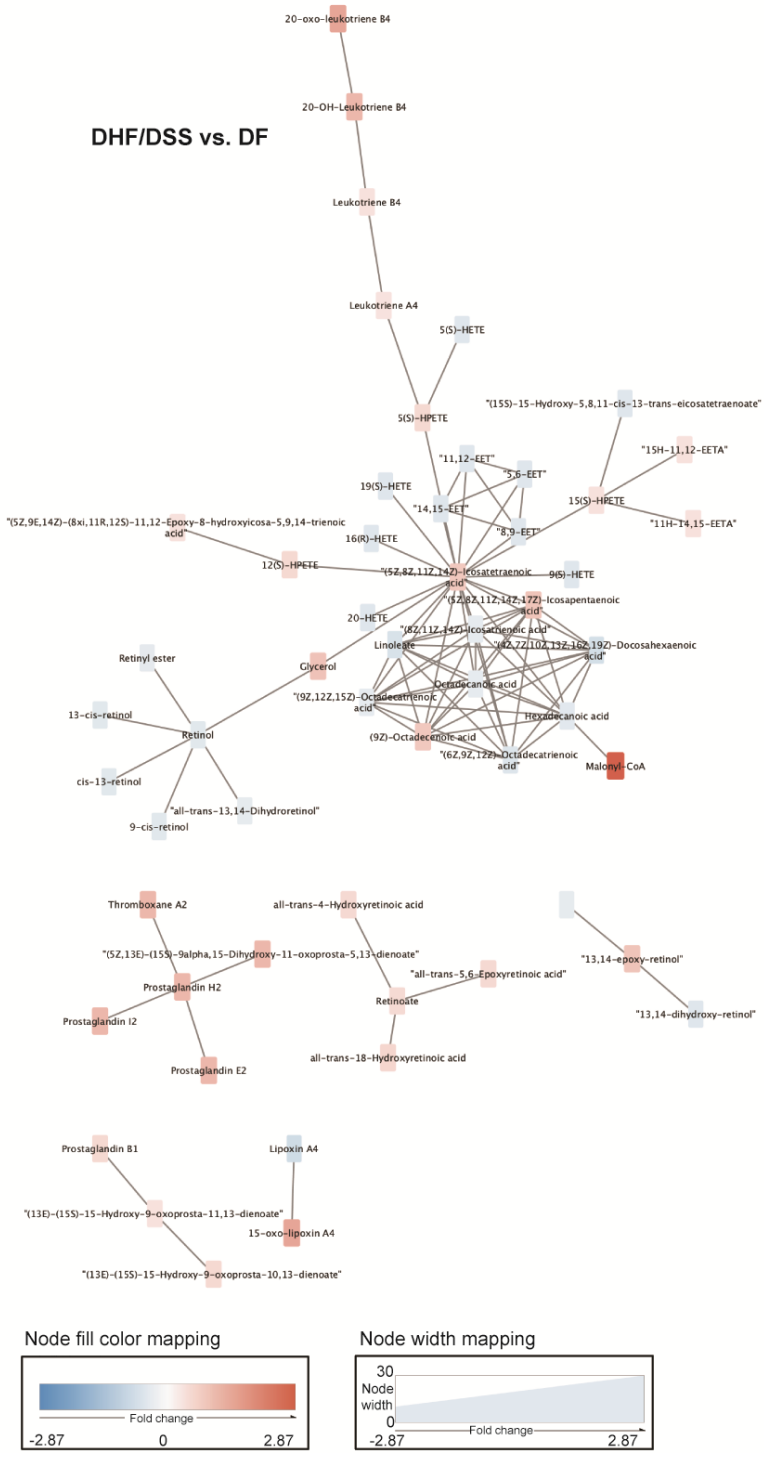

Supplemental Figure 6 Metabolic map of DHF/DSS vs. DF samples. Metabolites annotated by network analysis that are found when comparing DHF/DSS to DF samples. The node size and color are determined by the statistical differences between the samples with the values noted in the legend. The large nodes in red are metabolites that are upregulated in DHF/DSS samples and the small nodes in blue are metabolites that are decreased in DSS samples (increased in DF). The edges connecting the nodes represent enzymatic reactions that connect the metabolites and their length has no significance.

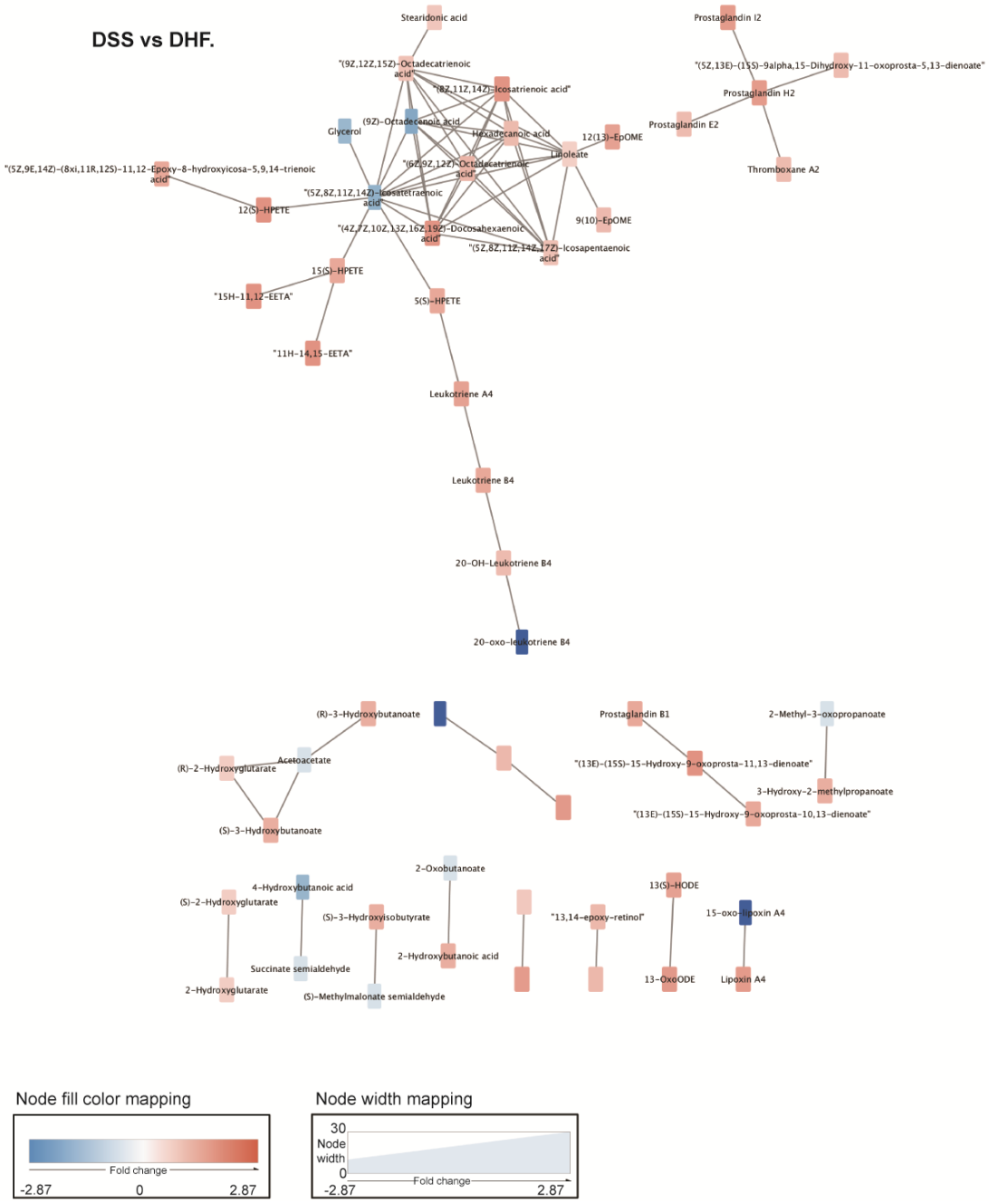

Supplemental Figure 7 Metabolic map of DSS vs. DHF samples. Metabolites annotated by network analysis that are found when comparing DSS to DF samples. The node size and color are determined by the statistical differences between the samples with the values noted in the legend. The large nodes in red are metabolites that are upregulated in DSS samples and the small nodes in blue are metabolites that are decreased in DSS samples (increased in DF). The edges connecting the nodes represent enzymatic reactions that connect the metabolites and their length has no significance.

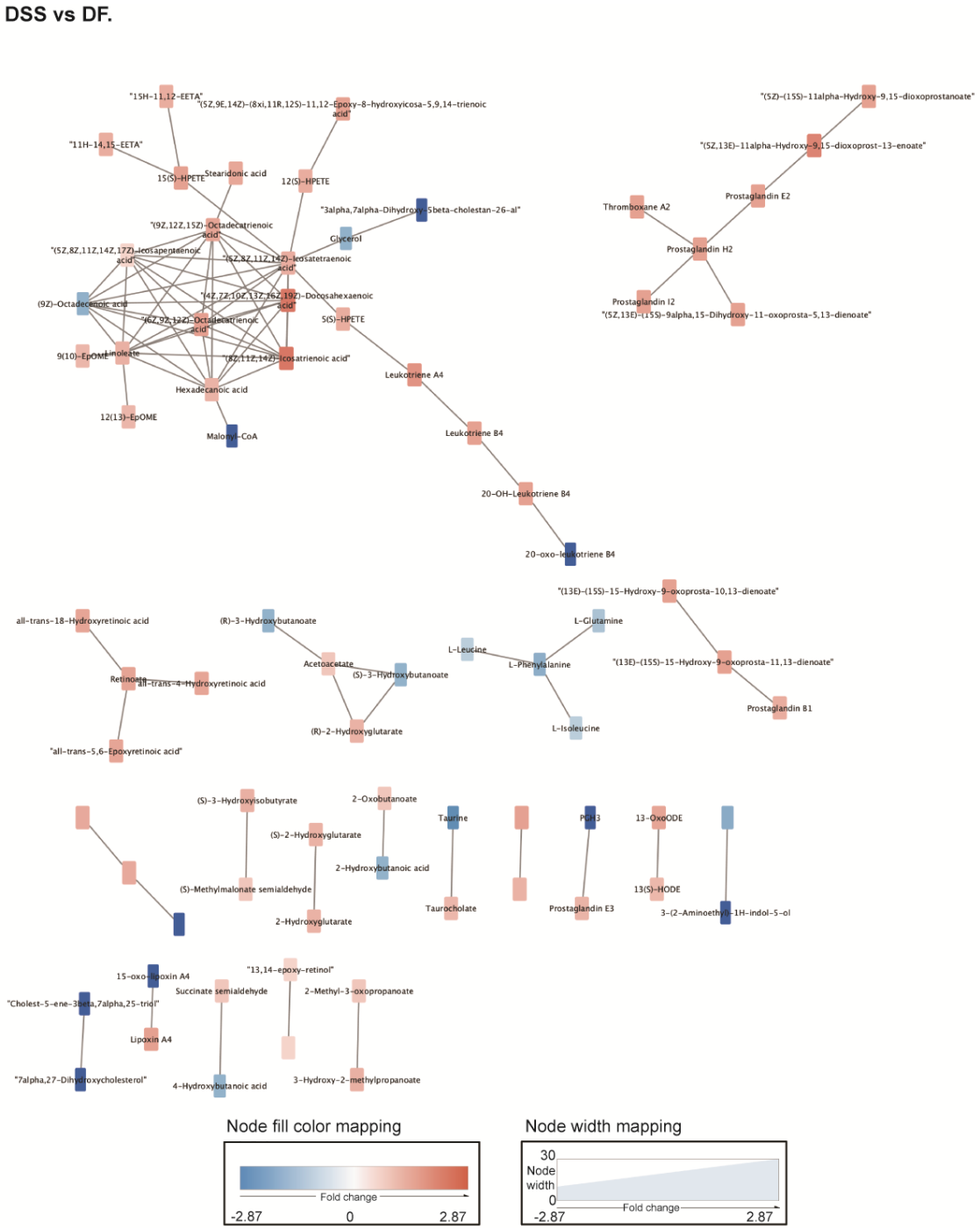

Supplemental Figure 8 Metabolic map of DSS vs. DF samples. Metabolites annotated by network analysis that are found when comparing DSS to DF samples. The node size and color are determined by the statistical differences between the samples with the values noted in the legend. The large nodes in red are metabolites that are upregulated in DSS samples and the small nodes in blue are metabolites that are decreased in DSS samples (increased in DF). The edges connecting the nodes represent enzymatic reactions that connect the metabolites and their length has no significance.

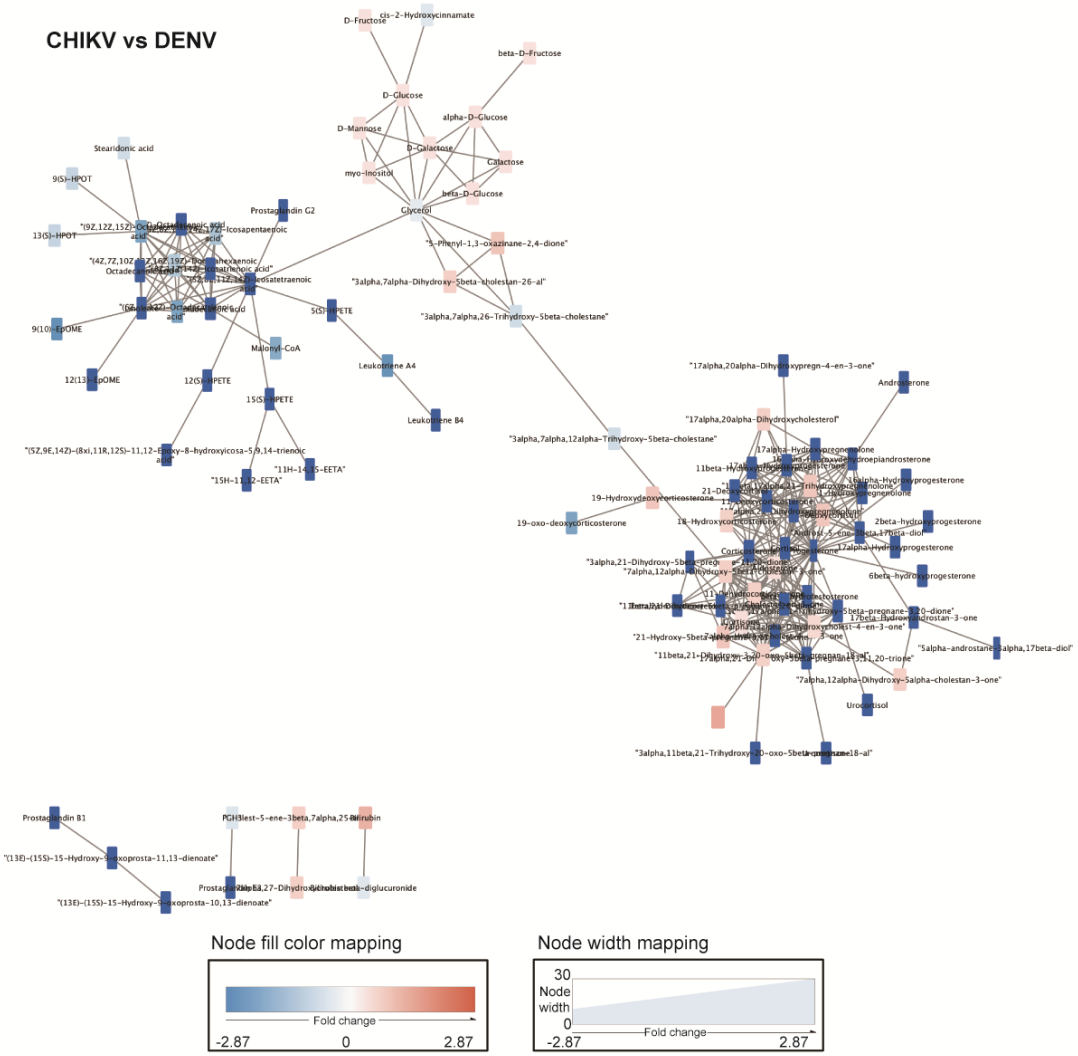

Supplemental Figure 9 Metabolic map of CHIKV vs. dengue samples. Metabolites annotated by network analysis that are found when comparing CHIKV to dengue samples. The node size and color are determined by the statistical differences between the samples with the values noted in the legend. The large nodes in red are metabolites that are upregulated in CHIKV samples and the small nodes in blue are metabolites that are decreased in CHIKV samples (increased in DEN). The edges connecting the nodes represent enzymatic reactions that connect the metabolites and their length has no significance.

Supplemental Tables

Supplementary Table 1 Pathways enriched in the indicated comparisons found in the positive ionization mode.

Time (hrs of infections)	DENV2 vs. mock	DENV2 vs. UVI	mock vs. UVI
6	Tryptophan metabolism C21-steroid hormone biosynthesis and metabolism CoA Catabolism	Tryptophan metabolism TCA cycle Linoleate metabolism Aspartate and asparagine metabolism Vitamin B5 - CoA biosynthesis from pantothenate	Bile acid biosynthesis Vitamin E metabolism Electron transport chain
18	Purine metabolism Arginine and Proline Metabolism Methionine and cysteine metabolism Pyrimidine metabolism Vitamin E metabolism Vitamin B5 - CoA biosynthesis from pantothenate Starch and Sucrose Metabolism Ascorbate (Vitamin C) and Aldarate Metabolism Aspartate and asparagine metabolism N-Glycan biosynthesis De novo fatty acid biosynthesis Xenobiotics metabolism CoA Catabolism Tryptophan metabolism	Pyrimidine metabolism Purine metabolism Vitamin B5 - CoA biosynthesis from pantothenate N-Glycan biosynthesis De novo fatty acid biosynthesis CoA Catabolism Vitamin B3 (nicotinate and nicotinamide) metabolism	Bile acid biosynthesis Vitamin E metabolism Propanoate metabolism Sphingolipid metabolism
30	Glycolysis and Gluconeogenesis	Purine metabolism Pyrimidine metabolism Vitamin B5 - CoA biosynthesis from pantothenate	TCA cycle Aminosugars metabolism Linoleate metabolism Glycosphingolipid biosynthesis - ganglioseries Xenobiotics metabolism Glycolysis and Gluconeogenesis Glycosphingolipid biosynthesis - globoseries Keratan sulfate biosynthesis
48	Vitamin E metabolism TCA cycle Phytanic acid peroxisomal oxidation	TCA cycle Glycolysis and Gluconeogenesis Lysine metabolism Vitamin B1 (thiamin) metabolism Valine, leucine and isoleucine degradation Purine metabolism Propanoate metabolism Phytanic acid peroxisomal oxidation Ascorbate (Vitamin C) and Aldarate Metabolism Ubiquinone Biosynthesis Glycine, serine, alanine and threonine metabolism Mono-unsaturated fatty acid beta-oxidation	Ubiquinone Biosynthesis Vitamin B1 (thiamin) metabolism

Supplementary Table 2 Pathways enriched in the indicated comparisons found in the negative ionization mode.

Time (hrs of infections)	DENV2 vs. mock	DENV2 vs. UVI	mock vs. UVI
6	Vitamin D3 (cholecalciferol) metabolism Purine metabolism Sialic acid metabolism Pyrimidine metabolism Aminosugars metabolism	Vitamin D3 (cholecalciferol) metabolism Purine metabolism Vitamin B9 (folate) metabolism Porphyrin metabolism	Vitamin D3 (cholecalciferol) metabolism Pyrimidine metabolism Sialic acid metabolism Aminosugars metabolism
18	Vitamin A (retinol) metabolism Purine metabolism Phosphatidylinositol phosphate metabolism Pyrimidine metabolism Glycolysis and Gluconeogenesis Porphyrin metabolism	Linoleate metabolism De novo fatty acid biosynthesis Fatty acid activation Glycerophospholipid metabolism Omega-3 fatty acid metabolism Arachidonic acid metabolism	Bile acid biosynthesis Vitamin E metabolism Glycolysis and Gluconeogenesis Vitamin B9 (folate) metabolism
30	Arachidonic acid metabolism Vitamin A (retinol) metabolism Omega-3 fatty acid metabolism Glycerophospholipid metabolism Aspartate and asparagine metabolism De novo fatty acid biosynthesis Phosphatidylinositol phosphate metabolism	De novo fatty acid biosynthesis Linoleate metabolism Di-unsaturated fatty acid beta-oxidation Fatty Acid Metabolism Vitamin A (retinol) metabolism Fatty acid activation Glycerophospholipid metabolism Leukotriene metabolism Arachidonic acid metabolism Omega-3 fatty acid metabolism	Bile acid biosynthesis Sialic acid metabolism C21-steroid hormone biosynthesis and metabolism Glycerophospholipid metabolism Di-unsaturated fatty acid beta-oxidation Fatty Acid Metabolism Aminosugars metabolism De novo fatty acid biosynthesis
48	Tryptophan metabolism Pyrimidine metabolism Glycolysis and Gluconeogenesis Sialic acid metabolism Hexose phosphorylation Carbon fixation Vitamin D3 (cholecalciferol) metabolism TCA cycle	De novo fatty acid biosynthesis Glycerophospholipid metabolism Arachidonic acid metabolism Vitamin A (retinol) metabolism Prostaglandin formation from arachidonate Fatty acid activation Omega-6 fatty acid metabolism Omega-3 fatty acid metabolism Linoleate metabolism Hexose phosphorylation Di-unsaturated fatty acid beta-oxidation Fatty Acid Metabolism Leukotriene metabolism	Tryptophan metabolism Prostaglandin formation from arachidonate Omega-6 fatty acid metabolism De novo fatty acid biosynthesis Leukotriene metabolism Androgen and estrogen biosynthesis and metabolism

Supplamentary Table 3 siRNA screen of the human unsaturated fatty acid biosynthesis pathway. The enzymes in the UFA biosynthesis pathway were identified based on the KEGG database (235). Here each enzyme is listed along with its gene ID, Accession number, GI number (GenInfo Identifier) and the sequence for the four siRNAs used to knockdown each gene.

Gene Symbol	GENE ID	Gene Accession	GI Number	Sequence 1	Sequence 2	Sequence 3	Sequence 4
ELOVL6	79071	NM_024090	13129087	CAAUGGACCUGUCAGCAAA	GGUCGGCACCUAAUGAAUA	CGAACUAGGAGAUACAAUA	GGGUGUAUAUCUAGAACGA
HSD17B12	51144	NM_016142	153792624	GAAAUCGGCAUCUUAGUGA	UAAGAUGACACAAUUGGUA	CGUAUGAGUAUCCUGAAUA	GAACUAAUAUUGUCGGGAA
PECR	55825	NM_018441	93102372	GAGGAUCUAUCGUCAAUAU	GGACCUUUCUGUUGUCAAA	AGGAGGAGGUGAAUAAUUU	GAAUGGGCCUGCAGUGGAA
PTPLB	201562	NM_198402	158819030	GAGAACUGCUCACAAUAUA	CGGCGUACCUGGUCAUCUA	AAUCAUCCGUUACUCCUUU	CAUGGACGAUCACGGAAAU
PTPLA	9200	NM_014241	82659104	UGAGAUAGUUCACUGUUUA	CAAUAAGACUUCCUAACAA	CCACAACUCUAUUUUCAUA	UGACAGAGAUCACUCGCUA
GPSN2	9524	NM_138501	50726974	UGGAGAUUCUGGACGCAAA	AUUACGAGGUGGAGAUUCU	GAGCUCAGCAGGUGAAACU	GAUUCUGGACGCAAAGACA
SCD	6319	NM_005063	53759150	GAUAUGCUGUGGUGCUUAA	AGAAUGAUGUCUAUGAAUG	CGACAUUCGCCCUGAUAUA	GGAGUACGCUAGACUUGUC
SCD5	79966	NM_024906	148596937	CAUAUUGGGUGGCUGUUUG	AGAACAUCGUCUGGAGGAA	GAGAAAGCUUGACGUCACU	CAGAAUGACAUCUUCGAGU
FADS2	9415	NM_004265	14141180	GCACUACGCUGGAGAAGAU	UGAAAUACCUGCCCUACAA	GGCAAGAACUCAAAGAUCA	GGCAAUGGCUGGAUUCCUA
ELOVL5	60481	NM_021814	52851443	CAAGGAAGCUGCGGAAGGA	GGUUUCUUCUGGACAAUUA	UCACACUGCUGUCUCUGUA	UCUCCAAACUCAUAGAAUU
FADS1	3992	NM_013402	14141179	GGAACCAUCUGCUACAUCA	GAGGAGCGGUGGCUAGUGA	GACUUGGCCUGGAUGAUUA	GCAUAGAGUACCAGUCCAA
ELOVL2	54898	NM_017770	157388944	CAAAUGGAGUGAUGAACAA	CCAGUCAUCUUAUAUGCUA	CGGUCAUGAGCCACGAUAA	CAAUAUGUUUGGACCGCGA
ACOX1	51	NM_007292	83641872	GGAAAGACUUCAAAUCAUG	GGGCAUGGCUAUUCUCAUU	CAAGUAAACCAGCGUGUAA	UUACAUGCCUUUAUCGUAC
ACOX3	8310	NM_001101667	156104865	GCAAGCGGAUCUUCGAGUA	ACAAGUGGCUGGUUUGCUA	GAUCGCUCCUCCUGACUUU	GAAUUAAGCCACGGCAGUA
HADHA	3030	NM_000182	105990523	GCUCUAACAUCAUUUGAAA	UCUCAGAAGUUAUGAAUGA	GACAAUAGAAUACCUAGAA	CGAAACAUGUGGCGGAAGA
ACAA1	30	NM_001607	6598316	GAGAUUGCCUGAUUCCUAU	GGGAUAACCUCUGAGAAUG	CCACCACGGUCCAUGAUGA	GAAAUAUUACUUCGCGCUU
ZAP128	10965	NM_006821	148727285	GGAAACAACUCCAGACUUU	GGAAGGACCUGACCAGAAG	GAGGUGGCCUGCUGGAGUA	GACCAAAGAUGGCUAUGCA
BACH	11332	NM_181866	75709215	GGCGGUACCUGCAGAUGAA	GCGCGGAGAUCACCUACAC	GCGCACCGACUUCCUGUCU	GACGAGAAGAAGCGCUUUG
PTE2B	122970	NM_152331	63999751	UAUAAGGAAUGCUCUCGUA	CCAAUAACAUGGACAACAU	CAUCGAGCCUCCUUACUUC	GAAGCGGGACGUACAGAUU
ACOT1	641371	NM_001037161	81230484	GGGACGAACCGGUGCGAAU	CUGCUGGAGUAUCGGGCUA	CCAAAGAUGGCUAUGCAGA	CAACAGAAAUCGCAUCAAG
BAAT	570	NM_001701	4502350	GGAAGGAGAUCCAGAGAUU	GACUAUCUAUGGCUAUUUA	CAAUUAAUAUCCACCAAUG	CCACGGUACUUAUUAAUGG

Supplamentary Table 4. Key resources Table. Included here is detailed information for all reagents and resources used in Chapter 3.

REAGENT or RESOURCE	SOURCE	IDENTIFIER
Antibodies		
anti- SCD Antibody (N-20)	Santa Cruz Biotechnology	Cat#: sc-14715 RRID: AB_2238791
anti- β-Actin (8H10D10) Mouse mAb	Cell signalling	Cat#: 12262 RRID: AB_2566811
anti-dsRNA monoclonal antibody	English & Scientific Consulting Bt	Cat#: 10010500 RRID: AB_2651015
anti-NS3	Dr. Richard Kuhn(Heaton et al. 2010a)	NA
anti-Envelope (4G2)	Dr. Richard Kuhn(Gentry et al. 1982)	NA
anti-Dengue 2 virus PrM protein antibody	Genetex	Cat#: GTX128093 RRID: AB_1240702
anti-Dengue 2 virus Capsid protein antibody	Genetex	Cat#: GTX103343 RRID: AB_1240697
Chicken anti-Goat IgG (H+L) Secondary Antibody, Alexa Fluor® 647 conjugate	Thermo Fisher Scientific	Cat#: A-21469 RRID: AB_2535872
Donkey anti-Mouse IgG Secondary Antibody, Alexa Fluor® 488 conjugate	Thermo Fisher Scientific	Cat#: R37114 RRID: AB_2556542
IRDye® 680RD Donkey anti-Goat IgG (H + L), 0.5 mg	Li-Cor	Cat#: 926-68074 RRID: AB_10956736
IRDye 800CW Goat anti-Mouse IgG (H + L), 0.5mg	Li-Cor	Cat#: 926-32210 RRID: AB_2687825
IRDye 800CW Goat anti-Rabbit IgG (H + L), 0.5mg	Li-Cor	Cat#: 926-32211 RRID: AB_10796098
IRDye® 680RD Goat anti-Mouse IgG (H+L), 0.5 mg	Li-Cor	Cat#:926-68070 RRID: AB_2651128
Bacterial and Virus Strains		
DENV1 (16007)	Dr. Clair Huang, CDC (Yoksan, 1986; Huang et al. 2000)	AF180818
DENV2 (16681)	Dr. Clair Huang, CDC (Yoksan, 1986; Kinney et al. 1997)	U87411
DENV3 (16562)	Dr. Clair Huang, CDC (Jirakanjanakit et al. 1999; Angsubhakorn et al. 1994; Goh et al. 2016)	KU725665
DENV4 (1036)	Dr. Clair Huang, CDC (Jirakanjanakit et al. 1999)	U18429
YFV 17D	Dr. Charles Rice (Rice et al. 1985)	NC_002031

KUNV	Dr. Alexander Khromykh (Khromykh & Westaway 1994)	AY274505
SINV	Dr. Richard Kuhn (Strauss et al. 1984)	NC_001547
ZIKA (PRVABC59)	Dr. Aaron Brault, CDC (Lanciotti et al. 2016)	KU501215
Chemicals, Peptides, and Recombinant Proteins		
siRNA library	Dharmacon (This paper)	Table S1
Lipofectamine® RNAiMAX Transfection Reagent	Invitrogen	13778075
SCD siRNA	Sigma	SASI_Hs01_00181371
siIRR: Custom siRNA	Dharmacon	CTM-278879
MISSION® esiRNA esiRNA human ELOVL2	Sigma-Aldrich	EHU033101-20UG
MISSION® esiRNA esiRNA targeting human ELOVL6	Sigma-Aldrich	EHU005171-20UG
MISSION® esiRNA esiRNA targeting human PECR	Sigma-Aldrich	EHU002471-20UG
MISSION® esiRNA esiRNA targeting mouse Acot1	Sigma-Aldrich	EMU214111-20UG
DAPI (4',6-Diamidino-2-Phenylindole, Dihydrochloride)	Invitrogen / Life Technologies	D1306
Stearoyl [1-14C] coA	American Radiolabled Chemicals	ARC 0756-10 µCi
SCD inhibitor	Medchem Express	HY-50709
C75	Cayman	10005270
Lovastatin	Sigma-Aldrich	PHR1285
Trizol	Lifetech	15596018
Trizol LS	Lifetech	10296-028
Bovine Serum Albumin (BSA), Fraction V, Fatty Acid Free for tissue culture	Gold Biotechnology	A-421-25
Oleic Acid	Sigma-Aldrich	O1008
Stearic Acid	Sigma-Aldrich	S4751
Oleic Acid-BSA	Sigma-Aldrich	O3008
Critical Commercial Assays		
Brilliant III Ultra-Fast SYBR qRT-PCR Master Mix	Agilent	600886
Experimental Models: Cell Lines		
Huh7	Dr. Charles Rice (Blight et al. 2002)	
BHK	ATCC	ATCC CCL-10
C636	ATCC	ATCC CRL-1660
A549	ATCC	ATCC CRM-CCL-185
HEL299	ATCC	ATCC CCL-137
Oligonucleotides		
DEN2 +strand (FWD): ACAAGTCGAACAACCTGGTCCAT	(Laue, Emmerich, & Schmitz, 1999	

DEN2 +strand (REV): GCCGCACCATTGGTCTTCTC	(Laue, Emmerich, & Schmitz, 1999	
Stearoyl-CoA desaturase 1 (FWD): TTGGGAGCCCTGTATGGGAT	This paper	
Stearoyl-CoA desaturase 1 (REV): TTTGTAAGAGCGGTGGCTCC	This paper	
GAPDH (FWD): TCCTGTTCGACAGTCAGCCG	This paper	
GAPDH (REV): AGTTAAAAGCAGCCCTGGTGA	This paper	
Recombinant DNA		
DENV2 luciferase replicon	Dr. Richard Kuhn (Heaton et al. 2010a)	
Software and Algorithms		
GraphPad Prism version 7.00 for Mac OS x	GraphPad Software, La Jolla California USA)	
R studio version 1.0.136	RStudio Team 2016	
ImageQuant TL	GE Health Care Life Sciences	
Volocity 6.3	Perkin Elmer	
FV10-ASW 4.2	Olympus	
Image Studio 5.2	Li-Cor	
LightCycler 96 SW 1.1	Roche	